UNIVERSITÀ DEGLI STUDI DI MILANO

DEPARTMENT OF PHYSICS

PhD School in Physics, Astrophysics and Applied Physics

CYCLE XXXVI

Steering the Quantum: from remote state preparation to quantum transport

Disciplinary Scientific Sector FIS/03

PhD Thesis of:
Massimo FRIGERIO

Supervisor: Matteo G.A. PARIS

Director of the School: Roberta VECCHI

A.Y. 2022-2023

Commission of the final examination:

External Referee 1:
Dr. Valentina Parigi (Laboratoire Kastler Brossel, Paris, France)

External Referee 2:
Prof. Elisabetta Paladino (Università degli Studi di Catania)

External Member 1:
Prof. Paolo Bordone (Università degli Studi di Modena e Reggio Emilia)

External Member 2:
Prof. Vittorio Giovannetti (Scuola Normale Superiore, Pisa)

Final examination:

Date: 21 December 2023

Università degli Studi di Milano, Dipartimento di Fisica "Aldo Pontremoli", Via Celoria 16, Milano, Italy

"I like the scientific spirit, the holding off,
the being sure but not too sure,
the willingness to surrender ideas when the evidence is against them:
this is ultimately fine, it always keeps the way beyond open
always gives life, thought, affection, the whole man,
a chance to try over again after a mistake
after a wrong guess."

W. Whitman

To my family and to Luca

Cover illustration:

Generated by successive iterations with the graphic artificial intelligence DALL-E 2. It is meant to represent a vessel made of light which is steered and conditioned by other types of light.

Internal illustrations:

All the internal illustrations are either original
or adapted from the author's own articles
listed at the beginning of this thesis.

MIUR subjects:

FIS/03

PACS:

03.65.w
03.65.Aa
03.65.Vf
03.67.a
42.50.p

List of Publications

As of October 2023

Refereed publications

1. **Steering Nonclassicality of Gaussian states**
   Massimo Frigerio, Stefano Olivares and Matteo G. A. Paris
   Physical Review A **103**, Issue no. 2, 022209 (Feb. 2021)
   DOI: 10.1103/PhysRevA.103.022209

2. **Generalized quantum-classical correspondence for random walks on graphs**
   Massimo Frigerio, Claudia Benedetti, Stefano Olivares and Matteo G. A. Paris
   Physical Review A **104**, Issue no. 3, L030201 (Sep. 2021)
   DOI: 10.1103/PhysRevA.104.L030201

3. **Exploiting Gaussian steering to probe non-Markovianity due to the interaction with a structured environment**
   Massimo Frigerio, Samaneh Hesabi, Davood Afshar and Matteo G. A. Paris
   Physical Review A **104**, Issue no. 5, 052203 (Nov. 2021)
   DOI: 10.1103/PhysRevA.104.052203

4. **Quantum-classical distance as a tool to design optimal chiral quantum walks**
   Massimo Frigerio, Claudia Benedetti, Stefano Olivares and Matteo G. A. Paris
   Physical Review A **105**, Issue no. 3, 032425 (Mar. 2022)
   DOI: 10.1103/PhysRevA.105.032425

5. **Quantum steering with Gaussian states: A tutorial**
   Massimo Frigerio, Claudio Destri, Stefano Olivares and Matteo G.A. Paris
   Physics Letters A **430**, 127954 (Apr. 2022)
   DOI: 10.1016/j.physleta.2022.127954

6. **Cost-effective estimation of single-mode thermal states by probabilistic quantum metrology**
   Massimo Frigerio, Stefano Olivares and Matteo G.A. Paris
   Quantum Science and Technology **7**, 035011 (May 2022)
   DOI: 10.1088/2058-9565/ac6dfe

7. **Swift chiral quantum walks**
   Massimo Frigerio and Matteo G.A. Paris
   Linear Algebra and its Applications **673**, pp. 28–45 (Sep. 2023)
   DOI: 10.1016/j.laa.2023.05.007

8. **Quantum routing of information using chiral quantum walks**
   Alberto Bottarelli, Massimo Frigerio and Matteo G.A. Paris
   AVS Quantum Science **5**, 2 (Apr. 2023)
   DOI: 10.1116/5.0146805

Publications under review

- **Enhanced quantum transport in chiral quantum walks**
  Emilio Annoni, Massimo Frigerio and Matteo G. A. Paris
  arXiv:2308.14747 [quant-ph] (Aug. 2023)

Publications in preparation

- **Tackling a sloppy Gaussian quantum statistical model**
  Massimo Frigerio and Matteo G. A. Paris
  t.b.a.

Publications in conference proceedings

- **Perspective and applications of chiral quantum walks**
  Massimo Frigerio
  Il Nuovo Cimento C (June 2022)
  DOI: 10.1393/ncc/i2022-22072-1

Contents

Introduction

Motivation

Quantum information science is a vast and rapidly developing field of research in physics, which accompanies and partially guides the parallel development of quantum technologies, with the common goal of harnessing quantum phenomena to achieve tasks that are classically unfeasible or to greatly improve current technological strategies. Despite not having well defined borders, with the risk of appearing sketchy to the uninitiated when compared to more cohesive topics such as, e.g., quantum field theory, it can be often recognized through a general feature: a contribution to quantum information science usually entails, theoretically and/or experimentally, a fine control of quantum degrees of freedom, be it direct or not, which is uncommon in all other branches of physics exploiting quantum mechanics. For example, particle physics is very rarely concerned with *preparing* exotic quantum states of the particles or in performing measurements in non-standard bases that do not have a clear macroscopic interpretation. In a similar fashion, quantum theory of matter aims at explaining physico-chemical properties of macroscopic states of matter without considering the possibility of a direct intervention on the quantum states of, say, the electrons in a solid. In striking contrast, experimental violation of Bell's inequalities, quantum teleportation and transport, quantum computation and essentially all topics in quantum information require a true control of quantum states and they often unveil the unperceived details of the quantum nature underlying everyday experience. Precisely because of this intersectional character, it finds application in a wide spectrum of modern physical research, encompassing cosmology, black holes physics, solid state physics, quantum computation, foundational questions on the quantum theory itself and it even propels and inspires the development of better classical algorithms. Of paramount importance in quantum information science is the ability to prepare desirable quantum states and to *steer* their evolution in a predictable, tuneable and useful way. This thesis would aspire to contribute to an infinitesimal development towards these goals.

Thesis overview

This thesis is structured as follows.

- In Chapter 1 we review the postulates of quantum mechanics and the main concepts of quantum information, with emphasis on foundational results that are often neglected in standard books on quantum mechanics, such as the Kochen-Specker theorem or the difference between locality and causality in the context of quantum correlations.

- In Chapter 2 we present the fundamentals of continuous-variable quantum information, Gaussian states, measurements and channels and we conclude with a short discussion on non-Gaussianity.

- In Chapter 3, after a pernickety exposition of the concept of quantum steering, we examine EPR steering for Gaussian states and nonclassical steering, drawing parallels and connections between them.

- In Chapter 4 the framework of quantum estimation theory and quantum metrology is laid down on the formal mathematical basis of abstract probability theory. Concepts such as the Quantum Fisher Information and quantum incompatibility in multi-parameter quantum metrology are discussed in some detail, and they are applied to two scenarios: the estimation of the temperature on photon-subtracted thermal states with probabilistic quantum metrology and the study of classical and quantum distinguishability of two parameters characterizing a sloppy quantum statistical model.

- In Chapter 5, marking the beginning of the second part of the thesis, we introduce a new subject: continuous-time quantum walks. Developing upon classical random walks on discrete structures, we present both discrete-time and continuous-time quantum walks on graphs. We also provide some elementary notions of graph theory that are relevant for the following chapters.

- In Chapter 6 we advance a generalization of continuous-time quantum walks to encompass Hamiltonian generators with complex couplings, thereby arriving at the notion of chiral quantum walks. We discuss their quasi-gauge invariance and their relation with Aharonov-Bohm phases for charged quantum particles interacting with a classical electromagnetic field.

- In Chapter 7, the last one, we further develop the theory of chiral quantum walks in the attempt to answer the question: what can they do and what they cannot do with respect to standard quantum walks? We show that chirality can be used e.g. to cure the problem of sedentarity, to induce directional quantum transport with high fidelity and to improve the transport performances of chain graphs by a new mechanism based on its action on the spectra.

All the material is either fully original or adapted from the author's published articles listed at the beginning of the thesis, in the effort to provide a cohesive overview of the research work done during my PhD studies, between November 2020 and October 2023.

Notation

We committed to maintaining consistency of notation throughout the thesis, although the vast variety of topics necessarily led to some overlaps of notations in different contexts. We use the hat, as in $\hat{\mathrm{H}}, \hat{\mathrm{U}}, \hat{\Pi}$ to denote all operators and we use boldface to emphasize the vectorial or matricial character of some operators, especially in continuous-variable systems, as in $\hat{\mathbf{R}}$, $\hat{\mathbf{\Pi}}_G$. Matrices are represented by uppercase straight letters such as $\mathrm{A}, \mathrm{L}, \mathrm{H}$. Calligraphic letters are mainly reserved to concepts related to Hilbert spaces, as in $\mathcal{H}, \mathcal{S}(\mathcal{H}), \mathcal{T}(\mathcal{H}), \mathcal{B}(\mathcal{H})$, although the notations for the fidelity and the classical Fisher Information make ecceptions to this rule.

Chapter 1

General theory of quantum information

1.1 The postulates of Quantum Mechanics

The mathematical theory of quantum mechanics in its modern form holds as its basis the operational interpretation [1], in which the fundamental concepts are the space of states, the preparations, the evolutions and the measurements. This paradigm, dating back to N. Bohr and J. Von Neumann in one of its earliest forms [2], aims at representing in a minimal way all the information needed to predict every outcome of every possible experiment in a given quantum mechanical setting, and nothing more. To each of these concepts corresponds a postulate, the result of historical selection of the minimal requests to describe the outcomes of succeeding experiments to unveil quantum behaviours: in the following we shall state and briefly discuss these postulates, together with an additional one, which is necessary to define how combined quantum mechanical systems should be formalised mathematically.

1.1.1 The Space of States Postulate

The first ingredient that is needed to build a mathematical theory to model Nature is ontological: what are the physical systems? How can we fully specify the states in which they present themselves to our investigations? In classical mechanics, the simplest entities are massive point particles: more precisely, they are specified by a constant m and they inhabit some manifold of possible positions at any given time. Their states at each time are specified by their position, a point on the manifold, and their velocity, a vector of the tangent space at that point. More complex classical systems can be still framed into this description by considering a mass density and internal forces preserving the integrity in the case of rigid bodies.

On the other hand, quantum mechanics is intrinsically[1] probabilistic, since even for the simplest nontrivial quantum system, the qubit, it is empirically established that no preparation of the system leads to a state in which all the possible observable quantities have deterministic values. The mathematical tool that has been historically found to be suitable to describe this behaviour is an Hilbert space, a (possibly infinite-dimensional) complex[2] vector space $\mathcal{H}$ endowed with a sesquilinear product $\forall \alpha, \beta \in \mathbb{C}, \forall |\mathbf{u}\rangle, |\mathbf{v}\rangle \in \mathcal{H} : \langle \alpha \mathbf{u} | \beta \mathbf{v} \rangle = \alpha^* \beta \langle \mathbf{u} | \mathbf{v} \rangle$ such that it is complete with respect to the norm induced by said

[1] Perhaps a better term would be *ontologically*.

[2] The underlying field of Hilbert spaces in quantum mechanics is the complex field, for reasons that will be hinted at later in this chapter.

product[3]. In quantum mechanics, the focus is almost exclusively on Hilbert spaces that are *separable*, that is to say they admit a countable orthonormal Schauder basis [3]. We remark also that Riesz Representation Theorem guarantees a one-to-one correspondence between vectors in $\mathcal{H}$ and elements of the dual space, thus justifying the Dirac bra-ket notation for scalar products.

To properly formalise the notion of quantum states, we shall introduce some minimal terminology [3, 4, 5]. Let us call $\mathcal{B}(\mathcal{H})$ the space of bounded operators on $\mathcal{H}$, recalling that boundedness imply continuity and vice versa, for linear operators on Banach spaces. By $\mathcal{T}(\mathcal{H})$ we will denote the space of trace-class linear operators. These are defined by first taking a generic bounded operator $\hat{A} \in \mathcal{B}(\mathcal{H})$ and defining $|\hat{A}| = \sqrt{\hat{A}^\dagger \hat{A}}$, $\hat{A}^\dagger$ being the adjoint of $\hat{A}$. If $\mathrm{Tr}|\hat{A}| = \sum_j \langle v_j || \sqrt{\hat{A}^\dagger \hat{A}} | v_j \rangle$ is convergent and finite for some complete orthonormal system (SONC) $\{|v_j\rangle\} \subset \mathcal{H}$, then it has the same value for *any* SONC and $\hat{A} \in \mathcal{T}(\mathcal{H})$; it can also be shown that the product of a bounded operator with a trace class operator is always in $\mathcal{T}(\mathcal{H})$. Another interesting quantity, when it is finite, is $\mathrm{Tr}\hat{A}^\dagger \hat{A}$: operators for which this is a finite number belong to the so-called Hilbert-Schmidt space, which is an Hilbert space with scalar product given by $\langle \hat{A}, \hat{B} \rangle = \mathrm{Tr}[\hat{A}^\dagger \hat{B}]$. Being an Hilbert space, the Hilbert-Schmidt space is self-dual, while for the trace-class operators we have the duality relation $\mathcal{T}'(\mathcal{H}) = B(\mathcal{H})$: the most general linear functional on trace-class operators is induced by an Hilbert-Schmidt product with some bounded operator.

Postulate 1.1.1: On quantum states

To each quantum system it is possible to associate a separable Hilbert space $\mathcal{H}$. A quantum state $\hat{\boldsymbol{\rho}}$ of the system is a positive semidefinite, trace-class linear operator on $\mathcal{H}$ with unit trace. The set of quantum states over $\mathcal{H}$ will be denoted by $\mathcal{S}(\mathcal{H})$:

$$\mathcal{S}(\mathcal{H}) \ := \ \{\hat{\boldsymbol{\rho}} \in \mathcal{T}(\mathcal{H}) \, | \hat{\boldsymbol{\rho}} \geq 0 \ \wedge \ \mathrm{Tr}[\hat{\boldsymbol{\rho}}] = 1\}$$

and it is a convex set: $\forall 0 \leq 1 \leq \lambda, \forall \hat{\boldsymbol{\rho}}_1, \hat{\boldsymbol{\rho}}_2 \in \mathcal{S}(\mathcal{H})$:

$$\lambda \hat{\boldsymbol{\rho}}_1 \ + \ (1 - \lambda) \hat{\boldsymbol{\rho}}_2 \ \in \ \mathcal{S}(\mathcal{H})$$

A state is said to be *pure* if it cannot be written as a nontrivial convex combination of other states.

A standard result characterizing pure states asserts that the following definitions are equivalent [6, 7]:

1. $\hat{\boldsymbol{\rho}}$ is pure
2. $\hat{\boldsymbol{\rho}}$ is a one-dimensional projector
3. $\mathrm{Tr}[\hat{\boldsymbol{\rho}}^2] = 1$

The number $0 \leq \mu := \mathrm{Tr}[\hat{\boldsymbol{\rho}}^2] \leq 1$ is called the *purity* of $\hat{\boldsymbol{\rho}}$.

[3]Completeness of normed vector spaces means that every Cauchy sequence is convergent. A complete normed vector space is also called a Banach space.

It is implicit in the operational interpretation that there should be a one-to-one correspondence between quantum states at the mathematical level and empirically distinguishable states of the system: that is, not only any state of the system can be represented by some $\hat{\boldsymbol{\rho}}$, but two distinct operators $\hat{\boldsymbol{\rho}}_1$ and $\hat{\boldsymbol{\rho}}_2$ describe physical states that could be discriminated, at least in principle, by some experiment. This is a significant advantage of using linear operators instead of vectors of $\mathcal{H}$ even to represent pure states, since vectors would require the additional definition of *rays* to become fully equivalent to physical states. *Preparing* a quantum state equates to being able to attach an operator $\hat{\boldsymbol{\rho}}$ to the state of the system: operationally, one would subject the system to multiple experimental protocols, post-selecting according to outcomes of measurements, in such a way that the final state reproduces faithfully the full statistics that can be derived from the operator $\hat{\boldsymbol{\rho}}$ at the theoretical level.

Much like any dynamical theory, quantum mechanics also has its dynamical laws. For isolated systems, no loss of information about the quantum state should occur during their evolution, meaning that pure states should map to pure states. Together with the inescapable request that the trace must be preserved, this implies the basic form of the evolution postulate [3, 4, 8]:

Postulate 1.1.2: On quantum evolution of isolated systems

An isolated quantum system that is described by a quantum state $\hat{\boldsymbol{\rho}}$ at a given time, will be described by another quantum state of the form $\hat{\mathrm{U}}\hat{\boldsymbol{\rho}}\hat{\mathrm{U}}^\dagger$ at any later time, where $\hat{\mathrm{U}}$ is a unitary operator generally dependent upon the elapsed time. In particular, its purity is constant.

It is generally the case that whenever the system is isolated, the collection of evolution operators $\hat{\mathrm{U}}_t$ at all times form a one-parameter continuous family inside the unitary group, labelled by the time t. Moreover, if no external drivings are operated on the system, this family constitutes an Abelian group with respect to the time parameter: $\hat{\mathrm{U}}_t\hat{\mathrm{U}}_{t'} = \hat{\mathrm{U}}_{t+t'}\ \forall t, t' \in \mathbb{R}$. In this case[4], the evolution law can be rewritten in differential form, bearing the name of *Von Neumann Evolution Equation* [3, 6, 7]:

$$i\hbar\frac{\partial\hat{\boldsymbol{\rho}}_t}{\partial t} = [\hat{\mathrm{H}}, \hat{\boldsymbol{\rho}}_t] \tag{1.1}$$

Here $\hat{\boldsymbol{\rho}}_t = \hat{\mathrm{U}}_t\hat{\boldsymbol{\rho}}\hat{\mathrm{U}}_t^\dagger$ and the symbol $[\hat{A}, \hat{B}] = \hat{A}\hat{B} - \hat{B}\hat{A}$ is the commutator, whereas $\hat{\mathrm{H}}$ is *the self-adjoint* operator corresponding to the additive family $\hat{\mathrm{U}}_t$ under Stone's Theorem on one-parameter unitary groups [3], according to $\hat{\mathrm{U}}_t = e^{-i\hat{\mathrm{H}}t/\hbar}$. The operator $\hat{\mathrm{H}}$ thus plays the role of the generator of time translations and it is called the *Hamiltonian*[5]. We recall that an operator is said to be self-adjoint if it is equal to its adjoint $\hat{\mathrm{H}} = \hat{\mathrm{H}}^\dagger$ *on its full domain*, which must be dense in $\mathcal{H}$. Crucially, this is different from the condition of Hermiticity, albeit they coincide in the finite dimensional case: after all, the entire construction of Hilbert spaces is an overkill for finite dimensional systems, as one can use the much simpler theory of finite-dimensional complex vector spaces. However,

[4] To be precise, the additional condition that the family $\hat{\mathrm{U}}_t$ is strongly continuous with respect to t, i.e. $\forall t_0 \in \mathbb{R}, \forall|\psi\rangle \in \mathcal{H} : \lim_{t\to t_0} \hat{\mathrm{U}}_t|\psi\rangle = \hat{\mathrm{U}}_{t_0}|\psi\rangle$ is required to ensure Stone's theorem and Von Neumann Equation. Differentiability with respect to t is a direct consequence.

[5] The main reason being that it plays the role of the energy operator and it allows to draw a parallel between Eq.(1.1) and the second of Hamilton's Equations of motion from classical mechanics.

in this thesis, we shall deal also with infinite-dimensional spaces that are necessary to describe the physics of the real world in a continuous spacetime, at least according to the most experimentally validated theory currently at our disposal, the quantum theory of fields. Despite this disclaimers, we will assume that every Hamiltonian we will deal with will be self-adjoint or at least essentially self-adjoint without proving it, but rather leveraging on very general theorems that apply in our standard cases (e.g. the Kato-Rellich Theorem, see [3]). Finally, it is worth mentioning that Eq.(1.1) reduces to the famed Schrödinger Equation when $\hat{\boldsymbol{\rho}}$ is pure and the vector notation for states is employed ($\hat{\boldsymbol{\rho}}_t = |\psi(t)\rangle\langle\psi(t)|$ with $|\psi(t)\rangle \in \mathcal{H}$):

$$i\hbar \frac{\partial}{\partial t}|\psi(t)\rangle \;=\; \hat{\mathrm{H}}|\psi(t)\rangle \tag{1.2}$$

For completeness, let us mention that when the Hamiltonian operator $\hat{\mathrm{H}}(t)$ has an explicit dependence on time, it is still possible to write a formal equation for the corresponding unitary evolution operator [3]:

$$\hat{\mathrm{U}}(t) \;=\; \mathrm{T}_{\leftarrow}\Big[\exp\big(-\frac{i}{\hbar}\int_{\tau=0}^{t}\hat{\mathrm{H}}(\tau)\mathrm{d}\tau\big)\Big] \tag{1.3}$$

where the notation $\mathrm{T}_{\leftarrow}[\bullet]$ indicates the *time ordering* of a string of time-labelled operator, i.e. the prescription of reordering the string such that operators labelled by smaller times should be put to the left. In practice, one almost never uses the formal definition of Eq.(1.3), but rather resorts to expansions such as the Dyson expansion or the Magnus expansion [3, 9, 10].

As a side note, the reduced Planck's constant $\hbar \simeq 1.05457 \times 10^{-34} J \cdot s$, playing the role of the *quantum of action* in quantum mechanics, will be treated as a conversion coefficient from time units to energy units, therefore we will put it equal to 1 by assuming appropriate units for time. An inherent ambiguity of a multiplicative factor will remain every time we encounter a product of the type $\hat{\mathrm{H}}t$, since one can scale t by some factor κ and $\hat{\mathrm{H}}$ by the inverse κ^{-1} leaving the product invariant: this ambiguity is irrelevant for our purposes, and it simply amounts to not having fixed an energy scale, since this is dependent upon the particular realisation of the abstract systems that we shall encounter from the quantum information perspective.

Up to this point, the indeterministic behaviour of quantum mechanics is preserved and, if we held true that the theory applies, at least in principle, at every scale up to our own, the contradiction with common experience is blatant. To overcome this limit and extract predictions for results of actual experiments from the theory, an additional postulate defining a quantum mechanical measurement is needed:

Postulate 1.1.3: On probabilities and the effect of measurement

Suppose that a measurement with a finite set of possible outcomes is performed on a quantum state $\hat{\boldsymbol{\rho}}$ of some quantum system. Then to each outcome "a" it corresponds a positive semidefinite operator $\hat{\Pi}_a$ such that the probability of obtaining that outcome upon measuring $\hat{\boldsymbol{\rho}}$ is:

$$p_a \;=\; \mathrm{Tr}[\hat{\Pi}_a \hat{\boldsymbol{\rho}}] \tag{1.4}$$

In particular, it must be that $\sum_a \hat{\Pi}_a = \mathbb{1}$ (thus $0 \leq \hat{\Pi}_a \leq \mathbb{1}$) and p_a is linear with respect to convex mixtures of quantum states. The operator $\hat{\Pi}_a$ is called an *effect*, whereas the collection of the effects defining a measurement is a *Positive Operator-Valued Measure* (POVM). If, moreover, the measurement is *non-destructive*, there will be operators $\hat{M}_a$ labelled by the same outcomes, possibly with multiplicity, and called *instruments* such that $\hat{\Pi}_a = \hat{M}_a^\dagger \hat{M}_a$ and the quantum state of the system after the measurement yielding the outcome a is:

$$\hat{\boldsymbol{\rho}}_a \;=\; \frac{1}{p_a} \hat{M}_a \hat{\boldsymbol{\rho}} \hat{M}_a^\dagger \tag{1.5}$$

Before discussing the mathematical aspects and generalisations of the measurement postulate, let us stress a pivotal point: Eq.(1.5) is *non-linear*, because one must re-normalise the state with the probability. Moreover, a lot of information about the original quantum state $\hat{\boldsymbol{\rho}}$ is generally lost when a specific outcome is selected by a measurement on it. At present, we *still* do not know how this can happen: we do not have a precise scale discriminating between an ordinary quantum interaction and a measurement (if it exists at all) and we do not know how a single outcome among all the possible ones is *realised* [11]; this problem, known as the *Measurement Problem*, has attracted a gigantic wealth of attention and efforts since the very early days of quantum mechanics, despite never resulting in any practical obstacle up to now because of the (still) very large gap between the scale of macroscopic instrument and the largest scale at which we attested quantum behaviour. A large number of ways out of this conceptual (and, sooner or later, also practical) issue have been put forward; just to mention a few, we can divide them into *interpretations* of quantum mechanics and *modifications* of the theory. Interpretations add context and phrasings to the postulates to try to talk away the measurement problem without modifying the theory: some examples are the Many-Worlds Interpretation [12, 13], Quantum Darwinism [14, 15, 16, 17], QBism [18], the Transactional Interpretation [19], Relational Quantum Mechanics [20] and Consistent Histories Approach [21]. The so-called *Copenhagen Interpretation* can be viewed as an acritical application of the postulates which is agnostic about the measurement problem. Modifications of quantum theory, instead, try to put forward new mechanisms, to be added to the postulates, that should explain how the collapse of a quantum state happens during a measurement, e.g. for spontaneous-collapse models, or how the indeterminacy of quantum mechanics would be only apparent, whereas (necessarily nonlocal) hidden variables govern the evolution of the state deterministically (e.g. the de Broglie - Bohm pilot wave theory in its modern versions [22, 23]). Of course, the topic is vast and complex, but for a modern, lucid point of view we recommend to start with the notions of ψ-ontic and ψ-epistemic interpretations (see [24, 25] and the related Pusey-Barrett-Rudolph theorem [26]).

The limitation of having a finite number of outcomes has been introduced here to limit the level of mathematical details, but it is not fundamental: we will later generalise the measurement postulate to numerable or even continuous outcomes with the help of abstract probability and measure theory. In either case, a special type of measurement is often considered, for which different outcomes are mutually exclusive, that is to say if the quantum state yields the outcome a and it is measured right afterwards, the outcome a will be realised with certainty and no other outcome will be possible. These are called Projection-Valued Measures (PVMs) because for them the operators $\hat{M}_a$ are *orthogonal* projectors (and consequently also the $\hat{\Pi}_a$). Notice that there can be instances of measurements whose effects are all projectors, but they are not orthogonal, as in the case of double-homodyne measurement that will be discussed in Section 2.7. A further subclass of PVMs are *maximally informative measurements*, whose projectors all have rank 1 and they are therefore associated with pure states; for these measurements, the state after the outcome a is found coincides with the projector itself and it is pure. Projection-valued measures are of particularly relevant also because of the Spectral Theorem, asserting that any self-adjoint operator $\hat{A}$ on an Hilbert space can be *resolved* in terms of a PVM, in the sense that there exist projectors $\hat{P}_a$ such that $\hat{A} = \int_a a\hat{P}_a \mathrm{d}a$, where the integral sign is symbolic for a generalised sum over continuous and discrete sets, forming the *spectrum* of $\hat{A}$ and the outcomes a are now real numbers. In light of this result, the self-adjoint operators are called *observables* because they define a PVM and they attach real values to the outcomes, allowing also to compute statistical quantities like the average $\langle \hat{A} \rangle_{\hat{\boldsymbol{\rho}}} = \mathrm{Tr}[\hat{\boldsymbol{\rho}}\hat{A}]$ and the variance $(\Delta \hat{A}^2)_{\hat{\boldsymbol{\rho}}} = \langle \hat{A}^2 \rangle_{\hat{\boldsymbol{\rho}}} - \langle \hat{A} \rangle_{\hat{\boldsymbol{\rho}}}^2$.

It is interesting to acknowledge that several important results of quantum information are already hidden in Eq.(1.5), for example the fact that we cannot determine an unknown quantum state by measuring it at a single-copy level, since the measurement will update the state in a way that is oblivious of all the other outcomes that were not realised. More precisely, a large number of copies of an unknown quantum state would be necessary to determine it: but either these copies are already given to us by the source of the unknown state, or we cannot make them starting from just one sample because of the no-cloning theorem [27].

The last postulate that we need to build our quantum engine concerns the description of multiple quantum systems. More generally, we need to specify how different degrees of freedom can be described in a encompassing framework that can also describe correlations and interactions between them.

Postulate 1.1.4: On combined quantum systems

If two degrees of freedom of a quantum system are described by the Hilbert spaces $\mathcal{H}_1$ and $\mathcal{H}_2$, the quantum state of the full system is an operator over their tensor product $\mathcal{H}_1 \otimes \mathcal{H}_2$. In particular, if the quantum states describing the two degrees of freedom are uncorrelated and specified by $\hat{\boldsymbol{\rho}}_1$ and $\hat{\boldsymbol{\rho}}_2$ respectively, the full quantum state is $\hat{\boldsymbol{\rho}}_1 \otimes \hat{\boldsymbol{\rho}}_2$. The same holds true when two different quantum systems are described jointly, e.g. for two distinguishable particles.

It has recently been argued that the Tensor Product Postulate is not actually a postulate because it can be derived from the others [28]. We will take the conservative approach of listing it with the others, while referring the interested reader to the mentioned

literature for further insights. The tensor product property, together with the existence of superpositions implied by the very structure of Hilbert spaces, gives rise to the rich phenomenology of quantum information, such as entanglement, violation of Bell's inequalities, quantum teleportation and enhanced quantum metrology to name just a few.

The possibility of compounding quantum systems through tensor products also elucidates some aspects of the previous postulates, that we shall discuss briefly in the following. Concerning the space of states' postulate, the tensor product guarantees that if $\hat{\boldsymbol{\rho}}$ is a mixed state on $\mathcal{H}$ there will exist an Hilbert space $\mathcal{H}_B$ and a pure state $|\psi\rangle \in \mathcal{H} \otimes \mathcal{H}_B$, called a *purification* of $\hat{\boldsymbol{\rho}}$, such that $\hat{\boldsymbol{\rho}} = \mathrm{Tr}_B[|\psi\rangle\langle\psi|]$, where $\mathrm{Tr}_B[\bullet]$ denotes the partial trace operation over $\mathcal{H}_B$; explicitly, given an orthonormal basis $\{|\varphi_j^B\rangle\}_{j=1}^{\dim B}$ of $\mathcal{H}_B$:

$$\mathrm{Tr}_B \mathrm{Tr}_B[|\psi\rangle\langle\psi|] \;=\; \sum_j \langle\varphi_j^B|\psi\rangle\langle\psi|\varphi_j^B\rangle \;\in\; \mathcal{S}(\mathcal{H}) \tag{1.6}$$

As for the evolution postulates, we can now consider quantum systems that are interacting with an environment and we can greatly generalise the set of linear maps defining quantum evolutions.

Postulate 1.1.5: On quantum evolutions for open quantum systems

The most general quantum evolution for a quantum system in a quantum state $\hat{\boldsymbol{\rho}}$ over the Hilbert space $\mathcal{H}$ is a completely positive (CP) linear map $\boldsymbol{\Phi}$:

$$\boldsymbol{\Phi} : \; \mathcal{S}(\mathcal{H} \;\rightarrow\; \mathcal{T}(\mathcal{H}) \tag{1.7}$$

In particular $\boldsymbol{\Phi}(\hat{\boldsymbol{\rho}})$ must be a positive-semidefinite, trace-class linear operator for any state $\hat{\boldsymbol{\rho}}$, $\mathrm{Tr}[\boldsymbol{\Phi}(\hat{\boldsymbol{\rho}})] \leq 1$ and given any other Hilbert space $\mathcal{H}_B$ of arbitrary dimension, with identity operator $\mathbb{1}_B$, also the map $\boldsymbol{\Phi} \otimes \mathbb{1}_B$ must preserve positivity of operators on $\mathcal{H} \otimes \mathcal{H}_B$. Moreover, either $\boldsymbol{\Phi}$ preserves the trace, or $\mathrm{Tr}[\boldsymbol{\Phi}(\hat{\boldsymbol{\rho}})] = \kappa \leq 1$ (it is *trace-nonincreasing*) and depends on $\hat{\boldsymbol{\rho}}$, so that the actual quantum state after the map is $\kappa^{-1}\boldsymbol{\Phi}(\hat{\boldsymbol{\rho}})$, which is non-linear in $\hat{\boldsymbol{\rho}}$. In this second case, the quantum map cannot be implemented deterministically and κ corresponds precisely to the probability of obtaining the desired output state.

Crucially, the positivity of a map is not sufficient to ensure the complete positivity: a typical counterexample is the partial transposition which, when acting on a subsystem of an entangled pure state, outputs an operator that is not positive semidefinite. Also, the remark about the impossibility of implementing in a deterministic way a map that is not trace preserving will become useful in later chapters; in particular, a non-trace preserving map can be seen as a result of a measurement followed by a post-selection over a subset of the possible outcomes. On the other hand, all completely positive and trace preserving (CPTP) maps can be seen as the result of the initial state interacting with another quantum system, representing its environment, and then tracing out (i.e. neglecting) the degrees of freedom of the latter. In formulae, if $\boldsymbol{\Phi}$ is CPTP and acts on $\hat{\boldsymbol{\rho}}$ defined on $\mathcal{H}$, there will exist an Hilbert space $\mathcal{H}_E$, a quantum state $\hat{\boldsymbol{\rho}}_E$ on it and $\hat{\mathrm{U}}$ unitary on $\mathcal{H} \otimes \mathcal{H}_E$ such that:

$$\boldsymbol{\Phi}(\hat{\boldsymbol{\rho}}) \;=\; \mathrm{Tr}_E\left[\hat{\mathrm{U}}(\hat{\boldsymbol{\rho}} \otimes \hat{\boldsymbol{\rho}}_E)\hat{\mathrm{U}}^\dagger\right] \tag{1.8}$$

and, vice versa, any procedure of this type induces a CPTP map on $\mathcal{H}$, where Tr_E is the partial trace over the environment's degrees of freedom. It is of utmost importance that the input state and the environment state are factorized at the beginning, otherwise the resulting map may not be CP. One might object that any initial entanglement between the input state and its environment should be attributed to some previous interaction, but either this interaction is specified and added to the map to get a CP evolution, or it would be unclear how one could change the input state at will while specifying in a non-ambiguous way the initial correlated state that should define the map.

There is yet another way to represent CP maps, which invokes Kraus Theorem [6, 7, 29] and suggests useful analogies with measurement operations. The theorem is the following:

Theorem 1.1.1: Kraus (1971)

Let $\mathcal{H}$ be an Hilbert space, $\mathcal{S}(\mathcal{H})$ its set of quantum states, $\mathcal{T}(\mathcal{H})$ the set of positive semidefinite trace-class operators ($\mathcal{S} \subset \mathcal{T}$) and $\mathbf{\Phi} : \mathcal{S}(\mathcal{H}) \to \mathcal{T}(\mathcal{H})$ a linear map. The following statements are equivalent:

(**K1**) The map $\mathbf{\Phi}$ is completely positive and trace-nonincreasing ($\mathrm{Tr}[\mathbf{\Phi}(\hat{\boldsymbol{\rho}})] \leq 1$)

(**K2**) The map $\mathbf{\Phi}$ can be written in Kraus form (or Operator Sum Representation):

$$\mathbf{\Phi}(\hat{\boldsymbol{\rho}}) = \sum_j \hat{K}_j \hat{\boldsymbol{\rho}} \hat{K}_j^\dagger \tag{1.9}$$

where $\hat{\boldsymbol{\rho}} \in \mathcal{T}(\mathcal{H})$, the sum is over a countable set and weakly convergent and $\sum_j \hat{K}_j^\dagger \hat{K}_j \leq \mathbb{1}$ (equality holds for CPTP maps).

Kraus operators are clearly reminiscent of the measurement operators that define a POVM: indeed, by definition, the operators $\hat{\Pi}_j = \hat{K}_j^\dagger \hat{K}_j$ define a POVM if they sum to $\mathbb{1}$, or part of it if their sum is smaller (as a positive operator). In the former case, we have a CPTP map that can be realised by performing a POVM measurement on the quantum state and disregarding the outcome, while in the latter case we are post-selecting over a subset of the possible outcomes and the map is not trace-preserving anymore. At the level of nomenclature, CP trace-nonincreasing linear maps are called *quantum operations*, whereas CPTP linear maps are termed *quantum channels*. These concepts can be generalised to cases in which the target Hilbert space is different from the starting one: in that case, the Kraus operators also link the corresponding Hilbert spaces and the unitary in Eq.(1.8) will be replaced by an isometry.

A similar result, due to the Soviet mathematician Mark A. Naimark, exists also for POVMs, essentially guaranteeing that they can always be achieved by letting the quantum system unitarily interact with another one, which is later measured projectively [6, 7, 29].

Theorem 1.1.2: Naimark's Dilation Theorem

Let $\{\hat{\Pi}_a\}_{a\in I}$ be a POVM with set of outcomes I on an Hilbert space $\mathcal{H}$. There exists an Hilbert space $\mathcal{H}_E$, a unitary operation $\hat{\mathrm{U}}$ on $\mathcal{H}\otimes\mathcal{H}_E$ and a projective measurement $\{\hat{P}_a\}_{a\in I'}$ on $\mathcal{H}_E$ such that:

$$\mathrm{Tr}_{\mathcal{H}}[\hat{\Pi}_a\hat{\boldsymbol{\rho}}] \;=\; \mathrm{Tr}_{\mathcal{H}\otimes\mathcal{H}_E}\left[\hat{P}_a\left(\hat{\mathrm{U}}\hat{\boldsymbol{\rho}}\otimes\hat{\boldsymbol{\rho}}_E^0\hat{\mathrm{U}}^\dagger\right)\right]$$

for some state $\hat{\boldsymbol{\rho}}_E^0\in\mathcal{S}(\mathcal{H}_E)$.

As a remark, we can invoke purifications and larger Hilbert spaces to choose $\hat{\boldsymbol{\rho}}_E^0$ to be a pure state. Moreover, any local unitary on $\mathcal{H}_E$ can be combined with $\hat{\mathrm{U}}$ without modifying the statement of the theorem; therefore, the state of the second system can be fixed to a specific pure state, $|\psi\rangle_E$, while only $\hat{\mathrm{U}}$ and $\hat{P}_a$ have to be tuned to reproduce the needed POVM. This constructions clearly reminds of the Von Neumann measurement scheme, in which the measurement apparatus (or at least its probe) is explicitly brought into the quantum description to let it interact unitarily with the system to be measured. Then, by virtue of the macroscopic nature of the apparatus and its internal properties, decoherence in the basis of the observable to be measured will occur and the state of the apparatus will collapse into a definite one, also causing the collapse of the system's state through the correlations established by the interaction.

As a final remark, all these results on POVMs and CP(TP) maps can be seen as consequences of the very general Stinespring's Dilation Theorem [7, 30], which we will not present in full form because it adds little to the exposition for our scopes.

1.2 Von Neumann Entropy, Fidelity and Relative Entropy

In this section we are going to overview some functionals of quantum states that are commonly employed in quantum information, starting with the Von Neumann Entropy. Given a probability distribution $\{p_j\}$, its entropy is defined to be $S(\{p_j\}) = -\sum_j p_j\log p_j$, where the sum is symbolic and it can be over discrete and/or continuous sets. Since, by the spectral theorem, one can associate a similar probability distribution to every quantum state $\hat{\boldsymbol{\rho}}\in\mathcal{S}(\mathcal{H})$, one can define the entropy of $\hat{\boldsymbol{\rho}}$ as [29]:

$$\hat{\boldsymbol{\rho}} := \sum_j p_j|\psi_j\rangle\langle\psi_j| \quad\Longrightarrow\quad S_{VN}(\hat{\boldsymbol{\rho}}) = -\mathrm{Tr}\left[\hat{\boldsymbol{\rho}}\log\hat{\boldsymbol{\rho}}\right] = -\sum_j p_j\log p_j \tag{1.10}$$

recalling that, for self-adjoint operators, $f(\hat{\boldsymbol{\rho}})$ is defined by diagonalizing $\hat{\boldsymbol{\rho}}$ and applying the function f to its eigenvalues[6]. The quantity $S_{VN}(\hat{\boldsymbol{\rho}})$ is the *Von Neumann Entropy* of the state, and it is zero if and only if the state is pure. Clearly, it is an alternative way to quantify the purity of a state, but it displays valuable properties that make it a prominent figure of merit in quantum information. To name the most relevant ones, it is concave

[6] A point which is not often emphasized is that positive semidefinite trace-class operators have purely discrete spectra.

with respect to convex combinations:

$$S_{VN}\left(\sum_j p_j \hat{\boldsymbol{\rho}}_j\right) \geq \sum_j p_j S_{VN}(\hat{\boldsymbol{\rho}}_j) \tag{1.11}$$

where $0 \leq p_j \leq 1$: in particular, it always decreases by taking mixtures of states. It is also *strongly subadditive* when considering tripartite systems, a result which is notoriously difficult to prove [29, 31]:

$$S_{VN}(\hat{\boldsymbol{\rho}}_{ABC}) + S_{VN}(\hat{\boldsymbol{\rho}}_B) \leq S_{VN}(\hat{\boldsymbol{\rho}}_{AB}) + S_{VN}(\hat{\boldsymbol{\rho}}_{BC}) \tag{1.12}$$

where $\hat{\boldsymbol{\rho}}_{ABC}$ is a generic state of the tripartite system, composed of subsystems A, B and C, and $\hat{\boldsymbol{\rho}}_B, \hat{\boldsymbol{\rho}}_{AB}, \hat{\boldsymbol{\rho}}_{BC}$ are the partial traces of $\hat{\boldsymbol{\rho}}_{ABC}$ with respect to AC, C and A, respectively. This implies, in particular, that it is subadditive $S_{VN}(\hat{\boldsymbol{\rho}}_{AB}) \leq S_{VN}(\hat{\boldsymbol{\rho}}_A) + S_{VN}(\hat{\boldsymbol{\rho}}_B)$, with equality holding if and only if $\hat{\boldsymbol{\rho}}_{AB} = \hat{\boldsymbol{\rho}}_A \otimes \hat{\boldsymbol{\rho}}_B$. Then, the difference:

$$\mathscr{J}\left[\hat{\boldsymbol{\rho}}_{AB}\right] := S_{VN}(\hat{\boldsymbol{\rho}}_A) + S_{VN}(\hat{\boldsymbol{\rho}}_B) - S_{VN}(\hat{\boldsymbol{\rho}}_{AB}) \tag{1.13}$$

which is called the *quantum mutual information*, intuitively quantifies by how much the bipartite state $\hat{\boldsymbol{\rho}}_{AB}$ fails to be a factorized states: in other words, it is a measure of the overall correlations between the two subsystems.

A second figure of merit that we shall introduce comes about when we try to quantify the *distance* of two quantum states. If the states are pure, let them be $|\psi\rangle$ and $|\phi\rangle$, it can be shown that any meaningful notion of distance between them is monotone and decreasing with their (squared) overlap $|\langle\psi|\phi\rangle|^2$, which is always between 0 and 1 for normalized states. Among the most commonly employed distances for pure states, we recall the *quantum angle* $\theta_{\psi,\phi}$ implicitly defined as:

$$\cos^2\theta_{\psi,\phi} = |\langle\psi|\phi\rangle|^2 \tag{1.14}$$

For qubits parametrized by the Bloch vector [29], the quantum angle coincides with the distance induced by the Fubini-Study metric [32].

The situation is remarkably different for mixed states, where two different quantities are often considered: the fidelity and the trace distance. The fidelity is defined[7] for any two quantum states $\hat{\boldsymbol{\rho}}$ and $\hat{\boldsymbol{\sigma}}$ on the same Hilbert space as [7, 29]:

$$\mathcal{F}\left[\hat{\boldsymbol{\rho}}, \hat{\boldsymbol{\sigma}}\right] := \left(\mathrm{Tr}\left[\sqrt{\sqrt{\hat{\boldsymbol{\rho}}}\hat{\boldsymbol{\sigma}}\sqrt{\hat{\boldsymbol{\rho}}}}\right]\right)^2 = \left\|\sqrt{\hat{\boldsymbol{\rho}}}\sqrt{\hat{\boldsymbol{\sigma}}}\right\|_1^2 \tag{1.15}$$

where again $\|\bullet\|_1$ denotes the trace norm. It is the direct generalization of the overlap, to which it is fully equivalent when $\hat{\boldsymbol{\rho}}$ and $\hat{\boldsymbol{\sigma}}$ are pure. In fact, we have the following more general result [33, 34]:

Theorem 1.2.1: Uhlmann's Theorem

Given two quantum states $\hat{\boldsymbol{\rho}}$ and $\hat{\boldsymbol{\sigma}}$ on the same Hilbert space $\mathcal{H}$ and let $|\psi_{\hat{\boldsymbol{\rho}}}\rangle, |\psi_{\hat{\boldsymbol{\sigma}}}\rangle$ denote two generic purifications of them. Then the following result holds:

$$\mathcal{F}\left[\hat{\boldsymbol{\rho}}, \hat{\boldsymbol{\sigma}}\right] = \max_{|\psi_{\hat{\boldsymbol{\rho}}}\rangle, |\psi_{\hat{\boldsymbol{\sigma}}}\rangle} |\langle\psi_{\hat{\boldsymbol{\rho}}}|\psi_{\hat{\boldsymbol{\sigma}}}\rangle|^2 \tag{1.16}$$

[7] MInd that some authors do not square the trace in the definition

In particular, it is symmetric, bounded between 0 and 1 and it is constant under the *same* unitary operation applied to both states. It takes the value 1 if and only if the $\hat{\boldsymbol{\rho}}$ and $\hat{\boldsymbol{\sigma}}$ coincide as operators.

Since the fidelity is close to 1 when two states are *closeby* and it is 0 when they are maximally distinguishable, a proper definition of distance based on the fidelity is given by:

$$D_B\left[\hat{\boldsymbol{\rho}}, \hat{\boldsymbol{\sigma}}\right] := \sqrt{2\left(1 - \sqrt{\mathcal{F}[\hat{\boldsymbol{\rho}}, \hat{\boldsymbol{\sigma}}]}\right)} \tag{1.17}$$

and it is known under the name of *Bures distance* [35]. Notice that it takes values in $[0, \sqrt{2}]$, and it can be shown that it satisfies the triangle inequality. It is also *contractive*, in the sense that for any CPTP map $\boldsymbol{\Phi}$ [7, 29]:

$$D_B\left[\boldsymbol{\Phi}\left[\hat{\boldsymbol{\rho}}\right], \boldsymbol{\Phi}\left[\hat{\boldsymbol{\sigma}}\right]\right] \leq D_B\left[\hat{\boldsymbol{\rho}}, \hat{\boldsymbol{\sigma}}\right] \tag{1.18}$$

a property making it the ideal notion of distance for certain applications. Indeed, it matches with the intuitive notion that a spontaneous, dissipative process should not increase the distinguishability between two quantum states. Analogously, one can define the Bures angle D_A as a generalization of the quantum angle:

$$D_A\left[\hat{\boldsymbol{\rho}}, \hat{\boldsymbol{\sigma}}\right] := \arccos\left(\sqrt{\mathcal{F}\left[\hat{\boldsymbol{\rho}}, \hat{\boldsymbol{\sigma}}\right]}\right) \tag{1.19}$$

Another commonly adopted notion of distance for mixed states is the *trace distance* [7, 29]:

$$\mathcal{T}\left[\hat{\boldsymbol{\rho}}, \hat{\boldsymbol{\sigma}}\right] = \frac{1}{2}\|\hat{\boldsymbol{\rho}} - \hat{\boldsymbol{\sigma}}\|_1 \tag{1.20}$$

It shares some common properties with the Bures distance, namely that it is symmetric, bounded between 0 and 1, invariant under unitary operations and contractive under CPTP maps and it obeys the triangle inequality, thereby defining a metric on the space of quantum states. It is bounded by the fideliy as follows:

$$1 - \sqrt{\mathcal{F}\left[\hat{\boldsymbol{\rho}}, \hat{\boldsymbol{\sigma}}\right]} \leq \mathcal{T}\left[\hat{\boldsymbol{\rho}}, \hat{\boldsymbol{\sigma}}\right] \leq \sqrt{1 - \mathcal{F}\left[\hat{\boldsymbol{\rho}}, \hat{\boldsymbol{\sigma}}\right]} \tag{1.21}$$

where the upper bound is saturated when both $\hat{\boldsymbol{\rho}}$ and $\hat{\boldsymbol{\sigma}}$ are pure.

One last quantity that we shall introduce is the *quantum relative entropy*. It can be seen as a quantum version of the *Kullback-Leibler divergence*, which is a measure of statistical distance between two probability distributions $\{p_n\}_{n\in\mathscr{X}}$ and $\{q_n\}_{n\in\mathscr{X}}$ with discrete or continuous sample space $\mathscr{X}$, defined by:

$$D_{KL}(\{p_n\}, \{q_n\}) = \sum_{n\in\mathscr{X}} p_n \log\left(\frac{p_n}{q_n}\right) \tag{1.22}$$

and it represents how well a theoretical distribution $\{q_n\}$ fits the information content of the probability distribution $\{p_n\}$ describing a dataset. It can be shown, using Jensen's inequality, that it is always nonnegative and it is 0 if and only if the two probability distributions coincide.

The *quantum relative entropy* between a quantum state $\hat{\boldsymbol{\rho}}$ and another quantum state $\hat{\boldsymbol{\sigma}}$ is defined as:

$$S\left(\hat{\boldsymbol{\rho}}\|\hat{\boldsymbol{\sigma}}\right) \;:=\; \mathrm{Tr}[\hat{\boldsymbol{\rho}}\log\hat{\boldsymbol{\sigma}}] - S_{VN}(\hat{\boldsymbol{\rho}}) \;=\; \mathrm{Tr}[\hat{\boldsymbol{\rho}}(\log\hat{\boldsymbol{\sigma}} - \log\hat{\boldsymbol{\rho}})] \tag{1.23}$$

It is also positive, by Klein's Inequality [7, 29], it is contractive and it is 0 if and only if the quantum states coincide. However, it is *not* symmetric. Notice also that if $\hat{\boldsymbol{\rho}}$ has a support which is not contained in that of $\hat{\boldsymbol{\sigma}}$, the quantum relative entropy of $\hat{\boldsymbol{\rho}}$ with respect to $\hat{\boldsymbol{\sigma}}$ will diverge.

1.3 GKSL Master Equation and Markovian dynamics

While CPTP maps are fully sufficient to describe the transformation of a quantum system as an input-output process, it is often also useful to represent the full dynamical evolution. We would then consider a 1-parameter continuous family of CPTP maps $\boldsymbol{\Phi}(t,0)$, parametrized by time t, such that [36, 37]:

$$\hat{\boldsymbol{\rho}}(t) \;=\; \boldsymbol{\Phi}(t,0)\left[\hat{\boldsymbol{\rho}}(0)\right] \tag{1.24}$$

Without further assumptions, no general characterization of such maps is known at present. Under the sole assumption that the maps are invertible, one can split $\boldsymbol{\Phi}(t,0) = \boldsymbol{\Phi}(t,s)\boldsymbol{\Phi}(s,0)$, since the continuity in t implies that we can stop the evolution at different, arbitrary times. However, in general, there is no guarantee that $\boldsymbol{\Phi}(t,s)$ is still completely positive, as it could be that *only the full map*, starting from time 0, is CPTP. If $\boldsymbol{\Phi}(t,s)$ is a positive (resp. completely positive) map $\forall 0 < s < t$ the dynamical map is called *P-divisible* (resp. *CP-divisible*). With the only innocent assumption tat $\boldsymbol{\Phi}(t,0)$ is invertible $\forall t > 0$, one can already deduce that the corresponding evolution can be written in a time-local form as [36, 38]:

$$\frac{d}{dt}\hat{\boldsymbol{\rho}}(t) \;=\; -i\left[\hat{\mathrm{H}}(t),\hat{\boldsymbol{\rho}}\right] \;+\; \sum_j \gamma_j(t)\left[\hat{\mathrm{A}}_j(t)\hat{\boldsymbol{\rho}}(t)\hat{\mathrm{A}}_j^\dagger(t) - \frac{1}{2}\left\{\hat{\mathrm{A}}_j^\dagger(t)\hat{\mathrm{A}}_j(t),\hat{\boldsymbol{\rho}}(t)\right\}\right] \tag{1.25}$$

where $\hat{\mathrm{H}}(t)$ is a time-dependent Hamiltonian operator and $\hat{\mathrm{A}}_j(t)$ are generic. Such equations describing the rate of change of $\hat{\boldsymbol{\rho}}$ at time t as a superoperator acting on $\hat{\boldsymbol{\rho}}(t)$ are often termed *master equations*.

If we do not assume divisibility to begin with (i.e. that $\boldsymbol{\Phi}(t,0)$ is invertible $\forall t > 0$), it is still an open problem to formulate fully general conditions under which the dynamics generated by Eq.(1.25) is CP-divisible. If the dynamical map satisfies a *semigroup property*:

$$\forall t,t' \in \mathbb{R}^+ : \quad \boldsymbol{\Phi}(t',0)\boldsymbol{\Phi}(t,0) \;=\; \boldsymbol{\Phi}(t+t',0) \tag{1.26}$$

then the Gorini-Kossakowski-Sudarshan-Lindblad (GKSL) Theorem [36, 38, 39, 40] implies that the Hamiltonian generator $\hat{\mathrm{H}}$, all the operators $\hat{\mathrm{A}}_j$ and all the rates γ_j must be time-independent; moreover, the associated dynamical map is CP-divisible if and only if all the rates are positive, $\gamma_j > 0$. If this is the case, Eq.(1.25) is said to be in the *Lindblad form* and there will be a superoperator $\mathcal{L}$, the Lindbladian:

$$\mathcal{L}\left[\bullet\right] \;=\; -i[\hat{\mathrm{H}},\bullet] \;+\; \sum_j \gamma_j\left[\hat{\mathrm{A}}_j \bullet \hat{\mathrm{A}}_j^\dagger - \frac{1}{2}\left\{\hat{\mathrm{A}}_j^\dagger\hat{\mathrm{A}}_j,\bullet\right\}\right] \tag{1.27}$$

such that the CP-divisible dynamical map satisfying the semigroup property is given by:

$$\mathbf{\Phi}(t) \;=\; e^{\mathcal{L}t} \tag{1.28}$$

On the other hand, if we assume divisibility but not the semigroup property, a generalization of the GKSL Theorem [36, 37, 38] implies that Eq.(1.25) is CP-divisible if and only if all the time-dependent rates $\gamma_j(t) \geq 0$ are non-negative at all times.

The semigroup structure together with the CP-divisibility, leading to the Lindblad form of the master equation also imply a very relevant property: the evolution of a state from a certain time onward just depends upon the state at that given time, and *not* upon the previous evolution of the state. In layman terms, the evolution is *memoryless*. This is the famous *Markovian property*, whose name descends from the corresponding notion in the theory of stochastic processes and Markov chains [41]. As a general definition, to which we shall refer in the following, an invertible dynamical map $\mathbf{\Phi}(t)$ is Markovian if it is P-divisible and non-Markovian otherwise; if the starting point is Eq.(1.25), then one usually demands directly CP-divisibility to define Markovian maps, amounting to $\gamma_j(t) \geq 0 \; \forall t > 0, \forall j$.

1.3.1 On the microscopic derivations of the master equation

Having introduced the dynamical maps from a purely mathematical viewpoint, it is now appropriate to provide a few minimal notions about their physical origins in the context of open quantum systems. The starting point is again Eq.(1.8), but this time we consider a generic, time-dependent one-parameter family of unitary transformations $\hat{\mathrm{U}}(t)$ coupling the environment with the system of interest. In the most elementary case, we can assume that $\hat{\mathrm{U}}(t)$ is generated by a time-independent Hamiltonian $\hat{\mathrm{H}} = \hat{\mathrm{H}}_S \otimes \mathbb{1}_E + \hat{\mathrm{H}}_{SE}$ where $\hat{\mathrm{H}}_S$ describes the unitary dynamics of the system alone and $\hat{\mathrm{H}}_{SE}$ contains the interactions between the system and its environment and also the dynamics of the environment itself. Going from Eq.(1.8) and $\hat{\mathrm{H}}$ to a master equation in Lindblad form requires a series of standard, yet subtle and questionable assumptions that we shall not spell out in details, but that can be found in classic textbooks with various degrees of rigorousness [6, 9, 36]. Among these assumptions, one has to assume that the time scale during which the environment relaxes back to its equilibrium state, dissipating any perturbation deriving from the interaction with the system, is far shorter than the time scale characterizing the system's evolution itself: this implies that any information about the system leaking into the environment is effectively lost and it will not cause any back-action on the system itself at later times. In a nutshell, it is the physical origin of the Markovian property. Nevertheless, this is *not* a universally valid property, and many interactions do *not* lead to a Markovian dynamics, or not even to a P-divisible mathematical map.

1.3.2 On non-Markovian dynamical maps and their characterization

The hallmark of non-Markovian dynamics is a departure from the standard dissipative character of Lindblad-type evolutions, leading to a constant loss of information into the environment. In non-Markovian evolutions, indeed, this information exchange is not necessarily monotonic in time, and it is possible for some systems to recover previously lost information, at least temporarily. The corresponding backflow of information attracted large attention in recent years [42, 43, 44, 45] due to its potential applications to

fight decoherence in quantum information science, of which entanglement recovery and revivals [46, 47, 48] and quantum reservoir engineering [45, 49] are prominent examples.

A variety of methods have been devised for the detection and quantification of non-Markovianity [50, 51, 52, 53, 54, 55, 56, 57]. One type of approach, including the BLP, RHP and LFS measures, named after the authors, is based on the contractive property of the trace-distance and related quantities under CPTP maps [53, 55, 56, 57]: if a given contractive measure of distance between two suitably chosen initial states is found to behave non-monotonically in time under a dynamical map, then the dynamics must be non-Markovian in the sense of not being CPTP divisible. Notice that the *full* dynamical map is always CPTP, therefore the distance between any two states at any time t is necessarily smaller than their distance at time 0. However it is possible that, for intermediate times $t' < t$, the distance at time t' is larger than that at time t, since some information about the original states has been recovered during the non-Markovian evolution. Another class of techniques developed to witness quantum non-Markovianity relies upon the effects of non-Markovian dynamics on quantum correlations and coherence [58, 59, 60, 61, 62]. The underlying idea is similar to distance-based measures: if we start from a bipartite system presenting certain quantum correlations, a purely dissipative process will only spoil them; if, on the other hand, we observe a momentary rise of quantum correlations after a certain time, some non-Markovian dynamics must be at play. In Section 3.4 we will see a direct application of a specific correlation, quantum steering, to the detection of non-Markovianity.

1.4 Additional results on the necessity of the postulates

The minimality and partial uniqueness of the postulates of quantum mechanics relies, in addition to an overwhelming amount of experimental tests that confirmed the theory at least up to macro-molecular scales, on several theorems that strongly limit alternative theories aimed at explaining the same phenomenology. The first result that we should mention is due to A. M. Gleason [63] and essentially establishes the necessity of Born's rule:

Theorem: Gleason's Theorem (1957)

If the dimension of the underlying Hilbert space $\mathcal{H}$ is greater or equal to 3, any map $v_{\hat{\rho}}$ satisfying the following assumptions:

(P1) To each projector $\hat{P} \in \mathcal{B}(\mathcal{H})$ a probability $v_{\hat{\rho}}(\hat{P})$ is associated:

$$0 \leq v_{\hat{\rho}}(\hat{P}) \leq 1\,, \quad v_{\hat{\rho}}(\hat{P}_1 + \hat{P}_2) = v_{\hat{\rho}}(\hat{P}_1) + v_{\hat{\rho}}(\hat{P}_2)$$

where $\hat{P}_1$ and $\hat{P}_2$ are generic mutually orthogonal projectors

(P2) $v_{\hat{\rho}}(\mathbb{1}) = 1$

can be represented as:

$$v_{\hat{\rho}}(\hat{P}) \;=\; \mathrm{Tr}[\hat{\rho}\hat{P}]$$

for some positive semidefinite, trace-class linear operator $\hat{\rho}$ on $\mathcal{H}$.

By requesting these properties only on the lattice of projectors, Gleason's theorem is

very powerful, and traditionally hard to prove. If a more stringent condition is imposed, namely that property (**P1**) is valid for all *effects*[8], together with linearity with respect to their convex linear combinations, a much simpler proof can be achieved [1].

The second result that we shall consider puts a stop to the deterministic dream of finding an hidden variable theory satisfying all the desirable assumptions of local realism. Among these assumptions, J. S. Bell (1966) and Simon B. Kochen jointly with E. Specker, confuted that of non-contextuality [64]: a measurement-non-contextual theory would describe a given projective measurement in the same way irrespective of other measurements with which it is considered to form a PVM. In other words, every measurement should be entirely specified by the probabilities that it associates with all the states and must *not* depend on its *context*. Relinquishing this condition leads to theories that are much less appealing for a realist, as they would represent with different mathematical objects physical operations that are empirically indistinguishable. The Kochen-Specker theorem [65] asserts that any hidden variable theory aiming at predicting all the results of quantum mechanics cannot be measurement-non-contextual:

Theorem: Kochen-Specker Theorem (1967)

If the dimension of the underlying Hilbert space $\mathcal{H}$ is greater or equal to 3, there will be a state and a set of measurements such that any attempt to assign definite values to the results of these measurement on the given state would require contextuality of the measurement operators.

On the same line is the revered theorem by John Stewart Bell (1928-1990), which has to do with the notion of locality. A local probabilistic theory is one in which the *statistics* of experiments performed at one place cannot be influenced by any other (classical or quantum mechanical) process that happened outside his past light-cone. It is important to stress that this does not imply the local behaviour of all the entities in the theory: for example, in the Copenhagen interpretation the wavefunction of an entangled state is *instantaneously* updated *everywhere* when just one of the parties is measured, but this does not result in a change in the local statistics. Only the *correlations* between measurements results can unveil these underlying description. On the other hand, if we also assume that the results of experiments are pre-determined by local hidden variables, Bell's result applies [66, 67, 68, 69]

Theorem 1.4.1: Bell's theorem

No local, non-superdeterministic hidden variables theory can reproduce all the possible correlations predicted by quantum mechanics

The proof of Bell's theorem relies on the construction of an inequality which is obeyed by all local hidden variables theories, but explicitly violated in appropriate quantum mechanical scenarios. In its recent and most adopted formulation, the Clauser-Horne-Shimony-Holt Inequality is used, involving two correlated parties each of which can operate two, non-orthogonal projective measurement on her side. Crucially, this inequality can be experimentally falsified *without relying on quantum theory*[9], allowing us to say that,

[8] We recall that effects are simply positive semidefinite operators that are upper bounded by $\mathbb{1}$

[9] Of course, quantum mechanics is used to envision the experiments, but then only the correlations matter, and they could have resulted from any other theory.

to the best of our knowledge, *local realism is not an universal law of physics*[10] [70, 71].

Despite the strong level of correlations unveiled by the violation of Bell's inequalities, the *No-Signaling Theorem* [72, 73, 74, 75] guarantees that *causality* is still preserved in quantum theory: given two distant agents sharing any arbitrarily correlated quantum state, there is no way for one of them to *instantaneously* influence the expectation values or the moments of any measurement performed by the other agent: no information can be instantaneously transmitted through quantum correlations. One can then ask if the non-local correlations displayed by quantum mechanics are the most general ones respecting special relativity and the notion of causality; the answer is surprisingly negative [76] and the study of non-local correlations beyond quantum mechanics is now an active area of research. It should be noted, however, that quantum mechanics is a fairly *rigid* and *self-sustaining* theoretical frame in this respect: most attempts to go beyond it have been shown to also predict peculiar phenomena or blatant violations of other predictions, such as the no-cloning theorem [76].

To conclude this section, let us mention a very recent result concerning the necessity of complex numbers in quantum mechanics. The actual need of complex numbers has been disputed since their introduction, and indeed in theories such as classical electromagnetism their role is purely for mathematical convenience and nothing more: the same theory, generalised to include complex numbers, allow for a more intuitive treatment of time-dependent phases and interference phenomena. On the other hand, it is always possible to represent complex numbers in $\mathbb{R}^2$, without never invoking the i, at the cost of introducing a more involved real structure. The sensible question is therefore whether such a real theory, or *any* other real theory, can reproduce the same results of complex quantum mechanics without significantly changing its axiomatic framework. A no-go result has been proved in [77] and it is recalled here:

Theorem 1.4.2: On the necessity of complex numbers in quantum mechanics (2021)

Assuming all the postulates of quantum mechanics[a], no alternative version of quantum mechanics based on Hilbert spaces over real numbers is fully compatible with the predictions of standard quantum mechanics with complex numbers. In particular, at least three correlated quantum systems are needed to prove a disagreement.

[a] Here the tensor product postulate must really be taken as a postulate, because we cannot derive it if we do not assume that the Hilbert spaces are over the complex field.

The authors proposed an experimental scenario in which an inequality derived by real quantum mechanics would be violated according to the standard theory. The prediction was recently confirmed by experiments [78].

[10] Loopholes must be appropriately tackled to claim this. At present, superdeterminism is the only loophole that cannot be excluded.

1.5 A very short digression on quantum speed limits

Having reviewed some standard notions capturing the *distance* between quantum states and having determined that CPTP maps can never reduce any (acceptable) distance measure between two initial states, we can however ask how far a state can evolve from the starting one during a continuous evolution in time. The question is particularly meaningful and simple to study for pure states and unitary evolutions, since the latter bear intrinsic time scales determined by the energy scale of their Hamiltonian generators. The key concept in this respect is that of quantum speed limits [79, 80, 81, 82]. Consider two states $|a\rangle, |b\rangle$ on an Hilbert space $\mathcal{H} \sim \mathbb{C}^N$ that have the *same* average energy with respect to a time-independent Hamiltonian operator $\hat{\mathrm{H}}$ on $\mathcal{H}$ (otherwise, they cannot be connected by the unitary evolution generated by $\hat{\mathrm{H}}$. Then the *quantum speed limit* τ_{QSL} is a lower bound on the time needed for the unitary evolution $e^{-it\hat{\mathrm{H}}}$ to rotate $|a\rangle$ to $|b\rangle$, and it is provided by the following expression:

$$\tau_{QSL} := \max\left\{ \frac{\arccos|\langle b|a\rangle|}{\Delta\hat{\mathrm{H}}} \, , \, \frac{2(\arccos|\langle b|a\rangle|)^2}{\pi(\langle\hat{\mathrm{H}}\rangle - E_0)} \right\} \tag{1.29}$$

where $\Delta\hat{\mathrm{H}} = \sqrt{\langle\hat{\mathrm{H}}^2\rangle - \langle\hat{\mathrm{H}}\rangle^2}$ is the standard deviation of energy of the states ($|a\rangle$ or $|b\rangle$), $\langle\hat{\mathrm{H}}\rangle$ their average energy and E_0 is the ground state's energy. Notice that they are tightly linked to the quantum angle $\arccos|\langle b|a\rangle|$, which indeed quantifies the distance between the states.

1.6 Entanglement and other quantum correlations

As mentioned in the short discussion on Bell's theorem, quantum correlations mark one of the most incisive departs from classical logic. Here we will only concern ourselves with *bipartite* correlations: whatever the number of quantum systems involved, we always assume a bipartition in two subgroups and we only study correlations *between* subgroups. To introduce the subject, it is best to start with pure states, which will be represented here by vectors in $\mathcal{H}$ instead of projectors and they should be interpreted as representatives of the equivalence class defining a ray. Let us consider a pure quantum state $|\Psi\rangle$ on an Hilbert space obtained through a tensor product $\mathcal{H}_A \otimes \mathcal{H}_B$, such that A and B label distinct and individually addressable quantum subsystems. We say that $|\Psi\rangle$ is *entangled* if it *cannot* be written as $|\Psi\rangle = |\phi\rangle_A \otimes |\varphi\rangle_B$ for any $|\phi\rangle_A \in \mathcal{H}_A$, $|\varphi\rangle_B \in \mathcal{H}_B$, otherwise we call it *separable*. Let us define for convenience $\dim\mathcal{H}_A = d_A$, $\dim\mathcal{H}_B = d_B$ and $d = \min(d_A, d_B)$. By applying singular values decomposition, it can be shown that *any* state in $\mathcal{H}_A \otimes \mathcal{H}_B$ can be written as $|\Psi\rangle = \sum_{j=1}^{d} \lambda_j |v_j\rangle_A \otimes |w_j\rangle_B$, where $\{|v_j\rangle_A\}_{j=1}^{d_A}$ and $\{|w_j\rangle_B\}_{j=1}^{d_B}$ are orthonormal bases in $\mathcal{H}_A$ and $\mathcal{H}_B$ respectively[11]. The real numbers[12] λ_j are termed *Schmidt coefficients*, they do not depend upon any ambiguity in the decomposition and the number of nonzero coefficient is the *Schmidt number*. Therefore, a pure quantum state is *entangled* if and only if its Schmidt number is greater than zero. Given

[11] This is a much stronger decomposition compared with a generic decomposition in a factorized orthonormal basis because there is only one summing index. Notice that only d elements are needed in the decomposition. The basis for the Hilbert space of largest dimension can be orthonormally completed at will, without changing the decomposition.

[12] Any complex phase can be reabsorbed in a redefinition of the vectors in the bases

the Schmidt decomposition, it is easy to see that:

$$\hat{\boldsymbol{\rho}}_A := \mathrm{Tr}_B[|\Psi\rangle\langle\Psi|] = \sum_{j=1}^{d} \lambda_j^2 |\phi\rangle_{AA}\langle\phi| \,, \qquad \hat{\boldsymbol{\rho}}_B := \mathrm{Tr}_A[|\Psi\rangle\langle\Psi|] = \sum_{j=1}^{d} \lambda_j^2 |\phi\rangle_{BB}\langle\varphi|$$

Therefore $\mu_A = \mathrm{Tr}_A[\hat{\boldsymbol{\rho}}_A^2] = \sum_{j=1}^{d} \lambda_j^4 = \mu_B$: the partial traces have the same eigenvalues, thus the same purity, which is 1 if and only if the state is *separable*. Alternatively but equivalently, entanglement of pure states can also be quantified by the Von Neumann Entropy of the partial traces [7, 29].

As we have seen, a separable pure state is always *factorized*, meaning that it consists of a single tensor product between states of each subsystem. Clearly, factorized states cannot show any correlation whatsoever when subjected to joint local measurements on both sides, since the respective results and probability distributions factorize as well. To sum it up, the only type of correlation that a pure state can exhibit is entanglement. It is interesting to note that the necessity of mixed states is often invoked on the basis of entanglement: consider a bipartite, pure entangled state and focus on one part of it. Then it is impossible to associate a pure quantum state with it, since it would *instantaneously* change by measurements on the other party and, even more compellingly in the case of a Bell's state, no local measurement would yield a single value with certainty when performed on the part. If we assume *preparation noncontextuality*, then, we are led to describe it in the same way as we describe a *statistical ensemble of pure states*, since they are empirically indistinguishable. Notice, however, that there is a formal difference in the theory between the two scenarios: to one part of an unmeasured entangled state *no one* can associate a pure quantum state with certainty, while a statistical mixture of pure states simply represents the lack of knowledge of the observer, while someone who prepared the state could know exactly the pure state in which it is found.

The situation changes radically when mixed states are also involved [83]. Since a mixed state is a statistical ensemble of pure quantum states, it is to be expected that also classical correlations could appear in this case, and the important question of distinguishing them from *truly quantum correlations* arises. The key idea was put forward in its modern form by Reinhard F. Werner in his seminal paper [84]: according to his definition, a generic bipartite quantum state $\hat{\boldsymbol{\rho}}_{AB}$ for two subsystems A and B described by Hilbert spaces $\mathcal{H}_A$ and $\mathcal{H}_B$, respectively, is *entangled* if it *cannot* be written as:

$$\hat{\boldsymbol{\rho}}_{AB} = \sum_j p_j \hat{\boldsymbol{\rho}}_j^A \otimes \hat{\boldsymbol{\rho}}_j^B \tag{1.30}$$

with $0 \leq p_j \leq 1$, $\sum_j p_j = 1$ and $\hat{\boldsymbol{\rho}}_j^A \in \mathcal{S}(\mathcal{H}_A), \hat{\boldsymbol{\rho}}_j^B \in \mathcal{S}(\mathcal{H}_B)$, otherwise it is defined to be separable. Separable mixed states are not necessarily factorized and they can display classical correlations; what makes this decomposition nontrivial is the request that the $\{p_j\}$ form a probability distribution. From an operational point of view, this definition is motivated by the fact that entangled states defined in this way cannot be prepared starting from separable states and using just *local operations and classical communication* (LOCC): this is then the characteristic feature of quantum correlations, while all correlations that can be recreated using LOCCs are classical according to this definition. Clearly the purity of the partial traces is not an indicator of entanglement anymore, moreover, unlike pure states, entangled mixed states do not necessarily violate any Bell's

inequality: in other words, although *all* separable states admit some local hidden variables model reproducing their correlations, this is also true for some entangled mixed states.

Finding a criterion that fully discriminates between separable and entangled mixed states is an arduous task. In general, this is done through the introduction of an *entanglement monotones* (or entanglement measures), a functional from the space of states $\mathcal{S}(\mathcal{H})$ to $[0, +\infty\}$ which is zero for every separable state, it is non-increasing under LOCCs and it is constant under local unitary operations [7, 29].

A prominent example of an entanglement measure is the *entanglement of formation* [85]: the idea is to generalise to mixed states the Von Neumann entropy of the partial traces, which is an entanglement measure on pure states, using a convex roof construction. In formulae:

$$E_f[\hat{\boldsymbol{\rho}}] \;:=\; \inf\left\{\sum_j p_j E_f[|\psi_j\rangle]\right\} \tag{1.31}$$

where $\hat{\boldsymbol{\rho}} = \sum_j p_j |\psi_j\rangle\langle\psi_j|$ is a convex decomposition of $\hat{\boldsymbol{\rho}}$ and the infimum is taken over all such decompositions, while $E_f[|\psi\rangle] := S_{VN}(\mathrm{Tr}_B[|\psi\rangle\langle\psi|])$, $|\psi\rangle \in \mathcal{H}_A \otimes \mathcal{H}_B$. Clearly $E_f[\hat{\boldsymbol{\rho}}] = 0$ if and only if $\hat{\boldsymbol{\rho}}$ is separable, it is invariant under local unitary evolutions and indeed it never increases under generic local quantum channels. However, it is not additive in the sense that the entanglement of formation of a pair of entangled states, taken as a whole quantum state, can be less than the sum of the entanglement of formation of each pair. However, the fact that one has to consider all possible convex decompositions is not very practical: after all, if this can be done efficiently, the definition of entanglement for mixed states could also be checked directly. This feature is shared by all measures of entanglement that are sufficiently general to apply in all dimensions and perfectly discriminate separable states from entangled states such as, e.g., the concurrence (see [86]).

1.6.1 Entanglement witnesses and PPT criterion

Due to the computational costs of computing the entanglement of formation and related perfectly discriminating measures, *entanglement witnesses* are often employed to certify entanglement. They rely on the fact that the set of separable states is a convex set, therefore ther will be tangent hyperplanes to it in the space of states such that all the states on one side of each of these planes must be entanglement, although not all the states on the other side are necessarily separable. A prototypical example are Bell's type inequalities: they define a linear condition on the state such that if the given quantity is greater than a certain threshold, the corresponding state must be entangled.

On a more general level, one can look for *entanglement criteria*, which do not have necessarily to be linear, but they still certify entanglement of a significant subset of states. The most commonly adopted is the Positive Partial Transpose (PPT) or Peres-Horodecki Criterion [83, 87], which leverages upon the fact that separable mixed states can be transposed at the level of one of the two parties and the resulting operator will still be a state:

$$\hat{\boldsymbol{\rho}} = \sum_j p_j \hat{\boldsymbol{\rho}}_j^A \otimes \hat{\boldsymbol{\rho}}_j^B \quad\Longrightarrow\quad \hat{\boldsymbol{\rho}}^{T_A} = \sum_j (\hat{\boldsymbol{\rho}}_j^A)^T \otimes \hat{\boldsymbol{\rho}}_j^B \in \mathcal{S}(\mathcal{H}_A \otimes \mathcal{H}_B) \tag{1.32}$$

where the apex T_A denotes partial transposition on subsystem A. However, if the state is entangled, this operation often results in a non-positive operator, which is also the

reason why the transpose operation is not a completely positive map. A measure of entanglement can be then defined as:

$$\mathcal{N}[\hat{\boldsymbol{\rho}}] \;:=\; \frac{\|\hat{\boldsymbol{\rho}}^{T_A}\|_1 - 1}{2} \tag{1.33}$$

which is called the *entanglement negativity*, or the related *logarithmic negativity*:

$$E_N[\hat{\boldsymbol{\rho}}] \;:=\; \log_2\|\hat{\boldsymbol{\rho}}^{T_A}\|_1 \;=\; \log_2\left(2\mathcal{N}[\hat{\boldsymbol{\rho}}]+1\right) \tag{1.34}$$

In both cases $\|\hat{X}\|_1 = \mathrm{Tr}\sqrt{\hat{X}^\dagger\hat{X}}$ is the *trace norm*, which is 1 if $\hat{X}$ is a valid quantum state. They are both *entanglement monotones*, meaning that they can only decrease under LOCCs and the logarithmic negativity is additive with respect to tensor products. The PPT criterion can fully discriminate entangled states when the subsystems have dimensions up to 3 and for some, but not all [88] Gaussian states [89].

Some entangled mixed states have the interesting property that, if a sufficiently large number of copies of them is available, appropriate LOCCs operations can be applied to produce Bell's entangled states from it, in a way that is compatible with the LOCCs Theorem (the total entanglement cannot increase). This type of entanglement is termed *distillable* and entangled states that are not distillable are *bound entangled*. An interesting property of the PPT criterion is that all the entangled states that are not detected by it are necessarily bound entangled, while it is still not known if the converse is also true.

1.6.2 Quantum Discord

We have seen that bipartite quantum states exhibiting nonlocal correlations are a strict subset of entangled states, also known as non-separable states. The question on whether non-separable states are the widest class of states exhibiting some form of *quantum* correlations is subtle and perhaps just a matter of interpretation: by their very definition, separable states can be prepared from factorized states via local operations and classical communications, hence they always admit a *local* description. However, this local description could still be necessarily quantum. To see this, let us consider two parties A and B and let us take two orthonormal bases $\{|j_A\rangle\}_{j=1}^{d_A}$ and $\{|k_B\rangle\}_{k=1}^{d_B}$ where d_A and d_B are the dimensions of the Hilbert spaces $\mathcal{H}_A$ and $\mathcal{H}_B$, respectively. We will say that a state $\hat{\boldsymbol{\rho}}_{AB}$ of the combined system is *classical-classical* if it can be decomposed in the following way [90]:

$$\hat{\boldsymbol{\rho}}_{AB}^{\mathrm{c/c}} \;=\; \sum_{j,k} p_{jk}^{AB}|j_A\rangle\langle j_A|\otimes|k_B\rangle\langle k_B| \tag{1.35}$$

where $0 \le p_{jk}^{AB} \le 1$ is a joint probability, for *some choice* of the respective orthonormal bases. Importantly, this is *not* the case for any separable state. Indeed, imagine to take a separable state whose density matrix has a non-degenerate spectrum, so that the decomposition of Eq.(1.30) is unique. Clearly, there is no a priori reason to demand that the density matrices $\{\hat{\boldsymbol{\rho}}_j^A\}$ are diagonal in the same orthonormal basis for different values of j, and similarly for $\{\hat{\boldsymbol{\rho}}_j^B\}$, so that the overall state will not be classical-classical, in general. Analogously, one can define classical-quantum states as those which can be decomposed as:

$$\hat{\boldsymbol{\rho}}_{AB}^{\mathrm{c/q}} \;=\; \sum_{j=1}^{d_A} p_j|j_A\rangle\langle j_A|\otimes\hat{\boldsymbol{\rho}}_j^B \tag{1.36}$$

and, in the opposite order, also quantum-classical states. Clearly, classical-classical states are a subset of both quantum-classical and classical-quantum states. The type of *asymmetric* quantum correlations exhibited by states that are *not* classical-classical go under the name of *quantum discord* [90, 91, 92] and, despite being weaker than the non-separability condition that defines entanglement, they can still be harnessed for certain tasks [93]. To characterize them, it is useful to consider the *quantum mutual information* of a bipartite state $\hat{\boldsymbol{\rho}}_{AB}$, defined as in Eq.(1.13), where $\hat{\boldsymbol{\rho}}_A = \mathrm{Tr}_B[\hat{\boldsymbol{\rho}}_{AB}]$ and $\hat{\boldsymbol{\rho}}_B = \mathrm{Tr}_A[\hat{\boldsymbol{\rho}}_{AB}]$. As we anticipated earlier, in intuitive terms the quantum mutual information captures the entirety of correlations in the composite state, both classical and quantum: the higher the local Von Neumann entropies and the lower the total entropy, the higher the total amount of correlations. In parallel, we also consider a scenario in which we do some projective measurement $\{\hat{\Pi}_A^a\}$ on subsystem A, with outcomes $\{a\}$, and we would like to quantify how much information we get about subsystem B from this procedure. This can be quantified by the following quantity:

$$\mathscr{J}_{\hat{\Pi}_A}[\hat{\boldsymbol{\rho}}_{AB}] = S_{VN}[\hat{\boldsymbol{\rho}}_B] - \sum_a p_a^A S_{VN}\left[\hat{\boldsymbol{\rho}}_{\hat{\Pi}_A}^{B|A=a}\right] \tag{1.37}$$

where:

$$p_a^A = \mathrm{Tr}_{AB}\left[(\hat{\Pi}_A^a \otimes \mathbb{1}_B)\hat{\boldsymbol{\rho}}_{AB}\right], \quad \hat{\boldsymbol{\rho}}_{\hat{\Pi}_A}^{B|A=a} = \frac{1}{p_a^A}\mathrm{Tr}_A\left[(\hat{\Pi}_A^a \otimes \mathbb{1}_B)\hat{\boldsymbol{\rho}}_{AB}\right] \tag{1.38}$$

If the subsystems are perfectly *classically* correlated in an orthonormal basis and we choose the optimal measurement on subsystem A, we will get the maximal amount of information about subsystem B and $\mathscr{J}_{\hat{\Pi}_A}[\hat{\boldsymbol{\rho}}_{AB}]$ will reach its maximal value. One can of course define the same quantity for projective measurements on subsystem B used to infer the state of subsystem A. The quantity $\mathscr{J}_{\hat{\Pi}_A}[\hat{\boldsymbol{\rho}}_{AB}]$ can be interpreted as the residual amount of correlations after the projective measurement on subsystem A, since one can show that:

$$\mathscr{I}\left[\sum_a (\hat{\Pi}_A^a \otimes \mathbb{1}_B)\hat{\boldsymbol{\rho}}_{AB}((\hat{\Pi}_A^a \otimes \mathbb{1}_B)\right] = \mathscr{J}_{\hat{\Pi}_A}[\hat{\boldsymbol{\rho}}_{AB}] \tag{1.39}$$

For classical-classical states, which are essentially classical probability distributions for two variables embedded in the quantum case, one has:

$$\mathscr{I}\left[\hat{\boldsymbol{\rho}}_{AB}^{\mathrm{c/c}}\right] = \max_{\{\hat{\Pi}_A\}} \mathscr{J}_{\hat{\Pi}_A}\left[\hat{\boldsymbol{\rho}}_{AB}^{\mathrm{c/c}}\right] = \max_{\{\hat{\Pi}_B\}} \mathscr{J}_{\hat{\Pi}_B}\left[\hat{\boldsymbol{\rho}}_{AB}^{\mathrm{c/c}}\right] \tag{1.40}$$

In words: the quantum mutual information of a classical-classical state coincides with the highest amount of information that can be extracted from any one of its two subsystems about the other one. If the state is *not* classical-quantum, however, the first inequality does not hold anymore: the maximal amount of information about B that subsystem A can extract with local measurements, $\max_{\{\hat{\Pi}_A\}} \mathscr{J}_{\hat{\Pi}_A}[\hat{\boldsymbol{\rho}}_{AB}]$, will be smaller than the total amount of correlations in the initial state, $\mathscr{I}[\hat{\boldsymbol{\rho}}_{AB}]$. Their difference is the *Quantum Discord* (QD) with respect to A:

$$\mathscr{Q}^A[\hat{\boldsymbol{\rho}}_{AB}] := \mathscr{I}[\hat{\boldsymbol{\rho}}_{AB}] - \max_{\{\hat{\Pi}_A\}} \mathscr{J}_{\hat{\Pi}_A}[\hat{\boldsymbol{\rho}}_{AB}] \tag{1.41}$$

where the maximization is taken over all projection-valued measurement. Similarly, if the state is *not* quantum-classical, the quantum discord with respect to B, $\mathscr{Q}^B[\hat{\boldsymbol{\rho}}_{AB}]$ will

be nonzero. The quantum discord completely captures this mismatch: $\mathscr{Q}^A = 0$ if and only if the state is classical-quantum, and similarly $\mathscr{Q}^B = 0$ if and only if it is quantum-classical, while if $\mathscr{Q}^A = \mathscr{Q}^B = 0$ the state must be classical-classical.

Separable states with positive quantum discord still exhibit some phenomena with no classical equivalents. For example, they cannot be *locally broadcasted* [94], i.e. their total correlations cannot be replicated on another bipartite system in an initially factorized state by just using local quantum channels and the original correlated state $\hat{\rho}_{AB}$. Other examples of properties exhibited by bipartite quantum states that are not classical-classical can be found, e.g., in [90, 92, 93, 95].

Part I

Continuous-variables Quantum Information

CHAPTER 2

A minimal introduction to continous-variable quantum information

In this Chapter we will present the fundamental concepts and main results underlying continuous-variable (CV) quantum information, whose applications range from quantum optics and the quantum description of the electromagnetic field, to quantum optomechanics, lattice models such as the Bose-Hubbard model and continuous-variable quantum computations, among others. The focus will be on key results to be referred to in the following chapters, rather than on derivations. After quantizing the electromagnetic field, we will introduce the phase-space methods that revolutionised the study of quantum optics almost five decades ago and we will describe in some detail Gaussian states and Gaussian operations. A final section will be devoted to non-Gaussian states, whose experimental preparation and manipulation is rapidly developing in recent years, mainly driven by their necessity to unlock the full power of CV quantum information. Our main references for quantum optics are the books *Quantum Optics* by Girish S. Agarwal [96] and the *Photons and Atoms: Introduction to Quantum Electrodynamics* by Claude Cohen-Tannoudji, Jacques Dupont-Roc and Gilbert Grynberg [97]. A shorter, practical overview can be found in [98]. Concerning CV quantum information and Gaussian states, we refer to [99] and [100], while an updated review on non-Gaussian states can be found in [101].

2.1 Basic notions and the non-relativistic quantisation of the electromagnetic field

Continuous-variable quantum information studies systems that display continuous degrees of freedom in some way, i.e. they admit observables (in the sense of self-adjoint, but not necessarily bounded operators) whose spectra is purely continuous. For all practical purposes, this is equivalent to saying that their underlying (separable) Hilbert space is infinite-dimensional. Our primer for CV quantum information will be systems of particles in three dimensional space, but our target is the description of a finite collection of modes of a quantum field. With respect to the general principles of quantum mechanics, some entities will be specified in greater detail in this context. First of all, the Hilbert space will now be $\mathcal{L}^2(\mathbb{R}^n)$, the space of complex-valued square-integrable functions on

$\mathbb{R}^n$, modulo almost-everywhere equivalence, endowed the natural Hermitian product:

$$\forall f, g \in \mathcal{L}^2(\mathbb{R}^n) \; : \quad \langle f|g\rangle := \langle f, g\rangle := \int_{\mathbb{R}^n} f^*(\vec{x}) g(\vec{x}) \mathrm{d}^n x$$

Keeping in mind that the Fourier operator is an isometry of these spaces into themselves, one usually identifies a space of *wavefunctions in the position representation* and the Fourier dual as the space of *wavefunctions in the momentum representation*.

The multiplicative operators $\hat{q}_j, j = 1, ..., n$ acting as $\hat{q}_j \psi(\vec{\tilde{x}}) = \tilde{x}_j \psi(\vec{\tilde{x}})$ in the position representation are called *position operators*. They are Hermitian but unbounded, with a continuous spectrum and they can be collected in an ordered vector $\hat{\vec{q}}$. Analogously, the multiplicative operators $\hat{p}_j$ acting in the same way in the momentum representation are called *momentum operators* and, by virtue of the Fourier operator, they can be represented as $\hat{p}_j = -i\hbar \dfrac{\partial}{\partial q_j}$ on an appropriate domain in $\mathcal{L}^2(\mathbb{R}^n)$ in the position representation[1]. Taken together, $\hat{\vec{q}}$ and $\hat{\vec{p}}$ are called *canonical quadrature operators*. On infinitely differentiable functions on $\mathbb{R}^n$ with compact support we can then claim that they satisfy the *canonical commutation relations*:

$$[\hat{q}_j, \hat{p}_k] \; = \; i\delta_{jk} \, \mathbb{1} \tag{2.1}$$

This relation is often abstracted as *the canonical quantisation relation* upon which quantum theories on continuous spaces are built. A straightforward consequence of it is that the underlying Hilbert space must be infinite-dimensional, otherwise taking the trace on both sides of Eq.(2.1) would lead to a contradiction. Even more compelling is the following result [3]:

Theorem 2.1.1: Stone - Von Neumann Theorem (1930-32)

Any two irreducible representations of the canonical commutation relations are unitarily equivalent.

This justifies the approach of taking these commutation relations as part of a systematic procedure aimed at quantising classical theories. The main ideas behind this approach, termed *geometric quantisation*, is to build a Lie algebra isomorphism: a map from polynomials on classical phase space to polynomial operators in the quadratures in the Hilbert space that preserves the corresponding symplectic structures, i.e. it maps Poisson's brackets between phase-space functions to the corresponding commutators between operators. Obvious difficulties immediately arise, since the product of classical variables is commutative, whereas quantum operators are not, introducing a well-known order ambiguity. In fact, the difficulty with this approach is even more radical [102, 103]:

Theorem 2.1.2: Groenewold - Van Hove (1946, 1951)

There is no linear *quantization map* from polynomials in $(\vec{q}, \vec{p}) \in \mathbb{R}^{2n}$ to polynomials in the irreducibly-represented operators $(\hat{\vec{q}}, \hat{\vec{p}})$ on $\mathcal{L}^2(\mathbb{R}^n)$ that is a Lie algebra isomorphism between Poisson brackets and commutators while respecting the canonical commutation relations.

[1] Again, we shall omit $\hbar$ from now on, assuming dimensionless units for positions and momenta

Due to this major hindrance, canonical quantisation achieves its scopes through the so-called *deformation quantisation*, where the Poisson brackets are *deformed* by adding terms proportional to powers of $\hbar$ ([2]) in such a way that the resulting *Moyal brackets* become isomorphic to quantum commutators, the isomorphism being realised by Wigner-Weyl quantisation. We shall not delve into the details of this rich subject in mathematical physics because it will be mostly unnecessary for us, but we refer the interested reader to some classic expositions [104, 105, 106, 107]. It is very instructive to notice that the Groenewold - Van Hove theorem does not hold if one restricts the ring of polynomials to be quantised: in particular, polynomials up to second degree can be quantised in a way compatible with commutators and canonical relations, although the mapping is far from unique. This fact often goes unrecognised, but it is at the heart of the simplicity of Gaussian quantum information, as we shall see in later sections.

Going back to Eq.(2.1), it is sometimes convenient to adopt a more compact notation, calling $\hat{\mathbf{R}} = (\hat{q}_1, \hat{p}_1, ..., \hat{q}_n, \hat{p}_n)$ and rewriting:

$$\left[\hat{R}_j, \hat{R}_k\right] \;=\; i\Omega_{jk} \tag{2.2}$$

where $\Omega := \bigoplus_{j=1}^{n} \boldsymbol{\omega}_j$ and $\boldsymbol{\omega}_j$ is a 2×2 matrix acting on the subspace $(\hat{q}_j, \hat{p}_j)$ and equal to $i\sigma_2$, where σ_2 is the second Pauli matrix $\sigma_2 = \begin{pmatrix} 0 & -i \\ i & 0 \end{pmatrix}$. They are *symplectic forms* in $\mathbb{R}^{2n}$ and $\mathbb{R}^2$, respectively, in the sense that they give rise to a symplectic vector space and the subset of the general linear group $\mathrm{GL}(2n, \mathbb{R})$ which preserves Ω by congruence is called the *real symplectic group* $\mathrm{Sp}(2n, \mathbb{R})$. An identity operator has been left implicit on the right-hand side of Eq.(2.2), to avoid confusion with the involved matrices. It is sometimes convenient to use the language of creation and annihilation operators in place of $\vec{\hat{q}}$ and $\vec{\hat{p}}$ to generate the algebra of observables. These are defined as:

$$\hat{a}_k = \frac{\hat{q}_k + i\hat{p}_k}{2}\;, \quad \hat{a}_k^\dagger = \frac{\hat{q}_k - i\hat{p}_k}{\sqrt{2}} \tag{2.3}$$

and they satisfy a corresponding commutation relation:

$$[\hat{a}_j, \hat{a}_k^\dagger] \;=\; \delta_{jk} \tag{2.4}$$

Recalling the standard results from the study of the quantum harmonic oscillator, these commutation relations imply the existence of a *vacuum state* $|0\rangle$ which is annihilated by every $\hat{a}_j$. Subsequent applications of powers of $\hat{a}_j^\dagger$ on the vacuum generate orthogonal states which are numbered by the sequence of integer exponents of each creation operator, and these states span the Hilbert space $\mathcal{L}^2(\mathbb{R}^n)$; more precisely, they form a complete orthonormal system.

2.1.1 The Fock space of n modes

The framework we have outlined up to now is taylored for the quantum mechanical description of a single point particle in $\mathbb{R}^n$. However, with a clever change of perspective, we can use the same mathematical tools to describe a multi-particle theory of identical

[2] The constant $\hbar$ reappears here just as a control parameter: tuning it towards smaller values suppresses the corrections, making the quantum commutator vanish, which can be interpreted as a kind of classical limit.

particles, with underlying single-particle Hilbert space $\mathcal{H}$. In this thesis, we will mainly consider systems of identical, *indistinguishable* bosons; this amounts to demanding that any N-particle state in $\mathcal{H}^{\otimes N}$ must be fully symmetric under the exchange of any pairs of single-particle *wavefunctions*, leaving the labels of the particles fixed. To be more explicit, we define a symmetrizing operator $\hat{\mathcal{P}}_S^{(N)}$ on $\mathcal{H}^{\otimes N}$ via:

$$\hat{\mathcal{P}}_S^{(N)}\left[|\psi_1\rangle_1 \otimes |\psi_2\rangle_2 \otimes \cdots \otimes |\psi_N\rangle_N\right] \quad =: \quad |\psi\rangle \vee |\psi_2\rangle \vee \cdots \vee |\psi_N\rangle \tag{2.5}$$

$$|\psi_1\rangle \vee \ldots |\psi_j\rangle \vee \ldots |\psi_k\rangle \cdots \vee |\psi_N\rangle \quad = \quad |\psi_1\rangle \vee \ldots |\psi_k\rangle \vee \ldots |\psi_j\rangle \cdots \vee |\psi_N\rangle \tag{2.6}$$

$$\tag{2.7}$$

where the symmetrized tensor product $\vee$ is *defined* by the second equation. Notice that the particle-label j in $|\bullet\rangle_j$ disappears when we consider the symmetrized state, since it no longer makes sense talking about "particle j" in a set of N truly indistinguishable particles. By $\mathcal{H}^{\vee N}$ we will denote the fully-symmetrized subspace of $\mathcal{H}^{\otimes N}$. We can now associate with each single-particle state $|\psi\rangle$ a pair of creation and annihilation operators, $\hat{a}^\dagger(|\psi\rangle)$ and $\hat{a}(|\psi\rangle)$, satisfying the following commutation relations:

$$\left[\hat{a}(|\psi\rangle), \hat{a}^\dagger(|\varphi\rangle)\right] \quad = \quad \langle\psi|\varphi\rangle \tag{2.8}$$

and use them to build states in $\mathcal{H}^{\vee N}$ via:

$$\hat{a}^\dagger(|\psi_1\rangle)\ldots\hat{a}^\dagger(|\psi_N\rangle)\,|0\rangle\!\rangle \quad = \quad |\psi_1\rangle \vee \cdots \vee |\psi_N\rangle \tag{2.9}$$

where $|0\rangle\!\rangle$ is the *unique* state with zero particles in it. In general $\hat{a}^\dagger(|\psi\rangle)$ will act on a state in $\mathcal{H}^{\vee N}$ to produce a state in $\mathcal{H}^{\vee(N+1)}$. If we suppose that $\mathcal{H}$ is finite-dimensional, with $\dim\mathcal{H} = n$ and with an orthonormal basis $\{|\phi_j\rangle\}_{j=1}^n$, we can finally build a *Fock space* of n modes as [3]:

$$\mathcal{F}^{(n)}(\mathcal{H}) \quad = \quad \bigoplus_{N=0}^{\infty} \mathcal{H}^{\vee N} \tag{2.10}$$

such that any state $|\Psi\rangle\!\rangle \in \mathcal{F}^{(n)}$ can be written as:

$$|\Psi\rangle\!\rangle \quad = \quad \sum_{k_1,\ldots,k_n=1}^{\infty} c_{k_1,\ldots,c_{k_n}} \left(\hat{a}_1^\dagger\right)^{k_1} \ldots \left(\hat{a}_n^\dagger\right)^{k_n} |0\rangle\!\rangle \tag{2.11}$$

where $\hat{a}_j^\dagger \equiv \hat{a}^\dagger(|\phi_j\rangle)$ and $c_{k_1},\ldots,c_{k_n} \in \mathbb{C}$ with $\sum_{k_1,\ldots,k_n}|c_{k_1},\ldots,c_{k_n}|^2 = 1$. Hence, once an orthonormal basis of the single-particle space $\mathcal{H}$ has been fixed, the states in the Fock space can be represented by a collection of complex numbers $\{c_{k_1},\ldots,c_{k_n}\}$ and the corresponding single-particle states in that basis define the *normal modes*. The restriction to $\mathcal{H}$ being finite-dimensional is for purely mathematical reasons, but notice that now the term "continuous-variable" does not refer to single-particle states anymore, but rather to the fact that we can have an arbitrary number of particles and therefore there will be observables with continuous spectra.

As a side note, the notions of being identical and being indistinguishable are somewhat blurred, but they can be rigorously defined appealing to a comparison with classical physics: identical particles also exist classically, but we always suppose to be able to address them separately with labels, even if they cannot be distinguished by any *intrinsic* property. On the other hand, indistinguishable particles are usually considered to be

a purely quantum type of entities, since the classical description of a multi-particle systems *requires* the possibility to label them. In quantum mechanics, instead, particles that are identical from the point of view of all their intrinsic properties must also be *indistinguishable*: one way to see this is to imagine that we attach label to two identical quantum particles localized at different positions, using their spatial degrees of freedom to distinguish them. Once their wavefunctions spread and they come to overlap in space, we can no longer be sure about which particle is which and the distinguishability is lost.

2.1.2 The canonical quantization of the electromagnetic field

Up to this point, our description fits the spatial quantum degree of freedom of a particle in $\mathbb{R}^n$. However, continuous-variable quantum mechanics is also the right formalism to describe a finite collection of modes of quantum fields. Since quantum field theory at low energies is really needed only for massless fields, the major application that is of interest in quantum information is provided by the electromagnetic field. Moreover, we shall always assume that a laboratory frame is at place and no relativistic boost will be needed, so that we can limit ourselves to the machinery of non-relativistic field theory. In this context, it is well known that the energy density at a spatial point where the electric field has the value $\vec{E}$ and the magnetic field has the value $\vec{B}$ is $w = \frac{\epsilon_0}{2}|\vec{E}|^2 + \frac{1}{2\mu_0}|\vec{B}|^2$. In vacuum and in the absence of nearby net charges and current densities, moreover, the field can only be an electromagnetic wave, such that $|\vec{E}| = c|\vec{B}|$ and $w = \epsilon_0|\vec{E}|^2$ and the total energy in a region $V \subseteq \mathbb{R}^3$ is:

$$H = \epsilon_0 \int_V E^2(\vec{x}) \mathrm{d}^3x \tag{2.12}$$

where we used the notation $|\vec{E}| = E$.

At this point, it turns out to be generally convenient to introduce the vector potential as an alternative description to fields. In all generality, the electric and magnetic fields in vacuum (even in the presence of nearby sources) can be expressed as:

$$\vec{E}(\vec{x}) \;=\; -\vec{\nabla}V(\vec{x}) \;-\; \frac{\partial \vec{A}(\vec{x})}{\partial t} \tag{2.13}$$

$$\vec{B}(\vec{x}) \;=\; \vec{\nabla} \times \vec{A}(\vec{x}) \tag{2.14}$$

where $V(\vec{x})$ is the scalar potential and $\vec{A}(\vec{x})$ is the vector potential. Taken together, they can be casted into a relativistic four-vector, whose relation with the four vector obtained out of the charge and current densities is an alternative way to express Maxwell's Equations. Despite having the advantage of leading to a simpler description, the potential fields are highly non-unique, as they display *gauge invariance*. This means that one can displace the potential in the following way:

$$V(\vec{x}) \;\mapsto\; V(\vec{x}) \;-\; \frac{\partial \Lambda(\vec{x})}{\partial t} \tag{2.15}$$

$$\vec{A}(\vec{x}) \;\mapsto\; \vec{A}(\vec{x}) \;+\; \vec{\nabla}\Lambda(\vec{x}) \tag{2.16}$$

where $\vec{\Lambda}(\vec{x})$ is a suitably regular scalar function, and the electric and magnetic fields will not change. At least classically, the $\vec{E}$ and $\vec{B}$ fields are in one-to-one correspondence

with physical consequences, therefore two potential fields configurations differing by a gauge transformation are physically equivalent [3]. For this reason, a *gauge fixing condition* is usually added to Maxwell's equations expressed in terms of potentials, to make them solvable without ambiguity. Finding a "good" gauge for the specific case can greatly simplify the description; if the description of electromagnetic radiation in a laboratory frame is the scope, a frequently adopted choice is the Coulomb gauge, imposing $\vec{\nabla}\cdot\vec{A} = 0$ in the whole spatial region. Furthermore, in the absence of nearby sources $V(\vec{x})$ can be put to zero. With these assumptions, Maxwell's Equations reduce to the wave equation, which we write here for $\vec{E}$:

$$\left(\nabla^2 - \frac{1}{c^2}\frac{\partial^2}{\partial t^2}\right)\vec{E}(\vec{x},t) \;=\; 0 \tag{2.17}$$

and $\vec{B} = \vec{E}/c$, so that this is the only equation to be solved. By separating the spatial and time dependent parts and with considering the *given* boundary conditions, one can solve the resulting Helmholtz Equation and determine the normal modes of the field. These are labelled by wavevectors $\vec{k}_n$, to which it corresponds a frequency of the temporal part of $\omega_n = c|\vec{k}_n|$, according to the linear dispersion relation of massless particles. The absence of sources then implies that all the normal modes (and therefore the fields themselves) are *transverse*, i.e. their polarization direction is orthogonal to the wavevectors. The standard example to fix the ideas is to consider electromagnetic radiation in a cubic box with sides of length L. The modes of the electric fields are then of the form[4]:

$$\vec{E}_{j,s}(\vec{x}) \;=\; \vec{\epsilon}_{j,s}E^0_j \sin(\vec{k}_j\cdot\vec{x})$$

where $\vec{\epsilon}_j$ is the polarization vector, the wavevector $\vec{k}_j$ has components $\frac{2\pi}{L}(n_x,n_y,n_z)$ with $n_x,n_y,n_z \in \mathbb{N}$, E^0_j is the amplitude and $\vec{\epsilon}_j\cdot\vec{k}_j = 0$. The index j should be interpreted as a multi-index listing the lattice of $\mathbb{N}^3$. A second index, s, is then needed to label the two linearly independent polarization directions orthogonal to $\vec{k}_j$.

The core idea of canonical quantization of the field enters here: we assume that the *field amplitude* associated with each spatial mode (with fixed wavevector and polarization) behaves like an independent, quantum degree of freedom attaining continuous values whose amplitude is described by a quantum state on $\mathcal{L}^2(\mathbb{R})$. This is in direct analogy with a point particle, whose position is classically described by a trajectory $\vec{x}(t)$, but it is becomes a random variable with amplitude $\psi(\vec{x})$ when we quantize the system. The position, instead, is now an operator acting on the Hilbert space: in much the same way, the field of each mode will become an operator. To apply this program in a judicious way, however, we should identify exactly *which* field should play the role of the position operator after quantization, and which will play the role of the momentum operator. Once again, classical mechanics comes to rescue, since one can use the classical Hamiltonian for the fields, given in Eq.(2.12), and find the right field-variables in which

[3] Despite some confusion in some expositions, this is still true in quantum mechanics. It is to be recognised that gauge transformations do have an influence on the wavefunction and they imply interesting phenomena such as the Aharonov-Bohm's phase, which will be discussed in detail later, but still all observable quantities are dependent just upon the values of $\vec{E}$ and $\vec{B}$.

[4] We assume vanishing field on the sides, amounting to a conductive box, just to simplify and neglect the cosine term.

Maxwell's Equations become the corresponding Hamilton's Equations[5]. The end result (see [77, 97] for the derivation) is the following:

$$\hat{\mathbf{E}}_{\perp}(\vec{x}) \;=\; \sum_n i\mathcal{E}_n\vec{\epsilon}_n\left[\hat{a}_n e^{i\vec{k}_n\cdot\vec{x}} - \hat{a}_n^{\dagger}e^{-i\vec{k}_n\cdot\vec{x}}\right] \tag{2.18}$$

$$\hat{\mathbf{B}}(\vec{x}) \;=\; \sum_n i\mathcal{B}_{\omega_n}\left(\vec{\kappa}_n\times\vec{\epsilon}_n\right)\left[\hat{a}_n e^{i\vec{k}_n\cdot\vec{x}} - \hat{a}_n^{\dagger}e^{-i\vec{k}_n\cdot\vec{x}}\right] \tag{2.19}$$

$$\hat{\mathbf{A}}_{\perp}(\vec{x}) \;=\; \sum_n \mathcal{A}_{\omega_n}\vec{\epsilon}_n\left[\hat{a}_n e^{i\vec{k}_n\cdot\vec{x}} + \hat{a}_n^{\dagger}e^{-i\vec{k}_n\cdot\vec{x}}\right] \tag{2.20}$$

where $\perp$ denotes the transverse components of the respective fields, $\omega_n = |\vec{k}_n|/c$, $\vec{\kappa}_n = \vec{k}_n/|\vec{k}_n|$ and:

$$\mathcal{E}_{\omega_n} \;=\; \sqrt{\frac{\hbar\omega_n}{2\epsilon_0 L^3}}\,, \quad \mathcal{B}_{\omega_n} \;=\; \frac{\mathcal{E}_{\omega_n}}{c}\,, \quad \mathcal{A}_{\omega_n} \;=\; \frac{\mathcal{E}_{\omega_n}}{\omega_n} \tag{2.21}$$

The Hamiltonian operator, instead, becomes:

$$\hat{\mathbf{H}} \;=\; \sum_n \hbar\omega_n\left(\hat{a}_n^{\dagger}\hat{a} + \frac{1}{2}\right) \tag{2.22}$$

2.2 The phase space of quantum optics

2.2.1 Characteristic function and Wigner function of quantum states

Building on the fact that the quadrature operators (or, alternative, the creation and annihilation operators) generate the algebra of observables, it is possible to represent any quantum state[6] on Fock space, $\hat{\boldsymbol{\rho}} \in \mathcal{S}\left(\mathcal{F}^{(n)}\right)$ through a function on a quantum phase-space $\mathbb{R}^{2n}$, called the *characteristic function* [99, 100]:

$$\chi\left[\hat{\boldsymbol{\rho}}\right]\left(\vec{\Lambda}\right) \;:=\; \mathrm{Tr}\left[\hat{\boldsymbol{\rho}}\,\hat{\mathbf{D}}\left(\vec{\Lambda}\right)\right] \tag{2.23}$$

where we introduced the *displacement operator*:

$$\begin{aligned}
&\hat{\mathbf{D}}\left(\vec{\Lambda}\right) \;:=\; \exp\left[-i\vec{\Lambda}^T\Omega\hat{\mathbf{R}}\right] \;=\; \bigotimes_{k=1}^{n} e^{\lambda_k\hat{a}_k^{\dagger}-\lambda_k^*\hat{a}_k} \;=\; \bigotimes_{k=1}^{n}\hat{\mathbf{D}}_k\left(\lambda_k\right)\\
&\vec{\Lambda} \;=\; \left(\mathrm{a}_1,\mathrm{b}_1,...,\mathrm{a}_n,\mathrm{b}_n\right)^T\in\mathbb{R}^{2n} \qquad \vec{\lambda}=\left(\lambda_1,...,\lambda_n\right)^T\in\mathbb{C}^n\\
&\text{where}\quad \lambda_k=\frac{1}{\sqrt{2}}\left(\mathrm{a}_k+i\mathrm{b}_k\right) \;=\; \left[\bar{U}\vec{\Lambda}\right]_{2k-1} \qquad \bar{U}:=\oplus_{j=1}^{n}\bar{u} \quad \bar{u}=\frac{1}{\sqrt{2}}\begin{pmatrix}1 & i\\ 1 & -i\end{pmatrix}
\end{aligned} \tag{2.24}$$

Notice that the matrix $\bar{U}$ is unitary, but the real vector $\vec{\Lambda}$ has double the entries of the complex vector $\vec{\lambda}$, thus $|\vec{\Lambda}|^2 = 2|\vec{\lambda}|^2$. It is also evident that $\hat{\mathbf{D}}^{\dagger}(\vec{\Lambda}) = \hat{\mathbf{D}}(-\vec{\Lambda})$, thus they are closed under the adjoint operation. Displacement operators bear their names due to their action on quadrature operators:

$$\hat{\mathbf{D}}(\vec{\Lambda})^{\dagger}\hat{\mathbf{R}}\hat{\mathbf{D}}(\vec{\Lambda}) \;=\; \hat{\mathbf{R}}+\vec{\Lambda} \tag{2.25}$$

[5] An even more pedantic approach would be to write down the Lagrangian, which defines the canonically conjugated variables; however, this is not very practical if the explicit relativistic invariance is not relevant.

[6] And, even more generally, any bounded operator $\hat{\mathrm{O}}$.

or, equivalently, they shift each annihilation operator $\hat{a}_k$ by $\lambda_k \in \mathbb{C}$. The fact that the expectation value of the displacement operators for each $\vec{\Lambda}$, i.e. the characteristic function, completely defines a quantum state (and indeed *any* bounded operator) is expressed by *Glauber formula* [98, 99]:

$$\hat{\mathrm{O}} \;=\; \int_{\mathbb{R}^{2n}} \mathrm{d}^{2n}\Lambda \; \chi[\hat{\mathrm{O}}](\vec{\Lambda}) \; \hat{\mathbf{D}}(-\vec{\Lambda}) \tag{2.26}$$

stating that displacement operators are *complete*, in the sense that any other operator can be expanded in terms of them with coefficients dictated by the Hilbert-Schmidt product. Indeed, displacement operators are orthogonal with respect to such product:

$$\mathrm{Tr}\left[\hat{\mathbf{D}}^{\dagger}(\vec{\Lambda}_1)\hat{\mathbf{D}}(\vec{\Lambda}_2)\right] \;=\; \pi^n \delta^{(2n)}(\vec{\Lambda}_1 - \vec{\Lambda}_2) \quad (\vec{\Lambda}_1, \vec{\Lambda}_2 \in \mathbb{R}^{2n}) \tag{2.27}$$

Through the displacement operators it is possible to write an expression which is *equivalent* to the canonical commutation relations, but involving just bounded operators, which is the mathematically rigorous way to define them. We report it in complex form and for a single mode, as it can be directly generalised to more general cases:

$$\forall \alpha, \beta \in \mathbb{C}: \quad \hat{\mathbf{D}}(\alpha)\hat{\mathbf{D}}(\beta) \;= \hat{\mathbf{D}}(\alpha+\beta) e^{\frac{1}{2}(\alpha\beta^* - \alpha^*\beta)} \tag{2.28}$$

Yet another equivalent description is provided by the Wigner function of a state $\hat{\boldsymbol{\rho}}$:

$$\begin{aligned} W\left[\hat{\boldsymbol{\rho}}\right]\left(\vec{X}\right) \;&=\; \frac{1}{(2\pi)^n}\int_{\mathbb{R}^n} \mathrm{d}^n q' \; \left\langle \vec{q} + \frac{1}{2}\vec{q}' \right| \; \hat{\boldsymbol{\rho}} \; \left| \vec{q} - \frac{1}{2}\vec{q}' \right\rangle \; e^{-i\vec{p}\cdot\vec{q}'} \\ \vec{X} \;&=\; (q_1, p_1, ..., q_n, p_n)^T \qquad \vec{q} = (q_1, ..., q_n)^T, \quad \vec{p} = (p_1, ..., p_n)^T \end{aligned} \tag{2.29}$$

The Wigner function is a quasiprobability distribution: the marginals of this distribution with respect to a given set of quadratures, one for each mode, provide the quantum probability distributions for the measurement of the remaining quadratures. When the function is everywhere positive, then it can be interpreted as a classical Liouville distribution on phase space but, even in that case, since non-commuting observables cannot be measured jointly, the Wigner function cannot be interpreted as *the* joint probability distribution associated with the quantum system for the qs and the ps variables. Nevertheless, a Wigner function which is positive semidefinite at all instants of a quantum experiment effectively provides an hidden variable model for the phenomenology, limiting the range of quantum behaviours that can be observed.

Since Eq.(2.29) is the Fourier transform of the expansion of $\hat{\boldsymbol{\rho}}$ on the eigenbasis of position operators, the full quantum state can be recovered from its Wigner function. In this sense, the Wigner function provides an encoding of the state in terms of a function (or a distribution) on phase space. For this reason we refer to this framework as the *phase space formulation of quantum mechanics*. The information contained in the characteristic function is the same, as one can show that:

$$W\left[\hat{\boldsymbol{\rho}}\right]\left(\vec{X}\right) \;=\; \frac{1}{(2\pi)^{2n}}\int_{\mathbb{R}^{2n}} \mathrm{d}^{2n}\vec{\Lambda} \; \exp\{i\vec{\Lambda}^T \Omega \vec{X}\} \; \chi\left[\hat{\boldsymbol{\rho}}\right]\left(\vec{\Lambda}\right) \tag{2.30}$$

so that, apart for a symplectic mixing performed by Ω, $W[\hat{\boldsymbol{\rho}}](X)$ is just the Fourier transform of $\chi[\hat{\boldsymbol{\rho}}](\vec{\Lambda})$. Notice that, with our conventions:

$$\chi[\hat{\boldsymbol{\rho}}](\vec{0}) \;=\; 1\,, \qquad \int_{\mathbb{R}^{2n}} \mathrm{d}^{2n}\vec{X} \; W[\hat{\boldsymbol{\rho}}](\vec{X}) \;=\; 1 \tag{2.31}$$

For some applications, it is convenient to use the modified characteristic function:

$$\tilde{\chi}\left[\hat{\boldsymbol{\rho}}\right]\left(\vec{\Lambda}\right) \;:=\; \mathrm{Tr}\left[\hat{\boldsymbol{\rho}}\,\exp\{-i\vec{\Lambda}^T\hat{\mathbf{R}}\}\right] \;=\; \mathrm{Tr}\left[\hat{\boldsymbol{\rho}}\,\hat{\mathbf{D}}(\Omega\vec{\Lambda})\right] \tag{2.32}$$

In this case, the Wigner function is precisely given by the Fourier transform of $\tilde{\chi}$

Part of the advantage of the phase space formulation becomes clear when we consider some standard quantum mechanical computations, such as taking expectation values of an observable $\hat{\mathrm{O}}$. After some work one can then arrive at the following *trace rules*:

$$\begin{aligned}\mathrm{Tr}\left[\hat{\boldsymbol{\rho}}\,\hat{\mathrm{O}}\right] &= \frac{1}{(2\pi)^n}\int_{\mathbb{R}^{2n}}\mathrm{d}^{2n}\vec{\Lambda}\;\chi\left[\hat{\boldsymbol{\rho}}\right](\vec{\Lambda})\;\chi[\hat{\mathrm{O}}](-\vec{\Lambda})\\ \mathrm{Tr}\left[\hat{\boldsymbol{\rho}}\,\hat{\mathrm{O}}\right] &= \pi^n\int_{\mathbb{R}^{2n}}\mathrm{d}^{2n}\vec{X}\;W\left[\hat{\boldsymbol{\rho}}\right](\vec{X})\;W[\hat{\mathrm{O}}](\vec{X})\end{aligned} \tag{2.33}$$

2.2.2 s-ordered Wigner functions and P-nonclassicality

The idea of expanding continuous-variable operators in normally, antinormally and symmetrically ordered power series of creation and annihilation operators dates back to the pioneering works of Roy J. Glauber (1925-2018) and E. C. G. Sudarshan (1931-2018), who studied the coherent properties of light and its mathematical representation through complex functions [108, 109, 110, 111]. The aim is to write expectation values of monomials like $\langle[\hat{x}^n\hat{p}^m]_o\rangle$ on generic quantum states $\hat{\boldsymbol{\rho}}$ as expectation values of the corresponding polynomial function x^np^n with respect to a (quasi-)probability distribution associated with $\hat{\boldsymbol{\rho}}$, where by $[\hat{x}^n\hat{p}^m]_o$ we denoted the product of operators with respect to some ordering rule "o": typically this would be all powers of $\hat{x}$ to the left, or to the right, or the symmetric sum over all possible orderings. Equivalently, one can work in the complex framework with creation and annihilation operators and monomials of the form $\alpha^n(\alpha^*)^m$. The Wigner function already does the job for symmetrically ordered products of $\hat{a}_k$ and $\hat{a}_k^\dagger$, while in more generality one can define a modified characteristic function $\chi_s[\hat{\boldsymbol{\rho}}](\vec{\Lambda}) = e^{\frac{s}{4}|\vec{\Lambda}|^2}\chi[\hat{\boldsymbol{\rho}}](\vec{\Lambda})$ where $s\in[-1,1]$ is a real parameter, and correspondingly the s-ordered Wigner functions:

$$W_s[\hat{\boldsymbol{\rho}}](\vec{X}) \;=\; \frac{1}{(2\pi)^{2n}}\int_{\mathbb{R}^{2n}}\mathrm{d}^{2n}\vec{\Lambda}\exp\{i\vec{\Lambda}^T\Omega\vec{X}\}\chi_s[\hat{\boldsymbol{\rho}}](\vec{\Lambda}) \tag{2.34}$$

such that for $s=0$ we recover the standard definitions of the characteristic and Wigner functions, while for $s=-1$ the latter is always a positive-semidefinite, regular function, which can be expressed in terms of the complex variables as:

$$Q[\hat{\boldsymbol{\rho}}](\vec{\alpha}) \;=\; W_{-1}[\hat{\boldsymbol{\rho}}](\vec{X}) \;=\; \frac{1}{\pi}\langle\vec{\alpha}|\hat{\boldsymbol{\rho}}|\vec{\alpha}\rangle \quad(\vec{\alpha}\in\mathbb{C}^n) \tag{2.35}$$

where the real argument $\vec{X}$ is connected with the complex representation $\vec{\alpha}$ by $\bar{U}$. This quantity is known as the Q-function or Husimi function. By its own definition it is apparent that it is a probability distribution with respect to a continuous set of complex outcomes, therefore it cannot emerge from a self-adjoint observable. It turns out that the Q-function describes expectation values of creation and annihilation operators in *antinormal* order. At the opposite end of the spectrum, for $s=1$, lies the Glauber P-function, which is often not even a function but it can always be represented as a distribution.

It describes the moments of $\hat{a}_k, \hat{a}_k^\dagger$ in *normal* order and it enters in the pivotal *Glauber-Sudarshan formula*:

$$\hat{\boldsymbol{\rho}} \;=\; \int_{\mathbb{C}^n} \mathrm{d}^n\alpha \; P(\vec{\alpha}) \; |\vec{\alpha}\rangle\langle\vec{\alpha}| \tag{2.36}$$

This is a very powerful result: not only it asserts that *any* continuous-variable quantum state can be expanded into (non-orthogonal) coherent states projectors, but it also makes apparent that only states with a singular P function can be entangled, since multimode coherent states are factorised and Eq.(2.36) becomes a separable state if P is a probability distribution.

It turns out that the P-function is tightly related to the possibility of describing a light field with Maxwell's Equations on a statistical ensemble of classical waves: if the P-function is a regular, positive-semidefinite distribution, the light which it describes is a statistical mixture of coherent states, the closest quantum state of light to a classical wave[7]. On the other hand, a CV quantum state $\hat{\boldsymbol{\rho}}$ is considered *nonclassical* whenever the *distribution* $P\left[\hat{\boldsymbol{\rho}}\right](\alpha)$ cannot be interpreted as a valid probability density, either because it can be represented by a function that attains negative values, or because a regularization of it does [109, 112, 113, 114, 115, 116, 117, 118, 119, 120, 121]. As a side note, we remark that several protocols have been devised to experimentally and theoretically certify the nonclassicality of light states (see e.g. [122, 123] and references therein).

It is possible to quantify the degree of nonclassicality of a quantum state $\hat{\boldsymbol{\rho}}$ by determining first the smallest number $s_m \in [-1, 1]$ such that $W_s[\hat{\boldsymbol{\rho}}](\vec{X})$ is not positive semidefinite anymore for all $s > s_m$, and then the *nonclassical depth* of $\hat{\boldsymbol{\rho}}$ is:

$$\tau[\hat{\boldsymbol{\rho}}] \;:=\; \frac{1 - s_m[\hat{\boldsymbol{\rho}}]}{2} \tag{2.37}$$

Another commonly employed measure of nonclassicality is the Mandel $\mathcal{Q}_M$ parameter, defined as:

$$\mathcal{Q}_M[\hat{\boldsymbol{\rho}}] \;:=\; \frac{\langle(\hat{a}^\dagger\hat{a})^2\rangle - \langle\hat{a}^\dagger\hat{a}\rangle^2 - \langle\hat{a}^\dagger\hat{a}\rangle}{\langle\hat{a}^\dagger\hat{a}\rangle} \tag{2.38}$$

which has the interpretation of being the ratio of the difference between the variance and the mean of the photon number distribution over the mean itself. If the variance is lower than the mean photon number, then $\mathcal{Q}_M < 0$ and the state must be nonclassical, as can be argued from Glauber-Sudarshan formula that all quantum states with positive semidefinite, regular P-function have $\mathcal{Q}_M > 0$. On the other hand, if $\mathcal{Q}_M > 0$, the test is inconclusive about nonclassicality.

Since the P-function and the Q-function are related by a Gaussian convolution[8], the P-function being the less regular of the two:

$$Q[\hat{\boldsymbol{\rho}}](\alpha) \;=\; \frac{1}{\pi}\int \mathrm{d}^2\beta P(\beta) e^{-|\alpha-\beta|^2} \tag{2.39}$$

we deduce that if $Q[\hat{\boldsymbol{\rho}}](\vec{\alpha}) = 0$ for some $\vec{\alpha} \in \mathbb{C}^n$ then the P-function must attain negative values, thus the state is nonclassical. However, the converse is not true: P-nonclassical

[7] This is due to the fact that it has nonzero expectation values for the fields with a minimal, constant uncertainty dictated by the uncertainty relations.

[8] Here expressed in complex notation and for a single mode

states can have everywhere-nonvanishing Q-functions. The inverse of Eq.(2.39) can be written via the Widder transform:

$$P(\alpha) \;=\; \exp\left(-\frac{\partial^2}{\partial\alpha\partial\alpha^*}\right) Q(\alpha,\alpha^*) \tag{2.40}$$

2.3 Gaussian states

Quadratic operators in the field's quadratures play a special role in continuous-variable quantum information, both because their algebra closes nicely, allowing for exact computations, and also because they can be used to describe a wide variety of states and operations in experimental quantum optics. The core definition for us will be the following [99]:

Definition 2.3.1: Gaussian states

A Gaussian state of n modes is a *thermal state* of a (possibly inhomogeneous) quadratic Hamiltonian operator $\hat{\mathbf{H}}$ which is bounded from below:

$$\hat{\boldsymbol{\rho}}_G \;:=\; \frac{e^{-\beta\hat{\mathbf{H}}}}{\mathrm{Tr}[e^{-\beta\hat{\mathbf{H}}}]}\;,\quad \beta\in\mathbb{R}^+ \tag{2.41}$$

where:

$$\hat{\mathbf{H}} = \frac{1}{2}(\hat{\mathbf{R}}-\vec{X})^T\cdot \mathrm{H}\cdot(\hat{\mathbf{R}}-\vec{X}) \tag{2.42}$$

and H is a symmetric, positive-definite ($\mathrm{H}>0$) real matrix, while $\vec{X}\in\mathbb{R}^{2n}$. The limit $\beta\to+\infty$ is included.

Notice that we can rewrite:

$$\hat{\mathbf{H}} \;=\; \hat{\mathbf{D}}(-\vec{X})\hat{\mathbf{H}}'\hat{\mathbf{D}}(\vec{X})\;,\quad \hat{\mathbf{H}}' = \frac{1}{2}\hat{\mathbf{R}}^T\cdot\mathrm{H}\cdot\hat{\mathbf{R}} \tag{2.43}$$

so that the vector $\vec{X}$ can be introduced by a simple displacement. To procede, we will now invoke two results from symplectic geometry [99]:

Theorem 2.3.1: Williamson Decomposition

Any positive definite $2n\times 2n$ real matrix H is congruent to a diagonal matrix of the form $\oplus_{j=1}^n\omega_j\mathbb{1}_2$ through a symplectic transformation:

$$S^T\mathrm{H}S \;=\; \oplus_{j=1}^n\omega_j\mathbb{1}_2\;,\qquad S\in\mathrm{Sp}(2n,\mathbb{R}),\;\; \omega_j\in\mathbb{R}^+ \tag{2.44}$$

Theorem 2.3.2

Let $\hat{\mathbf{H}} = \frac{1}{2}\hat{\mathbf{R}}^T \cdot \mathrm{H} \cdot \hat{\mathbf{R}}$ be an homogeneous quadratic Hamiltonian operator with $\mathrm{H} > 0$. Then its action on the vector of quadratures operators can be described by a linear symplectic transformation $S_H \in \mathrm{Sp}(2n)$:

$$e^{i\hat{\mathbf{H}}}\hat{\mathbf{R}}e^{-i\hat{\mathbf{H}}} \;=\; S_H \cdot \hat{\mathbf{R}} \tag{2.45}$$

such that $S_H = \Omega\mathrm{H}$. Vice versa, if $S_H = \Omega\mathrm{H}$ for a generic positive-definite real matrix H, there will exist an homogeneous quadratic Hamiltonian $\hat{\mathbf{H}}$ satisfying the above relation.

Theorem 2.3.3

Any real symplectic matrix $S \in \mathrm{Sp}(2n, \mathbb{R})$ can be written as a product of at most two matrices $S = S_A S_B$, where $S_A = e^{\Omega A}$, $S_B = e^{\Omega B}$ with A, B real and *symmetric* $2n \times 2n$ matrices.

Combining these results, we deduce that:

$$\begin{aligned}\frac{1}{2}\hat{\mathbf{R}}^T \cdot \mathrm{H} \cdot \hat{\mathbf{R}} \;&=\; \frac{1}{2}(S_H\hat{\mathbf{R}})^T \left(\bigoplus_{j=1}^{n} \omega_j \mathbb{1}_2\right)(S_H\hat{\mathbf{R}}) \;= \\ &=\; \hat{\mathbf{S}}^\dagger \left[\sum_{j=1}^{n} \frac{\omega_j}{2}(\hat{q}_j^2 + \hat{p}_j^2)\right]\hat{\mathbf{S}}\end{aligned} \tag{2.46}$$

where $\hat{\mathbf{S}} = \hat{\mathbf{S}}_A\hat{\mathbf{S}}_B$ and $\hat{\mathbf{S}}_A, \hat{\mathbf{S}}_B$ are the unitary operators associated with the symplectic matrices S_A, S_B through Theorem 2.3. We then arrive at:

$$\begin{aligned} e^{-\beta\hat{\mathbf{H}}} \;&=\; \hat{\mathbf{D}}(-\vec{X})\hat{\mathbf{S}}^\dagger \left[\otimes_{j=1}^{n} e^{-\beta\frac{\omega_j}{2}(\hat{q}_j^2+\hat{p}_j^2)}\right]\hat{\mathbf{S}}\hat{\mathbf{D}}(\vec{X}) \\ \mathrm{Tr}\left[e^{-\beta\hat{\mathbf{H}}}\right] \;&=\; \frac{1}{e^{\beta\frac{\omega_j}{2}} - e^{-\beta\frac{\omega_j}{2}}}\end{aligned} \tag{2.47}$$

Finally, we see that $\hat{q}_j^2 + \hat{p}_j^2$ is the standard Hamiltonian of an harmonic oscillator, which can be rewritten in terms of Fock states as $\hat{q}_j^2 + \hat{p}_j^2 = \sum_{n=0}^{\infty}(2m+1)|m\rangle_{jj}\langle m|$. Therefore, a generic Gaussian state assumes the following aspect [99]:

$$\hat{\boldsymbol{\rho}}_G \;=\; \left(\prod_{j=1}^{n}(1 - e^{-\beta\omega_j})\right)\hat{\mathbf{D}}(-\vec{X})\,\hat{\mathbf{S}}^\dagger \left[\bigotimes_{j=1}^{n}\sum_{m=0}^{\infty} e^{-\beta\omega_j m}|m\rangle_{jj}\langle m|\right]\hat{\mathbf{S}}\,\hat{\mathbf{D}}(\vec{X}) \tag{2.48}$$

Quantum states of the form $(1-\lambda^{-1})\sum_{n=0}^{\infty}\lambda^n|n\rangle\langle n|$ ($\lambda = e^{-\beta\omega}$) are called *thermal states* because they also describe the quantum state of thermal radiation emitted by a black body (apart for aspects concerning mode-coherence). We can then affirm that *every Gaussian state of n modes is the result of a unitary transformation generated by a symplectic operation, followed by a displacement, acting on a thermal state of the n modes*. In the next section, we will see how this characterization can be pushed further by studying in more details the unitary operations generated by quadratic Hamiltonians (or, equivalently, by

symplectic linear transformations on the vector of quadratures operators).

2.3.1 Thermal and coherent states

Two limits of Eq.(2.48) define the archetypal classical states of radiation. We already mentioned *thermal states*, corresponding to the case when $\vec{X} = 0$ (no displacement) and $\hat{\mathbf{S}} = \mathbb{1}$:

$$\begin{aligned} \hat{\boldsymbol{\nu}}_{th}\left(N_k\right) &= \frac{e^{-\beta_k \hat{a}_k^\dagger \hat{a}_k}}{\mathrm{Tr}\left[e^{-\beta_k \hat{a}_k^\dagger \hat{a}_k}\right]} = \frac{{N_k}^{\hat{a}_k^\dagger \hat{a}_k}}{(1+N_k)^{\hat{a}_k^\dagger \hat{a}_k + 1}} = \\ &= \frac{1}{1+N_k} \sum_{n=0}^{+\infty} \left(\frac{N_k}{1+N_k}\right)^n |n\rangle\langle n| \end{aligned} \tag{2.49}$$

where, for notational convenience, we redefined $\beta\omega_k = \beta_k$. The positive number $N_k = \left(e^{\beta_k} - 1\right)^{-1}$ is the expectation value of the number operator of mode k in the state $\hat{\boldsymbol{\nu}}_{th}(N_k)$. Their purity is easily computed to be:

$$\mu_{th}(N_k) = \frac{1}{1+2N_k} \tag{2.50}$$

so that the only pure thermal state is the vacuum ($N_k = 0$). All the formulae for single-mode thermal states immediately generalize to n-mode thermal states, because these are simply tensor products of single-mode Gaussian states and their CM is the corresponding direct sum of single-mode thermal CMs.

Another simple limit of Eq.(2.48) arises when we take again $\hat{\mathbf{S}} = \mathbb{1}$, but now $\vec{X} \neq 0$ and instead we let $\beta \to +\infty$. This brings the central thermal state to the vacuum, since only the term with $m = 0$ survives. We are therefore left with a pure state that we can represent in the ray notation as a displaced vacuum state, $\hat{\mathbf{D}}(\vec{X})|0\rangle$. Since the displacement operator acts independently on each mode, let us focus on the single-mode case and adopt the complex notation,

$$\hat{\mathrm{D}}(\alpha) = e^{\alpha\hat{a}^\dagger - \alpha^*\hat{a}} = e^{-\frac{1}{2}|\alpha|^2} e^{\alpha\hat{a}^\dagger} e^{-\alpha^*\hat{a}} \quad , \qquad \alpha \in \mathbb{C} \tag{2.51}$$

where the second inequality follows from the Backer-Campbell-Hausdorff formula $e^{\hat{A}}e^{\hat{B}} = e^{\hat{A}+\hat{B}+\frac{1}{2}[\hat{A},\hat{B}]+\cdots}$, which assumes a simple closed form when the two operators have a commutator proportional to the identity as is the case for $\hat{a}$ and $\hat{a}^\dagger$. Since $e^{-\alpha^*\hat{a}}|0\rangle = |0\rangle$, we find:

$$|\alpha\rangle := \hat{\mathrm{D}}(\alpha)|0\rangle = e^{-\frac{1}{2}|\alpha|^2} \sum_{n=0}^{+\infty} \frac{\alpha^n}{\sqrt{n!}} |n\rangle \tag{2.52}$$

These states are called *coherent states* and they enjoy special properties which make them pivotal in the study of quantum coherence of light. As a first thing, notice that they are eigenstates of the annihilation operator[9] $\hat{a}$ with *complex* eigenvalue α. Indeed, by invoking Eq.(2.25) we have:

$$\hat{a}|\alpha\rangle = \hat{\mathrm{D}}(\alpha)\hat{\mathrm{D}}^\dagger(\alpha)\hat{a}\hat{\mathrm{D}}(\alpha)|0\rangle = \hat{\mathrm{D}}(\alpha)(\hat{a}+\alpha)|0\rangle = \alpha|\alpha\rangle \tag{2.53}$$

[9] Interestingly, it can be proven that no normalizable eigenstates of the creation operator exist.

The same result can be obtained by the Fock space expansion, Eq.(2.52) and, vice versa, that expression can be derived by looking for normalizable eigenstates of $\hat{a}$. Moreover, again by Eq.(2.52), we see that their photon-number distribution is a *Poissonian* probability distribution:

$$p_n(\alpha) \;=\; |\langle n|\alpha\rangle|^2 \;=\; e^{-|\alpha|^2}\frac{|\alpha|^2}{n!} \tag{2.54}$$

therefore $|\alpha|^2$ is both the mean number of photons in the coherent state and the variance of it:

$$\langle\hat{N}\rangle_\alpha \;:=\; \langle\alpha|\hat{a}^\dagger\hat{a}|\alpha\rangle = |\alpha|^2 = (\Delta\hat{N})^2_\alpha \tag{2.55}$$

On the other hand, the variance of the photon-number distribution of a thermal state with mean photon number N_{th} is $(\Delta\hat{N})^2_{th} = N^2_{th} + N_{th} > N_{th}$ and grows quadratically with N_{th}: we say that thermal states have *super-Poissonian statistics*. Another interesting observation is that, since $\langle n|\hat{q}|n\rangle = \langle n|\hat{p}|n\rangle = 0$ and thermal states are diagonal in the Fock basis, the expectation value of the quadrature operators (or, equivalently, of the electric and magnetic field operators) is zero. Conversely, coherent states are always pure states and they possess coherence in the Fock basis. Indeed it is a straightforward application of Eq.(2.25) to show that:

$$\langle\alpha|\hat{q}|\alpha\rangle = \sqrt{2}\Re(\alpha)\;, \qquad \langle\alpha|\hat{p}|\alpha\rangle = \sqrt{2}\Im(\alpha) \tag{2.56}$$

where $\Re(\alpha)$ and $\Im(\alpha)$ represent the real and imaginary part of $\alpha \in \mathbb{C}$, respectively, giving a natural interpretation of the number α labelling a coherent state. Additionally, they belong to the class of states with minimal uncertainty, in the sense that they saturate the Heisenberg Uncertainty Inequality for the conjugated canonical quadrature operators:

$$(\Delta\hat{q}^2)_\alpha(\Delta\hat{p}^2)_\alpha \;=\; \frac{1}{4} \tag{2.57}$$

Coherent states are not orthogonal, indeed Eq.(2.28) implies:

$$\langle\beta|\alpha\rangle = \langle 0|\hat{\mathrm{D}}(-\beta)\hat{\mathrm{D}}(\alpha)|0\rangle = e^{-\frac{1}{2}(|\alpha|^2+|\beta|^2-2\alpha\beta^*)} \tag{2.58}$$

However, they form an *overcomplete* system, in the sense that they provide a resolution of the identity, which is a direct consequence of Glauber formula 2.26:

$$\frac{1}{\pi}\int_{\mathbb{C}^n} \mathrm{d}^n\alpha|\alpha\rangle\langle\alpha| \;=\; \mathbb{1} \tag{2.59}$$

but any finite number of them can be removed from the integration set without altering their completeness.

2.3.2 Phase-space representation of Gaussian states

It turns out that a *fully equivalent* way to Definition 2.3 to define Gaussian states is in terms of their Wigner (or characteristic) function being a Gaussian function [99, 100]:

$$\begin{aligned}
\chi\left[\hat{\boldsymbol{\rho}}_G\right]\left(\vec{\Lambda}\right) \;&=\; \exp\left\{-\frac{1}{2}\vec{\Lambda}^T\,\Omega^T\sigma\,\Omega\,\vec{\Lambda} \;-\; i\vec{\Lambda}^T\,\Omega\,\vec{X}_0\right\} \\
W\left[\hat{\boldsymbol{\rho}}_G\right]\left(\vec{X}\right) \;&=\; \frac{1}{(2\pi)^n\sqrt{\det[\sigma]}}\exp\left\{-\frac{1}{2}\left(\vec{X}-\vec{X}_0\right)^T\sigma^{-1}\left(\vec{X}-\vec{X}_0\right)\right\}
\end{aligned} \tag{2.60}$$

It is a simple task to prove that $\vec{X}_0 = \langle \hat{\mathbf{R}} \rangle_{\hat{\boldsymbol{\rho}}_G}$ is the vector of expectation values of the quadratures, also known as the *mean field*, whereas σ is a $2n \times 2n$ symmetric matrix going under the name of *covariance matrix* (CM), because it encodes the covariances between the quadratures:

$$[\sigma]_{jk} = \frac{1}{2}\left\langle \hat{R}_j \hat{R}_k + \hat{R}_k \hat{R}_j \right\rangle - \left\langle \hat{R}_j \right\rangle \left\langle \hat{R}_k \right\rangle \tag{2.61}$$

One might think that postulating a generic Gaussian Wigner function automatically defines a Gaussian state. However, it is intuitively clear that the uncertainty principle would forbid an arbitrarily narrow Gaussian peak in both q and p in phase space. Indeed, the CCRs imply a bound on the covariance matrix:

$$\sigma + \frac{i}{2}\Omega \geq 0 \tag{2.62}$$

which can be proven [124] by considering the operator $\hat{V} = (\hat{\mathbf{R}} - \langle \hat{\mathbf{R}} \rangle) \cdot \vec{Y}$, $Y \in \mathbb{C}^n$ being any complex vector; the positivity of $\hat{\boldsymbol{\rho}}$ implies that $\mathrm{Tr}[\hat{\boldsymbol{\rho}} \hat{V}^\dagger \hat{V}] \geq 0$ and by using the canonical commutation relations Eq.(2.2) the condition rewrites:

$$\vec{Y}^\dagger \cdot \left(\sigma + \frac{i}{2}\Omega\right) \vec{Y} \geq 0$$

which has to hold for any *complex* vector $\vec{Y}$, hence we arrive at Ineq.(2.62). Notice that it is necessary to consider the complex vectors, otherwise Ω would not contribute, being antisymmetric. Moreover, we deduced Ineq.(2.62) without ever supposing $\hat{\boldsymbol{\rho}}$ to be Gaussian, meaning that the covariance matrix of *any* quantum state will satisfy the inequality. It can then be shown that any time a CM satisfies Ineq.(2.62), the associated Wigner function will correspond to a valid Gaussian state, so that this is the only condition to be added.

To give some examples, let us represent thermal states and coherent states with their Wigner functions. In the first instance, the covariance matrix is $\sigma_{th} = (N_{th} + 1/2)\mathbb{1}_2$ and the expectation values of the quadratures are null, as discussed above. Their Wigner function is therefore:

$$W[\hat{\boldsymbol{\nu}}_{th}(N_{th})](x,p) = \frac{1}{\pi(2N_{th}+1)} e^{-\frac{x^2+p^2}{2N_{th}+1}} \tag{2.63}$$

For $N_{th} = 0$ we obtain the CM of the vacuum state $\sigma_0 = \mathbb{1}/2$. As for coherent states, the CM is the same of the vacuum one, while the expectation values of the quadratures are $x_0 = \sqrt{2}\Re(\alpha)$ and $p_0 = \sqrt{2}\Im(\alpha)$, so that their Wigner function is:

$$W[|\alpha\rangle\langle\alpha|](x,p) = \frac{1}{\pi} e^{-(x-x_0)^2-(p-p_0)^2} \tag{2.64}$$

An important quantity that can be expressed in terms of the CM for a Gaussian state is the purity. Indeed, by using the trace rules and its definition, one can show that:

$$\mu\left[\hat{\boldsymbol{\rho}}_G\right] = \frac{1}{2^n \sqrt{\det\left[\sigma\right]}} \tag{2.65}$$

2.4 Gaussian unitary operations

2.4.1 Euler or Bloch-Messiah decomposition

Another general theorem from symplectic geometry states the following [99]:

Theorem 2.4.1: (Bloch-Messiah decomposition)

Any real symplectic matrix $\mathrm{S} \in \mathrm{Sp}(2n, \mathbb{R})$ can be decomposed in the following way:

$$\mathrm{S} = \mathrm{O}\,\mathrm{Z}\,\mathrm{O}' \tag{2.66}$$

where $\mathrm{Z} = \bigoplus_{j=1}^{n} \mathrm{diag}(z_j, 1/z_j)$ is a diagonal matrix and $\mathrm{O}, \mathrm{O}' \in \mathrm{Sp}(2n, \mathbb{R}) \cap \mathrm{SO}(2n, \mathbb{R})$ are orthogonal symplectic matrices.

This is just the singular-value decomposition applied to the symplectic matrix, but the most relevant aspects rely on the specific form of the diagonal and orthogonal matrices. Notice that all the matrices in the product on the right side of Eq.(2.66) are symplectic, therefore we can distinguish between different unitary operations generated by quadratic Hamiltonians, whose action on the vector of quadratures operators is of these types.

2.4.2 Most general Gaussian unitary transformation

Gaussian unitary operations are those sending Gaussian states to Gaussian states by conjugation. Since only (up to) second order operators in the quadratures close between themselves under the commutator, Gaussian unitary operators are generated by linear and quadratic Hamiltonians, the most general being:

$$\begin{aligned}\hat{\mathbf{H}}_G \;=\; & \sum_{k=1}^{n} \left({f^{(1)}}_k \hat{a}_k^\dagger + {g^{(1)}}^*_k \hat{a}_k \right) + \\ & + \sum_{j \geq k=1}^{n} \left({g^{(1,1)}}_{j,k} \hat{a}_j^\dagger \hat{a}_k + {g^{(1,1)}}^*_{j,k} \hat{a}_k^\dagger \hat{a}_j \right) + \\ & + \sum_{j \geq k=1}^{n} \left({h^{(2)}}_{j,k} \hat{a}_j^\dagger \hat{a}_k^\dagger + {h^{(2)}}^*_{j,k} \hat{a}_k \hat{a}_j \right).\end{aligned} \tag{2.67}$$

We already saw that linear terms as in the first line of Eq.(2.67) generate displacement operators. Among the quadratic terms, the first distinction that we shall consider is between *passive* operations, which commute with the number operator $\hat{N} = \sum_{j=1}^{n} \omega_j \hat{a}_j^\dagger \hat{a}_j$, as those in the second line of Eq.(2.67), and *active* operation which change the expectation value of $\hat{N}$, in the third line.

We also observed that unitary operators generated by quadratic Hamiltonians linearly transform the quadrature operators according to a symplectic matrix. This means that if $\hat{\mathbf{H}}$ generates an n-modes Gaussian unitary operation $\hat{\mathbf{U}}_G$ acting on a Gaussian state $\hat{\boldsymbol{\rho}}_G$ as $\hat{\mathbf{U}}_G \hat{\boldsymbol{\rho}}_G \hat{\mathbf{U}}_G^\dagger$, there will be a symplectic matrix $\mathrm{S}_{\hat{\mathbf{H}}} \in \mathrm{Sp}(2n, \mathbb{R})$ and a vector

$\vec{d} \in \mathbb{R}^{2n}$ acting on phase-space and trasforming the CM and mean field of a generic Gaussian state according to:

$$\sigma_G \;\mapsto\; \mathrm{S}_{\hat{\mathbf{H}}}\,\sigma_G\,\mathrm{S}_{\hat{\mathbf{H}}}^T\,, \qquad \langle\hat{\mathbf{R}}\rangle_{\hat{\rho}_G} \;\mapsto\; \mathrm{S}_{\hat{\mathbf{H}}}\,\langle\hat{\mathbf{R}}\rangle_{\hat{\rho}_G} \,+\, \vec{d} \tag{2.68}$$

Given that $\vec{d}$ is implemented by a displacement operator (applied as the last), a full characterization of Gaussian unitary operations amounts to associating the symplectic matrix $\mathrm{S}_{\hat{\mathbf{H}}}$ to each quadratic Hamiltonian $\hat{\mathbf{H}}$.

2.4.3 Free evolutions and mode mixing

The single-mode, passive Gaussian operations with Hamiltonians $\hat{\mathbf{H}}_{0,j} = \omega_j \hat{a}_j^\dagger \hat{a}_j = \frac{\omega_j}{2}(\hat{p}_j^2 + \hat{q}_j^2)$ correspond to the free evolution of the modes. They act on the creation operators as:

$$e^{-it\hat{\mathbf{H}}_{0,j}}\,\hat{a}_k e^{it\hat{\mathbf{H}}_{0,j}} \;=\; e^{-i\delta_{jk}\omega_j t}\hat{a}_k \tag{2.69}$$

and their action on the corresponding quadratures $(\hat{q}_j, \hat{p}_j)$ can be represented through the following linear symplectic transformation[10]:

$$\mathrm{R}_{\omega_j t} \;=\; \begin{pmatrix} \cos\omega_j t & \sin\omega_j t \\ -\sin\omega_j t & \cos\omega_j t \end{pmatrix} \tag{2.70}$$

so that they simply cyclically rotate the two conjugated quadratures of the mode. Since it acts multiplicatively through a complex phase on annihilation and creation operators, free evolution is often called *phase shift*. On coherent states, the effect of the free evolution is to multiply their amplitude by a phase: $|\alpha e^{-i\omega_j t}\rangle$, so that their displaced Gaussian function rotates at constant angular velocity ω_j around the origin of phase space.

Another basic passive Gaussian unitary evolution arises when two modes are mixed together, an operation which, in the quantum optical setting, is physically implemented by mixing them into a *beam splitter*. This optical instruments are usually made out of two adjacent birefringent crystals aligned in different directions to form a cube. Light beams enter from two perpendicular input directions and, in a classical description, the incoming intensity of each of them is transmitted for a portion η to one output port, while proportionally to $1-\eta$ it is reflected to the second output port. The reflected and transmitted signals combine coherently in the output ports resulting in mode mixing. Besides the *transmissivity* η, a beam splitter is also characterised by a relative phase ϕ that it introduces between the two output beams. At the mathematical level, the quadratic Hamiltonian operator that effectively describes this interaction is $\hat{\mathbf{H}}_{BS}(\zeta) = \zeta\hat{a}_j^\dagger\hat{a}_k + \zeta^*\hat{a}_k^\dagger\hat{a}_j$ with $\zeta = \theta e^{i\phi} \in \mathbb{C}$. We will denote the respective unitary operation by:

$$\hat{\mathbf{U}}_{BS}(\zeta) \;:=\; e^{-i\hat{\mathbf{H}}_{BS}(\zeta)} \tag{2.71}$$

At the level of symplectic transformation acting on phase space, the mode mixing unitary $\hat{\mathbf{U}}_{BS}(\zeta)$ is implemented by:

$$\mathrm{S}_\zeta^{BS} \;=\; \begin{pmatrix} \cos\theta\,\mathbb{1}_2 & \sin\theta\,\mathrm{R}_\phi \\ -\sin\theta\,\mathrm{R}_\phi^T & \cos\theta\,\mathbb{1}_2 \end{pmatrix} \tag{2.72}$$

[10] Since it is a passive operation, it is also an orthonormal transformation

where $\mathrm{R}_\phi \in \mathrm{SO}(2)$ is the usual 2×2 rotation matrix of angle ϕ, introduced in Eq. (2.69). In general, the beam-splitter interaction can create *entanglement* between the inputs. However, its action on a tensor product of two coherent states simply mixes the respective amplitudes (taking $\phi = 0$ for simplicity):

$$\hat{\mathbf{U}}_{BS}(\theta)|\alpha\rangle \otimes |\beta\rangle \;=\; \big|(\alpha\cos\theta + \beta\sin\theta)\big\rangle \otimes \big|(-\alpha\sin\theta + \beta\cos\theta)\big\rangle \tag{2.73}$$

Using the P-function representation we can then claim that *only P-nonclassical states (on at least one input mode) can be entangled through a beam splitter*.

Given these two passive Gaussian operations, a general result that can be proven constructively states the following:

Theorem 2.4.2: On the decomposition of passive Gaussian transformations

Any *passive Gaussian unitary operation* on n modes corresponds to the action of an *orthonormal symplectic* $2n \times 2n$ *matrix* on phase space. Any such matrix can be decomposed into a finite product of phase shifters and two-mode mixers.

2.4.4 Single-mode squeezing

The kind of Hamiltonian evolution induced by terms $\propto \xi(\hat{a}^\dagger)^2 + h.c.$ generates single-mode, active Gaussian transformations. With reference to Eq.(2.66), these Hamiltonians describe the squeezing performed by the positive diagonal matrix Z. The unitary operator describing the transformation of the mode is[11]:

$$\hat{\mathbf{S}}^{(1)}(\xi) \quad := \quad \exp\left\{\frac{1}{2}\left[\xi\left(\hat{a}^\dagger\right)^2 - \xi^*\hat{a}^2\right]\right\} \tag{2.74}$$

This operator is then implemented on phase space by the following symplectic matrix:

$$\Sigma_\xi^{(1)} \;:=\; \cosh r\,\mathbb{1}_2 + \mathrm{K}_\xi \qquad \text{with} \qquad \mathrm{K}_\xi \;:=\; \sinh r \begin{pmatrix} \cos\varphi & \sin\varphi \\ \sin\varphi & -\cos\varphi \end{pmatrix} \tag{2.75}$$

with the polar decomposition of the complex coupling $\xi = re^{i\varphi} \in \mathbb{C}$. Acting on the vacuum, $\mathrm{S}_\xi^{(1)}$ creates a *squeezed vacuum state*. To compute its expression and also for future calculations, it is useful to consider a rewriting of $\hat{\mathbf{S}}_\xi^{(1)}$ based on the $\mathfrak{su}(1,1)$ algebra [96, 98]:

$$\hat{\mathbf{S}}_\xi^{(1)} = \exp\left(e^{i\varphi}\tanh r\frac{(\hat{a}^\dagger)^2}{2}\right)\exp\left[-(\ln\cosh r)\left(\hat{a}^\dagger\hat{a} + \frac{1}{2}\right)\right]\exp\left(-e^{i\varphi}\tanh r\frac{\hat{a}^2}{2}\right) \tag{2.76}$$

Applying this to the vacuum state gives:

$$|\xi\rangle \;:=\; \hat{\mathbf{S}}^{(1)}(\xi)|0\rangle \;=\; \frac{1}{\sqrt{\cosh r}}\sum_{n=0}^{+\infty} e^{in\varphi}(\tanh r)^n\frac{\sqrt{(2n)!}}{n!\,2^n}|2n\rangle \tag{2.77}$$

[11] The apex (1) reminds that this is single-mode squeezing.

The mean number of photons turns out to be $\langle\xi|\hat{a}^\dagger\hat{a}|\xi\rangle = \sinh^2 r$ and the variance is again super-Poissonian, $(\Delta\hat{N})^2_\xi = 2\sinh^2 r(\sinh^2 r + 1)$. This time, however, we see that $p_{2n+1}(\xi) = 0$: the photon-number probability distribution is zero for every odd Fock state. It can be shown that this can happen only if the state is P-nonclassical [112]. This property also implies that the mean field is zero for the squeezed vacuum, as the quadrature operators have non-vanishing matrix elements only between Fock states with different parity. On the other hand, the variance of the quadratures is (assuming $\varphi = 0$ for simplicity):

$$(\Delta\hat{q}^2)_\xi = \frac{1}{2}e^{2r}, \qquad (\Delta\hat{p}^2)_\xi = \frac{1}{2}e^{-2r} \tag{2.78}$$

In particular, we deduce that squeezed vacuum states are also minimal uncertainty states, but, unlike coherent states, their variance in one quadrature is *squeezed* below the uncertainty of the vacuum, hence their name.

Given the unitary Gaussian transformations that we considered so far, the Bloch-Messiah decomposition allows us to conclude that single-mode squeezers with real parameter ξ, phase shifters and beam splitters with $\phi = 0$ are sufficient to implement any Gaussian unitary transformation. Indeed, for $\varphi = 0$, we have that $\Sigma^{(1)}_\xi = \mathrm{diag}(e^r, e^{-r})$ which is exactly the type of diagonal matrices at the center of the decomposition in Eq.(2.66). Nevertheless, it is often convenient to define another squeezing operation, which can be decomposed in the previous ones.

2.4.5 Two-mode squeezing

Finally, Hamiltonians $\propto (\xi\hat{a}^\dagger_j\hat{a}^\dagger_k + h.c.)$ generate unitary evolutions analogous to the single-mode squeezing, but with the two quanta emitted in different modes, thus taking the name of *two-mode squeezing operations*. In The unitary operator is:

$$\hat{\mathbf{S}}^{(2)}(\xi) := \exp\left\{\xi\hat{a}^\dagger_j\hat{a}^\dagger_k - \xi^*\hat{a}_j\hat{a}_k\right\} \tag{2.79}$$

while the associated symplectic matrix acting on the quadratures is:

$$\Sigma^{(2)}_\xi := \begin{pmatrix} \cosh r\cdot\mathbb{1}_2 & \mathrm{K}_\xi \\ \mathrm{K}_\xi & \cosh r\cdot\mathbb{1}_2 \end{pmatrix} \tag{2.80}$$

with the 2×2 matrix K_ξ defined as in Eq.(2.75) and again $\xi = re^{i\varphi}$.

The action of $\hat{\mathbf{S}}^{(2)}(\xi)$ on the two-mode vacuum produces the so-called *twin beam states* (TWB):

$$\hat{\mathbf{S}}^{(2)}(\xi)|0,0\rangle = \sqrt{1-\tanh^2 r}\sum_{n=0}^{+\infty} e^{in\varphi}(\tanh r)^n|n,n\rangle \tag{2.81}$$

These states show perfect correlations in the Fock basis and, if a photon counter is at disposal, they can be used to herald pure Fock states. Also, the partial trace of a twin-beam state over one mode is a thermal state, which has the maximal Von Neumann entropy at fixed energy: for this reason, twin-beam states are maximally entangled at their given energy. In the limit of very large squeezing, $r\to\infty$, they approximate *Einstein-Podolski-Rosen (EPR) states*[12], considered in the homonymous *gedanken* experiment [125], which

[12] Apart for a local phase rotation

are common eigenstates of $\hat{q}_1 + \hat{q}_2$ and $\hat{p}_1 + \hat{p}_2$ with eigenvalue 0.

2.4.6 Williamson decomposition of the covariance matrix

The decomposition that we discussed in Theorem 2.3 applies to any positive-definite $2n \times 2n$ matrix, therefore it applies in particular to the covariance matrix σ of *any* quantum state. This means that we can decompose the CM as:

$$\sigma \;=\; \mathrm{S}^T \left(\bigoplus_{j=1}^{n} d_j \mathbb{1}_2 \right) \mathrm{S} \tag{2.82}$$

where S is a symplectic matrix, so that $\mathrm{S}^T \Omega \mathrm{S} = \Omega$ and $d_j \in \mathbb{R}$ are the *symplectic eigenvalues* of σ. We can then rewrite the uncertainty relation Eq.(2.62) as:

$$\sigma + \frac{i}{2}\Omega \geq 0 \implies \mathrm{S}^T \left(\bigoplus_{j=1}^{n} d_j + \frac{i}{2}\Omega \right) \mathrm{S} \geq 0 \implies \bigoplus_{j=1}^{n} d_j + \frac{i}{2}\Omega \geq 0 \tag{2.83}$$

the last equation then decomposes in several mode-by-mode conditions, each of which implies $d_j \geq \frac{1}{2}$. Thus, the uncertainty relations are fully equivalent to the condition that the symplectic eigenvalues of the CM are $\geq \frac{1}{2}$. It can be shown that the symplectic eigenvalues can be computed as the standard eigenvalues of the Hermitian matrix $i\Omega\sigma$.

2.5 Gaussian channels

If we depart from unitary evolutions, we can still consider the family of CP(TP) linear maps that preserve the set of Gaussian states. Also in this case, for CPTP maps it is possible to provide a full characterization of their action in terms of how they transform the CM and mean field of a generic input Gaussian state. Let us recall that trace-preserving CP maps are *deterministic*, in the sense that they can be implemented without the need of post-selection. In particular, CPTP Gaussian maps (Gaussian channels from now on) all arise, at least in principle, from an unitary coupling generated by a quadratic Hamiltonian with an ancillary system (or environment) in a Gaussian state, followed by partial tracing over the ancillary space. In terms of their action on the CM and mean field, the following theorem holds:

Theorem 2.5.1

Given an initial Gaussian state with covariance matrix σ and mean field (first-moments) vector $\vec{R}$, the action of a Gaussian channel on it is completely described in terms of two $2n \times 2n$ real matrices X and Y and a vector $\vec{r}_0 \in \mathbb{R}^{2n}$ transforming the moments according to:

$$\sigma \;\mapsto\; \mathrm{X}\sigma\mathrm{X}^T + \mathrm{Y} \tag{2.84}$$

$$\vec{R} \;\mapsto\; \mathrm{X}\cdot\vec{R} + \vec{r}_0 \tag{2.85}$$

The matrices X and Y must satisfy:

$$\mathrm{Y} + \frac{i}{2}\Omega \;\geq\; \frac{i}{2}\mathrm{X}\Omega\mathrm{X}^T \tag{2.86}$$

Conversely, any two matrices X and Y satisfying the condition above and acting as in Eq.(2.84) define a Gaussian quantum channel.

Notice that if X is the identity matrix, the only effect of the Gaussian channel is to *add noise*: to see this, one can notice that the action of a Gaussian channel $\mathbf{\Phi}$ with $\mathrm{X} = \mathbb{1}$ and $\mathrm{Y} > 0$ can be generated by displacing the input state with random displacing vectors $\vec{r}$ distributed according to a Gaussian distribution with CM Y:

$$\mathbf{\Phi}_{\mathrm{Y}}(\hat{\boldsymbol{\rho}}_G) \;=\; \int_{\mathbb{R}^{2n}} \mathrm{d}^{2n}r' \, \frac{e^{-\frac{1}{2}\vec{r'}^T \mathrm{Y}^{-1}\vec{r'}}}{\pi^n\sqrt{\det \mathrm{Y}}} \, \hat{\mathbf{D}}(\vec{r'})\hat{\boldsymbol{\rho}}_G\hat{\mathbf{D}}^\dagger(\vec{r'}) \tag{2.87}$$

Actually, this fact relies on a more general property of Gaussian states. Consider a $\hat{\boldsymbol{\rho}}_G$ with CM σ and first moments vector $\vec{r}_0$. By Williamson decomposition, there will exist a symplectic matrix S such that $\sigma - \frac{1}{2}\mathrm{S}^T\mathrm{S} \geq 0$, i.e. there exists a positive matrix Y such that $\sigma = \mathrm{Y} + \frac{1}{2}\mathrm{S}^T\mathrm{S}$. Since the second contribution is equivalent to the action of a symplectic unitary on vacuum, the Wigner function of $\hat{\boldsymbol{\rho}}_G$ can decomposed as follows:

$$W[\hat{\boldsymbol{\rho}}_G](\vec{R}) \;=\; \int_{\mathbb{R}^{2n}} \mathrm{d}^{2n}r \; e^{-\frac{1}{2}(\vec{R}-\vec{r})^T \mathrm{Y}^{-1}(\vec{R}-\vec{r})} \, W_0\left(\mathrm{S}^{-1}\vec{R} - \vec{r}\right) \tag{2.88}$$

where $W_0(\vec{R})$ is the Wigner function of the vacuum state. In other words, any Gaussian state can be prepared from the vacuum by first acting with a symplectic unitary transformations and then applying a noisy Gaussian channel with $\mathrm{X} = \mathbb{1}$.

2.6 Two-mode Gaussian states

If we consider just two modes, we can highlight many features of CV quantum information and study bipartite quantum correlations in a fairly general setting, without having to use too heavy notations. Let us label with the letter A (for Alice) the first mode, corresponding to operators $\hat{a}, \hat{a}^\dagger$, and with the letter B the second mode with operators $\hat{b}, \hat{b}^\dagger$. The most general bipartite Gaussian quantum state is characterized by 14 parameters: 10 of them coming from the symmetric 4×4 covariance matrix σ and the residual 4 defining the mean field $\langle\hat{\mathbf{R}}\rangle$. This vector influences the outcomes of most CV quantum measurements, but it does not interfere with properties such as entanglement or nonclassicality,

that are fully determined by the CM. Since σ is symmetric, it can be written in 2×2 block form:

$$\sigma \;=\; \begin{pmatrix} \mathrm{A} & \mathrm{C} \\ \mathrm{C}^T & \mathrm{B} \end{pmatrix} \tag{2.89}$$

From the point of view of quantum correlations, we can group different covariance matrices into equivalence classes related by *local* unitary transformations on each mode, i.e. by transformations of the type $\hat{\mathbf{U}}_A \otimes \hat{\mathbf{U}}_B$ acting on the bipartite state $\hat{\boldsymbol{\rho}}_{AB}$. Specifically, Local Unitary Gaussian Transformations (LGUTs) arise when $\hat{\mathbf{U}}_A$ and $\hat{\mathbf{U}}_B$ are unitaries generated by quadratic Hamiltonians in $\hat{a}, \hat{b}, \hat{a}^\dagger, \hat{b}^\dagger$. The corresponding symplectic transformations on the quantum phase space are of the form $\mathrm{S}_A \oplus \mathrm{S}_B \in \mathrm{Sp}(2) \oplus \mathrm{Sp}(2)$. Under LGUTs, one can identify *symplectic invariants* of the CM:

$$I_1 \;:=\; \det[\mathrm{A}], \quad I_2 \;:=\; \det[\mathrm{B}], \quad I_3 \;:=\; \det[\mathrm{C}], \quad I_4 \;:=\; \det[\sigma] \tag{2.90}$$

By exploiting these local transformations, some of the 10 parameters of the original CM can be eliminated. More in detail:

- 2 real parameters coming from the phase-shifts (or free evolutions) of each mode, of the form $\hat{\mathbf{U}}_\theta = e^{-i\theta \hat{a}_k^\dagger \hat{a}_k}$. This can be chosen so that the corresponding S_A and S_B, which are orthogonal in this case[13], diagonalize the A and B blocks respectively.
- 2 real parameters coming from single-mode squeezing (with no phases). They can be chosen to set the upper left and lower right 2×2 blocks proportional to the identity.
- 2 real parameters from another couple of orthogonal matrices, $V_1, V_2 \in O(2)$, to diagonalize the nondiagonal 2×2 blocks[14].

We are left with $10 - 6 = 4$ real parameters, with which we can parametrize the CM in *canonical form* [99]:

$$\sigma \;=\; \begin{pmatrix} a & 0 & c_1 & 0 \\ 0 & a & 0 & c_2 \\ c_1 & 0 & b & 0 \\ 0 & c_2 & 0 & b \end{pmatrix} \tag{2.91}$$

Note that, since for the canonical form:

$$I_1 \;=\; a^2, \quad I_2 \;=\; b^2, \quad I_3 \;=\; c_1 c_2, \quad I_4 \;=\; (ab - {c_1}^2)(ab - {c_2}^2) \tag{2.92}$$

and these are symplectic invariants for $\mathrm{Sp}(2) \oplus \mathrm{Sp}(2)$, it follows that a, b, c_1, c_2 are completely determined from the values of I_1, I_2, I_3, I_4, thus allowing to easily construct the canonical form of any 4×4 CM (up to a common sign flip of the c_i).

Finally, we quote the form of the symplectic eigenvalues $d_\pm$ of the covariance matrix σ in Eq.(2.89), in terms of its symplectic invariants:

$$d_\pm \;=\; \sqrt{\frac{\Delta(\sigma) \pm \sqrt{\Delta(\sigma)^2 - 4I_4}}{2}}, \qquad \Delta(\sigma) \;=\; I_1 + I_2 + 2I_3 \tag{2.93}$$

[13] Recall that $O(2) \subset \mathrm{Sp}(2)$

[14] They do not mess up with A and B blocks because they are already diagonal at this stage.

According to Williamson's theorem and the invariance of the Uncertainty relation under symplectic transformations, they satisfy $d_\pm \geq \frac{1}{2}$ and they are in fact equal to the diagonal elements of the CM of the unique bipartite thermal state related to σ by symplectic diagonalization.

2.6.1 Two-mode squeezed thermal states

A commonly studied class of two-mode Gaussian states are so-called *two-mode squeezed thermal states*:

$$\hat{\boldsymbol{\rho}}_{\text{TMST}} \;:=\; \hat{\mathbf{S}}^{(2)}(\xi)\;\left[\hat{\boldsymbol{\nu}}_{th}(N_1)\otimes\hat{\boldsymbol{\nu}}_{th}(N_2)\right]\;\hat{\mathbf{S}}^{(2)}(\xi)^\dagger \tag{2.94}$$

where, as before:

$$\hat{\mathbf{S}}^{(2)}(\xi) \;:=\; e^{\xi\hat{a}^\dagger\hat{b}^\dagger-\xi^*\hat{a}\hat{b}}\,, \qquad\qquad \xi:=re^{i\varphi} \tag{2.95}$$

We can explicitly calculate the form of the CM of a generic two-mode squeezed bipartite thermal state using Eq.(2.82) with $\mathbf{S}'=\Sigma_\xi^{(2)}$ given by Eq.(2.80) and $d_k = N_k+\frac{1}{2}$ for $k=1,2$. The result, assuming $\xi=r\in\mathbb{R}$ for neatness, is:

$$\sigma_{\text{TMST}} \;=\; \begin{pmatrix} a\,\mathbb{1}_2 & c\,\sigma_z \\ c\,\sigma_z & b\,\mathbb{1}_2 \end{pmatrix} \tag{2.96}$$

where $\sigma_z=\mathrm{diag}(1,-1)$ is the third Pauli matrix and:

$$\begin{cases} a \;:=\; \dfrac{1+N_1+N_2}{2}\cosh 2r \;+\; \dfrac{N_1-N_2}{2} \\ b \;:=\; \dfrac{1+N_1+\;N_2}{2}\cosh 2r \;-\; \dfrac{N_1-N_2}{2} \\ c \;:=\; \dfrac{1+N_1+N_2}{2}\sinh 2r \end{cases} \tag{2.97}$$

while the first-moments vector is zero, since no displacement is present. In particular, the CM is in canonical form (this is the main reason to choose $r\in\mathbb{R}$).

From now on we shall call two-mode squeezed thermal states, or more often TMST states, those whose CM is described by Eq.(2.96) and Eq.(2.97) with real two-mode squeezing parameter $r\in\mathbb{R}$ and, possibly, an arbitrary first-moments vector. The reason to restrict ourselves to this class of states is that they have a manageable number of free parameters while still comprising both entangled *and* separable states.

2.7 Gaussian measurements on Gaussian states

When it comes to measuring Gaussian states, it is natural to define a class of POVMs that respects their structure: when measuring a Gaussian states, their outcome should be distributed according to a (possibly degenerate) Gaussian distribution and the updated state after the measurement should still be Gaussian. The Gaussian positive operator-valued measures (POVM) respecting these requests are collections $\left\{\hat{\mathbf{\Pi}}_\alpha\right\}_{\alpha\in\mathcal{Q}}$ of positive Hermitian operators that sum to the identity operator and whose characteristic functions (or, equivalently, their Wigner functions) are Gaussians: in other words, they are

continuously labelled sets of non-normalized Gaussian states resolving the identity. In particular, the CM of each Gaussian effect $\hat{\mathbf{\Pi}}_\alpha$ has to satisfy the Uncertainty Relation 2.62.

We will focus just on single-mode measurements, for which the most general Gaussian POVM element is easily written as:

$$\hat{\mathbf{\Pi}}_\alpha \;=\; \frac{1}{\pi}\,\hat{\mathbf{D}}(\alpha)\,\hat{\boldsymbol{\rho}}_M\,\hat{\mathbf{D}}^\dagger(\alpha) \qquad \begin{cases} \alpha \in \mathbb{C} \\ \hat{\mathbf{D}}(\alpha) \;=\; e^{\alpha\hat{a}^\dagger - \alpha^*\hat{a}} \end{cases} \tag{2.98}$$

where $\hat{\mathbf{D}}(\alpha)$ is the usual displacement operator and $\hat{\boldsymbol{\rho}}_M$ is a single-mode Gaussian state with zero first-moments vector. In terms of the modified characteristic function, then:

$$\tilde{\chi}\left[\hat{\mathbf{\Pi}}_\alpha\right]\left(\vec{\Lambda}\right) \;=\; \frac{1}{\pi}\exp\left\{-\frac{1}{2}\vec{\Lambda}^T\sigma_M\,\vec{\Lambda} \;-\; i\vec{\Lambda}^T\,\vec{X}(\alpha)\right\} \qquad \vec{\Lambda} \;:=\; \begin{pmatrix} q \\ p \end{pmatrix} \tag{2.99}$$

where $\vec{X}(\alpha) = (\lambda_1, \lambda_2)^T$, $\alpha = \frac{1}{\sqrt{2}}(\lambda_1 + i\lambda_2)$ is the outcome of the measurement, which appears in the first-moments vector only, and σ_M is the CM of $\hat{\boldsymbol{\rho}}_M$. Notice that the outcome α can be complex because it is not forced to be the eigenvalue of any Hermitian operator. In particular, there can be non-commuting Hermitian operators having the real and imaginary part of α as eigenvalues respectively, but since we are not restricting ourselves to projective measurements, this does not preclude us from measuring α altogether.

Apart from a displacement, every single-mode Gaussian state is a squeezed thermal state, therefore:

$$\sigma_M \;=\; \sigma^{(1)}(\xi_M)\,\sigma_{th}\,(N_M)\;\sigma^{(1)}\,(\xi_M) \tag{2.100}$$

where $\sigma_{th}(N_M) = (N_M + \frac{1}{2})\mathbb{1}_2$, N_M is an average number of thermal photons, $\sigma^{(1)}(\xi_M)$ is the symplectic transformation corresponding to the single-mode squeezing unitary transformation (2.75) and $\xi_M = r_M e^{i\phi}$ is the single-mode squeezing parameter. This is a consequence of the classification of all Gaussian states combined with the observation that the only single-mode unitary Gaussian operations are free evolution (that we can always ignore by redefining the quadratures), single-mode squeezing and displacement (which does not affect σ_M). Thus, a single-mode Gaussian generalized measurement is characterized by just five real numbers, three of which are in its covariance matrix. Moreover, Gaussian *projective* measurements are obtained whe $N_M = 0$, i.e. when the central Gaussian state $\hat{\boldsymbol{\rho}}_M$ in Eq.(2.98) is a squeezed vacuum state.

The probability of occurrence of the outcome $\alpha \in \mathbb{C}$ upon a single-mode Gaussian measurement described by the POVM $\{\hat{\mathbf{\Pi}}_\alpha\}_{\alpha\in\mathbb{C}}$ on the last mode (without loss of generality) of an n-mode Gaussian state $\hat{\boldsymbol{\rho}}$ is:

$$p_\alpha \;=\; \mathrm{Tr}_{1,\ldots,n}\left[\hat{\boldsymbol{\rho}}\,\left(\mathbb{1}_{n-1}\otimes\hat{\mathbf{\Pi}}_\alpha\right)\right] \tag{2.101}$$

where the trace is performed over the entire Fock space $\mathcal{F}^{(n)}$ of n modes. The conditional state of the remaining $n-1$ modes after the outcome α is observed is instead:

$$\hat{\boldsymbol{\tau}}_\alpha \;=\; \frac{1}{p_\alpha}\mathrm{Tr}_n\left[\hat{\boldsymbol{\rho}}\,\left(\mathbb{1}_{n-1}\otimes\hat{\mathbf{\Pi}}_\alpha\right)\right] \tag{2.102}$$

The phase space formulation via Wigner calculus provides a convenient route to carry on the computation. Let us start from a general bipartite Gaussian state $\hat{\boldsymbol{\rho}}_G$ with CM in 2×2-block form:

$$\sigma \;=\; \begin{pmatrix} \mathrm{A} & \mathrm{C} \\ \mathrm{C}^T & \mathrm{B} \end{pmatrix} \tag{2.103}$$

and zero first-moments vector, subjected to a single-mode Gaussian measurement on its second mode, characterized by a 2×2 CM σ_M and a first-moments vector $\vec{X}(\alpha)$ defined as before. Using the trace rules for the modified characteristic functions of $\hat{\boldsymbol{\rho}}_G$ and $\mathbb{1} \otimes \hat{\boldsymbol{\Pi}}_\alpha$ in Eq.(2.101) we get can compute p_α as:

$$p_\alpha \;=\; \frac{1}{(2\pi)^2} \int_{\mathbb{R}^2 \times \mathbb{R}^2} d^2\Lambda_1 d^2\Lambda_2 \; \tilde{\chi}\left[\hat{\boldsymbol{\rho}}\right](\Lambda_1, \Lambda_2) \; \tilde{\chi}\left[\hat{\boldsymbol{\Pi}}_\alpha\right](-\Lambda_2) \; 2\pi\delta^2(-\Lambda_1) \tag{2.104}$$

where $2\pi\delta(-\Lambda_1)$ arises from the characteristic function of the identity operator of the first mode, $\mathbb{1}^{(1)}$. Inserting Eq.(2.99) for the characteristic function of the measurement and performing the integrals, we finally arrive at:

$$p_\alpha \;=\; \frac{1}{\pi\sqrt{\det\left(\mathrm{B} + \sigma_M\right)}} \exp\left[-\frac{1}{2} X^T(\alpha) \left(\mathrm{B} + \sigma_M\right)^{-1} X(\alpha)\right] \tag{2.105}$$

which is a Gaussian probability density function for $\alpha \in \mathbb{C}$ centered in 0 and with a matrix of covariances given by $(\mathrm{B} + \sigma_M)$. Had we chosen an initial bipartite state with nonzero first-moments vector, this would have simply translated the center of the Gaussian function to the value of the first-moments of the initial state's second mode.

To compute $\hat{\boldsymbol{\tau}}_\alpha$ we use again the trace rules in Eq.(2.102) and then we take the characteristic function:

$$\begin{aligned} \tilde{\chi}\left[\hat{\boldsymbol{\tau}}_\alpha\right](\Lambda_1) \;&=\; \mathrm{Tr}_1\left[\frac{1}{p_\alpha}\mathrm{Tr}_2\left[\hat{\boldsymbol{\rho}}\left(\mathbb{1} \otimes \hat{\boldsymbol{\Pi}}_\alpha\right)\right] e^{-i\Lambda_1^T \hat{\boldsymbol{R}}_1}\right] \;= \\ &=\; \frac{1}{p_\alpha} \int_{\mathbb{R}^2} \frac{d^2\Lambda_2}{2\pi} \; \tilde{\chi}\left[\hat{\boldsymbol{\rho}}\right](\Lambda_1, \Lambda_2) \; \tilde{\chi}\left[\hat{\boldsymbol{\Pi}}_\alpha\right](-\Lambda_2) \;= \\ &=\; \frac{1}{p_\alpha} \int_{\mathbb{R}^2} \frac{d^2\Lambda_2}{2\pi^2} \; \exp\left[-\frac{1}{2}\vec{\Lambda}^T \sigma' \vec{\Lambda} \;+\; i\Lambda_2^T \vec{X}(\alpha)\right] \end{aligned} \tag{2.106}$$

with the following notation:

$$\vec{\Lambda} \;=\; \begin{pmatrix} \Lambda_1 \\ \Lambda_2 \end{pmatrix} \in \mathbb{R}^4, \quad \sigma' \;=\; \begin{pmatrix} \mathrm{A} & \mathrm{C} \\ \mathrm{C}^T & \mathrm{B} + \sigma_M \end{pmatrix}, \quad \vec{X}(\alpha) = \begin{pmatrix} \lambda_1 \\ \lambda_2 \end{pmatrix} \in \mathbb{R}^2 \tag{2.107}$$

and, as usual, $\alpha = \frac{1}{\sqrt{2}}(\lambda_1 + i\lambda_2)$. Introducing the change of variables $\Lambda' = \Lambda_2 + (\mathrm{B} + \sigma_M)^{-1}\mathrm{C}\Lambda_1$, the exponent of the integrand becomes:

$$\begin{aligned} &-\frac{1}{2}\Lambda'^T \left(\mathrm{B} + \sigma_M\right)\Lambda' \;-\; i\Lambda'^T X(\alpha) \;+ \\ &-\frac{1}{2}\Lambda_1^T \left[\mathrm{A} - \mathrm{C}^T\left(\mathrm{B} + \sigma_M\right)^{-1}\mathrm{C}\right]\Lambda_1^T \;-\; i\Lambda_1^T \mathrm{C}^T \left(\mathrm{B} + \sigma_M\right)^{-1} X(\alpha) \end{aligned}$$

After integrating over Λ', the characteristic function of the conditional state is given by:

$$\tilde{\chi}\left[\hat{\boldsymbol{\tau}}_\alpha\right](\Lambda_1) \;=\; \exp\left[-\frac{1}{2}\Lambda_1^T \sigma_c \Lambda_1 - i\Lambda_1^T X_c\right] \tag{2.108}$$

where we defined the conditioned CM and first-moments vector as:

$$\sigma_c \;:=\; \mathrm{A} - \mathrm{C}^T\,(\mathrm{B}+\sigma_M)^{-1}\,\mathrm{C}\,, \qquad X_c \;:=\; \mathrm{C}^T\,(\mathrm{B}+\sigma_M)^{-1}\,X(\alpha) \tag{2.109}$$

We can examine this result introducing the concept of the so-called *Schur complement* (see [126], p. 25).

Definition 2.7.1: Schur complement

Let σ be a $2n \times 2n$ symmetric matrix in block form according to Eq.(2.103). Then, if A is invertible, the *Schur complement* of matrix A in σ is given by:

$$\sigma/\mathrm{A} \;:=\; \mathrm{B} \;-\; \mathrm{C}^T\mathrm{A}^{-1}\mathrm{C} \tag{2.110}$$

and similarly, if B is invertible, the Schur complement of B in σ is:

$$\sigma/\mathrm{B} \;:=\; \mathrm{A} \;-\; \mathrm{C}^T\mathrm{B}^{-1}\mathrm{C} \tag{2.111}$$

Therefore, we can say that the conditional matrix σ_c is precisely the Schur complement of $\mathrm{B}+\sigma_M$ in $(\sigma+\mathbb{1}\oplus\sigma_M)$. The positivity of σ_c is guaranteed by the following theorem [99, 126, 127] [15]:

Theorem 2.7.1: Schur complement

Let σ be a $2n \times 2n$ symmetric matrix in block form according to Eq.(2.103), such that A, B are both invertible. Then σ is positive (semi)definite if and only if one of the two (equivalent) conditions is fulfilled:

- A is positive definite and its Schur complement in σ is positive (semi)definite.
- B is positive definite and its Schur complement in σ is positive (semi)definite.

In our circumstance, given that $\sigma+\mathbb{1}\oplus\sigma_M$ is positive semidefinite, Theorem 2.7 implies that σ_c is too. But the same theorem also implies that σ_c still fulfills the Uncertainty Relations. Indeed, let us consider the following matrix inequalities for σ and σ_M:

$$\begin{aligned} \sigma + \frac{i}{2}\boldsymbol{\omega}_1 \oplus \boldsymbol{\omega}_2 \;&\geq\; 0 \\ \sigma_M - \frac{i}{2}\boldsymbol{\omega}_2 \;&\geq\; 0 \end{aligned} \tag{2.112}$$

Note that the second one is the complex-conjugate (or, equivalently, the transpose) of the Uncertainty Relations for σ_M. Summing them and using the block form, we find:

$$\begin{pmatrix} \mathrm{A} + \frac{i}{2}\boldsymbol{\omega}_1 & \mathrm{C} \\ \mathrm{C}^T & \mathrm{B}+\sigma_M \end{pmatrix} \;\geq\; 0 \tag{2.113}$$

[15] See also *Haynsworth inertia additivity formula* in the mathematical literature.

Using Theorem 2.7 on this last equation, we conclude that the Schur complement of $\mathrm{B}+\sigma_M$ in the above matrix must be positive semidefinite, therefore:

$$\mathrm{A}+\frac{i}{2}\boldsymbol{\omega}_1-\mathrm{C}^T\left(\mathrm{B}+\sigma_M\right)^{-1}\mathrm{C} \;=\; \sigma_c \;+\; \frac{i}{2}\boldsymbol{\omega}_1 \;\geq\; 0 \tag{2.114}$$

so that σ_c satisfies the Uncertainty Relations for mode 1. Thus the conditional state is a legitimate, physical Gaussian state.

Eq.(2.109) also displays a fundamental property: the conditional state CM σ_c *does not depend on the outcome* $\alpha\in\mathbb{C}$ *of the performed measurement*, but only depends upon the CMs of both the initial state and the measurement.

2.7.1 Extremal cases: homodyne and heterodyne measurements

There are at least two important classes of single-mode Gaussian measurements, whose operators are projectors:

- **Homodyne measurements**: These are described by *orthogonal* projections onto the eigenstates of a generic quadrature:

$$\left\{|x_\phi\rangle\langle x_\phi|\right\}_{x\in\mathbb{R}}\;, \qquad \begin{cases}\hat{x}_\phi \;:=\; \cos\phi\,\hat{q}\;-\;\sin\phi\,\hat{p}\\ \hat{x}_\phi|x_\phi\rangle \;=\; x_\phi|x_\phi\rangle\end{cases} \tag{2.115}$$

  The Wigner function of a quadrature-eingenstate projector is a Dirac delta distribution, which can be interpreted as the limit of the linear integral operators generated by increasingly peaked Gaussian functions. Moreover, they do respect the Gaussian character of a multimode state after these measurements have been performed on some of its modes: they are indeed Gaussian measurements. The characteristic function of the homodyne measurement on the quadrature $\hat{x}_\phi$ can still be described by Eq.(2.99), by taking suitable limits on σ_M. With the notation that we are going to introduce in the next session, homodyne measurement on the $\hat{q}$ quadrature, for example, would correspond to the $\mu_{sm}\to 0$ limit[16] of Eq.(2.100) with fixed $\phi=0$, while the one for the $\hat{p}$ quadrature is generated by the same limit, but with $\phi=\pi$. As long as μ_m remains finite, these limits correspond to a diagonal σ_M with one divergent diagonal element whilst the other one is null. As a consequence, inserting the expression for σ_M in Eq.(2.99) and *then* taking the limit, would ultimately yield:

$$\tilde{\chi}\left[|x\rangle\langle x|\right]\left(\vec{\Lambda}\right) \;\propto\; \delta\left(\Lambda_1\right)\,e^{i\Lambda_2\lambda_2} \qquad\Longrightarrow\qquad W\left[|x\rangle\langle x|\right]\left(\vec{X}\right) \;\propto\; \delta\left(X_2-\lambda_2\right) \tag{2.116}$$

  where, again, $\lambda_2=X_2(\alpha)=\sqrt{2}\cdot\mathrm{Im}[\alpha]$. Equivalently, they can be seen as the limits of Eq.(2.100) for infinite squeezing in the $\hat{x}_\phi$ quadrature direction, for any finite $N_M\geq 0$[17]. In the quantum optics setting, experimental implementation of homodyne measurement is approximately possible, for example, by mixing the mode

[16] μ_{sm} is inversely related to the squeezing of the measurement, so that $\mu_{sm}\to 0$ implies infinitely squeezed measurement. μ_m, instead, is the purity of the positive operators of the measurement.

[17] Notice that any finite noise becomes irrelevant in the homodyne limit, so that homodyne measurements are effectively parametrized just by their phases.

to be measured on a balanced beam-splitter with another mode of the same frequency, called the *local oscillator* (LO), excited in a very energetic ($|\alpha| \gg 1$) coherent state $|\alpha\rangle$, such as the ones approximately produced by high-power well-stabilized lasers. The action of the 50/50 beam-splitter on the two modes is described by Eq.(2.72) with $\phi = \frac{\pi}{4}$ and $\theta = 0$, because no additional phases should be introduced. The two output modes are then measured by two photodiodes and the difference between the two photocurrents is seen to approach the values for the measurement of the quadrature, whose phase is dictated by that of $\lambda \in \mathbb{C}$, in the correct limit of infinite energy LO.

- **Heterodyne measurements** These are implemented by *non-orthogonal* projections (hence, truly generalized measurements) onto single-mode coherent states:

$$\left\{\hat{\mathbf{\Pi}}_\alpha\right\}_{\alpha\in\mathbb{C}} \quad := \quad \{|\alpha\rangle\langle\alpha|\}_{\alpha\in\mathbb{C}} \tag{2.117}$$

They are described by Eq.(2.99) with $\sigma_M = \frac{1}{2}\cdot\mathbb{1}_2$, i.e. minimal uncertainties in both quadratures: it is the best approximation, without violating the Uncertainty Relations, to the classical idea of measuring both $\hat{q}$ and $\hat{p}$. The name *heterodyne* stems from the quantum optical experimental implementation of this measurement, which also requires the mixing of the mode to be measured with another mode, but at a different frequency in this case.

2.8 Separability of Gaussian states

For pure bipartite Gaussian states $|\psi_G\rangle\!\rangle$, one can quantify their entanglement by directly computing the Von-Neumann entropy of the partial traces in terms of their CM:

$$S_V\left[\hat{\boldsymbol{\rho}}_A\right] \;=\; f_{VN}\left(\sqrt{\det\sigma_A}\right) \tag{2.118}$$

$$f_{VN}(x) \;:=\; \left(x+\frac{1}{2}\right)\log\left[x+\frac{1}{2}\right] \;-\; \left(x-\frac{1}{2}\right)\log\left[x-\frac{1}{2}\right] \tag{2.119}$$

where $\hat{\boldsymbol{\rho}}_A = \mathrm{Tr}_B\left[|\psi_G\rangle\!\rangle\langle\!\langle\psi_G|\right]$ and σ_A is its covariance matrix; of course, the same result would be obtained taking the trace over subsystem A.

In general, however, having to deal with mixed states, Peres-Horodecki Criterion can be directly used to construct an entanglement monotone for Gaussian states. For a bipartite Gaussian state of two modes, applying a partial transpose on the second mode is equivalent to a mirror reflection of the momentum-like quadrature of that mode, performed by the following matrix acting on quantum phase space:

$$\hat{T}_B \quad\longrightarrow\quad \Delta_B \;:=\; \begin{pmatrix} 1 & 0 & 0 & 0 \\ 0 & 1 & 0 & 0 \\ 0 & 0 & 1 & 0 \\ 0 & 0 & 0 & -1 \end{pmatrix} \;=\; \mathbb{1}_2^A \oplus \mathrm{diag}(1,-1) \tag{2.120}$$

This is a consequence of the fact that transposition coincides with complex conjugation on Hermitian operators, and complex conjugation is in turn equivalent to time-reversal in the Schrödinger equation, that is mechanical inversion of the motion.

Looking back at the characteristic function of a Gaussian state $\hat{\boldsymbol{\rho}}$, the action of the matrix Δ_B corresponds to a change in the covariance matrix of $\hat{\boldsymbol{\rho}}$:

$$\sigma \quad \longrightarrow \quad \tilde{\sigma} \;:=\; \Delta_B\, \sigma\, \Delta_B \tag{2.121}$$

We conclude that the partially transposed Gaussian state is still a legitimate (Gaussian) quantum state if and only if the two necessary and the positivity and the uncertainty inequality on $\tilde{\sigma}$ are met:

$$\begin{cases} \tilde{\sigma} \;\geq\; 0 \\ \tilde{\sigma} \;+\; \dfrac{i}{2}\Omega \;\geq\; 0 \end{cases} \tag{2.122}$$

While it is easy to show that the positivity condition is always satisfied by looking at the eigenvalue equation for $\tilde{\sigma}$, the second condition, imposing the Uncertainty Relations on the partially transposed bipartite state, is nontrivial. Exploiting once again the invariance of the Uncertainty Relation (2.62) under symplectic transformations and the symplectic diagonalization theorem, the second condition is reduced to the requirement that both the symplectic eigenvalues of $\tilde{\sigma}$ should be greater than $\frac{1}{2}$.
To compute the symplectic eigenvalues of $\tilde{\sigma}$, we proceed by steps. As a first thing, we apply Δ_B on both sides to the canonical form Eq.(2.91) and then we compute the new symplectic invariants according to Eq.(2.92):

$$\tilde{I}_1 \;=\; I_1 \qquad \tilde{I}_2 \;=\; I_2 \qquad \tilde{I}_3 \;=\; -I_3 \qquad \tilde{I}_4 \;=\; I_4 \tag{2.123}$$

We then apply Eq.(2.93) to get the desired result:

$$\tilde{d}_{\pm} \;=\; \sqrt{\frac{\Delta(\tilde{\sigma}) \pm \sqrt{\Delta(\tilde{\sigma})^2 - 4I_4}}{2}}, \qquad \Delta(\tilde{\sigma}) \;=\; I_1 + I_2 - 2I_3 \tag{2.124}$$

Since ppt criterion is necessary and sufficient for bipartite Gaussian states and the fulfillment of the Uncertainty Relation for $\tilde{\sigma}$ is necessary and sufficient for the ppt criterion to hold, we can state:

Theorem 2.8.1: Separability criterion for Gaussian states

A bipartite Gaussian state $\hat{\boldsymbol{\rho}}$ is separable if and only if the smallest symplectic eigenvalue $\tilde{d}_-$ of its partially mirror-reflected covariance matrix $\tilde{\sigma}$ is greater or equal to $\frac{1}{2}$. Otherwise, it is entangled.

The amount by which $\tilde{d}_-$ fails to be greater than $\frac{1}{2}$ can be used to quantify Gaussian entanglement:

Definition 2.8.1

The quantity:

$$\epsilon \;:=\; \max\left\{0\,,\; -\log[2\tilde{d}_-]\right\} \tag{2.125}$$

is an entanglement monotone called **entanglement negativity**.

Entanglement negativity attains its minimum value of 0 for all separable states, because for them $\tilde{d}_- \geq \frac{1}{2}$ as said before. At fixed energy expectation value, ϵ is maximal for two-mode squeezed vacuum states among all bipartite Gaussian states. In terms of the symplectic invariants, it is also possible to compute in closed form the entanglement of formation of Gaussian states with respect to some bipartition. In the simple case of TMST states, it can be seen that it is monotone with the entanglement negativity, thus providing the same information.

2.9 Gaussian Quantum Discord

In the Gaussian context, the maximization implicit in the definition of quantum discord, Eq.(1.41) through the classical correlations is naturally restricted to *Gaussian* POVMs. However, for a vast class of Gaussian states, this restriction does not change the result and Gaussian Quantum Discord (GQD) is equivalent to QD for them [128].

In terms of symplectic invariants, GQD can be explicitly computed for two-mode Gaussian states as[90, 129]:

$$\mathcal{D}_{A|B}\left[\hat{\boldsymbol{\rho}}_{AB}\right] \;=\; f_{VN}\left[\sqrt{I_2}\right] \;-\; f_{VN}\left[d_+\right] \;-\; f_{VN}\left[d_-\right] \;+\; f_{VN}\left[\sqrt{E^{min}_{A|B}}\right] \tag{2.126}$$

where:

$$E^{min}_{A|B} \;:=\; \begin{cases} \left[\dfrac{2|I_3| + \sqrt{4I_3^2 + (4I_2-1)(4I_4-I_1)}}{4I_2-1}\right]^2 & \text{if} \quad \dfrac{4(I_1I_2-I_4)^2}{(4I_4+I_1)(4I_2+1)I_3^2} \;\leq\; 1 \\ \\ \dfrac{I_1I_2 - I_3^2 + I_4 - \sqrt{(I_1I_2 - I_3^2 + I_4)^2 - 4I_1I_2I_4}}{2I_2} & \text{otherwise.} \end{cases} \tag{2.127}$$

while f_{VN} is the function introduced in Eq.(2.119) and $d_\pm$ are the two symplectic eigenvalues given in Eq.(2.93).
The first expression in Eq.(2.127) applies, in particular, to TMST states, for which the POVM needed in the maximization is the one corresponding to double-homodyne detection, while the second expression applies when the maximization is achieved through homodyne measurements.

As a final note, it has been shown [90] that bipartite Gaussian states with zero GQD must be *factorized*: in other words, Gaussian states cannot have *purely classical* correlations, they either have some quantum correlations (positive GQD), or they are not correlated at all.

2.10 Limitations of Gaussian quantum information

Gaussian states are limiting cases of the whole set of quantum states of CV systems in many respect [130, 131]. We will list here a few:

- The only states saturating the Heisenberg Inequality for the canonical operators are pure Gaussian states. Equivalently, the covariance matrix of a non-Gaussian state is always strictly greater than that of some pure Gaussian state
- Gaussian states maximize the Von Neumann entropy at fixed CM [132]
- Gaussian states are the least entangled among all states with the same CM

Analogously to the renowned result in statistics, a quantum version of the Central Limit Theorem can be proven, essentially stating that when an asymptotically large number of copies of a generic non-Gaussian state are sampled by an averaged displacement operator, the resulting state is Gaussian (see [131] for the exact statement).

Given its neat theoretical formulation, Gaussian quantum information is an ideal playground to study concepts such as quantum uncertainty and interference, nonclassical aspects of light and quantum metrology, among others. However, there are several quantum phenomena that cannot manifest themselves in a purely Gaussian setting. The root of this limitation is the positivity of the Wigner function, which entails an hidden variable description in terms of phase space coordinates. This is not, however, a *classical* phase space description, because perfectly resolving measurements in quantum phase space do not exist; it has been called an *epistemically restricted classical theory* (or *epistricted theory*) [133], the restriction relying on the symplectic structure of *classical* phase space. Epistricted theories can show entanglement, complementarity, no-cloning, dense coding, teleportation and many other quantum features, but they do not display contextuality nor violations of Bell's inequalities. To clarify this point, it is important to specify that entangled Gaussian states *can* be used to violate Bell's inequalities and they are indeed often employed to this end, but non-Gaussian measurements (such as photon counting measurements) are required; indeed, in many respects, non-Gaussian measurements are as good as non-Gaussian states as quantum resources.

Another prominent field in which Gaussian quantum information is not sufficient in itself is universal quantum computation (in its continuous-variables formulations [134, 135]). It has been acknowledged for more than 20 years that protocols involving only Gaussian quantum states and Gaussian operations (including measurements) can always be simulated *efficiently* by classical algorithms, thus they are idle for a possible quantum advantage [136]. More specifically, states with Wigner functions attaining negative values are *necessary* for universal quantum computation. It has recently been argued that Wigner negativity is in fact *equivalent* to contextuality for pure states [137], a phenomenon that cannot be displayed by epistricted classical theories.

2.10.1 Some facts about non-Gaussian states

If we consider only pure states, the set of Gaussian states can be characterized in terms of their Wigner functions, thanks to Hudson's Theorem [138, 139]:

Theorem 2.10.1: R. L. Hudson (1974)

Every continuous-variable pure state whose Wigner function is everywhere positive in phase-space is a Gaussian state

Therefore, Wigner negativity and non-Gaussianity are actually the same concept for pure states. At the same time, from a resource-theoretic point of view, it can be shown that universal quantum computation with CV (pure[18]) states can be achieved by adding a single non-Gaussian gate, the cubic gate [134, 135, 140] to the set of unitary Gaussian operations. The situation radically changes when we include mixed states. The definition of Gaussian states (2.3) implies that *any* CV state whose Wigner function is not a Gaussian function in phase-space is automatically non-Gaussian. But this also applies to generic mixtures of Gaussian states sampled according to a non-Gaussian (classical) probability distribution, therefore it does not reflect any quantum property of these states. The logical consequence is to introduce the following definition:

Definition 2.10.1: Quantum non-Gaussianity

A state $\hat{\boldsymbol{\rho}}$ of a CV bosonic system of n modes is *quantum non-Gaussian* if it cannot be written as a convex combination of Gaussian states

Clearly, without loss of generality, one can assume that the Gaussian states in the convex decomposition are pure. A further difference from the pure case is due to the fact that quantum non-Gaussian states can still have a Wigner function which is positive everywhere, an example is the mixture of the vacuum state and the first Fock state:

$$\hat{\boldsymbol{\rho}}_\eta \;=\; (1-\eta)|0\rangle\langle 0| \;+\; \eta|1\rangle\langle 1| \tag{2.128}$$

which is quantum non-Gaussian for $\eta \geq 0.476$ and it has a positive Wigner function for $\eta < \frac{1}{2}$. Given this diverse and complex scenario, it is desirable to have at our disposal some functionals quantifying the non-Gaussianity (and, possibly, only the *quantum* non-Gaussianity) of non-Gaussian states. We should stress that this is necessary for two reasons, each of which requires its own set of approaches: on the one hand, it is theoretically useful to give structure and organize the wild variety of non-Gaussian states, perhaps defining a hierarchy among them and linking them to resource theories; on the other hand, we would like to be able to *certify* quantum non-Gaussianity, or even just Wigner negativity, in an experimental setting where the full knowledge of the Wigner function is difficult to obtain and it is often plagued by large errors. This second step is of course of utmost importance if one aspires at applying the resource of non-Gaussianity to tasks such as CV quantum computation. Among the theoretical measures of non-Gaussianity we mention the ones based on the Hilbert-Schmidt distance [141] and on the quantum relative entropy [142], where in both cases the idea is to use a distance on the space of states and to measure it between the purported non-Gaussian state and the closes Gaussian one, which is often the unique Gaussian state having the same CM and mean-field vector of the non-Gaussian state at stake [143]. Wigner negativity can be quantified via the negative volume [144] and related measures, if a full knowledge of the Wigner function is available. On the other hand, quantifiers based on the value of the Wigner function at the origin or on the conditional entropy with respect to the reference Gaussian states are amenable to experimental applications [145, 146]. In the multi-mode context, and particularly for photon-added and photon-subtracted states, more specific protocols have been advanced [147, 148, 149]. As for quantum non-Gaussianity, perhaps the most powerful theoretical tool to characterize this property is the stellar rank [150], while several witnesses were devised independently [151, 152, 153].

[18] In theoretical quantum computation, pure states are almost always the standard, while mixed states are mainly used when noise modeling is considered.

CHAPTER 3

Gaussian Quantum Steering

The term *steering* in quantum mechanics was initially introduced by E. Schrödinger in 1935 [154] in relation to the Einstein-Podolski-Rosen paradox [125], regarding his realisation that quantum correlations could be used to remotely modify, or *steer*, a distant quantum state by acting on its correlated party. It later became clear that quantum correlations respect *causality*: no local experiment can detect any instantaneous influence deriving from operations on a (quantum) correlated, distant subsystem: only *correlated results*, to be later compared by bringing the two observes together, can unveil the correlations. In 2007, H. Wiseman et al. [155, 156] introduced the modern definition of quantum steering as a quantum correlation that is more stringent than entanglement, but not as demanding as Bell's nonlocality [157]: in their construction, that we shall review in Section 3.1, quantum steering arises from the impossibility of finding a local hidden variable description *of one side* of a bipartite state when local measurements are performed on the other side. Going far beyond its original role in the foundational aspects of quantum mechanics, quantum steering is nowadays considered a relevant quantum resource, e.g. for cryptographic tasks such as one-sided device-independent quantum key distribution [158] and in the remote preparation of exotic quantum states, such as nonclassical or even non-Gaussian states of the electromagnetic field. In this Chapter, we will first present a detailed exposition of the notion of quantum steering arising from a task involving two parties, highlighting a number of subtleties in the form of hidden assumptions in the standard presentations and finally arriving to the formulation in terms of assemblages. In Section 3.2 we specialize these concepts to Gaussian steering for continuous-variable systems, connecting it to the EPR paradox; in an apparent change of direction, in Section 3.3 we tackle the problem of remote generation of nonclassicality with two-mode Gaussian states and we arrive at the conclusion that it is very intimately related with EPR steering. Finally, in Section 3.4 we apply a measure of EPR steering to the problem of quantifying the non-Markovianity of a Gaussian quantum channel known as the Quantum Brownian Motion channel, assuming different spectral functions that characterize the corresponding thermal environment.

3.1 The notion of quantum steering: checking an untrusty device

To introduce the modern definition of quantum steering we will construct a step-by-step scenario in which two parties, Alice and Bob, share a purported quantum state $\hat{\boldsymbol{\rho}}_{AB}$ and Bob's measurement apparatus is deemed untrustworthy. The bipartite state is generated by a black box with two outputs, A and B, that should emit repeatedly the *declared, entangled quantum state* $\hat{\boldsymbol{\rho}}_{AB}$, such that subsystem A goes to Alice and subsystem B goes to Bob. They both know the declared state $\hat{\boldsymbol{\rho}}_{AB}$, but they do not trust the black box.

Moreover, they both have "universal" measuring devices that should be able to perform any quantum measurement on their subsystems, but Bob's device cannot be trusted for whatever reason. Their task is to check that the actual states outputted by the black box are indeed entangled, for example because they would like to later use them for a quantum cryptography protocol.

Suppose that Bob sets his device to measure the observable X on his subsystem. Then, if everything is right, he must get the possible results b according to a probability distribution given by:

$$p_X(b) \;=\; \mathrm{Tr}_{AB}\left[\left(\mathbb{1}_A \otimes \hat{\mathbf{\Pi}}_b^X\right)\hat{\boldsymbol{\rho}}_{AB}\right] \tag{3.1}$$

where $\hat{\mathbf{\Pi}}_b^X$ is the POVM element corresponding to a measurement of the observable X resulting in the outcome b. If he does not get the expected probability for any choice of observable, then he will know that either the black box, his device, or both are corrupted. Let us suppose, therefore, that this first test passes, that is, all probabilities Bob computes with Eq. (3.1) are correct. Of course, this is not enough to trust the "black box plus Bob's measurement device" assembly, because we are only accessing local degrees of freedom of subsystem B of the purported state $\hat{\boldsymbol{\rho}}_{AB}$. Alice can do the same with her subsystem and, since her device is trustworthy, she would conclude that her subsystem is correctly described by $\hat{\boldsymbol{\rho}}_A = \mathrm{Tr}_B\hat{\boldsymbol{\rho}}_{AB}$. Still, many states besides $\hat{\boldsymbol{\rho}}_{AB}$ can have the correct partial traces, without actually being equivalent to $\hat{\boldsymbol{\rho}}_{AB}$: Alice and Bob must now check *correlations* between their subsystems. If also Bob's device were trustworthy, they could simply do a full tomography and verify if the black box is actually able to prepare the purported state. However, with our assumptions, they should find another way. After a little thought, they come up with the following idea: if the state outputted by the black box is really entangled, and if Bob's device works fine, then a measurement on subsystem B should change the quantum state of subsystem A conditioned upon the outcome of the measurement. Alice cannot immediately check that this influence took place, by the no-signaling theorem, but she can do that if Bob tells her the measurement outcome he found; indeed, if he measures X and gets b, Alice predicts that her quantum state will be:

$$\hat{\boldsymbol{\rho}}_{A|b,X} \;=\; \frac{1}{p_X(b)}\mathrm{Tr}_B\left[\left(\mathbb{1}_A \otimes \hat{\mathbf{\Pi}}_b^X\right)\hat{\boldsymbol{\rho}}_{AB}\right] \tag{3.2}$$

where $p_X(b)$ is correctly given by Eq.(3.1), as previously certified. Now, if $\hat{\boldsymbol{\rho}}_{AB}$ is separable, we could write it as:

$$\hat{\boldsymbol{\rho}}_{AB} \;=\; \int d\lambda\, p(\lambda)\hat{\boldsymbol{\rho}}_{A,\lambda} \otimes \hat{\boldsymbol{\rho}}_{B,\lambda} \tag{3.3}$$

where the integral sign is symbolic and possibly includes discrete sums and $p(\lambda)$ is a probability distribution. In that case, we can define $p_X(b|\lambda) = \mathrm{Tr}\left[\hat{\mathbf{\Pi}}_b^X\hat{\boldsymbol{\rho}}_{B,\lambda}\right]$ and we can write:

$$\hat{\boldsymbol{\rho}}_{A|b,X} \;=\; \frac{1}{p_X(b)}\int d\lambda p(\lambda)p_X(b|\lambda)\hat{\boldsymbol{\rho}}_{A,\lambda} \;=\; \int d\lambda p(\lambda|b,X)\hat{\boldsymbol{\rho}}_{A,\lambda} \tag{3.4}$$

The last step was derived by applying Bayes theorem and *defining* $p(\lambda|b,X)$ to be the probability that a particular value of λ described the initial factorized state, upon measuring X on Bob's subsystem and getting the result b. Eq.(3.4) is a local hidden state (LHS) model on Alice's side, since it implies that Alice gets states $\hat{\boldsymbol{\rho}}_{A,\lambda}$ at each run, according to the probability distribution $p(\lambda)$, and then she makes a Bayesian update to

$\hat{\boldsymbol{\rho}}_{A|b,X}$ after being reported the outcome b from Bob: as far as she is concerned, there was no "action at a distance" but simply an updated knowledge of the hidden variable λ that specifies the quantum state of his subsystem. It must be stressed that Bayes theorem not always applies in quantum mechanics, and the operative meaning of the probability $p(\lambda|b, X)$ can be obscure with our assumptions. However, this is not problematic for us: we are defining that probability from measurable quantities and we only care that it *is* a probability distribution, which is immediately checked. We now come to the final, key point: there exist *entangled* quantum states $\hat{\boldsymbol{\rho}}_{AB}$ such that the corresponding *conditional* states $\hat{\boldsymbol{\rho}}_{A|b,X}$ on Alice's side cannot be described by a single LHS model as in Eq.(3.4) for all possible choices of measurements X on Bob's side. With such states, even if they cannot trust neither the black box that prepares them nor Bob's measurement apparatus, they can check that the shared state is entangled by picking appropriate choice of measurements X on Bob's side and checking that Alice's conditional states are the expected $\hat{\boldsymbol{\rho}}_{A|b,X}$. These states are called *steerable by Alice*. Notice that we proved that separable states cannot be steerable, therefore also that steering implies entanglement. However, it turns out that a generic entangled state $\hat{\boldsymbol{\rho}}_{AB}$ *could* have a LHS model for Bob's conditional states and for all possible measurements on Alice's side: not all entangled states are steerable [156]. Notice also that the LHS model does not require us to trust Bob's apparatus: we simply ask if there can be *any* two probability distributions $p_X(b|\lambda)$ and $p(\lambda)$ and ensemble $\hat{\boldsymbol{\rho}}_{A,\lambda}$ of density operators making Eq.(3.4) work, with the constraint that $\int d\lambda p_X(b|\lambda) = p_X(b)$ but with no further requests on how the stochastic map $p_X(b|\lambda)$ was derived. It is worth mentioning that in the original formulation and standard expositions one considers Bob as the agent who also prepares the bipartite states $\hat{\boldsymbol{\rho}}_{AB}$ and he is untrustworthy altogether: Alice only trusts the fact that what she measures respects quantum mechanics, but she does not trust any claim by Bob; Bob will communicate his purported outcomes b at each run and Alice is free to either check at each time that the *unconditional* state is always $\hat{\boldsymbol{\rho}}_A$ *or* that, taking into account Bob's datum b, her state is actually influenced by such an outcome. If she finds that the unconditional states are always the same, but that the correlation with Bob's outcome is such that the states $\hat{\boldsymbol{\rho}}_{A|b,X}$ cannot arise from a local hidden state model on her side, then she will be convinced that Bob is really preparing bipartite entangled states and he is sending her one half of them. To be fully redundant: as far as Alice is concerned, the state $\hat{\boldsymbol{\rho}}_{A|b,X}$ is simply *whatever state she gets each time Bob's claim to have measured X and obtained the outcome b*: she does not trust that, but she simply reconstructs the states associated with each one of Bob's reported data $\{b, X\}$, e.g. by tomography. It is Bob's task, then, to chose the most convenient set of observables $X_1, X_2...$ such that the corresponding conditional states on Alice's side do not admit a LHS model.

There are still some hidden assumptions in this picture. A crucial one is that the probability $p(\lambda)$ according to which the black box prepares the factored state $\hat{\boldsymbol{\rho}}_{A,\lambda} \otimes \hat{\boldsymbol{\rho}}_{B,\lambda}$ at each run *does not depend on the choice of measurement X* on Bob's side. If the black box were controlled by Bob, for example, this would require that *it is Alice to decide what measurement she would like him to perform*, and that she makes her decision only *after* she got her part of the state. If Alice does not believe any assumption about what kind of states $\hat{\boldsymbol{\rho}}_{AB}$ can be prepared by the black box, it is simple to argue that it is indeed *necessary* for Alice to ask Bob to perform multiple types of *mutually incompatible* measurements. To show that, it is sufficient to consider a pure entangled state which can be expanded in

two different orthonormal, factorized bases:

$$\sum_n c_n |\phi_n\rangle_A \otimes |u_n\rangle_B = \sum_m d_m |\psi_m\rangle_A \otimes |v_m\rangle_B \tag{3.5}$$

If Bob were to measure his state in the same $\{|u_n\rangle\}$ basis at each run, Alice would simply get a random state from the ensemble $\sum_n c_n^2 |\phi_n\rangle\langle\phi_n|$, and Bob's outcome would tell her the actual value of n for that particular run. Clearly, these observations can be explained also by classical correlations, and they would not convince Alice that the original state was indeed entangled. On the other hand, if Alice can ask him to measure in the $\{|v_m\rangle\}$ basis on some of the runs, she could check that in those cases she gets different conditional states, drawn from the same ensemble (since the partial trace must be the same) being resolved in a different way by Bob's outcomes. In the following, we will see that if Alice accepts some assumptions about what kind of states $\hat{\boldsymbol{\rho}}_{AB}$ can be generated by the black box, it can become unnecessary for her to choose Bob's measurement: Bob can choose a single observable to be measured on his subsystem at each run to convince her that the output state of the black box, among those she considers possible, is an entangled one.

Before proceeding further, we should formalise our conclusions with a few definitions [155, 156, 159]:

Definition 3.1.1: Quantum Steering and Steering assemblages

Let $\hat{\boldsymbol{\rho}}_{AB}$ a quantum state of a bipartite quantum system with underlying Hilbert space $\mathcal{H}_A \otimes \mathcal{H}_B$. Given a projection-valued measure $\{\hat{\mathbf{\Pi}}_b^X\}_{b\in\Lambda_X}$, labelled by X, with outcomes in $\Lambda_X \subseteq \mathbb{R}$ and acting on $\mathcal{H}_B$, the following set of *non-normalized quantum states* in $\mathcal{T}(\mathcal{H}_A)$:

$$\left\{\tilde{\hat{\boldsymbol{\rho}}}_{A|b,X} := \mathrm{Tr}_B\left[\left(\mathbb{1}_A \otimes \hat{\mathbf{\Pi}}_b^X\right)\hat{\boldsymbol{\rho}}_{AB}\right]\right\}_{b\in\Lambda_X} \tag{3.6}$$

is called a *steering assemblage* for subsystem A.

A steering assemblage is said to admit a *local hidden state (LHS) model* if there exists a probability distribution $p(\lambda)$ and a set of states $\hat{\boldsymbol{\rho}}_{A,\lambda}$ such that:

$$\hat{\boldsymbol{\rho}}_A := \mathrm{Tr}_B\left[\hat{\boldsymbol{\rho}}_{AB}\right] = \int d\lambda p(\lambda)\hat{\boldsymbol{\rho}}_{A,\lambda} \tag{3.7}$$

$$\forall b \in \Lambda_X : \quad \tilde{\hat{\boldsymbol{\rho}}}_{A|b,X} = \int d\lambda\, p(\lambda) p_X(b|\lambda)\hat{\boldsymbol{\rho}}_{A,\lambda} \tag{3.8}$$

for *some* X-dependent and λ-dependent probability distribution $p_X(b|\lambda)$ over the space of outcomes Λ_X.

If there exists a set of PVMs $\{X_1, ..., X_n\}$ such that the corresponding steering assemblages do not admit *a unique* LHS model $\{p(\lambda), \hat{\boldsymbol{\rho}}_{A,\lambda}\}$ on subsystem A, we say that the state $\hat{\boldsymbol{\rho}}_{AB}$ is $B \to A$ *quantum steerable*.

As it is clear from these definitions, quantum steering is an *asymmetric* form of quantum correlation [160, 161, 162]: a bipartite state can be $B \to A$ steerable and not $A \to B$

steerable, or vice-versa. Of course, it can also be two-way steerable. Moreover, since the whole scenario to check $B \to A$ steerability can be framed in terms of Bob trying to convince Alice that they share an entangled state, it is clear that quantum steering (in either direction) is a stronger correlation than quantum entanglement [157], while it is necessarily weaker than Bell's nonlocality since a Bell test would convince *both* Alice and Bob that they share an entangled state without any further assumption. Finally, from a computational perspective, we note that the steerability of a set of assemblages can be judged via semidefinite programming [159, 163].

3.2 EPR steering and Gaussian steering

Considering its roots in the EPR paradox, it is of particular interest to study quantum steering in CV quantum information. Intuitively, the connection can be understood by the following reasoning: imagine that Alice and Bob share an EPR state, such that whenever Bob measures the momentum quadrature of his subsystem and finds the value $\vec{p}$, he immediately knows that Alice's subsystem is now in an eigenstate of her momentum quadrature with eigenvalue $-\vec{p}$, and similarly if he measures the position quadrature finding the value $\vec{q}$, he knows that Alice's subsystem is in the eigenstate of her position quadrature with eigenvalue $-\vec{q}$; Alice can then check, at each run, that her subsystem is in the eigenstate correctly predicted by Bob, but this cannot be compatible with a LHS on her side, since for the local hidden state to describe both the assemblages resulting from Bob measuring $\hat{q}_B$ or $\hat{p}_B$, it would have to violate the Uncertainty Relations. This means that the EPR experiment is effectively a quantum steering task, in the sense described in the previous section.

Let us start by studying CV quantum steering for bipartite Gaussian states. As we discussed in Section 2.7, the (classical and quantum) correlations of any bipartite Gaussian state $\hat{\boldsymbol{\rho}}_{AB}$ are entirely determined by its CM σ, since the first-moments vector can be modified at will by local operations. In the same papers where quantum steering in its modern form was firstly defined [155, 156], it was shown that if a bipartite Gaussian state is steerable, then Gaussian measurements are enough to generate the needed assemblages to prove it. Furthermore, it was proven that a necessary and sufficient condition for steering by Gaussian measurements on Bob's modes is the *violation* of the following matrix inequality:

$$\sigma + \frac{i}{2} \left(\Omega_A \oplus \mathbb{O}_B \right) \geq 0 \tag{3.9}$$

The key idea behind the proof is that Ineq.(3.9) is both necessary and sufficient for the existence of a $2n_A \times 2n_A$ CM for Alice's modes, $\tilde{\sigma}$, which is physical, $\tilde{\sigma} + i\Omega_A/2 \geq 0$ and such that $\sigma_{A,c} - \tilde{\sigma} \geq 0$ for all possible conditional CMs $\sigma_{A,c}$, that is for all possible measurement's covariance matrices σ_M in Eq.(2.109). Then $\tilde{\sigma}$ could be exploited by Bob to concoct an ensemble $\{p_{\vec{\beta}}, \hat{\boldsymbol{\rho}}_{\tilde{\sigma}}^{\vec{\beta}}\}$ that works as an effective LHS on Alice's side. Therefore, if such a matrix $\tilde{\sigma}$ exists, no matter what kind of Gaussian measurement is performed on Bob's modes, Alice won't be convinced that the initial state must have been entangled and, by definition, $\hat{\boldsymbol{\rho}}_{AB}$ is *not steerable* (with Gaussian measurements) by Bob. Conversely, whenever Ineq.(3.9) is *violated* (meaning that the matrix on the left-hand side has at least one negative eigenvalue) there will exist Gaussian measurements such that the corresponding conditional states could not have been simulated by a predetermined ensemble chosen by Bob.

Further intuition on Gaussian steering can be gained by considering the simplest scenario, where $\hat{\boldsymbol{\rho}}_{AB}$ is a two-mode state with mode A sent to Alice and mode B controlled by Bob. Then $\hat{\boldsymbol{\rho}}_{AB}$ is steerable with Gaussian measurements by Bob if and only if there is no physical, unique single-mode covariance matrix $\tilde{\sigma}$ which is *narrower*, with respect to all possible quadrature combinations of Alice's mode, than all the conceivable conditional covariance matrices. In other words, if any Gaussian function in Alice's phase space which is narrower than the Wigner functions of all possible conditional states *at the same time in* $\hat{q}_A$ *and* $\hat{p}_A$ is necessarily *unphysical*, then the state is steerable. Clearly, this relates to the connection with the EPR paradox that we sketched at the beginning of this section: partly due to this reason, and also to clearly distinguish the different steering notions by their names, from now on we will refer to steering with CV quantum systems as *EPR steering*.

3.3 Nonclassical steering

In this section we will define nonclassical steering for two-mode Gaussian states as the process of remotely generating P-nonclassicality on one mode by Gaussian measurements on the other one. We will then compare it to the standard notion of quantum steering to provide an intuition for the relations between these different notions and also to argue for the application of nonclassicality as a witness for quantum steering in continuous-variable systems. Indeed, the necessity for experimentally accessible properties that would allow to demonstrate steering was already pointed out in the original paper [155, 156] and was later addressed by a number of protocols (see [164] and references therein).

Looking at the characteristic function in Eq.(2.60) and assuming a two-mode Gaussian state $\hat{\boldsymbol{\rho}}_{AB}$, it is straightforward to conclude from Eq.(2.34) that the state is nonclassical if and only if the least eigenvalue of σ is smaller than $\frac{1}{2}$. In the following, we will be interested in characterizing how quantum correlations in the joint Gaussian quantum state $\hat{\boldsymbol{\rho}}_{AB}$ may be exploited to influence the nonclassicality of one mode (say B) by Gaussian measurements on the other one (mode A).

Let us assume that the CM of $\hat{\boldsymbol{\rho}}_{AB}$ is in canonical form, as in Eq.(2.91), since LGUTs are not relevant when considering a quantum correlation. The *unconditional state* of mode A, defined either as the state that Alice uses to describe her mode without knowing anything about Bob's mode *or* as the state she assigns to her mode by assuming that Bob has performed some measurement on his mode without letting her know the outcome, is given by $\hat{\boldsymbol{\rho}}_A = \mathrm{Tr}_B\left[\hat{\boldsymbol{\rho}}_{AB}\right]$ and has a CM $\sigma_A = \mathrm{A}$. Since the uncertainty relations imply that $a \geq \frac{1}{2}$ in the canonical form, this means that $\hat{\boldsymbol{\rho}}_A$ must be classical. The same holds true for mode B, thus we may say that given a two-mode Gaussian state $\hat{\boldsymbol{\rho}}_{AB}$ in canonical form, neither of the two modes has any intrinsic nonclassicality. Based on this observation, we can ask whether a two-mode Gaussian state in canonical form can be used to prepare a nonclassical state of one mode by performing a generalized Gaussian measurement on the other mode. We are thereby led to the following definition [165]:

Definition 3.3.1: Weak Nonclassical Steering

A two-mode Gaussian state $\hat{\boldsymbol{\rho}}_{AB}$ in canonical form is *weakly nonclassically steerable* (WNS) from mode B to mode A ($B \to A$) if there exists a Gaussian POVM $\{\hat{\boldsymbol{\Pi}}_\alpha\}_{\alpha\in\mathbb{C}}$ on mode B such that the *conditional state of mode* A

$$\hat{\boldsymbol{\rho}}_{c,\alpha} = \frac{1}{p_\alpha}\mathrm{Tr}_B\left[\hat{\boldsymbol{\rho}}_{AB}\left(\mathbb{1}_A \otimes \hat{\boldsymbol{\Pi}}_\alpha\right)\right] \tag{3.10}$$

is *P-nonclassical*, where $p_\alpha = \mathrm{Tr}_{AB}[\hat{\boldsymbol{\rho}}_{AB}(\mathbb{1}_A \otimes \hat{\boldsymbol{\Pi}}_\alpha)]$ is the probability of observing the outcome $\alpha \in \mathbb{C}$.

One must bear in mind that EPR steering is already a *nonclassical phenomenon*, since it involves quantum correlations whose effects on the steered side cannot be reproduced by any local hidden variable model [155, 156]. Notwithstanding this, we introduce here the term *nonclassical steering* because we are bringing in the additional notion of P-nonclassicality which is conceptually disjoint from the nonclassical character of quantum correlations. Therefore one should not interpret nonclassical steering as a somehow *less classical* variant of EPR steering, but rather as a different phenomenon that aims at capturing the ability to remotely influence P-nonclassicality within correlated CV quantum states. Having settled their definition, let us now deduce a simple criterion to discern weakly nonclassically steerable states:

Lemma 3.3.1

The least classical (i.e. with highest possible nonclassical depth) conditional state $\hat{\boldsymbol{\rho}}_{c,\alpha}$ of mode A attainable with Gaussian measurements on mode B of a two-mode Gaussian state $\hat{\boldsymbol{\rho}}_{AB}$ in canonical form is reached by quadrature detection on mode B, either of the $\hat{q}_B$ quadrature if $|c_2| \geq |c_1|$, or of the $\hat{p}_B$ quadrature otherwise.

The proof of this result can be found in our original works [165, 166] and it relies on a direct computation of the conditional CM through Eq.(2.109) for the most general single-mode Gaussian measurement on mode B. This result can be readily converted into a criterion for WNS by simply using the explicit form of the conditional CM for quadrature measurements on mode B:

Lemma 3.3.2: WNS criterion

A two-mode Gaussian state $\hat{\boldsymbol{\rho}}_{AB}$ in canonical form is WNS ($B \to A$) if and only if the parameters of its CM satisfy:

$$a - \frac{c^2}{b} < \frac{1}{2}, \quad c = \max\{|c_1|, |c_2|\} \tag{3.11}$$

We call this property *weak* nonclassical steering because it does not imply entanglement. Indeed, there are (non isolated) choices for the values of a, b, c_1, c_2 that correspond to physical states ($\sigma > 0$ and fulfilling UR) that are separable and WNS, e.g. $a = b = 13.9$, $c_1 = 4.6$, $c_2 = -13.7$. Besides, there exist WNS states with $c_1 c_2 > 0$, which is a sufficient

condition for separability. Intuitively, the issue is that a single, optimal Gaussian measurement is sufficient for Bob to show Alice that a state is WNS, but the assumption of a canonical two-mode Gaussian state is too generic and a single choice of measurement cannot be sufficient to demonstrate EPR steering, which in turn implies that it cannot prove entanglement. In fact, it has been shown [165] that WNS can be achieved with Gaussian states with arbitrarily low Gaussian Quantum Discord.

Motivated by these examples, we seek a stronger condition than the one provided in Definition 3.3 to explore other quantum correlations that can arise while studying the remote generation of P-nonclassicality with Gaussian states in canonical form. Recalling that Proposition 3.3 identifies quadrature measurements as the best Gaussian measurements to induce nonclassicality, we introduce the following more stringent notion of nonclassical steering:

Definition 3.3.2: Strong Nonclassical Steering

A two-mode Gaussian state $\hat{\boldsymbol{\rho}}_{AB}$ in canonical form is called *strongly nonclassically steerable* (SNS) ($B \to A$) if the measurement of *any* quadrature on mode B generates a nonclassical conditional state of mode A.

Following the same argument used in [166] to prove Proposition 3.3, we can deduce the following criterion:

Lemma 3.3.3: SNS criterion

A two-mode Gaussian state $\hat{\boldsymbol{\rho}}_{AB}$ in canonical form is SNS ($B \to A$) if and only if the parameters of its CM satisfy:

$$a - \frac{c'^2}{b} < \frac{1}{2}, \quad c' = \min\{|c_1|, |c_2|\} \tag{3.12}$$

In order to generalize these definitions from two-mode Gaussian states in canonical form to *all* Gaussian states of two modes, we should take into account (local) single-mode squeezing transformations, which may alter the nonclassicality of each mode independently of their quantum correlations. However, since any two-mode Gaussian state can be brought to its *unique* canonical form through LGUTs without altering the correlations, we can extend the definitions in the following way:

Definition 3.3.3: Nonclassical Steering for two-mode Gaussian states

A generic two-mode Gaussian state $\hat{\boldsymbol{\rho}}_{AB}$ is called weakly (strongly) nonclassically steerable if the *unique* Gaussian state $\hat{\boldsymbol{\rho}}'_{AB}$ *in canonical form* related to $\hat{\boldsymbol{\rho}}_{AB}$ by LGUTs is weakly (strongly) nonclassically steerable.

In order to extend also the criteria for WNS/SNS, we need to specify the effect of LGUTs on σ_c. We recall that any LGUT on a two-mode system is described by an element $\mathrm{S}_A \oplus \mathrm{S}_B$ acting on quantum phase space, where $\mathrm{S}_{A(B)} \in \mathrm{Sp}_{A(B)}(2, \mathbb{R})$. The 2×2 blocks of a generic σ, decomposed as in Eq.(2.103), are transformed according to:

$$\mathrm{A}' = \mathrm{S}_A \mathrm{A} \mathrm{S}_A^T \quad \mathrm{B}' = \mathrm{S}_B \mathrm{A} \mathrm{S}_B^T \quad \mathrm{C}' = \mathrm{S}_A \mathrm{C} \mathrm{S}_B^T \tag{3.13}$$

Let us now suppose that $\mathrm{S}_A \oplus \mathrm{S}_B$ brings the initial σ in canonical form, so that $\mathrm{A}' = a'\mathbb{1}_2$, $\mathrm{B}' = b'\mathbb{1}_2$ and $\mathrm{C}' = \mathrm{diag}(c'_1, c'_2)$. The conditional CM σ_c resulting from a Gaussian measurement with CM σ_M on the initial state with CM σ can be rearranged as:

$$\sigma_c = \mathrm{S}_A^{-1}\left[\mathrm{A}' - \mathrm{C}'\left(\mathrm{B}' + \sigma'_M\right)^{-1}\mathrm{C}'^T\right](\mathrm{S}_A^T)^{-1} \tag{3.14}$$

where the CM of the measurement has been redefined according to $\sigma'_M = \mathrm{S}_B\sigma_M\mathrm{S}_B^T$. We see that performing the measurement (associated with) σ_M on the two-mode state with CM σ is equivalent to perform the modified measurement σ'_M on the canonical form state related to σ and then performing the transformation induced by S_A on the resulting conditional CM. This means that we can simply factor out the action of S_A^{-1} because it does not interfere with the steering process. Meanwhile, as long as S_B does not introduce infinite squeezing, we can still approach the desired limit of σ'_M, acting on the state in canonical form, by taking a limit of σ_M with a suitable phase. Finally, to get the necessary and sufficient conditions for WNS and SNS in the general case, we can now rewrite Ineq.(3.11) and Ineq.(3.12), replacing a, b, c_1, c_2 with their expressions in terms of symplectic invariants of Eq.(2.92):

Lemma 3.3.4: General criteria for nonclassical steering

A generic two-mode Gaussian state $\hat{\boldsymbol{\rho}}_{AB}$ is *weakly nonclassically steerable* from mode $B \to A$ if and only if its symplectic invariants satisfy the inequality:

$$\frac{I_1 I_2 - {I_3}^2 + I_4 - \sqrt{\left(I_1 I_2 - {I_3}^2 + I_4\right)^2 - 4 I_1 I_2 I_4}}{2 I_2 \sqrt{I_1}} < \frac{1}{2}\,. \tag{3.15}$$

while it is *strongly nonclassically steerable* if they satisfy the stronger inequality:

$$\frac{I_1 I_2 - {I_3}^2 + I_4 + \sqrt{\left(I_1 I_2 - {I_3}^2 + I_4\right)^2 - 4 I_1 I_2 I_4}}{2 I_2 \sqrt{I_1}} < \frac{1}{2}\,. \tag{3.16}$$

Strong nonclassical steering obviously implies weak nonclassical steering, but it also implies entanglement. We will show this implicitly by proving a stronger result:

Theorem 3.3.1

A two-mode Gaussian state $\hat{\boldsymbol{\rho}}_{AB}$ that is SNS $B \to A$ is also EPR-steerable in the same direction, therefore also entangled.

Proof. As stated in Ineq.(3.9), EPR steerability $B \to A$ of a Gaussian state by Gaussian measurements amounts to the *violation* of the inequality $\sigma + \frac{i}{2}\boldsymbol{\omega}_A \oplus \mathbb{O}_B \geq 0$ by its CM. Exploiting LGUT-invariance, we can restrict the comparison between EPR steerability and SNS to Gaussian states in canonical form. In this case, keeping in mind that $a > \frac{1}{2}$, violation of the above inequality reduces to [156, 167] $(a - c_1^2/b)(a - c_2^2/b) < 1/4$, which is certainly true under the SNS Ineq.(3.12). □

Notice that, by combining Ineq.(3.15) and Ineq.(3.16) with the EPR steerability $B \to A$ criterion for a two-mode Gaussian state in canonical form, $(a - c_1^2/b)(a - c_2^2/b) < 1/4$, we

can readily express also Ineq.(3.9) in terms of symplectic invariants:

$$4I_4 < I_2 \tag{3.17}$$

which most clearly shows the asymmetric nature of this quantum correlation, since $I_2 = b^2$ appears on the right-hand side. Again, the related inequality for EPR steerability $A \to B$ can be obtained by replacing I_2 with I_1 in Ineq.(3.17).

It is remarkable that the quantities on the left sides of (3.11) and (3.12) are precisely conditional variances appearing in the Reid EPR-criterion [168, 169], whose test is already experimentally accessible [161, 170]. The idea is that, when Bob measures either the $\hat{q}_B$ or the $\hat{p}_B$ quadrature of his mode, the conditional states of Alice will have minimal variances along orthogonal quadratures; the EPR paradox arises if the product of these minimal quadratures is less than $\frac{1}{4}$, which naively seems to contradict the Uncertainty Relations. As already noted, this is precisely the condition of EPR steering. This is also in agreement with the well-known result stating that quadrature measurements are the best choice for Gaussian EPR steering [171].

3.3.1 Gaussian Steering Triangoloids

Let us now focus on the relevant class of two-mode squeezed thermal states (TMST) [172, 173, 174] that we introduced in Section 2.6.1. The parameters of their CMs are given by Eq.(2.97), where we rename $N_1 = N_A, N_2 = N_B$, denoting the average number of thermal photons in each mode. These states are particularly convenient to study quantum correlations in two-mode Gaussian states, as they are described by only 3 parameters but they include separable states, entangled states that are not steerable and, as we will see in the following, also steerable states. Moreover, having a degree of asymmetry quantified by $N_A - N_B$, their steering properties can be asymmetric.

Since TMST are all and only those states whose CM is in canonical form with the additional constraint that $c_1 = -c_2 = c$, for them the conditions for WNS and SNS coincide, by Eq.(3.11) and Eq.(3.12): the most nonclassical conditional state on mode A is obtained by *any* quadrature measurement on mode B. From the proof of Theorem 3.3, it is also clear that TMST states are EPR-steerable from one mode to the other *if and only if* they are nonclassically steerable (strongly and therefore also weakly) in the same direction. This observation provides a new, somehow surprising, role for the notion of P-nonclassicality: it is *the* property that Alice should check, after Bob's measurement on his mode, to certify that the shared TMST state is indeed entangled; we note that this fact could find applications in one-sided device-independent quantum key distribution [158]. Note that the *universal* steerability condition for TMST states becomes:

$$\cosh 2r \;>\; 1 + \frac{2N_A(1+2N_B)}{1+N_A+N_B} \tag{3.18}$$

which is readily interpreted as a lower bound on the two-mode squeezing needed to make the TMST steerable $B \to A$.

In order to illustrate nonclassical steering for TMST states, we employ plots of *triangoloids*. They are described by considering the two relevant quantities that characterize the conditional state, as far as its nonclassicality is concerned: its purity μ_c, and the conditional squeezing purity μ_{sc}. This second parameter arises by noting that the conditional state of Alice's mode, being a single-mode Gaussian state, will be described by a

displaced, squeezed thermal state; if we call r_c the corresponding squeezing parameter, as in Eq.(2.75), we can define $\mu_{sc} = (1 + 2\sinh^2 r_c)^{-1}$. The convenience of using these two parameters relies on the fact that they are both bounded between 0 and 1. Moreover, for TMST states, their functional dependence upon the Gaussian POVM and the initial parameters (N_A, N_B, r) can be worked out analytically [166]. For a fixed TMST state, we can thus plot the region of achievable conditional states in the (μ_c, μ_{sc})-space, as obtained by considering all the POVM's parameters. These are the curvilinear triangles (triangoloids) in Fig.3.1, where we also displayed the nonclassical region (light-green region), i.e. those parameters corresponding to nonclassical states of mode A (see [165] for further details):

$$\mu_{sc} < \frac{2\mu_c}{1 + {\mu_c}^2} \tag{3.19}$$

It follows that the TMST state associated with a given triangoloid is nonclassically steerable $B \to A$ when the parameters N_A, N_B and r of the state are such that the triangoloid intersects the nonclassical region, as in the right panel of Fig.3.1, because only in that scenario there will be some Gaussian POVM on mode B yielding a nonclassical state of mode A. We shaded the intersection area according to the nonclassical depths, with lighter regions corresponding to higher nonclassicality. As it may be also appreciated graphically, the decisive point for nonclassical steering of a TMST is the blue, lower vertex of the triangoloid, attained by quadrature detection on mode B: if this point is outside the nonclassical region, all other points of the triangoloid are outside too and an intersection between the nonclassical region and the triangoloid will no longer be possible. Notice that the equivalence of EPR steering and nonclassical steering for TMSTs has a neat graphical interpretation: the light-green nonclassical region is *the largest* region such that a TMST whose triangoloid intersects it is necessarily entangled. Indeed, suppose that a larger region in the (μ_c, μ_{sc}) square exists such that whenever the triangoloid intersects it, one can be sure that the state is entangled; since these diagrams can be drawn by Bob from the data gathered by measurements on his mode only, it would mean that the intersection with such a larger region would *convince* Bob that the state was entangled, so it must have been steerable. However, we proved that the largest region such that an intersection of the triangoloid implies steering is precisely the nonclassical region.

The equivalence between nonclassical steering (of the weak and/or strong type) with EPR steering for TMST states is insightful also for another reason: it shows that, if Alice is willing to accept some hypotheses about the shared quantum states, EPR steering $B \to A$ is possible even with a single type of measurement. In the present case, if she believes that the original two-mode state was a TMST Gaussian state and that Bob's measurement apparatus, as unreliable as it could be, is only capable of performing Gaussian measurements, then she will be convinced that the TMST state was also entangled if and only if, upon getting the outcome from Bob, she finds out that her conditional state is nonclassical. To achieve this, it is sufficient for Bob to do a single type of projective measurement of a (generic) quadrature on his mode and report the outcome: there is no need for Alice to ask in advance what kind of measurement he should perform in each run. We conclude by mentioning that a thorough description of triangoloids and their role in the study of nonclassical steering can also be found in [165], where the propagation of a TMST state through a thermal environment and its detrimental effect on these quantum correlations was also explored.

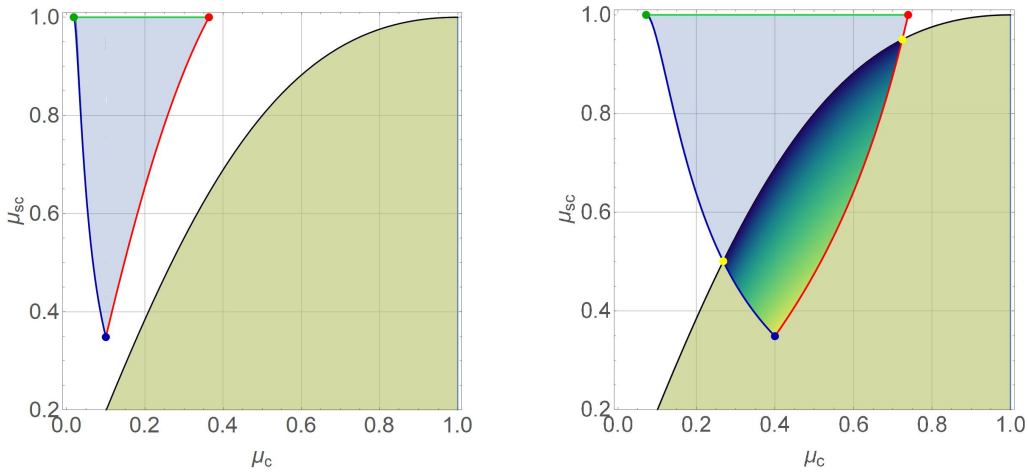

Figure 3.1: (Left): Triangoloid for TMST state with $N_A = N_B = 4.5$ and $r = 1.2$, μ_c is the purity of the conditional state, while $\mu_{sc} = (1+2\sinh^2 r_c)^{-1}$ quantifies the conditional squeezing. The light-green region contains all nonclassical conditional states. (Right): triangoloid for $N_A = N_B = 0.75$ and $r = 1.2$.

3.4 Probing non-Markovianity with quantum steering

In this section we shall see how quantum steering can be used to detect the non-Markovianity of a specific Gaussian channel: the Quantum Brownian Motion (QBM) channel, originating from the interaction with Ohmic and sub-Ohmic environments characterized by a Lorentz-Drude cutoff. The asymmetric behaviour of steering and its stricter requirements as a quantum correlation compared with entanglement make it an interesting candidate to build a more stringent measure of non-Markovianity, at the same time involving only accessible quantities in the Gaussian regime.

3.4.1 Steerability and non-Markovianity measures

Various criteria and measures have been discussed for the recognition and quantification of CV quantum steering, such as the quantity introduced in [167]. According to them, Gaussian steering of mode B by mode A of a two-mode CV state can be quantified by the *Gaussian $A \to B$ steerability* that for a two-mode state reads:

$$\mathcal{S}^{A\to B} = \max\left\{0, \frac{1}{2}\ln\frac{\det \mathrm{A}}{\det \sigma^{AB}}\right\}. \tag{3.20}$$

where, as before, A is the diagonal block in the CM σ^{AB} pertaining to mode A of the bipartite state $\hat{\boldsymbol{\rho}}_{AB}$. Whenever the dimensionless quantity $\mathcal{S}^{A\to B}$ is positive, it indicates the amount by which the state of mode A has a smaller purity than the overall state of the two modes. As shown in [167], for Gaussian states it is positive if and only if mode A can steer mode B. By exchanging the labels A and B, one readily obtains $\mathcal{S}^{B\to A}$, a measure of Gaussian steering of mode A by measuring mode B. Consider now a two-mode Gaussian state that is described by a CM $\sigma(0)$ at the initial time. Under Gaussian, Markovian CPTP maps acting independently on each one of the modes, the time derivative of

the steering measure is always non-positive:

$$\mathcal{D}_{\mathcal{E}}^{\rightarrow}(t) \;:=\; \frac{d\mathcal{S}^{A\rightarrow B}(\sigma(t))}{dt} \leq 0 \tag{3.21}$$

where $\sigma(t)$ is the CM at time t and $\mathcal{E}_t$ is a Gaussian, single-mode CPTP quantum evolution under scrutiny, acting on the steering mode A. This is a simple consequence of the CP-divisibility of Markovian maps and the known fact that $\mathcal{S}^{A\rightarrow B}$ cannot exceed its initial value under generic *local* Gaussian operations on the modes and classical communication [175]. Similarly, one can define $\mathcal{D}_{\mathcal{E}}^{\leftarrow}$ when $\mathcal{E}_t$ acts on the *steered* mode B and $\mathcal{D}_{\mathcal{E}}^{\leftrightarrow}$ for $\mathcal{E}_t$ acting independently on both modes: also these quantities will be non-negative if $\mathcal{E}_t$ describes a Markovian quantum evolution. However, if the quantum evolution $\mathcal{E}_t$ is not CP-divisible in time, i.e. it is non-Markovian, the map that evolves the state between any two consecutive time instants need not be a CPTP map, and consequently, $\mathcal{S}^{A\rightarrow B}$ can behave non-monotonically during the whole time evolution. Therefore, any positive value of $\mathcal{D}_{\mathcal{E}_t}^{\star}$, with $\star = \rightarrow, \leftarrow, \leftrightarrow$, indicates the violation of Markovianity for the channel under study [58]. To build a measure of non-Markovianity for Gaussian quantum channels, we will start with a twin-beam (TWB) state with two-mode squeezing parameter r fixed by the total energy, since they are the maximally correlated Gaussian states at a given energy, which as necessarily to be fixed and bounded in order to have a well-posed problem. Calling σ_0^{AB} their CM, our measure of non-Markovianity for a single-mode Gaussian channel $\mathcal{E}$ is defined as:

$$\mathcal{N}^{\star}\left[\mathcal{E}_t\right](r) \;=\; \int_{\mathcal{D}_{\mathcal{E}}>0} D_{\mathcal{E}}^{\star}\left(t; r\right) dt \tag{3.22}$$

where it is assumed that $\mathcal{E}_t$ acts on the steering mode, the steered mode or on both of them independently, depending on $\star = \rightarrow, \leftarrow, \leftrightarrow$. In the case of a Gaussian quantum evolution $\mathcal{E}_t^{(n)}$ acting on n modes, one can extend the previous definitions in the following way. Consider n modes labeled by $a_1, ..., a_n$ and call them subsystem A, and additional n modes labeled by $b_1, ..., b_n$ composing subsystem B. As initial state, one can take the tensor product of n TWB states, each of which involves mode a_i from system A and mode b_i from system B, all with the same two-mode squeezing parameter r. Subsystem A will be the steering party, while subsystem B will be the steered party. Using the general definition of Gaussian steerability in terms of the symplectic eigenvalues of the Schur complement [167], we can define as before $\mathcal{D}_{\mathcal{E}^{(n)}}^{\star}$ and $\mathcal{N}^{\star}[\mathcal{E}_t^{(n)}](r)$ for $\star = \rightarrow, \leftarrow, \leftrightarrow$ and $\mathcal{E}_t^{(n)}$ acting respectively on subsystem A, subsystem B, or independently on both of them. This achieves the goal of defining a generic measure of non-Markovianity for any Gaussian quantum evolution.

3.4.2 Quantum Brownian Motion

We will now shortly sketch a description of the Gaussian channel we will consider in the following, the *quantum Brownian motion* (QBM) channel, a paradigmatic model of interaction with an environment, that allows us to explore our measure of non-Markovianity in the analytically approachable setting of Gaussian states and enables comparisons with other existing measures. Besides, it finds application e.g. in quantum optomechanics [176]. The CV system of interest is a quantum harmonic oscillator with frequency ω_0 and unit mass, and it is coupled to a bath consisting of an ensemble of harmonic oscillators.

[177]. An initially factorized state for the system and the bath evolves unitarily under the Hamiltonian of the channel, which is [177]:

$$\hat{H}_1 = \frac{\hat{p}^2}{2} + \frac{1}{2}\omega_0^2\hat{q}^2 + \sum_n \left(\frac{\hat{P}_n^2}{2m_n} + \frac{1}{2}m_n\omega_n^2\hat{Q}_n^2 \right) + \alpha\hat{q}\sum_n k_n\hat{Q}_n \tag{3.23}$$

where $\hat{p}$ and $\hat{q}$ (resp. $\hat{P}$ and $\hat{Q}$) are quadrature operators of the system (resp. of the bath). The relative strengths of interaction and the coupling constant are denoted by k_n and α, respectively. Then the environment is traced out to find the state of the system at each time. The initial state of the bath is assumed to be a thermal state at temperature $T = \beta^{-1}$ with respect to the corresponding free Hamiltonian of the bath. Assuming weak coupling and secular approximation, the master equation can then be recast in this form [178, 179] [1]:

$$\frac{d\hat{\boldsymbol{\rho}}}{dt} = \frac{\Delta(t)+\gamma(t)}{2}\left[2\hat{a}\hat{\boldsymbol{\rho}}\hat{a}^\dagger - \hat{a}^\dagger\hat{a}\hat{\boldsymbol{\rho}} - \hat{\boldsymbol{\rho}}\hat{a}^\dagger\hat{a}\right] + \frac{\Delta(t)-\gamma(t)}{2}\left[2\hat{a}^\dagger\hat{\boldsymbol{\rho}}\hat{a} - \hat{a}\hat{a}^\dagger\hat{\boldsymbol{\rho}} - \hat{\boldsymbol{\rho}}\hat{a}\hat{a}^\dagger\right] \tag{3.24}$$

which is to be understood in the interaction picture. The time-dependent terms $\Delta(t)$ and $\gamma(t)$ represent the diffusion and damping coefficients, respectively. Assuming a thermal environment at temperature T, described by a spectral density $J(\omega)$, these coefficients $\gamma(t)$ and $\Delta(t)$ can be computed by [36, 177]:

$$\gamma(t) = \alpha^2\int_0^t d\tau\int_0^\infty d\omega J(\omega)\sin(\omega\tau)\sin(\omega_0\tau) \tag{3.25}$$

$$\Delta(t) = \alpha^2\int_0^t d\tau\int_0^\infty d\omega\, J(\omega)\coth\left[\frac{\omega}{2T}\right]\cos(\omega\tau)\cos(\omega_0\tau) \tag{3.26}$$

where $\coth\left[\frac{\beta\omega}{T}\right] = 2N(\omega)+1$ and $N(\omega) = (1+\exp\{-\beta\omega\})^{-1}$ is the mean number of thermal photons in the bath at frequency ω. The master equation Eq.(3.24) is time-local, but it does not satisfy the semigroup property, since the damping and diffusion coefficients are time dependent. Depending upon the form of the spectral density $J(\omega)$ of the environment, the coefficients $\Delta(t) \pm \gamma(t)$ may or may not describe a Markovian Gaussian map. In particular, it is known that the quantum map described by Eq.(3.24) is non-Markovian if $\Delta(t) < |\gamma(t)|$ at some point in time; in that case, it is said to be in non-Lindblad form, but it still preserves the positivity of the density matrix [179, 180]. In this study, the origin of the purported non-Markovianity is a spectral density for the bath with Lorentz-Drude cutoff [36, 178, 181]:

$$J(\omega) = \frac{2\omega^s}{\pi}\frac{\omega_c^{3-s}}{\omega_c^2+\omega^2} \tag{3.27}$$

where ω_c is the cutoff frequency. In Eq. (3.27), the cases $s = 1$ and $s < 1$ correspond to an Ohmic and sub-Ohmic spectral density, respectively, while the super-Ohmic case cannot be dealt with Lorentz-Drude cutoff due to ultraviolet divergence of the frequency integrals. Whenever $\omega_0/\omega_c \ll 1$, at least in the Ohmic case, the dynamics of the system is expected to be Markovian on the ground of the longer characteristic time of the system compared to the relaxation time of the bath. Therefore, in the following we will assume $\omega_0 > \omega_c$ and consider an environment both at low and high temperature, each in the

[1] From now on, we assume appropriate units such that $\hbar = k_B = 1$

Ohmic $s = 1$ and sub-Ohmic $s = \frac{1}{2}$ scenarios. Explicit formulas for $\gamma(t)$ and $\Delta(t)$ in the Ohmic cases can be derived, while for the $s = \frac{1}{2}$ sub-Ohmic spectral density we resorted to numerical integration.

To discuss our measures of non-Markovianity $\mathcal{N}^{\star}$, two situations must be considered; in the first one, only one mode of the initial TWB state exploited to probe non-Markovianity is subjected to the QBM channel, while the second mode undergoes the free unitary evolution. In this first scenario, adopting the notation:

$$\Gamma(t) \;=\; \int_0^t 2\gamma(s)ds \tag{3.28}$$

$$\Delta_\Gamma(t) \;=\; e^{-\Gamma(t)} \int_0^t e^{\Gamma(s)}\Delta(s)ds \tag{3.29}$$

the evolution of the covariance matrix, which is the TWB CM σ_0^{AB} at the initial time, when mode A is subjected to the QBM channel is as follows [178]:

$$\sigma_t^{AB} = \left[e^{-\frac{\Gamma(t)}{2}}\mathbb{I}_A \oplus \mathbb{I}_B\right]^T \sigma_0^{AB} \left[e^{-\frac{\Gamma(t)}{2}}\mathbb{I}_A \oplus \mathbb{I}_B\right] \;+\; \Delta_\Gamma(\mathbb{I}_A \oplus \mathbb{O}_B) \tag{3.30}$$

with the obvious changes when the QBM channel acts on mode B instead. To evaluate $\mathcal{N}^{\leftrightarrow}$, instead, both modes are individually and locally subjected to the channel. The evolution of the covariance matrix is now [178]:

$$\sigma_t^{AB} \;=\; \left[e^{-\frac{\Gamma(t)}{2}}\mathbb{I}_A \oplus e^{-\frac{\Gamma(t)}{2}}\mathbb{I}_B\right]^T \sigma_0^{AB} \left[e^{-\frac{\Gamma(t)}{2}}\mathbb{I}_A \oplus e^{-\frac{\Gamma(t)}{2}}\mathbb{I}_B\right] \;+\; \Delta_\Gamma(\mathbb{I}_A \oplus \mathbb{I}_B) \tag{3.31}$$

In the weak coupling regime $\alpha \ll 1$ that was already implicit in the derivation of the master equation, we can expand Δ_Γ to first order in $\Gamma(t)$; then, recalling that $\Gamma(t) \sim O(\alpha^2)$ and truncating the expansion up to second order in α, we can simply write:

$$\Delta_\Gamma \simeq \int_0^t \Delta(s)ds \tag{3.32}$$

From the structure of Eq.(3.30) and Eq.(3.31), it is clear that the blocks $\mathrm{A}, \mathrm{B}, \mathrm{C}$ will still be diagonal and we can write them at any time as $\mathrm{A}(t) = a(t)\,\mathbb{I}_2$, $\mathrm{B}(t) = b(t)\,\mathbb{I}_2$, and $\mathrm{C}(t) = c(t)\,\mathrm{diag}(1, -1)$, where $\mathbb{I}_2$ is the 2×2 identity matrix. In particular, the reduced CMs for mode A and mode B will stay proportional to the identity at all times, therefore the free evolution of the modes will not have any effect and the state is once more a two-mode squeezed thermal state (TMST) at all times. Our task thus boils down to computing the three functions $a(t), b(t), c(t)$ for the three scenarios and then the corresponding non-Markovianity measures. Eq.(3.30) and Eq.(3.31), being referred just to the CMs, allow to check the complete positivity of the channel under investigation in the Gaussian sector and we consider the QBM channel always under this assumption.

3.4.3 Non-Markovianity of an Ohmic environment

Using Eqs.(3.30,3.31) and the definitions in Eq.(3.22), we now evaluate the non-Markovianity measures $\mathcal{N}^{\rightarrow}, \mathcal{N}^{\leftarrow}$ and $\mathcal{N}^{\leftrightarrow}$ for Ohmic and sub-Ohmic environments both at low and high temperatures. We assume a cutoff frequency $\omega_c = 1$ and we fix $\omega_0 = 7$ as the

frequency of the system modes. Since ω_c is significantly smaller than ω_0, we expect to detect a non-Markovian behavior, as previously discussed. The two-mode squeezing parameter of the TWB initial state of the system will be fixed at $r = 2$, which is both an experimentally achievable value in quantum optics and a good representative for the whole class of TWB states: indeed we checked that for any $r \gtrsim 2$ the qualitative behavior that we shall discuss is essentially unaltered. We shall start by the Ohmic environment, having $s = 1$ in the spectral density Eq.(3.27). In Fig.3.2(a) the low temperature ($T = 1.5$) case is displayed. The measure $\mathcal{N}^{\rightarrow}$ corresponding to the steering mode only (mode A) interacting with the environment is the smaller one for all considered values of the coupling constant (red, dashed curve), while $\mathcal{N}^{\leftrightarrow}$ is always the larger one (black, solid curve), corroborating the intuition that the sensitivity of the system to the non-Markovian character of the QBM channel is stronger when both modes can interact with two independent copies of the same structured environment. Moreover, all of the measures are monotonically increasing functions of the coupling and behave as $\sim \alpha^2$ in the $\alpha \to 0$ limit. Therefore, for low temperature Ohmic environments, the larger the coupling, the better the estimation of non-Markovianity by Gaussian steering with TWB states.

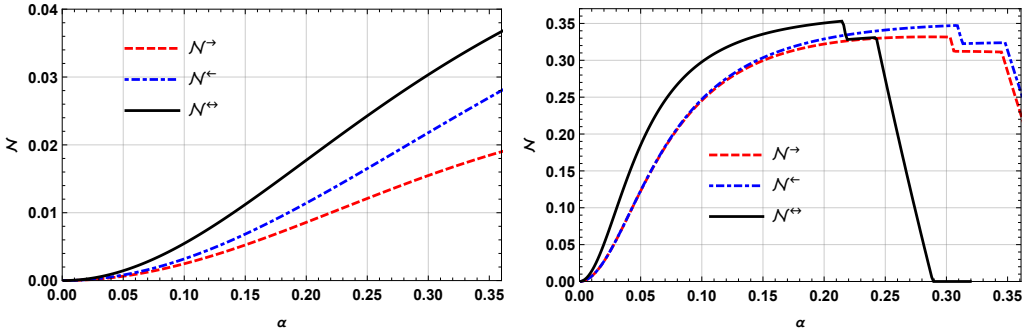

(a) $T = 1.5$ (b) $T = 100$

Figure 3.2: Non-Markovianity ($\mathcal{N}$) vs coupling constant (α) for a QBM channel with a structured environment described by an Ohmic spectral density with cutoff frequency $\omega_c = 1$ at temperature $T = 1.5$ (left) and $T = 100$ (right). The CV system at initial time is a TWB state with frequency $\omega_0 = 7$ and two-mode squeezing parameter $r = 2$. The three curves correspond to: mode A undergoing the QBM channel evolution and mode B evolving freely ($\mathcal{N}^{\rightarrow}$, red, dashed curve), mode B subjected to the QBM channel and mode A evolving freely ($\mathcal{N}^{\leftarrow}$, blue, dotted-dashed curve) and both modes evolving through two independent, identical QBM channels ($\mathcal{N}^{\leftrightarrow}$, black, solid curve). In all three cases, mode A is the steering mode and mode B is the steered mode.

Considering now a high temperature ($T = 100$) Ohmic environment, the same qualitative analysis of the low temperature situation applies for small values of the coupling constant ($\alpha \lesssim 2.1$), as can be seen in Fig.3.2(b). The values of $\mathcal{N}^{\star}$ are an order of magnitude higher than those of the low-temperature environment, indicating that not only quantum steering is degraded faster at high temperatures, but it can also be temporarily restored in a significant portion. However, at still higher values of α, $\mathcal{N}^{\leftrightarrow}$ suddenly dips to zero with a steep linear slope, and the other two measures soon follow. These are not numerical artifacts, and they are essentially due to the transition into a non-steerable state.

3.4.4 Non-Markovianity of a sub-Ohmic environment

We now switch to an environment described by a sub-Ohmic spectral density with $s = \frac{1}{2}$. At low temperature ($T = 1.5$) the behavior closely mimics the Ohmic case, with $\mathcal{N}^{\rightarrow}$ being the smaller measure and all of them monotonically increasing with α and quadratic in the $\alpha \to 0$ limit, see Fig.3.3(a). Notice, however, that from the quantitative aspect there is a substantial difference: according to our measures, the non-Markovianity of a sub-Ohmic environment with $s = \frac{1}{2}$ is about thirty times larger than that of an Ohmic environment at the same temperature and with the same cutoff frequency.

Finally, let us consider the QBM channel with a sub-Ohmic environment with $s = \frac{1}{2}$ and at high temperature ($T = 100$). The non-Markovianity measures $\mathcal{N}^{\star}$ as functions of the coupling constant α are plotted in Fig.3.3(b). Again the values of all the measures are greater than those for the corresponding low temperature environment, but for $\alpha \gtrsim 0.1$ the plot of $\mathcal{N}^{\leftrightarrow}$ starts to drop gradually, and the other two measures soon follow the same trend. This decrease is considerably slower than that of Fig.3.2(b) for the Ohmic high temperature bath. Also for this case, the upshot is that for strong enough couplings with high temperature environment, Gaussian steerability is less effective at witnessing the non-Markovian character of the QBM channel.

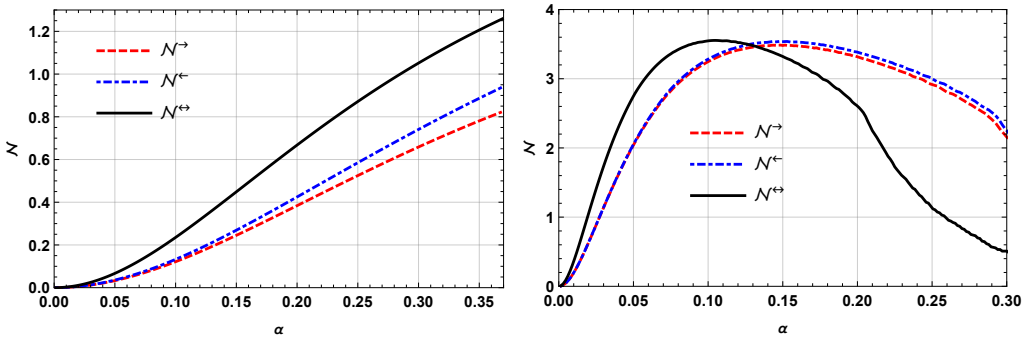

(a) $T = 1.5$ (b) $T = 100$

Figure 3.3: The three non-Markovianity measures ($\mathcal{N}$) vs. coupling constant (α) for a QBM channel with a structured environment described by a sub-Ohmic spectral density with $s = \frac{1}{2}$, cutoff frequency $\omega_c = 1$ at low temperature $T = 1.5$ (left) and high temperature $T = 100$ (right). The probing CV system is prepared as before.

3.4.5 Explaining the trends of steerability-based non-Markovianity measures

We have seen that the non-Markovianity of the sub-Ohmic environment, according to all of our measures, is considerably higher than that of the Ohmic environment. To have a better understanding of this behavior, and also of the sudden decrease of $\mathcal{N}^{\star}$ for $\alpha \gtrsim 0.2$ in the case of high temperature environments, it is useful to have a look at the time dependence of the steerability in the two cases. Fig.3.4 displays the time-derivative of the Gaussian steerability $\mathcal{S}^{A\to B}$ in the three cases for an Ohmic, low temperature environment ($\omega_c = 1$, $T = 1.5$, $\omega_0 = 7$, $r = 2$). There is a single time interval, between $t \simeq 0.3$ and $t \simeq 0.8$, during which there is a backflow of steerability and the derivative is positive. This time interval is approximately the same disregarding of whether the bath interacts with mode A, mode B, or both modes independently. Moreover, we checked

that it is not significantly influenced by either α or by r (at least for $r > 2$). Notice also that the ordering of the curves for the steerability is different from the ordering of the corresponding non-Markovianity measures. Indeed, Gaussian steerability decreases the least when only the steered mode (mode B) interacts with the bath (blue, dotted-dashed curve), while it decreases most rapidly when both modes are interacting with independent, identical environments (black, solid curve). However, in the latter case, the backflow is also more significant (higher peak in Fig.3.4), yielding greater values of non-Markovianity according to our measures. Indeed, by definition $\mathcal{N}^{\star}$ is just the area between the time axis and the positive arc of the corresponding curve in Fig.3.4 (under the red curve for $\mathcal{N}^{\rightarrow}$, the blue curve for $\mathcal{N}^{\leftarrow}$ and the black curve for $\mathcal{N}^{\leftrightarrow}$). At higher temperatures, this first time interval is still unchanged, but a second, later interval of increasing $\mathcal{S}^{A\rightarrow B}$ appears between $t \simeq 1.4$ and $t \simeq 1.7$ as can be noticed from Fig.3.5(a), partially explaining the quantitative difference in non-Markovianity between low and high temperature Ohmic environments. As α increases the backflow increases too, but the Gaussian steerability curves of Fig.3.5(a) also slide down towards the time axis and they become zero at earlier times, in compliance with common intuition suggesting that a stronger interaction will degrade quantum correlations faster.

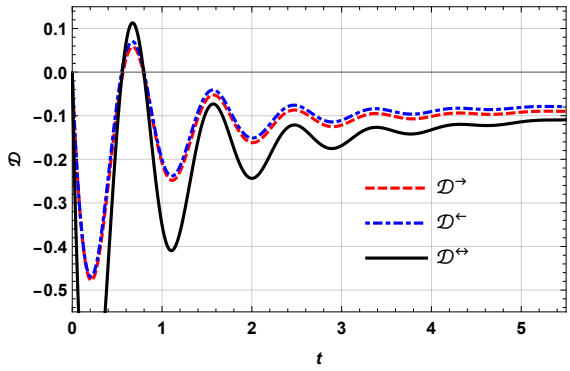

Figure 3.4: Time derivative of Gaussian steerability $A \rightarrow B$ of a TWB state as a function of time for an Ohmic environment at low temperature ($T = 1.5$) and coupling constant $\alpha = 0.15$.

This explains the trends observed in Fig.3.2(b): after a certain value of α, the Gaussian steerability goes to zero before the end of the second time interval in which backflow can occur (first dip in Fig.3.2(b)). At still higher values of α, also the first backflow time interval occurs after the Gaussian steerability has already vanished, and $\mathcal{N}^{\star}$ consequently drops to zero too. This is not seen when the bath is at a lower temperature, because then quantum steering lasts longer and the backflow can always manifest before Gaussian steerability vanishes.

Fig.3.5(b), on the other hand, shows that even at low temperature ($T = 1.5$), a sub-Ohmic environment with $s = \frac{1}{2}$ induces cyclic backflows of Gaussian steerability $\mathcal{S}^{A\rightarrow B}$ from the bath back into the system, for all three possible ways of coupling the modes of the system with the bath. This gives a quantitative understanding of the difference between non-Markovianity of Ohmic vs. sub-Ohmic environments, and also justifies the slower decrease of $\mathcal{N}^{\star}$ with α at higher temperature observed in Fig.3.3(b), since now only a minor decrement in non-Markovianity occurs whenever a single time interval of increasing $\mathcal{S}^{A\rightarrow B}$ slides past the time when Gaussian steerability vanishes. For the sub-Ohmic case too, this decrease with α is observed just for the high temperature bath. Overall, the issue of decreasing sensitivity to non-Markovianity for stronger couplings

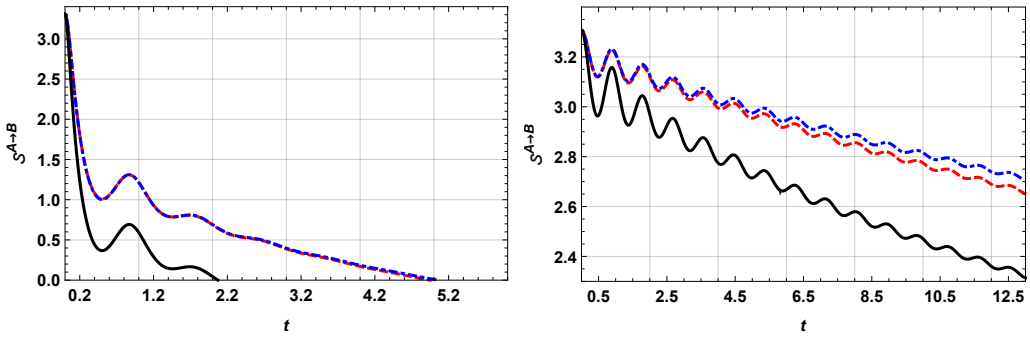

(a) $T = 100$, Ohmic

(b) $T = 1.5$, sub-Ohmic

Figure 3.5: Gaussian steerability $A \to B$ of a TWB state as a function of time for an Ohmic environment at high temperature ($T = 100$, left) for a sub-Ohmic environment ($s = \frac{1}{2}$) at low temperature ($T = 1.5$, right). The coupling constant is $\alpha = 0.2$ in both instances.

with high temperature environments can be overcome by starting with a TWB state having a greater two-mode squeezing parameter r, so that Gaussian steerability will not be destroyed before the characteristic time scale of the non-Markovian evolution had time to happen.

We emphasize that in our analysis we also took into account values of α which could be partially beyond the weak coupling limit that is implicit in the derivation of the Lindblad equation. Therefore it might be the case that in a strict weak coupling limit, only the first portion of the trends discussed so far will be reliable. However, this does not affect the validity of our arguments, because the model described by the final master equation with specified time-dependent diffusion and damping coefficients $\Delta(t)$ and $\gamma(t)$ does not impose any constraint on the value of the coupling constant.

As a final remark, we mention that from an experimental point of view this method provides a viable opportunity to quantify the non-Markovianity of a Gaussian quantum channel since, considering e.g. $\mathcal{N}^{\leftrightarrow}$ as the most sensitive measure, it requires preparing a TWB state, sending both modes through two independent copies of the channel and measuring the variances of one quadrature for each mode ($a(t)$ and $b(t)$) as well as the covariance of a quadrature of the first mode with a quadrature of the second mode ($c(t)$), at different times. Using these data, one can compute $\mathcal{S}^{A\to B}(t)$ and consequently $\mathcal{N}^{\leftrightarrow}$, once a reasonably long set of values has been acquired.

Chapter 4

Quantum Metrology

The problem of inferring unknown parameters with increasing accuracy and precision is pivotal in science in general. Most of the times, we are not dealing with direct *measurements*, since the quantities that we would like to estimate are not directly observable. A striking example is provided by particle collisions: almost everything that particle detectors ever reveal are electromagnetic signals, what is measured is a stream of impulses of current. From these, particle physicists inferred all the currently known fundamental interactions of the Standard Model. In the context of quantum information, an entanglement monotone can be taken as another example: if we know the exact quantum state of the bipartite system we can in principle compute it, but there is no observable whose expectation value computes the entanglement monotone on that state for us. Quantum mechanics complicates things in at least three ways:

- Quantum coherence is fragile and projective measurements destroy the previous quantum state, so that measuring them precisely can be challenging
- On the other hand, the fact that quantum states are so easily altered by their environment suggest that they could be used as very precise probes
- Observables in quantum mechanics are not always mutually compatible: measuring more than one parameter on a quantum state is a task whose achievable precision can be fundamentally limited by quantum uncertainty.

Generally speaking, we could divide the approaches into two categories. On the one hand we can consider *Quantum Hypothesis Testing* [182], dealing with a finite number of options we are trying to discriminate between, usually divided into quantum state discrimination [183, 184] and quantum channel discrimination [185, 186]. A typical example could be classifying an ensemble of states into entangled ones and separable ones, without spoiling the entanglement too much. The constraints imposed by the no-cloning theorem, the measurement-induced collapse, the limited amount of available measurements and, sometimes, also the rate at which we can discriminate states, are the main obstacles to face. In other scenarios, instead, we speak about *Quantum Estimation Theory* (QET), or *Quantum Metrology* [187, 188, 189, 190] which deals with *quantum statistical models*, that will be accurately defined in the next Sections: these are subsets of the collection of states of a physical system encoding continuous or discrete parameters that we are trying to estimate. The estimation process involves selecting the optimal measurement setting to be performed on the states defining the statistical models and then post-processing the resulting probability distributions, according to classical estimation theory, to infer the value of an *estimator* of the true parameters values. Besides optimizing the measurement strategy, also the *encoding* can often be selected by choosing

appropriate *probe states* on which the parameters will be encoded. In the end, the desired result will be a purported value for each of the parameters that we attempted to estimate *and* their respective variances. While these variances can depend on the classical post-processing and on specific circumstances, informative and valuable lower bounds on them can be derived on purely theoretical grounds. We can then further distinguish between:

- **Global Estimation Theory**, in which case the measurement is optimized *independently* of the true parameters values and, respectively, the lower bounds on the variances will not depend on the parameters themselves

- **Local Estimation Theory**, in which the optimal measurement depends on the true values of the parameters and so do the lower bounds, *but without implying full previous knowledge of them*. Concretely, one would get a first rough estimate of the parameters values and then she would select accordingly the best fitting measurement in that occurrence.

In what follows, we will focus exclusively on Local Quantum Estimation Theory of real, continuous parameters. We will first begin in Section 4.1 by reviewing axiomatic probability theory and classical estimation theory, providing the basis of any estimation scheme. Subsequently, in Section 4.2 we will introduce quantum statistical models and the central figure of merit, the Quantum Fisher Information, accompanied by the respective Quantum Cramér-Rao bound which constitutes the ultimate inferior limit to the variance of any estimator for a single parameter, dictated solely by the rules of quantum mechanics. Single-parameter quantum estimation theory will be applied to the problem of temperature estimation of photon-subtracted thermal states in Section 4.3, which will also give us the opportunity to discuss the role of post-selection protocols in quantum metrology. As a last topic, in Section 4.4 we will briefly overview the subtle field of multiparameter quantum metrology and we will discuss its applications to a sloppy quantum model for the estimation of two consecutive phases in a Mach-Zender interferometer.

To close our introduction, let us mention a few of the many and diverse applications of quantum metrology. From a merely theoretical viewpoint, quantum metrology is the natural setting to generalize the uncertainty relations and the celebrated Heisenberg Inequality, as was recognized by S. L. Braunstein, C. M. Caves and G. J. Milburn almost 30 years ago [191]. The possibility of harnessing entanglement to beat the *shot-noise limit* in optical interferometry also attracted a wealth of attentions [189, 190, 192, 193], although some examples in which entanglement is not needed to improve precision have also been studied [194, 195]. Quantum metrology assisted by nonclassical features of laser light, such as squeezing, has also been essential to construct extremely sensitive detectors such as those required for gravitational waves detection at LIGO and VIRGO [196, 197]. Another prominent field of application of quantum estimation theory has to do with those scenarios in which the interaction between the pobe and the sample has to be very weak in order to avoid damaging the sample itself, e.g. in biologal applications [198]. On a similar spirit, *quantum illumination* tries to exploit quantum correlations between modes of light to reconstruct the optical properties of an object with minimal interaction [199, 200, 201, 202].

4.1 Classical Fisher Information and estimators

The aim of this section is to introduce the mathematical preliminaries that are necessary to arrive at the notion of *statistical models*. We will start with abstract probability theory, define statistical models and discuss the classical estimation process. The goal is to find a balance between mathematical rigor and conciseness, hoping to provide a short and to-the-point guide without neglecting the formal subtleties characterizing the subject.

4.1.1 Minimal elements of abstract probability theory

Suppose that we are given a space such as $\mathbb{R}^n$ and we want to define a sensible notion of *measure* for subsets of it. It turns out that this cannot be done in a meaningful way for *all* possible subsets: there is a collection of subsets which are *measurable* and all the others are not, depending of course on the way in which we construct the measure (see e.g. the Banach-Tarski paradox). In formal terms:

Definition 4.1.1: Measurable space

A *measurable space* (X, Ω) is a set X together with a collection of subsets Ω of X, called a σ-algebra, fulfilling the following axioms:

- **[AMS1]** $X \in \Omega$
- **[AMS2]** If $A \in \Omega$, then its complement is also in the σ-algebra: $X \setminus A \in \Omega$
- **[AMS3]** If $\{A\}_{n\in\mathbb{N}}$ is a finite or countable collection of elements in Ω, then their *union* is also in Ω:
$$\bigcup_{n\in\mathbb{N}} A_n \in \Omega$$

In particular, any *intersection* of *finitely many* sets in Ω is in Ω and $\varnothing \in \Omega$. The sets in Ω are called *measurable*. A function $f : X \to Y$ between two measurable spaces (X, Ω) and (Y, Σ) is said to be a *measurable function* if and only if the preimage of every measurable set $A \in \Sigma$ is a measurable set in X:

$$\forall A \in \Sigma : \quad f^{-1}(A) := \{v \in X : \ f(v) \in A\} \ \in \ \Omega\} \tag{4.1}$$

From axioms **[AMS1-2]** it follows that $\varnothing \in \Omega$ and from axioms **[AMS1-3]** one can also deduce that any *countable intersection* of measurable sets is measurable. Moreover, the intersection of two σ-algebras on X defines another valid σ-algebra. Two trivial σ-algebras are $\Omega = \{X, \varnothing\}$ and $\Omega = \mathcal{P}(X)$, where $\mathcal{P}(X)$ denotes the power set of X, i.e. the set of all subsets of X. The reason to define σ-algebra is that the above axioms are necessary and sufficient to define a concept of *measure* for any measurable set, leading to the following notion:

Definition 4.1.2: Measure space, measurable functions

A *measure space* (X, Ω, μ) is a measure space (X, Ω) equipped with a function $\mu : \Omega \to \mathcal{B}$ where $\mathcal{B}$ is a Banach space ($\mathbb{R}^+$ for real-valued positive measures) and:

- **[AMS4]** $\mu(\varnothing) = 0$ where 0 is the zero vector in $\mathcal{B}$
- **[AMS5]** μ is σ-additive: if $\{E_n\}_{n\in\mathbb{N}}$ is a finite or countable collection of *measurable* subsets of X that are *pairwise disjoint*, then:

$$\mu\left(\bigcup_{n\in\mathbb{N}} E_n\right) = \sum_{n=0}^{\infty} \mu\left(E_n\right)$$

- **[AMS6]** If $\mathcal{B} = \mathbb{R}^+$, then $\mu(E) \geq 0 \; \forall E \in \Omega$

An important example of measurable space on a set X arises when X is also a topological space:

Definition 4.1.3

A *topological* space (X, τ) is a set X together with a collection of subsets $\tau \subseteq \mathcal{P}(X)$, called a *topology*, respecting the following axioms:

- **[AT1]** $X \in \tau$ and $\varnothing \in \tau$
- **[AT2]** If $A_1, A_2 \in \tau$, then $A_1 \cap A_2 \in \tau$
- **[AT3]** If $\{A\}_{n\in\mathbb{N}}$ is a finite or countable collection of elements in τ, then their *union* is also in τ:

$$\bigcup_{n\in\mathbb{N}} A_n \in \tau$$

The elements of τ are called *open sets*. In particular, when $X = \mathbb{R}^n$, the standard notion of open sets defines the *standard topology* on X.

When (X, τ) is a topological space, when can look for the smallest σ-algebra containing τ, which is the collection of sets generated by arbitrary combination of complements, countable unions and countable intersections of elements in τ. This is called the *Borel σ-algebra* $\mathscr{B}(X)$ on (X, τ). Given all these notions, we can introduce the axiomatic definition of probability according to Kolmogorov:

Definition 4.1.4: Probability space, random variable

A *probability space* is a Borel measure space $(X, \tau, \mathscr{B}(X), \mu)$ with $\mathscr{B}(X)$ being the Borel σ-algebra of the topology τ, and the *probability measure* μ has values in $[0, 1]$: $\mu : \mathscr{B}(X) \to [0, 1]$, with $\mu(\varnothing) = 0$ and $\mu(X) = 1$. A random variable $\mathbb{M} : X \to Y$ is a *measurable function* from the probability space X to a measurable space (Y, Σ).

The target measurable space (Y, Σ) naturally inherits the structure of a probability

space through $\mathbb{M}$ via:

$$\forall A \in \Sigma : \qquad \nu(A) \;:=\; \mu\left(\mathbb{M}^{-1}(A)\right) \in [0,1] \tag{4.2}$$

The idea behind this whole construction by Kolmogorov is that the measurable sets in X are the meaningful, elementary events, while the probability μ defines the statistical state of the system, in the sense that the probability associated with each event $E \in \Sigma$, given by $\mu(E)$, is the probability of the event of finding the system in a state in E. A random variable $\mathbb{M} : X \to Y \subseteq \mathbb{R}$ defines a *measurement setting* on the system, whereas a measurable set $A \in \mathscr{B}(\mathbb{R})$ defines a range of (real) outcomes of the measurement. The probability that the outcome of the measurement $\mathbb{M}$ is in the range A, given the state μ of the system, via Eq.(4.2).

For our purposes, it will be sufficient to assume that Y is always a discrete or continuous subset of $\mathbb{R}$ endowed, respectively, with the *counting measure*[1] or the *Lebesgue measure*, i.e. the standard measure in real spaces deriving from the Borel σ-algebra generated by the standard topology. If the set Y is discrete, the random variable $\mathbb{M}$ is termed *simple*. Leveraging on Lebesgue's theory of integration and starting first from simple random variables, one can define the *integration* of a random variable $\mathbb{M}$ to compute its *expectation value* $\mathrm{E}(\mathbb{M})$:

$$\mathrm{E}(\mathbb{M}) \;:=\; \int_{\Omega} \mathbb{M}\, d\mu \tag{4.3}$$

In particular, if X is finite, then $\Omega = \{A_1, ..., A_n\}$ and the integral reduces to a sum $\mathrm{M}(\mathbb{M}) = \sum_{j=1}^{n} m_j \mu(A_j)$ where $m_j := \mathbb{M}(A_j)$ is the value of the random variable when the event A_j occurs, while $\mu(A_j)$ represents its probability of occurring.

Similarly to the standard construction for real functions, one can use Lebesgue integration on the target space $Y \subseteq \mathbb{R}$ of a random variable to define square-integrable random variables, modulo "almost everywhere" equivalence. We shall denote with $L^2(X, Y)$ the set of square-integrable random variables from the probability space X to the target space Y. Given a collection of such random variables, $\{\mathbb{X}_j\}_{j=1}^{n} \in L^2(X, \mathbb{R})$, their *covariances* are given by the following expectation values:

$$\mathrm{Cov}\left(\mathbb{X}_j, \mathbb{X}_k\right) \;:=\; \mathrm{E}\left[\left(\mathbb{X}_j - \mathrm{E}(\mathbb{X}_j)\right)\left(\mathbb{X}_k - \mathrm{E}(\mathbb{X}_k)\right)\right] \tag{4.4}$$

Together they form the *covariance matrix*, whose diagonal entries are called the *variances* of the respective random variables.

To set the stage for quantum metrology, we will also introduce here the *positive operator-valued measures*, which we encountered in Chapter 1 in an informal way.

[1] The counting measure on a finite set associates to each subset its cardinality.

Theorem 4.1.1

Let $\mathcal{H}$ be an Hilbert space, $\mathcal{S}(\mathcal{H})$ the convex set of quantum states, $(X, \mathscr{B}(X))$ be a measurable space with $X \subseteq \mathbb{R}^n$ finite, countable or continuous. An *effect* $\hat{\mathrm{E}}$ is a linear map $\hat{\mathrm{E}} : \mathcal{S}(\mathcal{H}) \to [0,1]$ associating with each quantum state $\hat{\boldsymbol{\rho}} \in \mathcal{S}(\mathcal{H})$ a probability through Born's rule 1.4. We denote by $\mathcal{E}(\mathcal{H})$ the convex set of effects on $\mathcal{H}$. A *positive operator-valued measure* (POVM) on X is a function $F : \mathscr{B}(X) \to \mathcal{E}(\mathcal{H})$ such that:

1. $\forall B \in \mathscr{B}(X) : \quad 0 \leq F(B) \leq \mathbb{1}$, i.e. F associates with each measurable set a positive operator bounded by the identity operator
2. $F(\varnothing) = 0$ and $F(X) = \mathbb{1}$
3. It is additive under union of pairwise disjoint sets:

$$\{M_j\}_{j=1}^n \text{ s.t. } \forall j \neq k \in \{1, ..., n\} : \quad M_j \in \mathscr{B}(X) \ \wedge \ M_j \cap M_k = \varnothing \implies$$
$$\implies \quad F\left(\bigcup_{j=1}^{n} M_j\right) = \sum_{j=1}^{n} F(M_j) \tag{4.5}$$

where, if $n \to +\infty$, the sum is convergent in the weak topology

The last ingredient that we need to talk about classical and quantum estimation theory is the notion of *probability density function*. This comes about when considering measures that are *absolutely continuous* with respect to the Lebesgue measure ι on $\mathbb{R}$, i.e. to each set that has measure 0 according to Lebesgue they also assign measure 0:

$$\mu \ll \iota \quad \iff \quad \forall A \in \mathscr{B}(\mathbb{R}) : \ \iota(A) = 0 \implies \mu(A) = 0 \tag{4.6}$$

where $\mu \ll \nu$ reads "the probability measure μ is absolutely continuous with respect to the probability measure ν". Such probability measures can all be related one to another via the *Radon-Nikodim Theorem*:

Theorem 4.1.2: Radon-Nikodim

Let μ and μ' be two probability measures on the same measurable space $(X, \mathscr{B}(X))$ and let μ be absolutely continuous with respect to μ', $\mu \ll \mu'$. There will exist a function $p : X \to \mathbb{R}^+$ such that, for any Borel set $B \in \mathscr{B}(X)$:

$$\mu(B) = \int_B p \, d\nu \tag{4.7}$$

The function p, formally written as $p = d\mu/d\nu$, is the *Radon-Nikodim derivative* of μ with respect to ν. When X is a continuous space and ι is the Lebesgue measure, the function p is called the *probability density function* associated with the probability measure μ. Alternatively, if $X \subseteq \mathbb{R}$ is discrete, the Radon-Nikodim derivative of μ with respect to the *counting measure* on X is called a *probability mass function*. When we do not wish to specify if we are talking about a discrete or continuous measure space, we call them *probability distributions*.

4.1.2 Classical statistical models and Fisher Information

The idea of a statistical model comes about when we would like to know the probability density function describing the results of a measurement with continuous outcomes on a given state, but we only have access to a finite sample of M observed outcomes. Oftentimes, the goal is more ambitious, as we wish to reconstruct the full state or, in other words, all the probability density functions resulting from all possible measurements. We assume, however, to be free to choose the type of measurement by which we get the finite collection of sampled outcomes.

Definition 4.1.5: Classical statistical model

Given a probability space $(X, \mathscr{B}(X), \mu)$, a *classical statistical model* on it is defined by a continuous parametric family of probability densities $p_{\vec{\lambda}} : X \to [0,1]$, depending smoothly[a] upon the m real parameters $\vec{\lambda} \in \Lambda \subseteq \mathbb{R}^m$.

[a] Meaning that, as functions of $\vec{\lambda}$, all the probability density functions are C^∞.

It is often assumed that the association $\vec{\lambda} \mapsto p_{\vec{\lambda}}$ is injective, however we will partially relax this assumption when considering *sloppy statistical models* in future sections. Notice that the topological assumptions on X together with the smooth assumptions on the parametrization imply that a statistical model defines a *smooth manifold structure* on a subfamily of probability distributions on X, where the association $p_{\vec{\lambda}} \mapsto \vec{\lambda}$ provides a *chart* on (an open subset of) the manifold[2]. The manifold resulting from a statistical model is a *statistical manifold*.

We now introduce the central quantity in metrology, the Fisher Information matrix. From a geometrical viewpoint, it is the most natural metric to adopt on a statistical manifold, thereby quantifying distances between nearby probability distributions corresponding to slightly varied values of the parameters. At the same time, through the Cramér-Rao Theorem, as we shall see, this metric directly translates into a bound on the maximal precision that one can hope to achieve when estimating the true probability distribution from a finite sample.

Definition 4.1.6: Fisher Information

Let $\{p_{\vec{\lambda}}(x)\}_{\vec{\lambda}\in\mathbb{R}^m}$ be a classical statistical model. Its *Fisher Information matrix*, denoted by $\mathscr{F}[\vec{\lambda}]$ is defined entry-wise as:

$$\mathscr{F}_{jk}[\vec{\lambda}] \quad := \quad \int_X p_{\vec{\lambda}}(x)\, \partial_{\lambda_j} \left[\log p_{\vec{\lambda}}(x)\right]\, \partial_{\lambda_k} \left[\log p_{\vec{\lambda}}(x)\right]\, dx \tag{4.8}$$

and it is an $m \times m$ positive semidefinite metric. Moreover, if the map $\vec{\lambda} \mapsto p_{\vec{\lambda}}$ is everywhere locally invertible, then $\mathscr{F}$ is a positive-definite matrix and it defines a *Riemannian metric* on the statistical manifold.

One would expect that a parameter-independent transformation of the random vari-

[2] To be completely general, one would have to admit the possibility that the smooth association of parameters to probability distributions can be valid only locally, with different, smoothly compatible charts applying to different open neighbours in the functional space of probability distributions

able defining a statistical model will not increase the information content of the model. If the Fisher Information reflects our intuitive notion of the meaning of the word information, then, it should be non-increasing (with respect to the partial ordering of completely positive matrices) under such a transformation acting on the random variable: this is indeed the case and, moreover, according to Chentsov Theorem, it is the only metric on the statistical manifold with this property, modulo a constant rescaling.

Let us now imagine that we sample M times a random variable $\mathbb{M} : Y \to X$, where $X \subseteq \mathbb{R}$ is either discrete or continuous. This set of outcomes will be a point in X^M and we wish to use it to reconstruct the probability distribution $\tilde{p} : X \to [0,1]$ that would be computed from the full knowledge of the state of the system. The standard approach is to use the framework of statistical models, so that instead of having to reconstruct a full function, we need to find the right parameters $\vec{\lambda}^*$ in some $\mathbb{R}^m$ determining the function, $p_{\vec{\lambda}^*} = \tilde{p}$. An *estimator* is precisely a way to infer the right parameters given the M outcomes:

Definition 4.1.7

Given the M outcomes in X^M of a random variable $\mathbb{M} : Y \to X$, an *estimator* is a random variable $\Theta^{(M)} : X^M \to \Lambda$, where $\Lambda \subseteq \mathbb{R}^m$ is the space of parameters. It is called *unbiased* if:

$$\forall \vec{\lambda} \in \Lambda : \quad \mathrm{E}_{\vec{\lambda}}\left[\Theta^{(M)}\right] = \vec{\lambda} \tag{4.9}$$

where $\mathrm{E}_{\vec{\lambda}}[\bullet]$ denotes the expectation value of a random variable with respect to the probability distribution $p_{\vec{\lambda}}$ in the statistical model. It is called *asymptotically unbiased* if the above condition holds for $M \to \infty$.

As for any other random variable, one can compute the covariance matrix for the estimator. In particular, one considers the components of $\Theta^{(M)}$, which is a function from $X^M \to \Lambda \subseteq \mathbb{R}^m$, so that $\left(\Theta^{(M)}\right)_j : X^M \to \Lambda_j \subseteq \mathbb{R}$, as m random variables. The covariance, if the estimator is unbiased, is given by:

$$\left[\mathrm{Cov}(\Theta^{(M)})\right]_{jk} := \mathrm{E}_{\vec{\lambda}}\left[\left((\Theta^{(M)})_j - \lambda_j\right)\left((\Theta^{(M)})_k - \lambda_k\right)\right] \tag{4.10}$$

If an estimator performs better than another one, for the same dimension M of the sample, its covariance matrix should be smaller; at the same time, we cannot expect, in general, to have zero mean-squared errors if M is finite. A lower bound is provided by the Cramér-Rao Inequality:

Theorem 4.1.3: Cramér-Rao

Given a statistical model $\{p_{\vec{\lambda}}\}_{\vec{\lambda}\in\Lambda}$ and *any unbiased estimator* $\Theta^{(M)}$ for a random variable distributed according to the probability distribution $\tilde{p} = p_{\vec{\lambda}^*}$, its covariance matrix is bounded from below, in the sense of partial ordering of completely positive matrices, by:

$$\mathrm{Cov}\left(\Theta^{(M)}\right) \;\geq\; \frac{1}{M}\,\mathscr{F}^{-1}\left[p_{\vec{\lambda}^*}\right] \tag{4.11}$$

where $\mathscr{F}^{-1}$ denotes the matrix inverse of the Fisher Information matrix, computed for the true value $\vec{\lambda}^*$ of the set of parameters.

An unbiased estimator is *efficient* if it saturates the Cramér-Rao bound. For finite M and for some statistical model, it can happen that no efficient estimator exists. A more reasonable request is to ask that the bound is saturated in the limit $M \to \infty$[3]: estimators fulfilling this condition are called *asymptotically efficient* and they always exist, the most well-known examples being the Bayes estimator and the maximum-likelihood estimator.

4.2 Quantum Estimation Theory

If we want to translate the ideas that we just introduced to the quantum setting, the first place to start is to replace Eq.(4.2), that computes the probability for the outcome of a measurement $\mathbb{M}$ to lie in the set $A \in \mathscr{B}(\mathbb{R})$ if the state is the probability measure $\mu : \Sigma \to [0,1]$. The equivalent prescription in quantum mechanics is Born's rule, Eq.(1.4): the probability measure μ is replaced by a quantum state $\hat{\boldsymbol{\rho}}$, the measurement $\mathbb{M}$ by a POVM F, and given a Borel set $A \in \mathscr{B}(X)$, $X \subseteq \mathbb{R}$, the probability of getting an outcome in A while measuring F on $\hat{\boldsymbol{\rho}}$ is $\mathrm{Tr}\left[\hat{\boldsymbol{\rho}}\hat{\Pi}_A\right]$ where $\hat{\Pi}_A = F(A) \in \mathcal{E}(\mathcal{H})$ is the effect associated with A via the POVM. Via this procedure, we thus have a probability measure $\mu_F^{\hat{\boldsymbol{\rho}}}$:

$$\mu_F^{\hat{\boldsymbol{\rho}}} : \mathscr{B}(X) \to [0,1] \quad \text{s.t} \quad \mu_F^{\hat{\boldsymbol{\rho}}}(A) = \mathrm{Tr}[\hat{\boldsymbol{\rho}}\hat{\Pi}_A] \tag{4.12}$$

of which we can take the Radon-Nikodim derivative with respect to the counting or Lebesgue measure, depending on whether $X \subseteq \mathbb{R}$ is discrete or continuous. The net result is that, once a state $\hat{\boldsymbol{\rho}}$ and a POVM F have been fixed, we obtain again a probability distribution $\tilde{p} = d\mu_F^{\hat{\boldsymbol{\rho}}}/d\iota$.

In order to compute the corresponding Fisher Information matrix, however, we should define what is a *quantum* statistical model. Indeed, if in the classical case we were just interested in estimating $\tilde{p}$ from a sampling of the associated random variable, hence we embedded $\tilde{p}$ in a parametric family of probability distributions, in the quantum case we are often interested in estimating some parameter specifying a quantum channel. The typical and most studied case is that of *unitary models*, in which one considers a parametric Hamiltonian $\hat{\mathrm{H}}(\vec{\lambda})$ and tries to infer the parameters value by first letting a probe state $\hat{\boldsymbol{\rho}}_0$ evolve unitarily under $\hat{\mathrm{H}}(\vec{\lambda})$ for a fixed amount of time and then measuring it with some POVM to get the desired probability distribution. A less obvious case is the

[3] One should multiply by M both sides of the inequality before taking the limit, to get a nontrivial result.

estimation of temperature of a quantum environment in a thermal state: in this case a convenient approach would be to take a probe state of a quantum system whose size is negligible with respect to the environment, and coupling it to the latter to achieve thermalization. The end result is still described by a CPTP map taking all quantum states of the probe system to the thermal state with the desired temperature.

Definition 4.2.1: Quantum Statistical Model

Given an Hilbert space $\mathcal{H}$, a *quantum statistical model* $\mathrm{S}_{\mathcal{Q}} : \Lambda \subseteq \mathbb{R}^m \to \mathcal{S}(\mathcal{H})$ is a smooth injective mapping from the parameters space Λ to a family of quantum states $\{\hat{\boldsymbol{\rho}}_{\vec{\lambda}}\}_{\vec{\lambda}\in\Lambda}$. It is often assumed that the rank of $\hat{\boldsymbol{\rho}}_{\vec{\lambda}}$ does not depend upon the parameters.

Given a quantum statistical model $S_{\mathcal{Q}}$ and a POVM F, we can define a *classical* statistical model via $p_{\vec{\lambda}}(A) = \mathrm{Tr}\left[\hat{\boldsymbol{\rho}}_{\vec{\lambda}} F(A)\right]$ and we can compute the Fisher Information of the latter. The crucial difference is that in the classical case the random variable $\mathbb{M}$ was fixed *before* constructing the classical statistical model, whereas in the quantum setting, once a quantum statistical model is given, one can still choose the type of measurement (POVM) by which the associated classical statistical model is computed.

4.2.1 Quantum Fisher Information for single parameters

If the quantum statistical model involves a single parameter ($m = 1$, $\Lambda \subseteq \mathbb{R}$), the Fisher Information reduces to a real, positive function of this single parameter and it provides a scalar lower bound for the variance of any unbiased estimator through the Cramér-Rao inequality. It is then meaningful to ask what is the POVM F which maximizes the Fisher Information of the resulting probability distribution, so that the variance of an asymptotically efficient estimator can be minimized. In general, the answer will depend on the true value of the parameter λ, but it is of utmost importance to stress that such a dependence does *not* enter in the derivations needed to compute the Fisher Information: those derivatives only act on the λ-dependence of the *quantum statistical model* and *not* on the λ-dependent optimized POVM. Under these assumptions, we can state the following result:

Definition 4.2.2: Symmetric Logarithmic Derivative

Given a single-parameter quantum statistical model $\{\hat{\boldsymbol{\rho}}_\lambda\}$, a *Symmetric Logarithmic Derivative* (SLD) $\hat{\mathrm{L}}_\lambda$ is a *self-adjoint operator* fulfilling the following *Lyapunov Equation*:

$$\partial_\lambda \hat{\boldsymbol{\rho}}_\lambda \;=\; \frac{1}{2}\left(\hat{\boldsymbol{\rho}}_\lambda \hat{\mathrm{L}}_\lambda + \hat{\mathrm{L}}_\lambda \hat{\boldsymbol{\rho}}_\lambda\right) \tag{4.13}$$

whose general solution, in the eigenbasis of $\hat{\boldsymbol{\rho}}_\lambda = \sum_n {\rho^\lambda}_n |{\psi^\lambda}_n\rangle\langle{\psi^\lambda}_n|$ is:

$$\hat{\mathrm{L}}_\lambda \;=\; 2\sum_{n,m} \frac{\langle{\psi^\lambda}_n|\partial_\lambda \hat{\boldsymbol{\rho}}_\lambda|{\psi^\lambda}_n\rangle}{{\rho^\lambda}_n + {\rho^\lambda}_m} |{\psi^\lambda}_m\rangle\langle{\psi^\lambda}_n| \tag{4.14}$$

and it is implied that the sum extends only to terms for which ${\rho^\lambda}_n + {\rho^\lambda}_m \neq 0$.

Equivalently, if the dependence on λ of the eigenvalues and eigenvectors of $\hat{\boldsymbol{\rho}}_\lambda$ is discerned, one can rewrite Eq.(4.14) as:

$$\begin{aligned}\hat{\mathrm{L}}_\lambda &= \sum_n {\rho^\lambda}_n \left(\partial_\lambda \log {\rho^\lambda}_n\right) |{\psi^\lambda}_n\rangle\langle{\psi^\lambda}_n| \; + \\ &+ 2 \sum_{n\neq m} \frac{{\rho^\lambda}_n - {\rho^\lambda}_m}{{\rho^\lambda}_n + {\rho^\lambda}_m} \langle{\psi^\lambda}_m|\partial_\lambda {\psi^\lambda}_n\rangle \, |{\psi^\lambda}_m\rangle\langle{\psi^\lambda}_n|\end{aligned} \tag{4.15}$$

Definition 4.2.3: Quantum Fisher Information

The Fisher Information computed as:

$$\left(\mathscr{F}_\lambda \left[\mathrm{Tr}[\hat{\boldsymbol{\rho}}_\lambda \hat{\Pi}_{\lambda^*}(x)]\right]\right)_{\lambda=\lambda^*} = \mathrm{Tr}\left[\hat{\boldsymbol{\rho}}_{\lambda^*} \hat{\mathrm{L}}^2_{\lambda^*}\right] \tag{4.16}$$

where $\hat{\Pi}_{\lambda^*}(x)$ is the POVM obtained from the spectral projectors on the eigenvectors of the symmetric logarithmic derivative $\hat{\mathrm{L}}_\lambda$ is called the *Quantum Fisher Information* (QFI), it depends solely on the quantum statistical model, and it will be denoted by $\mathcal{Q}_{\{\hat{\boldsymbol{\rho}}_\lambda\}}(\lambda)$.

Theorem 4.2.1: Braunstein-Caves

Given a single-parameter quantum statistical model $\{\hat{\boldsymbol{\rho}}_\lambda\}$, the maximum of the Fisher Information over all possible parameter-independent POVMs around the generic state $\hat{\boldsymbol{\rho}}_{\lambda^*}$ of the quantum statistical model is equal to the Quantum Fisher Information evaluated in λ^*:

$$\max_{F\in\mathrm{POVMs}} \mathscr{F}_{\lambda^*}\left[\mathrm{Tr}[\hat{\boldsymbol{\rho}}_{\lambda^*} F(x)]\right] = \mathcal{Q}_{\{\hat{\boldsymbol{\rho}}_\lambda\}}(\lambda^*) \tag{4.17}$$

The Quantum Fisher Information, inserted in the Cramér-Rao Inequality 4.11, results in the so-called *quantum Cramér-Rao bound*:

$$\mathrm{Cov}\left(\Theta^{(M)}[\lambda]\right) \geq \frac{1}{M\mathcal{Q}_{\hat{\boldsymbol{\rho}}_{\tilde{\lambda}}}(\lambda^*)} \tag{4.18}$$

We stress that the possibility of saturating this bound depends on two steps: first one should define an appropriate *observable*, as a self-adjoint operator, through the projectors $\hat{\Pi}_\lambda(x)$ derived from the diagonalization of the symmetric logarithmic derivative. Measuring M times the observable on the quantum state encoding the value of the true parameter, one gets an *estimator* computed as the *mean* of these values: this fact depends on the choice of the observable, and it can be shown that the right observable to achieve this is $\hat{\mathrm{O}}_\lambda = \lambda\mathbb{1} + \frac{\hat{\mathrm{L}}_\lambda}{\mathcal{Q}(\lambda)}$. With this, one can already prove that:

$$\mathrm{Tr}[\hat{\boldsymbol{\rho}}_\lambda \hat{\mathrm{O}}_\lambda] = \lambda \tag{4.19}$$

$$\langle \Delta\hat{\mathrm{O}}_\lambda{}^2 \rangle = \frac{1}{\mathcal{Q}(\lambda)} \tag{4.20}$$

where Eq.(4.19) shows that the estimator is *asymptotically*[4] unbiased, while Eq.(4.20) indicates that the estimator will saturate the quantum Cramér-Rao bound, at least asymp-

[4]One would have to collect a large number of outcomes to expect convergence to the correct mean value

totically, because of the Central Limit Theorem.

It is useful to rewrite the QFI in several explicit forms, to clarify its meaning. We will start by using the formulas (4.14-4.15) into (4.16):

$$\mathcal{Q}(\lambda) = 2\sum_{n,m} \frac{\left|\langle\psi^\lambda{}_m|\partial_\lambda\hat{\boldsymbol{\rho}}_\lambda|\psi^\lambda{}_n\rangle\right|^2}{\rho^\lambda{}_n + \rho^\lambda{}_m} \tag{4.21}$$

$$= \sum_n \rho^\lambda{}_n \left(\partial_\lambda \log \rho^\lambda{}_n\right)^2 + 2\sum_{n\neq m} \frac{(\rho^\lambda{}_n - \rho^\lambda{}_m)^2}{\rho^\lambda{}_n + \rho^\lambda{}_m} \left|\langle\psi^\lambda{}_m|\partial_\lambda\psi^\lambda{}_n\rangle\right|^2 \tag{4.22}$$

The second expression (4.22) makes it clear that if the quantum statistical model contains mixed states there is an additional term, the first one, which is simply the Fisher Information of the eigenvalues distribution of $\hat{\boldsymbol{\rho}}_\lambda$, i.e. of the populations of the corresponding pure states. If the model is composed only of pure states, $\hat{\boldsymbol{\rho}}_\lambda = |e_\lambda\rangle\langle e_\lambda|$, then one can go back to the Lyapunov Equation and check that the SLD and QFI for the pure quantum statistical model are:

$$\hat{\mathrm{L}}^{\mathrm{pure}}_\lambda = |\partial_\lambda e_\lambda\rangle\langle e_\lambda| + |e_\lambda\rangle\langle\partial_\lambda e_\lambda| \tag{4.23}$$

$$\mathcal{Q}^{\mathrm{pure}}(\lambda) = 4\left[\langle\partial_\lambda e_\lambda|\partial_\lambda e_\lambda\rangle + \left(\langle\partial_\lambda e_\lambda|e_\lambda\rangle\right)^2\right] \tag{4.24}$$

We highlight that the term $\langle\partial_\lambda e_\lambda|e_\lambda\rangle$ in Eq.(4.24) is purely imaginary, which can be seen by the fact that:

$$0 = \partial_\lambda 1 = \partial_\lambda\left(\langle e_\lambda|e_\lambda\rangle\right) = \langle\partial_\lambda e_\lambda|e_\lambda\rangle + \text{c.c.}$$

where c.c. is short for complex conjugate. Thus, the square in Eq.(4.24) is actually negative and the QFI is maximized when $|\partial_\lambda e_\lambda\rangle$ is orthogonal to $|e_\lambda\rangle$ and it has a large modulus, implying that small variations of the parameter radically change the associated pure state.

4.2.2 Unitary quantum statistical models

To conclude our preliminary survey on single-parameter quantum estimation, let us take on a specific example that was briefly mentioned before. We consider a smooth parametric family of Hamiltonian operators $\hat{\mathrm{H}}(\lambda)$ acting on an Hilbert space $\mathcal{H}$ and inducing the unitary evolution $\hat{\mathbf{U}}_\lambda(t) = e^{-it\hat{\mathrm{H}}(\lambda)}$. Calling $\hat{\boldsymbol{\rho}}_0$ our generic probe state, the quantum statistical model will be defined by states of the form:

$$\hat{\boldsymbol{\rho}}_{\lambda;t} := e^{-it\hat{\mathrm{H}}(\lambda)}\hat{\boldsymbol{\rho}}_0 e^{it\hat{\mathrm{H}}(\lambda)} \tag{4.25}$$

where time enters as an additional parameter, with different times defining different models. Inside the parametric family of Hamiltonians, we suppose that it lies the actual Hamiltonian of a physical system that we wish to probe; λ could be, for example, the coupling strength of a (quantum) spin with a magnetic moment and an external, classical magnetic field, or the amplitude of the field itself. It is clear that the eigenvalues of $\hat{\boldsymbol{\rho}}_{\lambda;t}$ will not depend on λ, since the evolution is unitary; the maximization of the QFI over all probe states $\hat{\boldsymbol{\rho}}_0$ can thus be reduced to pure probe states only, since any convex

combination of them will result in the corresponding convex combination of QFIs. We can then apply Eq.(4.24) to the pure model $|\psi_{\lambda;t}\rangle = e^{-it\hat{\mathrm{H}}(\lambda)}|\psi_0\rangle$ to get:

$$\mathcal{Q}^{U}(\lambda,t) \;=\; 4\left[\left\langle|\partial_\lambda\hat{\mathbf{U}}_\lambda(t)|^2\right\rangle_0 \;+\; \left\langle\hat{\mathbf{U}}^\dagger_\lambda(t)\partial_\lambda\hat{\mathbf{U}}_\lambda(t)\right\rangle^2_0\right] \tag{4.26}$$

where $|\hat{\mathrm{A}}|^2 = \hat{\mathrm{A}}^\dagger\hat{\mathrm{A}}$ and $\langle\bullet\rangle_0 = \langle\psi_0|\bullet|\psi_0\rangle$. A further subclass of these unitary models arises when the dependence of the Hamiltonian upon the parameter is linear, i.e. $\hat{\mathrm{H}}(\lambda) = \lambda\hat{\mathrm{G}}$. While for the generic case we cannot differentiate the unitary evolution operator by simply bringing down the derivative of the Hamiltonian[5], in this simpler scenario we can do that and arrive at a concise answer:

$$\mathcal{Q}^{\text{cov.}}(t) \;=\; 4t^2\mathrm{Var}\left(\hat{\mathrm{G}};|\psi_0\rangle\right) \;= 4t^2\left[\langle\hat{\mathrm{G}}^2\rangle_0 - \langle\hat{\mathrm{G}}\rangle^2_0\right] \tag{4.27}$$

where, importantly, the dependence of the QFI on the parameter λ to be estimated is disappeared; quantum statistical models with such a property are often termed *covariant*. The time parameter can clearly be reabsorbed in a rescaling of λ, since only their product appears in $\hat{\mathbf{U}}_{\lambda;t}$ when the model is covariant. The Cramér-Rao Inequality, therefore, reduces to the well-known uncertainty relation:

$$\mathrm{Var}\left(\Theta^{(M)}\left[\lambda\right];|\psi_0\rangle\right)\;\mathrm{Var}\left(\hat{\mathrm{G}};|\psi_0\rangle\right) \;\geq\; \frac{1}{4N} \tag{4.28}$$

Since λ is a real parameter with the dimensions of time (after the rescaling) and $\hat{\mathrm{G}}$ is the operator generating the time translations, the above inequality should be understood as akin to the energy-time uncertainty relation, which can be better defined in terms of quantum speed limits, rather than the standard uncertainty relations for canonically conjugated operators. Notice that we wrote $\Theta^{(M)}\left[\lambda\right]$ in the left-hand side of Eq.(4.28) because the related variance is associated with an *estimator*, whose optimization can lead to the saturation of the inequality. As for the most informative probe state $|\psi_0\rangle$ that one can use for these simple unitary covariant models, it is apparent that any balanced superposition of the ground state and highest excited state of $\hat{\mathrm{G}}$ maximizes the variance of $\hat{\mathrm{G}}$, thus providing the smallest lower bound on the variance of the estimator for λ.

[5]Indeed, in general, the derivative does not commute with the Hamiltonian itself, nor do commute two Hamiltonians in the family for different values of λ.

4.3 Temperature estimation of photon-subtracted thermal states and cost effectiveness

As a concrete example of a one-parameter, mixed quantum statistical model, let us consider thermal states of a single mode [98], characterized by an average number of photons $\lambda = (e^{\beta} - 1)^{-1}$, where $\beta = \hbar\omega/(k_B T)$, T is the temperature parameter of the state and ω is the frequency of the mode. In the number basis, the state can be expressed as:

$$\hat{\boldsymbol{\nu}}_\lambda := \sum_{n=0}^{+\infty} p_n(\lambda)\, |n\rangle\langle n| \,, \tag{4.29}$$

$$p_n(\lambda) := \frac{1}{1+\lambda}\left(\frac{\lambda}{1+\lambda}\right)^n . \tag{4.30}$$

For analytic convenience, the parameter to be estimated will be λ rather than β^{-1}. Although the Fisher Information for λ and β^{-1} are related by a temperature-dependent conversion factor dictated by propagation of uncertainty, this is the same factor for all the considered quantities, and it cannot influence the comparisons and the relevant conclusions we are going to draw. In what follows, we shall compare the QFI of this quantum statistical model with that obtained by first applying single-photon subtraction to the thermal states.

4.3.1 Ideal single-photon subtraction

Ideally, the subtraction of a single photon is implemented on the Hilbert space by the action of the annihilation operator $\hat{a}$ of the corresponding mode. If $\hat{\boldsymbol{\nu}}_\lambda^-$ is the ideal single-photon subtracted thermal state:

$$\hat{\boldsymbol{\nu}}_\lambda^- := \mathcal{E}^-\left[\hat{\boldsymbol{\nu}}_\lambda\right] = \frac{\hat{a}\,\hat{\boldsymbol{\nu}}_\lambda \hat{a}^\dagger}{\mathrm{Tr}[\hat{\boldsymbol{\nu}}_\lambda \hat{a}^\dagger \hat{a}]} = \frac{1}{\lambda}\hat{a}\,\hat{\boldsymbol{\nu}}_\lambda \hat{a}^\dagger \,. \tag{4.31}$$

its photon-number probability distribution will be:

$$p_n^-(\lambda) \;=\; \frac{n+1}{(1+\lambda)^2}\left(\frac{\lambda}{1+\lambda}\right)^n . \tag{4.32}$$

Notice that the average number of photons in the ideal single-photon subtracted thermal state is:

$$\mathrm{Tr}[\hat{\boldsymbol{\nu}}_\lambda^- \hat{a}^\dagger \hat{a}] \;=\; 2\lambda$$

and, perhaps counter-intuitively, this is greater than λ, the average number of photons in the starting thermal state before the photon is subtracted [203]. This can be seen as a consequence of the fact that the vacuum state is always the most probable number state in a thermal distribution, and it is removed from the mixture by single-photon subtraction.

To compute the Fisher Information resulting from standard measurement protocols in quantum optics, we also need the probability distributions associated with $\hat{\boldsymbol{\nu}}_\lambda^-$, whose expressions are easier to derive starting from an operator representation of these states. As we saw in Chapter 2:

$$\hat{\boldsymbol{\nu}}_\lambda \;=\; (1 - e^{-\beta}) e^{-\beta \hat{a}^\dagger \hat{a}} \,. \tag{4.33}$$

Applying the ideal single-photon subtraction map $\mathcal{E}^-$ to this expression:

$$\begin{aligned}\hat{\boldsymbol{\nu}}_\lambda^- &= (1-e^{-\beta})^2\left[\mathbb{I}+\hat{a}^\dagger\hat{a}\right]e^{-\beta\hat{a}^\dagger\hat{a}}\\ &= (1-e^{-\beta})^2\left[\mathbb{I}-\frac{\partial}{\partial\beta}\right]e^{-\beta\hat{a}^\dagger\hat{a}}\,.\end{aligned}\tag{4.34}$$

The last expression is very convenient to readily evaluate the homodyne and heterodyne distributions of $\hat{\boldsymbol{\nu}}_\lambda^-$ from the well-known corresponding distributions of the thermal state $\hat{\boldsymbol{\nu}}_\lambda$.

In a completely analogous way, the single-photon added thermal state defined by:

$$\hat{\boldsymbol{\nu}}_\lambda^+ := \mathcal{E}^+\left[\hat{\boldsymbol{\nu}}_\lambda\right] = \frac{1}{\lambda+1}\hat{a}^\dagger\hat{\boldsymbol{\nu}}_\lambda\hat{a}\,,\tag{4.35}$$

can be rewritten as:

$$\begin{aligned}\hat{\boldsymbol{\nu}}_\lambda^+ &= (e^\beta-1)(1-e^{-\beta})\,\hat{a}^\dagger\hat{a}\,e^{-\beta\hat{a}^\dagger\hat{a}}\\ &= -(e^\beta-1)(1-e^{-\beta})\frac{\partial}{\partial\beta}e^{-\beta\hat{a}^\dagger\hat{a}}\,.\end{aligned}\tag{4.36}$$

The corresponding photon-number distribution is:

$$p_n^+(\lambda) = \frac{n}{\lambda(1+\lambda)}\left(\frac{\lambda}{1+\lambda}\right)^n.\tag{4.37}$$

and the average photon number is $2\lambda+1$ in this case.

The Husimi Q-function of these states are easily evaluated from Eq.(4.33), Eq.(4.34) and Eq.(4.35):

$$Q_\lambda(\alpha) = \frac{1}{\pi(1+\lambda)}\exp\left[-\frac{|\alpha|^2}{1+\lambda}\right],\tag{4.38}$$

$$Q_\lambda^-(\alpha) = \frac{1+\lambda(1+|\alpha|^2)}{\pi(1+\lambda)^3}\exp\left[-\frac{|\alpha|^2}{1+\lambda}\right],\tag{4.39}$$

$$Q_\lambda^+(\alpha) = \frac{|\alpha|^2}{\pi(1+\lambda)^2}\exp\left[-\frac{|\alpha|^2}{1+\lambda}\right].\tag{4.40}$$

Analogously, the probability distributions associated with the quadrature $\hat{x}=\frac{\hat{a}+\hat{a}^\dagger}{\sqrt{2}}$ for $\hat{\boldsymbol{\nu}}_\lambda$, $\hat{\boldsymbol{\nu}}_\lambda^-$ and $\hat{\boldsymbol{\nu}}_\lambda^+$ are, respectively:

$$X_\lambda(x) = \frac{1}{\sqrt{\pi}\sqrt{1+2\lambda}}\exp\left[-\frac{x^2}{1+2\lambda}\right],\tag{4.41}$$

$$X_\lambda^-(x) = \frac{1+\lambda(3+2x^2+2\lambda)}{\sqrt{\pi}(1+2\lambda)^{5/2}}\exp\left[-\frac{x^2}{1+2\lambda}\right],\tag{4.42}$$

$$X_\lambda^+(x) = \frac{\lambda+2(\lambda^2+x^2(1+\lambda))}{\sqrt{\pi}(1+2\lambda)^{5/2}}\exp\left[-\frac{x^2}{1+2\lambda}\right].\tag{4.43}$$

Among Gaussian measurements, it has been shown in [204] that either heterodyne detection (whose statistics is described by the Husimi Q-function) or homodyne detection are provably optimal to estimate the temperature of thermal states. However, it is not obvious if this holds for the photon-subtracted and photon-added thermal states.

4.3.2 Realistic single-photon subtraction

Photon-subtraction is a cornerstone of many quantum optical protocols, particularly as a backdoor to non-Gaussian states of electromagnetic radiation [205, 206, 207, 208, 209], as well as to test fundamental aspects of quantum mechanics [210, 211, 212, 213, 214] and to improve quantum teleportation with continuous variables [215, 216]. The standard way to implement approximate single-photon subtraction on a state in quantum optics involves sending it onto a high transmittance beam-splitter, with the vacuum state in the orthogonal port, and performing on-off detection on the weak, reflected signal [217]. In the limit of infinitesimal reflectivity of the beam-splitter and perfect efficiency of the on-off detection, whenever the detectors catches a signal, it will be a single photon and the transmitted, output state will be single-photon subtracted according to the ideal map $\mathcal{E}^-$ introduced above. The action of the beam-splitter is described by the unitary operator:

$$\hat{\mathbf{U}}_{\rm BS}(\zeta) \;=\; \exp\left[\zeta \hat{a}^\dagger \hat{b} - \zeta^* \hat{a}\hat{b}^\dagger\right] . \tag{4.44}$$

where $\hat{a}$ is the mode operator of the field we are interested in and $\hat{b}$ is the mode operator of the orthogonal port. The parameter $\zeta = \theta e^{i\phi}$ quantifies the transmissivity and the additional phase introduced by the beam-splitter. It is convenient to express the BS unitary operator as:

$$\hat{\mathbf{U}}_{\rm BS}(\zeta) \;=\; \exp\left[-e^{-i\phi}\tan\theta\;\hat{a}\hat{b}^\dagger\right]\left(\cos^2\theta\right)^{\frac{1}{2}(\hat{a}^\dagger\hat{a}-\hat{b}^\dagger\hat{b})}\exp\left[e^{i\phi}\tan\theta\;\hat{a}^\dagger\hat{b}\right] \tag{4.45}$$

derived from Eq.(4.44) by exploiting the rules of the two-boson representation of the $\mathfrak{su}(2)$ Lie algebra provided by the operators $\hat{J}_+ = \hat{a}^\dagger\hat{b}$, $\hat{J}_- = \hat{a}\hat{b}^\dagger$ and $\hat{J}_3 = \frac{1}{2}[\hat{J}_+, \hat{J}_-] = \frac{1}{2}(\hat{a}^\dagger\hat{a} - \hat{b}^\dagger\hat{b})$. We will assume $\phi = 0$ and $\eta = \cos^2\theta$ will be the beam-splitter *transmittance*. If $\theta = 0$, then $\eta = 1$ and $\hat{\mathbf{U}}_{\rm BS} = \mathbb{I}$, so that the input state is fully transmitted. Our input for the two modes, instead, is $\hat{\boldsymbol{\nu}}_\lambda \otimes |0\rangle\langle 0|$. Carrying out the computation, we get:

$$\hat{\mathbf{U}}_{\rm BS}(\theta)\left[\hat{\boldsymbol{\nu}}_\lambda \otimes |0\rangle\langle 0|\right]\hat{\mathbf{U}}^\dagger_{\rm BS}(\theta) \;=\; \frac{1}{1+\lambda}\sum_{n=0}^{+\infty}\sum_{k,k'=0}^{n}\left(\frac{\lambda}{1+\lambda}\right)^n \tag{4.46}$$

$$\times\sqrt{\binom{n}{k}\binom{n}{k'}}(1-\eta)^{\frac{k+k'}{2}}\eta^{n-\frac{k+k'}{2}}|n-k\rangle\langle n-k'|\otimes|k\rangle\langle k'|$$

At this point, an on-off detection with efficiency $0 < \epsilon \leq 1$ is performed on the second mode. This is described by a POVM with two effects:

$$\hat{\Pi}_0 \;=\; \sum_{m=0}^{+\infty}(1-\epsilon)^m|m\rangle\langle m|\,, \tag{4.47}$$

$$\hat{\Pi}_1 \;=\; \mathbb{I} - \hat{\Pi}_0 \;=\; \sum_{m=0}^{+\infty}\left[1-(1-\epsilon)^m\right]|m\rangle\langle m|\,. \tag{4.48}$$

Whenever the detector clicks, meaning that the outcome is 1, the state of the first mode will be the approximate single-photon subtracted thermal state. This happens with probability:

$$\wp_1(\lambda;\eta,\epsilon) \;=\; \mathrm{Tr}\left[\left(\mathbb{I}\otimes\hat{\Pi}_1\right)\hat{\mathbf{U}}_{\rm BS}(\theta)\left[\hat{\boldsymbol{\nu}}_\lambda\otimes|0\rangle\langle 0|\right]\hat{\mathbf{U}}^\dagger_{\rm BS}(\theta)\right] \;=\; \frac{\lambda\epsilon(1-\eta)}{1+\lambda\epsilon(1-\eta)} \tag{4.49}$$

Denoting with $\hat{\boldsymbol{\rho}}_\lambda$ the approximate single-photon subtracted thermal state and by Tr_B the partial trace over the second output mode of the beam-splitter:

$$\begin{aligned}\hat{\boldsymbol{\rho}}_\lambda &= \frac{1}{\wp_1}\mathrm{Tr}_B\left[\left(\mathbb{I}\otimes\hat{\Pi}_1\right)\hat{\mathbf{U}}_{\mathrm{BS}}(\theta)\left[\hat{\boldsymbol{\nu}}_\lambda\otimes|0\rangle\langle 0|\right]\hat{\mathbf{U}}_{\mathrm{BS}}^\dagger(\theta)\right] = \\ &= \frac{1}{\wp_1}\frac{1}{1+\eta\lambda}\sum_{n=0}^{+\infty}\left(\frac{\eta\lambda}{1+\eta\lambda}\right)^n\left[1-\left(\frac{1+\eta\lambda}{1+\lambda(\eta+(1-\eta)\epsilon)}\right)^{n+1}\right]|n\rangle\langle n| \end{aligned} \tag{4.50}$$

Looking at Eq.(4.50), apart from the factor in square brackets and the normalization, the usual distribution of a thermal state with average number of photons $\eta\lambda$ can be recognized: this would be the state of the first mode after the beam-splitter if no detection took place on the reflected beam. Moreover, both Eq.(4.46) and the final result in Eq.(4.50) involve P-classical states. Indeed, the former is the result of a P-classical state mixed with the vacuum by a beam-splitter, while the final state is diagonal in the number basis and with non vanishing photon-number probability for any $n \geq 0$, hence it must be P-classical too; this also implies that their Wigner functions are everywhere non-negative in phase space. However, the state in Eq.(4.50) is non-Gaussian[6], having a Wigner function which is a linear combination of two Gaussians in phase space. Indeed, while $\hat{\Pi}_0$ is Gaussian, the operator $\hat{\Pi}_1$ corresponding to the successful subtraction is not. Checking the fidelity between the realistic state Eq.(4.50) and the ideal one in Eq.(4.34) for the reference values $\eta = 0.95$ and $\epsilon = 0.97$, it turns out to be greater than 0.9 for values of $\lambda \lesssim 70$, confirming that it is a good approximation to the ideal state.

4.3.3 Fisher Information for single-photon subtracted thermal states

All the states considered above are diagonal in the number basis, as in Eqs.(4.29), (4.32), (4.37), and (4.50); therefore, only the first contribution is present in the general formula for the QFI, Eq.(4.22), and it amounts to the (classical) FI of the photon-number probability distributions $P_n(\lambda)$:

$$\mathscr{F}[\{P_n(\lambda)\}] = \sum_{n=0}^{+\infty}\frac{[\partial_\lambda P_n(\lambda)]^2}{P_n(\lambda)} \tag{4.51}$$

By the same token, also the SLDs are diagonal in the Fock basis. In other words, the problem of estimating λ on these states is a classical estimation problem embedded in a quantum setting. In this sense, single-photon detection is a *classical* detection strategy for this special scenario. Also, no entanglement is created by the beam-splitter, given that the input state is P-classical.

Therefore the Quantum Fisher Information $\mathcal{Q}$ of $\hat{\boldsymbol{\nu}}_\lambda, \hat{\boldsymbol{\nu}}_\lambda^-$ and $\hat{\boldsymbol{\nu}}_\lambda^+$ is, respectively:

$$\mathcal{Q}\left[\hat{\boldsymbol{\nu}}_\lambda\right] = \mathscr{F}\left[\{p_n(\lambda)\}\right] = \frac{1}{\lambda(1+\lambda)}, \tag{4.52}$$

$$\mathcal{Q}\left[\hat{\boldsymbol{\nu}}_\lambda^-\right] = \mathscr{F}\left[\{p_n^-(\lambda)\}\right] = \frac{2}{\lambda(1+\lambda)} = \mathcal{Q}\left[\hat{\boldsymbol{\nu}}_\lambda^+\right]. \tag{4.53}$$

[6] It is not, however, *quantum* non-Gaussian, since it is simply a non-Gaussian mixture of Gaussian states

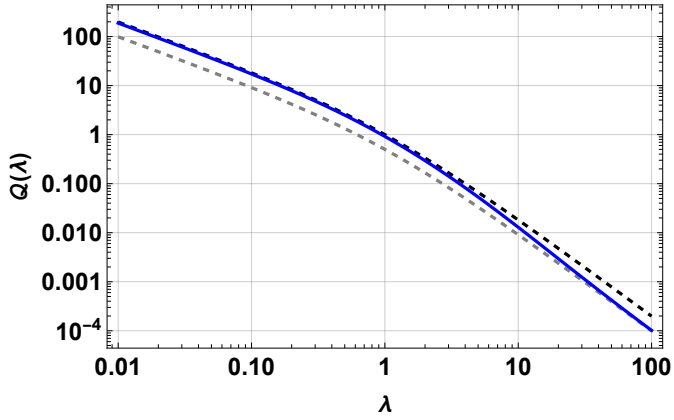

Figure 4.1: Quantum Fisher Information as a function of the average photon number $\lambda = (e^{\beta} - 1)^{-1}$ for thermal state (dashed gray), ideal single-photon subtracted / added thermal state (solid black) and realistic single-photon subtracted thermal state (blue) for a beam-splitter with transmittance $\eta = 0.95$ and on-off detection with efficiency $\epsilon = 0.99$. Mind the log-scale on both axes.

We see that both ideal single-photon subtraction and addition double the QFI. The same computation for the photon-number distribution of the realistic single-photon subtracted thermal state, Eq.(4.50) leads to a series that we were not able to sum in a closed form. However, by performing the sum numerically and plotting the resulting QFI as a function of λ against the results of Eq.(4.52,4.53), we confirmed that the advantage in the QFI can still be attained by the realistic single-photon subtraction protocol, as shown in Fig.4.1 for plausible values of beam-splitter transmittance and detector efficiency ($\eta = 0.95$ and $\epsilon = 0.99$).

The QFI of the realistic single-photon subtraction converges to the ideal case in the limit $\lambda \to 0$: indeed, when the initial thermal state has a small average number of photons, the realistic protocol well-approximates the ideal scenario, because whenever the detector clicks, there is a high chance that just a single photon was actually caught. However, this is in spite of the probability of success $\wp_1(\lambda)$ of the protocol itself, and we address this issue later. When $\lambda \gg 1$, instead, the realistic single-photon subtracted thermal state performs no better than the initial thermal state itself.

4.3.4 Exploring other cost-effective measurement strategies

Despite the fact that the number basis is the one that translates our estimation task on thermal quantum states into a classical one, experimentally resolving the full photon-number distribution is a formidable work. Hence, it is interesting to study whether the advantage over the QFI of the unprocessed thermal state persists if we consider easier-to-implement measurements on the ideal and realistic single-photon subtracted thermal states. We will take into account three detection strategies: homodyne detection of the $\hat{x}$ quadrature, heterodyne (also called double-homodyne) detection and on-off detection with efficiency ϵ, whose effects are in Eq.(4.47,4.48).

Starting with homodyne measurements, Fig.4.2 shows that it always performs worse

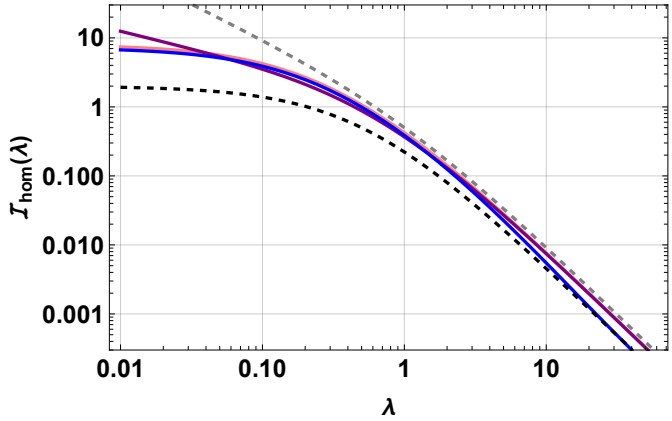

Figure 4.2: Fisher Information of homodyne distribution as a function of the initial average photon number $\lambda = (e^{\beta} - 1)^{-1}$ for thermal states (dashed black), ideal single-photon subtracted / added thermal states (solid pink / purple) and realistic single-photon subtracted thermal states (solid blue) for a beam-splitter with transmittance $\eta = 0.95$ and on-off detection with efficiency $\epsilon = 0.97$. Mind the log-scale on both axes. Quantum Fisher Information of thermal states (dashed gray) is also shown for reference.

than the QFI of the initial thermal state. However, the FI of the homodyne distributions X_λ^-, X_λ^+ and $\langle x|\hat{\boldsymbol{\rho}}_\lambda|x\rangle$ are greater than the FI of X_λ over a wide range of values of λ, while for $\lambda \gg 50$ the approximate single-photon subtracted thermal state provides less information than the initial thermal state under homodyne detection.

Considering heterodyne detection instead, we found that $\hat{\boldsymbol{\nu}}_\lambda^\pm$ and $\hat{\boldsymbol{\rho}}_\lambda$ outperform even the QFI of the initial thermal state, in the range $\lambda \gtrsim 1$, while they perform better than the heterodyne distribution of $\hat{\boldsymbol{\nu}}_\lambda$ for a greater range of values, but $\hat{\boldsymbol{\rho}}_\lambda$ eventually becomes worse than $\hat{\boldsymbol{\nu}}_\lambda$ for this detection strategy. These trends are displayed in Fig.4.3.

Finally, let us discuss the cheapest strategy, on-off detection. With the idea of exploiting a resource we already harnessed for the photon subtraction, we will assume the same detection efficiency ϵ. The realistic scenario can thus be summarized by a black box with one input for the initial thermal state and two output for the signal of the two identical on-off detectors, put at the two ends of the beam-splitter. The signal of the first detector is recorded whenever the second detector clicks, meaning that single-photon subtraction happened. This corresponds to relatively compact and easy-to-build apparatus.

Fig.4.4 shows that the FI of the on-off distributions for $\hat{\boldsymbol{\nu}}_\lambda^-$ and $\hat{\boldsymbol{\rho}}_\lambda$ are significantly greater than the QFI of the initial thermal state for $\lambda \lesssim 0.5$ and are still better than the FI of the on-off distribution of $\hat{\boldsymbol{\nu}}_\lambda$ for $\lambda \lesssim 2$. On the other hand, the ideal photon-added state $\hat{\boldsymbol{\nu}}_\lambda^+$ isi remarkably inefficient with this detection strategy; the reason can be seen in the fact that the ideal photon-added state, unlike the initial thermal state, will almost always make an efficient on-off detector click and the on-off statistics will depend very weakly on the initial parameter of the thermal distribution.

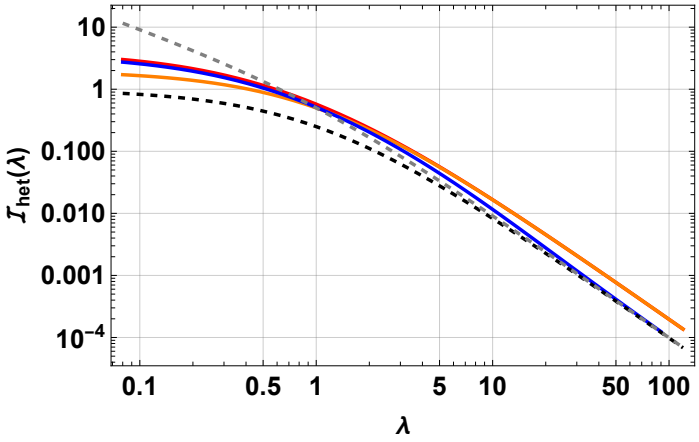

Figure 4.3: Fisher Information of heterodyne distributions as a function of the initial average photon number $\lambda = (e^{\beta} - 1)^{-1}$ for thermal states (dashed black), ideal single-photon subtracted / added thermal states (solid red / orange) and realistic single-photon subtracted thermal states (solid blue) for a beam-splitter with transmittance $\eta = 0.95$ and on-off detection with efficiency $\epsilon = 0.97$. Mind the log-scale on both axes. Quantum Fisher Information of thermal states (dashed gray) is also shown for reference.

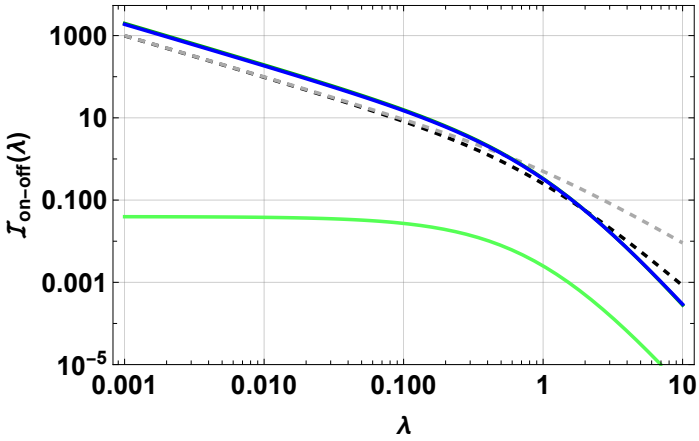

Figure 4.4: Fisher Information of on-off distributions as a function of the initial average photon number $\lambda = (e^{\beta} - 1)^{-1}$ for thermal states (dashed black), ideal single-photon subtracted states (solid blue curve), photon-added thermal states (solid light-green) and realistic single-photon subtracted thermal states (solid blue curve, coinciding with the ideal photon-added state in this range) for a beam-splitter with transmittance $\eta = 0.95$ and on-off detection with efficiency $\epsilon = 0.97$. Mind the log-scale on both axes. Quantum Fisher Information of thermal states (dashed gray) is also shown for reference.

4.3.5 Exploiting all the information from the realistic single-photon subtraction protocol

In evaluating the Fisher Information of the probability distributions associated with the realistic single-photon subtracted thermal state, we disregarded a crucial issue: the real-

istic protocol is not always successful. If we repeat the protocol M times on identically prepared thermal states $\hat{\boldsymbol{\nu}}_\lambda$, according to Eq.(4.49) we will prepare:

$$M' \;=\; M\wp_1(\lambda) \;=\; \frac{M\lambda\epsilon(1-\eta)}{1+\lambda\epsilon(1-\eta)}\,. \tag{4.54}$$

approximate single-photon subtracted thermal states $\hat{\boldsymbol{\rho}}_\lambda$. Since the CR bound writes:

$$\mathrm{Var}\big[\Theta^{(M)}(\lambda)\big] \;\geq\; \frac{1}{M'\,\mathscr{F}[\hat{\boldsymbol{\rho}}_\lambda]} \;=\; \frac{1}{M\wp_1(\lambda)\mathscr{F}[\hat{\boldsymbol{\rho}}_\lambda]}\,. \tag{4.55}$$

for the variance of any unbiased estimator $\Theta^{(M)}(\lambda)$ of λ, we deduce that having a reduced number of accepted single-photon subtracted thermal states effectively translates into a reduction of the Fisher Information extractable by any measurement, by a λ-dependent factor which is precisely the probability of success $\wp_1(\lambda)$. However, when the subtraction protocol fails we still have a final state that can be measured:

$$\hat{\boldsymbol{\rho}}_\lambda^{\oslash} \;=\; \frac{1}{\wp_0(\lambda)}\frac{1}{1+\lambda(\eta+(1-\eta)\epsilon)}\sum_{n=0}^{+\infty}\left(\frac{\eta\lambda}{1+\eta\lambda+\lambda(1-\eta)\epsilon}\right)^n |n\rangle\langle n| \tag{4.56}$$

where $\wp_0(\lambda) = 1-\wp_1(\lambda) = \frac{1}{1+\lambda(1-\eta)\epsilon}$. By writing:

$$\frac{\tilde{\lambda}}{\tilde{\lambda}+1} \;=\; \frac{\eta\lambda}{1+\eta\lambda+\lambda(1-\eta)\epsilon} \quad\Longrightarrow\quad \tilde{\lambda} \;=\; \frac{\eta\lambda}{1+(1-\eta)\epsilon\lambda}$$

we can re-express Eq.(4.56) as:

$$\hat{\boldsymbol{\rho}}_\lambda^{\oslash} \;=\; \frac{1}{1+\tilde{\lambda}}\sum_{n=0}^{+\infty}\left(\frac{\tilde{\lambda}}{1+\tilde{\lambda}}\right)^n |n\rangle\langle n|\,. \tag{4.57}$$

Thus, whenever the realistic single-photon subtraction protocol fails, the resulting state is again a thermal state, but with a new average photon number $\tilde{\lambda}$. The QFI with respect to λ of $\hat{\boldsymbol{\nu}}_{\tilde{\lambda}}$ will therefore be:

$$\mathcal{Q}\left[\hat{\boldsymbol{\nu}}_{\tilde{\lambda}};\lambda\right] \;=\; \left(\frac{\partial\tilde{\lambda}}{\partial\lambda}\right)^2 \mathcal{Q}\left[\hat{\boldsymbol{\nu}}_{\tilde{\lambda}};\tilde{\lambda}\right] \;=\; \frac{\eta}{(1+\epsilon(1-\eta)\lambda)^2}\frac{1}{\lambda(1+\eta\lambda+(1-\eta)\epsilon\lambda)} \tag{4.58}$$

which is smaller than $\mathcal{Q}\left[\hat{\boldsymbol{\nu}}_\lambda;\lambda\right]$, the QFI of the starting thermal state. Additional information can be gained from the very same probability distribution of success for the approximate single-photon subtraction. Specifically, the corresponding FI is:

$$\mathscr{F}\left[\{\wp_0,\wp_1\}\right] \;=\; \frac{\left(\partial_\lambda\wp_1\right)^2}{\wp_1} + \frac{\left(\partial_\lambda\wp_0\right)^2}{\wp_0} \;=\; \frac{\epsilon(1-\eta)}{\lambda(1+\lambda\epsilon(1-\eta))^2} \tag{4.59}$$

Overall, the full information that we can extract from the approximate single-photon subtraction protocol on $\hat{\boldsymbol{\nu}}_\lambda$, assuming the best possible detection strategy on the output states, is [218]:

$$\mathscr{F}_{\mathrm{tot}} \;:=\; \mathscr{F}[\{\wp_0,\wp_1\}] \;+\; \wp_1\mathcal{Q}\left[\hat{\boldsymbol{\rho}}_\lambda\right] \;+\; \wp_0\mathcal{Q}\left[\hat{\boldsymbol{\rho}}_\lambda^{\oslash}\right] \tag{4.60}$$

By computing it explicitly, it appears as if all the advantage we found with the realistic single-photon subtracted thermal state is precisely cancelled by the weighted sum in Eq.(4.60), so that the total extractable information coincides with the initial QFI of $\hat{\boldsymbol{\nu}}_\lambda$ (a similar result for photon-subtraction on Gaussian states was found in [219]). This can be understood by noting that $\mathscr{F}_{\rm tot}$ is necessarily upper-bounded by the QFI of the output state of the beam splitter before the post-selection, Eq.(4.46): this is best understood in the black box description that we mentioned above, since all the collected outcomes (including the one encoded in the acceptance probabilities) can be viewed as a single string of outcome for a measurement performed on the joined state of the two output modes. Since this is just the result of the BS unitary evolution of the vacuum with the initial state whose temperature we wanted to estimate, the QFI for the temperature parameter will be the same as for the thermal state we started with.

One can also derive a lower bound on $\mathscr{F}_{\rm tot}$, taking advantage of a convexity property of the QFI [220]: if a family $\hat{\varrho}_\lambda$ of quantum states encoding a parameter λ is decomposed into a convex mixture according to:

$$\hat{\varrho}_\lambda \;=\; \sum_a p^a_\lambda \hat{\varrho}^a_\lambda \tag{4.61}$$

where p^a_λ is a probability distribution over the variable a, depending upon the parameter λ, then:

$$\mathcal{Q}\left[\hat{\varrho}_\lambda\right] \;\leq\; \sum_a p^a_\lambda \mathcal{Q}\left[\hat{\varrho}^a_\lambda\right] \;+\; \mathscr{F}\left[\{p^a_\lambda\}\right] \tag{4.62}$$

This is called an *extended convexity property* for the QFI, since it states that the Quantum Fisher Information of a mixture is no greater than the average of the QFI of the states in the ensemble *plus* the classical FI of the probability distribution of the ensemble. For us, the convex combination is:

$$\hat{\varrho}_\lambda \;=\; \wp_1(\lambda)\hat{\boldsymbol{\rho}}_\lambda \;+\; \wp_0(\lambda)\hat{\boldsymbol{\rho}}^{\varnothing}_\lambda \;=\; \hat{\boldsymbol{\nu}}_{\eta\lambda} \tag{4.63}$$

which is simply the statement that if we ignore the outcome of the on-off detector in the realistic single-photon subtraction protocol, the outcome will be again a thermal state, with an average number of photons reduced by the beam-splitter transmittance: $\eta\lambda$. The extended convexity property (4.62) then implies:

$$\mathcal{Q}\left[\hat{\boldsymbol{\nu}}_{\eta\lambda};\lambda\right] \;=\; \frac{\eta}{\lambda(1+\eta\lambda)} \;\leq\; \mathscr{F}_{\rm tot} \tag{4.64}$$

As $\eta \to 1$, the lower bound converges to the QFI of $\hat{\boldsymbol{\nu}}_\lambda$, while in general, for $0 < \eta < 1$ it is strictly smaller than $\mathcal{Q}\left[\hat{\boldsymbol{\nu}}_\lambda\right]$.

Despite its theoretical interest, the above result is of little relevance from a practical perspective, since photon-number detection is experimentally very challenging anyway. We will thus explore whether the total extractable information from the realistic single-photon subtracted thermal state can be larger than the FI of the initial state for sub-optimal, but experimentally more relevant detection strategies.

In Fig.4.5 we plotted the total information retrieved by the realistic photon-subtraction scheme, but assuming *heterodyne detection* on the output states of the beam splitter (blue curve), compared to the Fisher Information for the heterodyne distribution of the initial thermal state. For $\lambda \lesssim 0.3$, the post-selection provides larger information, even taking

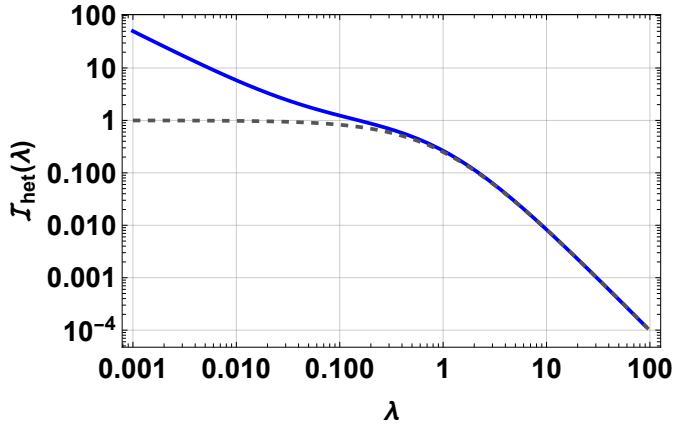

Figure 4.5: Total information retrieved from realistic photon-subtraction protocol followed by heterodyne detection of the output (blue curve) and Fisher Information of the heterodyne distribution of $\hat{\boldsymbol{\nu}}_\lambda$ for comparison (dashed, gray curve). The detection efficiency of the on-off measurement is $\epsilon = 0.99$ and the transmittance of the BS is $\eta = 0.95$.

into account the photon-subtraction probabilities. Analogously, in Fig.4.6, both for the post-selection scenario (blue curve) and for the one without post-selection (gray, dashed curve), we chose as final measurement an on-off photon detection with the same efficiency $\epsilon = 0.99$. Now the advantage of the conditional strategy is seen for $\lambda \gtrsim 2$.

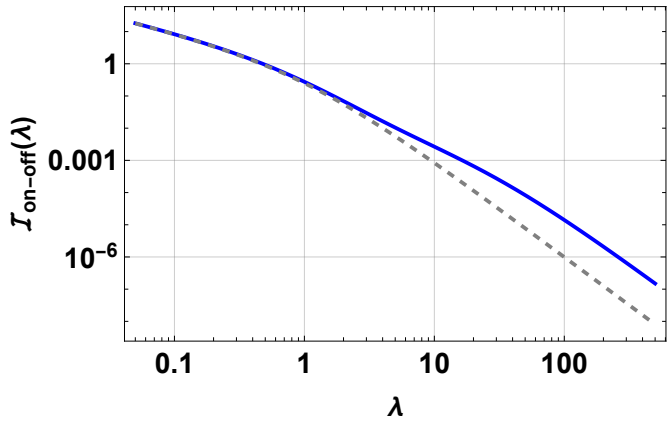

Figure 4.6: Total information retrieved from realistic photon-subtraction protocol followed by on-off detection of the output (blue curve) and Fisher Information of the heterodyne distribution of $\hat{\boldsymbol{\nu}}_\lambda$ for comparison (dashed, gray curve). The detection efficiency of the on-off measurements is $\epsilon = 0.99$ and the transmittance of the BS is $\eta = 0.95$.

4.3.6 Cost-effectiveness of the postselected protocol

In order to take into account the amount of resources required to implement the different detection schemes, let us introduce the so-called *cost parameters* [221, 222]. We denote by C_P the cost of the preparation of the initial quantum state, by C_S the cost of the post-

selection process (i.e., essentially that of an on-off measurement) and by C_M the cost of the final measurement which, when photon-subtraction is considered, is performed only when the post-selection is effective. Whenever the post-selection fails, we will perform the least expensive measurement, which is on-off detection with the same efficiency ϵ, on the resulting state $\hat{\boldsymbol{\rho}}_\lambda^{\oslash}$. The Fisher Information, with respect to the initial parameter λ, extractable from the resulting statistics is readily calculated:

$$\mathscr{F}^{\oslash} = \frac{\epsilon\eta}{\lambda(1+\epsilon\lambda)^2(1+\epsilon(1-\eta)\lambda)}\,. \tag{4.65}$$

The information-cost ratio for the post-selection strategy, $\mathcal{R}_{ps}$, is then given by [221, 222]:

$$\mathcal{R}_{ps} = \frac{\wp_1\mathscr{F}_M\left[\hat{\boldsymbol{\rho}}_\lambda\right] + \wp_0\mathscr{F}^{\oslash} + \mathscr{F}\left[\{\wp_0,\wp_1\}\right]}{C_P + C_S + \wp_1 C_M + \wp_0 C_S}\,. \tag{4.66}$$

where $\mathscr{F}_M\left[\hat{\boldsymbol{\rho}}_\lambda\right]$ is the Fisher Information for the measurement strategy labelled by M performed on the successfully post-selected state $\hat{\boldsymbol{\rho}}_\lambda$ and we attributed the same post-selection cost C_S also to the on-off measurement on the rejected state with the $\wp_0 C_S$ term in the denominator. In the standard quantum estimation protocol, without performing the photon-subtraction, the information-cost ratio would be:

$$\mathcal{R}_0 = \frac{\mathscr{F}_M\left[\hat{\boldsymbol{\nu}}_\lambda\right]}{C_P + C_M}\,. \tag{4.67}$$

Since C_M is usually the largest among the costs and the realistic photon-subtraction strategy pays it only for the more informative states $\hat{\boldsymbol{\rho}}_\lambda$, it is clear that it is possible to have $\mathcal{R}_{ps} > \mathcal{R}_0$. To provide just an example of this fact, let's assume $C_P = 1$, $C_S = 0.5$ and $C_M = 10$. We will take the same C_M both for $\mathcal{R}_{ps}$ and $\mathcal{R}_0$, but we will assume heterodyne detection on $\hat{\boldsymbol{\rho}}_\lambda$ and the optimal, photon-number measurement on $\hat{\boldsymbol{\nu}}_\lambda$ (so that $\mathscr{F}_M\left[\hat{\boldsymbol{\nu}}_\lambda\right] = \mathcal{Q}\left[\hat{\boldsymbol{\nu}}_\lambda\right]$). This is perhaps unrealistic, since a measurement that has to resolve the full photon-number distribution will be more difficult to perform than heterodyne detection, however it makes our point even stronger, since if $\mathcal{R}_{ps} > \mathcal{R}_0$ when the measurement costs are considered the same, it will be true a fortiori when more plausible values are inserted. The comparison is depicted (in logarithmic scale) in Fig.4.7 as a function of λ, where the blue curve refers to $\mathcal{R}_0$ and the dashed gray curve to $\mathcal{R}_{ps}$.

Clearly, at least for low temperature thermal states, the realistic photon-subtraction strategy followed by heterodyne detection has a better information-cost ratio than the optimal measurement on the initial thermal state that achieves the QCR bound. The term $\wp_0\mathscr{F}^{\oslash}$ in the numerator of $\mathcal{R}_{ps}$ is typically negligible, and one can work with the more compact expression

$$\mathcal{R}_{ps} \simeq \left(\wp_1\mathscr{F}_M\left[\hat{\boldsymbol{\rho}}_\lambda\right] + \mathscr{F}\left[\{\wp_0,\wp_1\}\right]\right)/(C_P + C_S + \wp_1 C_M)\,.$$

On the other hand, it would be meaningless to discard the $\mathscr{F}\left[\{\wp_0,\wp_1\}\right]$ term, since this information is already available anyway. In Fig.4.8 we also plotted the region in the parameters space of C_S, C_M and λ where $\mathcal{R}_{ps} > \mathcal{R}_0$ to show that the choice of the costs is not too critical for our result, for most values of λ.

Finally, let us remark that, for $\lambda \ll 1$, there is always a cheap, very effective strategy, which is to perform an on-off measurement directly on $\hat{\boldsymbol{\nu}}_\lambda$; indeed, such a measurement yields a good approximation to the full photon-number distribution in that limit. However, this strategy is doomed to failure for large enough values of λ, implying that our post-selection protocol is the most efficient of all the considered ones in a wide range of

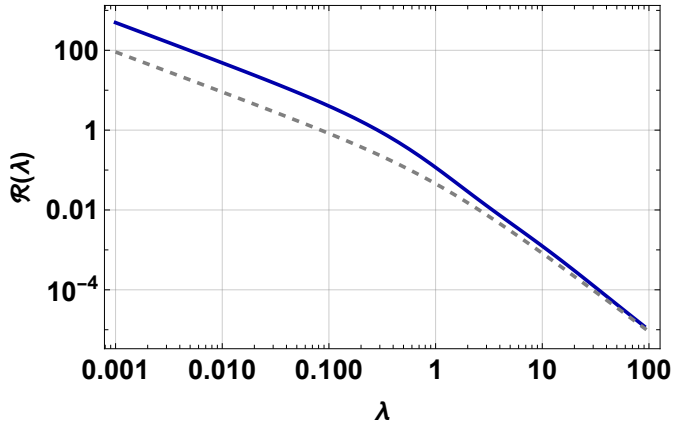

Figure 4.7: Information-cost ratio for the realistic photon subtraction protocol followed by homodyne detection ($\mathcal{R}_{ps}$, solid blue curve) and for the initial thermal state subjected to the optimal photon-number measurement ($\mathcal{R}_0$, dashed gray curve), as functions of the parameter λ to be estimated. The cost of preparation was assumed to be $C_P = 1$, that of post-selection $C_S = 0.5$ and the measurement cost is $C_M = 10$. The detection efficiency of the on-off measurements is $\epsilon = 0.99$ and the transmittance of the BS is $\eta = 0.95$.

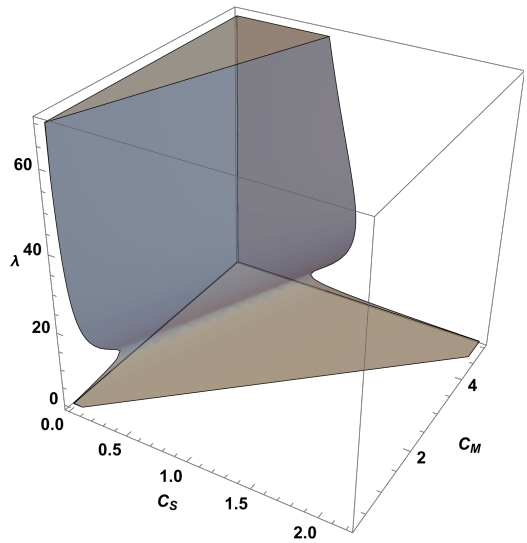

Figure 4.8: Region in parameters space of C_S, C_M and λ where $\mathcal{R}_{ps} > \mathcal{R}_0$, implying that the probabilistic protocol is better from a cost-effective standpoint. We fixed $C_P = 1$ without loss of generality, since only the ratios between the other costs and C_P can influence the inequality.

temperatures. In this respect, we adopted the framework of *local* quantum metrology, but our results indicate that the optimal measurement can be determined with very limited a priori knowledge of the true value of the parameter λ. Recently, a paradigm for global quantum thermometry has also been considered altogether [223]

4.3.7 On the role of weak measurements and post-selection in quantum metrology

The example of photon-subtracted thermal states that we just discussed poses a question on whether the quantum Cramér-Rao (QCR) bound can be exceeded by more elaborate measurement strategies that cannot be described by a (parameter-independent) POVM on the initial state, as for example measurements implemented by coupling the system with an ancilla and then measuring the ancilla in such a way that the conditional state of the system, post-selected according to the outcome of the measurement, gives an higher QFI for the parameter, as if the post-selection were able to concentrate the information in the final state: this is the framework of *probabilistic quantum metrology* [222, 224, 225, 226, 227, 228, 229]. However, general results show that these strategies cannot overcome the QCR bound[218, 230, 231], ultimately due to a compensation between the enhanced QFI of the post-selected states and the probability of success of the post-selection process. Moreover, the same conclusion holds true if one considers all the information available from the strategy, i.e. by adding to the count the Fisher information of the measurement's outcomes and the QFI of the discarded states of the system [232]. On the other hand, the optimal measurement specified by the symmetric logarithmic derivative, despite fixing the ultimate quantum bound, is often unreasonable to implement in an experimental setting, which is the natural purpose of quantum metrology. Therefore, as a first point, probabilistic quantum metrology may actually achieve an advantage over the direct measurement procedure when sub-optimal, realistic measurement strategies are employed. This has been studied, e.g., in the context of the estimation of the gain of a nondeterministic linear amplifier [233], and in quantum magnetometry with nitrogen-vacancy centers of diamond [234]. Secondly, taking into account the experimental cost of implementing different detection methods, the overall information-cost ratio could be drastically improved by deciding to spend a higher amount of resources only in the trials with a successful post-selection outcome.

In a recent work [221] about post-selected quantum metrology for unitary models, the authors prove the necessity of a form of nonclassicality, namely the negativity of a generalized Kirkwood-Dirac distribution, to achieve an improvement of the information-cost ratio with post-selection, see also [235]. In our case, no form of state nonclassicality is at play, because we are always dealing with fully classical states according to Glauber's definition, which is widely regarded as the most general notion of nonclassicality (but we also refer to [236] for subtle issues in this respect, especially when weak measurements are involved). This does not contradict the results of [221], since they considered unitary models and they maximized over the probing state, while temperature cannot be considered a unitarily-imprinted parameter and no further maximization can be made. Therefore, the results we just outlined show that the restriction in [221] to unitary models is actually necessary to arrive at their conclusion and, with more general assumptions, an improvement of the information-cost ratio with probabilistic metrology is also possible with classical probes.

4.4 Basic notions of multi-parameter quantum metrology

The problem of quantum estimation and of the computation of a lower bound for variances becomes significantly more contrived when we want to estimate more than one parameter of a quantum statistical model. A quick way to partially understand why this is the case is to consider the maximization over all the POVMs that is implicit in the definition of the QFI for a single parameter. If we have two parameters, say λ_1 and λ_2, the best POVM for the estimation of λ_1 can depend upon the value of λ_2, and vice versa. Even worse, the POVMs that maximize the QFI for λ_1 and λ_2 separately will not commute, in general, and it becomes entirely unclear what the best strategy for their joint estimation would be and what error should be associated with it.

The first step that we face when trying to generalize the QFI to more than one parameter is the definition of the Symmetric Logarithmic Derivative. Indeed, one may define it for a statistical model parametrized by $\vec{\lambda} = (\lambda_1, ..., \lambda_d)^T \in \mathbb{R}^d$ as:

$$\partial_{\lambda_j} \hat{\boldsymbol{\rho}}_{\vec{\lambda}} \;=\; \frac{\hat{\mathrm{L}}_j^S \hat{\boldsymbol{\rho}}_{\vec{\lambda}} + \hat{\boldsymbol{\rho}}_{\vec{\lambda}} \hat{\mathrm{L}}_j^S}{2} \tag{4.68}$$

In a similar fashion, we can also introduce the *Right Logarithmic Derivatives* (RLD) as the operators $\hat{\mathrm{L}}_j^R$ satisfying [237]:

$$\partial_{\lambda_j} \hat{\boldsymbol{\rho}}_{\vec{\lambda}} \;=\; \hat{\boldsymbol{\rho}}_{\vec{\lambda}} \hat{\mathrm{L}}_j^R \tag{4.69}$$

In terms of them, we can introduce the SLD Quantum Information Matrix $\boldsymbol{\mathcal{Q}}(\vec{\lambda})$ and the RLD Quantum Information matrix $\boldsymbol{\mathcal{J}}(\vec{\lambda})$:

$$\mathcal{Q}_{jk}(\vec{\lambda}) \;=\; \mathrm{Tr}\left[\hat{\boldsymbol{\rho}}_{\vec{\lambda}} \frac{\hat{\mathrm{L}}_j^S \hat{\mathrm{L}}_k^S + \hat{\mathrm{L}}_k^S \hat{\mathrm{L}}_j^S}{2}\right] \tag{4.70}$$

$$\mathcal{J}_{jk}(\vec{\lambda}) \;=\; \mathrm{Tr}\left[\hat{\boldsymbol{\rho}}_{\vec{\lambda}} \hat{\mathrm{L}}_k^R \hat{\mathrm{L}}_j^{R\,\dagger}\right] \tag{4.71}$$

4.4.1 On the geometry of quantum metrology

It is worth making a small detour to appreciate the tight relation between the SLD-QFI matrix and the Bures distance, Eq.(1.17), giving rise to an insightful connection between quantum metrology and the geometry of the quantum statistical model. It can be shown that [32, 34, 35]:

$$\left(\mathcal{D}_B\left[\hat{\boldsymbol{\rho}}_{\vec{\lambda}}, \hat{\boldsymbol{\rho}}_{\vec{\lambda}+d\vec{\lambda}}\right]\right)^2 \;=\; \frac{1}{2}\mathcal{Q}_{jk}(\vec{\lambda})\, \mathrm{d}\lambda_j \mathrm{d}\lambda_k \tag{4.72}$$

Therefore we can state that, apart for a constant factor, the SLD Quantum Fisher Information matrix defines a *metric* on the quantum statistical model, seen as a smooth variety inside the space of quantum states $\mathcal{S}(\mathcal{H})$, which coincides with the Bures metric derived as the double differential of the Bures distance with respect to variations in the parameter. The intuition is clear: the larger the SLD-QFI, the farther are two quantum states in the model labelled by infinitesimally close values of the parameters, hence the better they could be distinguished, at least in principle. The corresponding *curvature* tensor associated with the SLD-QFI metric can be computed as:

$$\mathcal{U}_{jk}(\vec{\lambda}) \;=\; -\frac{i}{2}\mathrm{Tr}\left[\hat{\rho}_\lambda \left[\hat{\mathrm{L}}_j^S\,,\, \hat{\mathrm{L}}_j^S\right]\right] \tag{4.73}$$

and it is known as the *Uhlmann curvature* [238]. As it is the case for the standard notions of curvature in differential geometry [239, 240], this quantity measures the infinitesimal change of a quantum state $\hat{\rho}_\lambda$ in the model when it is parallely transported along a closed path in parameter's space around the starting point, therefore it is also a generalization of the *Berry curvature* [240, 241]. In general, and especially for two-parameters models, the determinant of the curvature is the most significant scalar quantity to capture the *shape* of the manifold, since it coincides with the notion of Gaussian curvature for two-dimensional surfaces embedded in $\mathbb{R}^3$ [239].

4.4.2 Scalar Cramér-Rao bounds and the R-quantity

As was the case for the single-parameter scenario, also here SLD-QFI and RLD-QFI matrices provide lower bounds for the covariance matrices of any estimator $\Theta[\vec{\lambda}]$ of the n parameters:

$$\mathrm{Cov}\left(\Theta^{(M)}\left[\vec{\lambda}\right]\right) \geq \frac{1}{M}\,\boldsymbol{\mathcal{Q}}^{-1}(\vec{\lambda}^*) \tag{4.74}$$

$$\mathrm{Cov}\left(\Theta^{(M)}\left[\vec{\lambda}\right]\right) \geq \frac{1}{M}\,\boldsymbol{\mathcal{J}}^{-1}(\vec{\lambda}^*) \tag{4.75}$$

where M is the number of measurements performed on identical copies of the state $\hat{\boldsymbol{\rho}}_{\vec{\lambda}^*}$. However, while for a single parameter the first bound, based on the SLD-QFI, was always attainable with the POVM defined by the eigenbasis of the SLD itself, the two bounds in Eq.(4.74) and Eq.(4.75) cannot be saturated by any POVM in the general case.

Scalar Cramér-Rao bounds can also be formulated by introducing a weight matrix $\mathbf{W}$, which is a general $d \times d$ positive matrix specifying d independent linear combinations of the parameters and how much weight should be associated to their respective variances. Using the shorthand notation $\mathbf{C}(\vec{\lambda})$ for $\mathrm{Cov}(\Theta^{(M)}[\vec{\lambda}])$, we can write the scalar CRBs as:

$$\mathrm{Tr}\left[\mathbf{W}\mathbf{C}(\vec{\lambda})\right] \geq \frac{1}{M}\,\mathbf{B}^S(\vec{\lambda},\mathbf{W}) \tag{4.76}$$

$$\mathrm{Tr}\left[\mathbf{W}\mathbf{C}(\vec{\lambda})\right] \geq \frac{1}{M}\,\mathbf{B}^R(\vec{\lambda},\mathbf{W}) \tag{4.77}$$

where:

$$\mathbf{B}^S(\vec{\lambda},\mathbf{W}) := \mathrm{Tr}\left[\mathbf{W}\boldsymbol{\mathcal{Q}}^{-1}(\vec{\lambda})\right] \tag{4.78}$$

$$\mathbf{B}^R(\vec{\lambda},\mathbf{W}) := \mathrm{Tr}\left[\mathbf{W}\mathrm{Re}\left(\boldsymbol{\mathcal{J}}^{-1}(\vec{\lambda})\right)\right] + \|\sqrt{\mathbf{W}}\mathrm{Im}\left(\boldsymbol{\mathcal{J}}^{-1}(\vec{\lambda})\right)\sqrt{\mathbf{W}}\|_1 \tag{4.79}$$

The advantage of formulating the problem in terms of a scalar linear function of the covariances is to be able to define the *most informative scalar bound* as:

$$\mathbf{B}^{MI}(\vec{\lambda},\mathbf{W}) := \max_{\{\hat{\Pi}\}} \mathrm{Tr}\left[\mathbf{W}\mathscr{F}_{\hat{\Pi}}(\vec{\lambda}^*)\right] \tag{4.80}$$

where $\mathscr{F}_{\hat{\Pi}}(\vec{\lambda}^*)$ is the *classical* Fisher Information matrix resulting from the measurement of the POVM $\{\hat{\Pi}\}$ on the quantum statistical model and evaluated at the true value of the parameters $\vec{\lambda}^*$. Notice that this quantity, being a classical FI, provides a bound which

can always be saturated by an asymptotically efficient estimator in the limit $M \to \infty$, whereas the bounds provided by the SLD-QFI and RLD-QFI do not share this property because they cannot be directly interpreted as classical Fisher Information matrices deriving from a well-defined measurement scheme.

It can be shown that a bound $\mathbf{B}^H(\vec{\lambda}, \mathbf{W})$ introduced by Holevo [242, 243] is always at least as informative as both the SLD-QFI bound and the RLD-QFI bound:

$$\mathbf{B}^{MI}(\vec{\lambda}, \mathbf{W}) \;\geq\; \mathbf{B}^H(\vec{\lambda}, \mathbf{W}) \;\geq\; \max\left[\mathbf{B}^S(\vec{\lambda}, \mathbf{W})\,,\; \mathbf{B}^R(\vec{\lambda}, \mathbf{W})\right] \tag{4.81}$$

However, the Holevo bound is often too hard to compute explicitly, which is also the reason why we do not provide its general expression here. While generally inferior to the most informative bound, the Holevo bound coincides with $\mathbf{B}^{MI}$ in special cases, in particular for *pure* quantum statistical models, and it can be saturated by performing collective measurements on an asymptotically large number of copies of the state.

Given the practical limitations affecting the Holevo bound in most scenarios, the following constraint on the difference between $\mathbf{B}^H$ and $\mathbf{B}^S$ is particularly valuable:

$$\mathbf{B}^S(\vec{\lambda}, \mathbf{W}) \;\leq\; \mathbf{B}^H(\vec{\lambda}, \mathbf{W}) \;\leq\; \left(1 + \mathscr{R}(\vec{\lambda}\right) \mathbf{B}^S(\vec{\lambda}, \mathbf{W}) \;\leq\; 2\mathbf{B}^S(\vec{\lambda}, \mathbf{W}) \tag{4.82}$$

where $0 \leq \mathscr{R} \leq 1$, called the R-quantity (or sometimes the *quantumness*) is defined via [244]:

$$\mathscr{R}(\vec{\lambda}) \;:=\; \|i\boldsymbol{\mathcal{Q}}^{-1}(\vec{\lambda})\,\boldsymbol{\mathcal{U}}(\vec{\lambda})\|_\infty \tag{4.83}$$

where $\|\bullet\|_\infty$ is the infinity-norm, equal to the largest eigenvalue of its argument, while $\boldsymbol{\mathcal{U}}(\vec{\lambda})$ is the Uhlmann curvature, as defined in Eq.(4.73) which is sometimes referred to as the *asymptotic incompatibility matrix* in this context. Notice that the Uhlmann curvature, whose only nonzero terms are necessarily off-diagonal, depends upon the commutator of the symmetric logarithmic derivatives pertaining to different parameters: considering only two parameters for clarity, if the two SLDs commute they can be simultaneously diagonalized and $\boldsymbol{\mathcal{U}} = \mathscr{R} = 0$, thus the Holevo bound coincides with the SLD-QFI bound. The meaning is apparent: it is possible to find a single projective measurement that achieves the best precision in the estimation of both parameters together and this can be used to saturate the SLD-QFI bound; a quantum statistical model whose symmetric logarithmic derivatives commute pairwise for any value of $\vec{\lambda}$ is said to be *quasi-classical* [245]. It should be stressed that Eq.(4.82) also entails that the *scaling* of the SLD-QFI bound (in terms of whatever type of resources one attributes to the statistical model) is already optimal, since the difference with the Holevo bound is by a factor of 2 at most.

In the special case of a two-parameters model which will be relevant for us in the next Section, Eq.(4.83) simplifies into:

$$\mathscr{R}(\lambda_1, \lambda_2) \;=\; \sqrt{\frac{\det \boldsymbol{\mathcal{U}}(\lambda_1, \lambda_2)}{\det \boldsymbol{\mathcal{Q}}(\lambda_1, \lambda_2)}} \tag{4.84}$$

where the numerator inside the square root is the *Gaussian curvature* of the quantum statistical manifold at the point (λ_1, λ_2). Finally, an important aspect to highlight is that the R-quantity is invariant under reparametrizations; indeed, given an everywhere locally invertible change of coordinates $\vec{\lambda}'(\vec{\lambda})$ with Jacobian matrix $\mathbf{J}(\vec{\lambda}') = \frac{\partial \vec{\lambda}}{\partial \vec{\lambda}'}$, the SLD-QFI and the Uhlmann curvature both transform according to $\bullet \mapsto \mathbf{J} \bullet \mathbf{J}^T$.

4.5 Sloppy (quantum) statistical models: a case study

It can sometimes happen that a statistical model (either classical or quantum) is not invertible in an open neighbourhood $\Omega_{\vec{\lambda}}$ around a point $\vec{\lambda}$ of parameters space, meaning that different parameters configurations can be locally assigned to the same state, making it impossible to reconstruct them accurately from the statistical model. More generally, even if the statistical model is invertible in $\Omega_{\vec{\lambda}}$, it might happen that the Fisher Information (or the QFI, for quantum statistical model) is almost degenerate, having a determinant close to 0. In these cases, we say that the (classical or quantum) statistical model is *sloppy*. The degeneracy of the (quantum) Fisher Information matrix signals that there is some reparametrization, not necessarily a linear one[7], such that, in terms of the new parameters, one or more of them have an almost vanishing value of the (quantum) FI and the statistical model is effectively only dependent upon the other parameters. It should be intuitively clear that the sloppiness of a statistical model is an issue about the *encoding* of the parameters into the set of states; for example, imagine that we want to estimate the parameters of a CV unitary operator acting on a single mode by first rotating its quadratures by an angle θ and then displacing the mean field by $\alpha \in \mathbb{C}$. If we decide to encode (θ, α) on a thermal state, the dependence upon θ will be completely lost: the obvious option would be to change the probe state into another which does not commute with $e^{i\theta \hat{a}^\dagger \hat{a}}$. Clearly, if the agents determining the two parameters can be addressed independently, we are not actually dealing with a true two-parameters model and we could just estimate them individually with single-parameter quantum metrology: in this section, therefore, we assume to have *limited control* about the single agents.

4.5.1 The model: two phase shifters in a Mach-Zender interferometer

We will address a very simple sloppy model, presented in Fig.4.9 to investigate the relationship between sloppiness and quantum incompatibility; we consider a Mach-Zender interferometer with a factorized Gaussian input state of two modes whose CM and first moments are given by:

$$\sigma_0^{(1)} = \frac{1}{2}\begin{pmatrix} e^{2r} & 0 & 0 & 0 \\ 0 & e^{-2r} & 0 & 0 \\ 0 & 0 & e^{2r} & 0 \\ 0 & 0 & 0 & e^{-2r} \end{pmatrix}, \qquad \vec{d}_0 = \begin{pmatrix} q\cos\beta \\ q\sin\beta \\ 0 \\ 0 \end{pmatrix} \tag{4.85}$$

In words, $\hat{\boldsymbol{\rho}}_{1,2}^{(0)} = \hat{\boldsymbol{\rho}}_{1;r,q,\beta}^{(0)} \otimes \hat{\boldsymbol{\rho}}_{2;r,0,0}^{(0)}$ is the tensor product of two single-mode squeezed vacuum states with the same squeezing parameter r and a displacement of the first mode given by $(q\cos\beta, q\sin\beta)^T$. The beam-splitter at the entrance of the interferometer is described by a mixing angle ϕ, such that the transmissivity is $\cos^2\phi$, and a relative phase θ as in Eq.(2.72). Notice that a relative phase in the squeezing angle of one of the input states can be reabsorbed in θ. The parameters to be estimated are the phase shifts λ_1 and λ_2 imprinted on the mode occupying the upper horizontal arm of the interferometer by two consecutive phase shifters. The second beam splitter, the mirrors and everything afterwards are irrelevant as long as the Quantum Fisher Information is concerned, as they amount to a parameter-independent unitary change of the quantum statistical model, which is reabsorbed when considering all possible POVMs.

[7] Of course, locally in the parameters space any reparametrization is linear on the FI matrix because it acts by congruence on it, but the Jacobian can depend upon the values of the parameters.

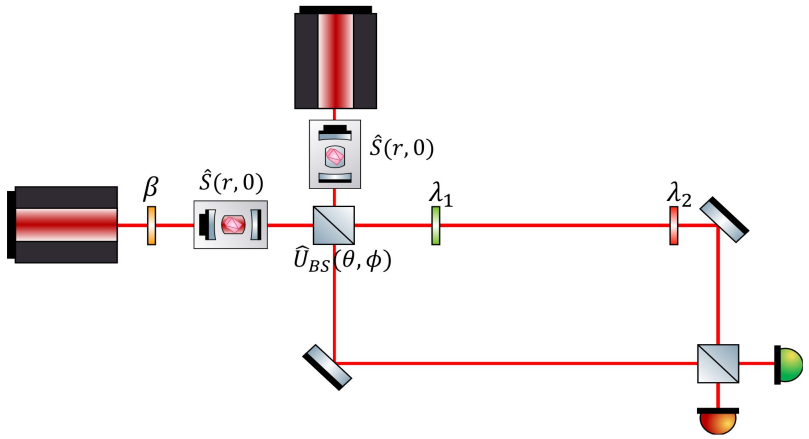

Figure 4.9: A Mach-Zender interferometer with two equally squeezed inputs with squeezing parameter r, and a relative displacement of the first mode with respect to the second in the quadrature $(\cos\beta, \sin\beta)$. The beam splitter has a transmissivity $\cos^2\phi$ and a relative phase θ between the inputs. The parameters λ_1 and λ_2 to be estimated are encoded by two consecutive phase shifters on the upper arm of the interferometer.

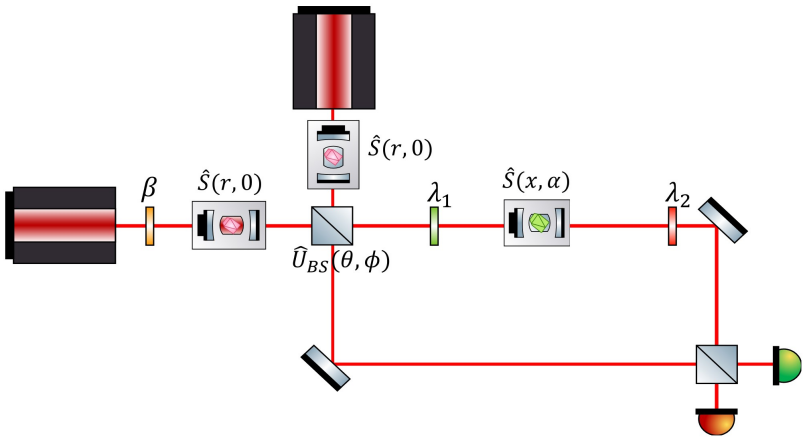

Figure 4.10: The same scheme of Fig.4.9 is reproposed with an additional single-mode squeezer $\hat{S}(x,\alpha)$ in between the phase shifters.

The sloppiness of this model is apparent from the fact that the two phase shifters contribute to an overall phase shift of $\lambda_1 + \lambda_2$ of one mode with respect to the other, so that the difference $\lambda_1 - \lambda_2$ is completely undetermined if only the output states are known. A realistic scenario described by such a model that we can have in mind to ponder on it could be a continuous medium of unknown and continuously varying refractive index that imparts a total phase shift and we would like to estimate how different sections of it contribute to the overall shift. At any rate, we are assuming to be unable to address individually the two phase shifters with targeted measurement protocols and the only chance we have to distinguish λ_1 and λ_2 is to put an active element, which we will call a *scrambler*, in between. We will content ourselves with the analysis of the Gaussian scenario and the only nontrivial scrambler that we should consider is another single-mode squeezer, parametrized by a squeezing factor of e^{-2x} and a squeezing angle α, as in Fig.4.10. An intermediate displacement would also be sufficient to partially uncouple the two parameters, but the discrimination of λ_1 and λ_2 would then be limited to the first-moments vector of the final Gaussian state, resulting in uninteresting conclusions.

Overall, we can write the general output state as:

$$\begin{aligned} \hat{\mathbf{U}}_{\phi,\theta,x,\alpha}(\lambda_1,\lambda_2) \;&:=\; \hat{\mathbf{U}}_R(\lambda_2)\,\hat{\mathbf{S}}^{(1)}_{x,\alpha}\,\hat{\mathbf{U}}_R(\lambda_1)\hat{\mathbf{U}}_{BS}(\theta,\phi) \\ \\ \hat{\boldsymbol{\rho}}(\lambda_1,\lambda_2;r,&\phi,\theta,x,\alpha,q,\beta) \;= \\ =\; \hat{\mathbf{U}}_{\phi,\theta,x,\alpha}(\lambda_1,\lambda_2)&\left[\hat{\boldsymbol{\rho}}^{(0)}_{1;r,q,\beta}\otimes\hat{\boldsymbol{\rho}}^{(0)}_{2;r,0,0}\right]\left(\hat{\mathbf{U}}_{\phi,\theta,x,\alpha}\right)^{\dagger}(\lambda_1,\lambda_2) \end{aligned} \tag{4.86}$$

where $\hat{\mathbf{U}}_R(\lambda) = e^{-i\lambda\hat{a}^\dagger\hat{a}}$ and the other operators are defined as in Section 2.4. Appreciate the fact that, while the initial sloppy model was fully covariant with respect to λ_1 and λ_2, meaning that the (degenerate) QFI matrix would have been independent upon the true values of the parameters, the model with the scrambler in Eq.(4.86) above is only covariant with respect to λ_2, while it can be argued that λ_1 and α only enter in the model through the combination $\gamma = \alpha + 2\lambda_1$, meaning that the phase α can be exploited to improve the local estimation if the QFI around the true value of λ_1 is not optimized.

4.5.2 QFI and Uhlmann curvature for the pure states model

We should now compute the SLD-QFI matrix for the scrambled quantum statistical model we just described. This would be a very tedious task, but the following general formulas for pure Gaussian models comes to a rescue [246, 247, 248]:

$$\mathcal{Q}_{jk} \;=\; \frac{1}{4}\mathrm{Tr}\left[\left(\sigma_{\vec{\lambda}}^{-1}\partial_j\sigma_{\vec{\lambda}}\right)\left(\sigma_{\vec{\lambda}}^{-1}\partial_k\sigma_{\vec{\lambda}}\right)\right] \;+\; 2(\partial_j\vec{d}^{T}_{\vec{\lambda}})\cdot\sigma_{\vec{\lambda}}^{-1}\cdot(\partial_k\vec{d}_{\vec{\lambda}}) \tag{4.87}$$

where $\sigma_{\vec{\lambda}}$ and $\vec{d}_{\vec{\lambda}}$ are respectively the CM and the first-moments vector of the pure Gaussian states $|\psi_G(\vec{\lambda})\rangle$ defining the model and $\partial_j \equiv \partial_{\lambda_j}$. Remarkably, this expression is the same as the classical Fisher Information for a classical statistical model consisting of Gaussian probability density functions with CM $\sigma_{\vec{\lambda}}$ and expectation values $\vec{d}_{\vec{\lambda}}$. Here we have the opportunity to emphasize a subtle aspect: when considering a *mixed states* quantum statistical model, it can happen that a variation of the parameters' values induces a sudden jump of the rank of $\hat{\boldsymbol{\rho}}_{\vec{\lambda}}$; when this is the case, general formulas like Eq.(4.87) are not valid anymore and one must resort to more sophisticated ones

[246, 249, 250]. Armed with Eq.(4.87), we can compute the entries of the QFI matrix for our statistical model:

$$\begin{aligned}\mathcal{Q}_{11}(r,\phi,\theta,q,\beta) &= 2\cosh^2 2r + 2q^2\Big\{\cosh 2r + \\ &+ \left[\cos 2\beta\cos 2\phi + \cos(2\beta+\theta)\sin\theta\sin(2\phi)^2\right]\sinh 2r\Big\}\end{aligned} \tag{4.88}$$

$$\begin{aligned}\mathcal{Q}_{22}(r,\theta,\phi,x,\gamma,q=0) &= 2\Big(\cosh 2r\,\cosh 2x + \sinh 2r\,[\cos\theta\cos(\gamma+\theta) + \\ &+ \cos 2\phi\sin\theta\sin(\gamma+\theta)]\sinh 2x\Big)^2\end{aligned} \tag{4.89}$$

$$\begin{aligned}\mathcal{Q}_{12}(r,\theta,\phi,x,\gamma,q=0) &= 2\cosh^2 2r + \\ &+ 2\left[2-\sin^2(2\phi)\sin^2\theta\right]\sinh^2(2r)\sinh^2 x + \\ &+ \Big[\cos\theta\cos(\gamma+\theta) + \\ &+ \cos(2\phi)\sin\theta\sin(\gamma+\theta)\Big]\sinh 4r\sinh 2x\end{aligned} \tag{4.90}$$

In the equations for $\mathcal{Q}_{22}$ and $\mathcal{Q}_{12}$ we put $q=0$ since the term proportional to q is rather involved and uninformative, moreover we introduced $\gamma=\alpha+2\lambda_1$ since this is the only combination of these parameters appearing in their expressions.

Notice that the q-independent term of $\mathcal{Q}_{11}$ is just $2\cosh^2 2r$, while the q-dependent term can be maximized by putting $\beta=\theta=0$ and $\phi=n\pi$, or $\theta=\frac{\pi}{2}$, $\beta=-\frac{\pi}{4}$ and $\phi=\frac{(2n+1)\pi}{4}$, with $n\in\mathbb{N}$. Its value at the maximum is:

$$\mathcal{Q}_{11}^{max} = 2\cosh^2(2r)+2e^{2r}q^2 \tag{4.91}$$

For constant input energy (i.e. constant r) we can now maximize $\mathcal{Q}_{22}$. The absolute maximum is achieved for $\phi=\theta=\gamma=0$, dubbed the *maximum configuration* from now on, and yields:

$$\mathcal{Q}_{22}^{max} = 2\cosh^2\left[2(r+x)\right] \tag{4.92}$$

and it is compatible with the maximum of $\mathcal{Q}_{11}$ even for $q\neq 0$. However, this result is of little relevance for at least to reasons: we had to put $\gamma=0$, which amounts to fine-tuning α according to the true value λ_1 of the first unknown parameter, and we also end up with a solution corresponding to removing the initial beam-splitter from our scheme ($\phi=0$). This fact has a clear interpretation: if we want to estimate λ_1 and λ_2 with the best possible accuracy and *disregarding their compatibility* we have to focus all the incoming squeezing onto the upper arm of the interferometer where the phase shifters are placed. To be more explicit, we highlight that any mode mixing by the initial beam splitter will necessarily reduce the *local* single-mode squeezing, while at the same time generating some amount of two-mode squeezing. Thus, removing the beam splitter actually maximizes the squeezing on the phase shifters while, at the same time, it partially trivializes the problem to a single-mode one.

If we consider, instead, the other combination of parameters maximizing the q-dependent term, dubbed the *optimal configuration* from now on, we obtain for $\mathcal{Q}_{22}$:

$$\mathcal{Q}_{22}^{opt} := \mathcal{Q}_{22}(r, \theta = \frac{\pi}{2}, \phi = \frac{\pi}{4}, q = 0, \beta = -\frac{\pi}{4}) \tag{4.93}$$

$$\mathcal{Q}_{22}^{opt} = 2\cosh^2 2r \ \cosh^2 2x \tag{4.94}$$

The ratio between $\mathcal{Q}_{22}^{opt}$ over $\mathcal{Q}_{22}^{max}$ is:

$$\frac{1}{4} \leq \frac{\cosh^2 2r \cosh^2 2x}{\cosh^2 [2(r+x)]} = \frac{1}{4}\left(1 + \frac{\cosh[2(r-x)]}{\cosh[2(r+x)]}\right)^2 \leq 1 \tag{4.95}$$

the lower bound being achieved in the limit of $r, x \to \infty$, while the upper bound is reached for either $r = 0$ or $x = 0$. Importantly, we see that the scaling of the QFI for the parameter λ_2 in the optimal configuration is the same as the scaling at its maximum, Eq.(4.92) and it differs from it by at most a factor of $\frac{1}{4}$. Additionally, if in the best setting with $\phi = \theta = 0$ we do not assume to know λ_1, so that we can not impose $\gamma = 0$ to get the overall maximum configuration, in the worst-case scenario it could happen that $\gamma = \pi$ and we end up with:

$$\mathcal{Q}_{22}^{inf} = \mathcal{Q}_{22}(r, \theta = 0, \phi = 0, \gamma = \pi, q = 0) = 1 + \cosh[4(r-x)] \tag{4.96}$$

In this case, the ratio $\mathcal{Q}_{22}^{inf}/\mathcal{Q}_{22}^{opt}$ evaluates to $(\tanh 2x \tanh 2r - 1)^2 \leq 1$. Thus the optimal configuration can even be more informative than the maximum configuration if we do not assume to know λ_1.

Let us now make a crucial observation: the optimal configuration also makes the estimation problem *fully covariant*: indeed, both $\mathcal{Q}_{22}^{opt}$ in Eq.(4.94) and $\mathcal{Q}_{12}^{opt}$, whose value is:

$$\mathcal{Q}_{12}^{opt} = 2\cosh^2 2r + 2\sinh^2 2r \sinh^2 x \tag{4.97}$$

are now independent from both λ_1 and λ_2.

As a measure of the sloppiness in the various configurations, we can consider the determinant of the full matrix $\boldsymbol{\mathcal{Q}}$. Its value is exponentially growing with r and x both in the maximum and optimal configurations, but the ratio $\det \boldsymbol{\mathcal{Q}}^{max}/\det \boldsymbol{\mathcal{Q}}^{opt}$ is always bounded between 0 and 2 and it quickly goes to 0 for large values of the initial squeezing r, whatever the value of x. This indicates that, as we could have expected, the optimal configuration is better at lifting the sloppiness of the model independently of the energy introduced by the scrambler, quantified by x.

As a final step, we should examine the *quantum* incompatibility of the parameters. Analogously to the formula Eq.(4.87), one compute the Uhlmann curvature for pure Gaussian quantum models as [246]:

$$\mathcal{U}_{jk}(\vec{\lambda}) = \frac{1}{4}\mathrm{Tr}\left[\Omega\sigma_{\vec{\lambda}}\left(\Omega\partial_i\sigma_{\vec{\lambda}}\Omega\partial_j\sigma_{\vec{\lambda}} - \Omega\partial_j\sigma_{\vec{\lambda}}\Omega\partial_i\sigma_{\vec{\lambda}}\right)\right] + 4\partial_i\vec{d}_{\vec{\lambda}}^{\,T}\sigma_{\vec{\lambda}}^{-1}\Omega\sigma_{\vec{\lambda}}^{-1}\partial_j\vec{d}_{\vec{\lambda}} \tag{4.98}$$

Only the off-diagonal entries can be nonzero and clearly $\mathcal{U}_{jk} = -\mathcal{U}_{kj}$. For our two-parameters model, we then have $\det \boldsymbol{\mathcal{U}} = \mathcal{U}_{12}^2$. The value of $\mathcal{U}_{12}$ can actually be written

in a convenient closed form also for $q \neq 0$:

$$\begin{aligned} &\mathcal{U}_{12}(\lambda_2; r, \theta, \phi, x, \gamma, q, \beta) \;= \\ =\;& 2\Big[\cos(\gamma+\theta)\cos 2\phi \sin\theta - \cos\theta \sin(\gamma+\theta)\Big]\sinh 2r \sinh 2x + \\ &- 4q^2 \cos^2\phi^2 \sin 2(\beta-\lambda_2)\sinh 2x \end{aligned} \tag{4.99}$$

It is simple to check that $\mathcal{U}_{12}^{opt} = 0$, so that also the $\mathscr{R}$ parameter is zero in the optimal configuration and the parameters can be jointly estimated via the projection-valued measure diagonalizing simultaneously both the symmetric logarithmic derivatives. Moreover, the result is true *for any value of* λ_1 *and* λ_2 since, once again, the problem becomes covariant in the optimal configuration.

To conclude, it is worth pondering about the physical situation associated with the optimal configuration; since we have $\phi = \frac{\pi}{4}$, the beam-splitter is now a balanced one. For $\theta = \frac{\pi}{2}$, moreover, the input state after the BS turns out to be a *twin-beam state*, apart for the relative displacement and irrelevant local phases that can be reabsorbed into an immaterial redefinition of λ_1. Therefore, in this setting, the local squeezing impinging onto the phase shifters is zero, while the entanglement is maximal. This could be related to its effectiveness at decoupling the two parameters, since entanglement could play a role at fully exploiting the two-mode space to independently encode λ_1 and λ_2, whereas in the maximum configuration the reduction to a single-mode problem could have limited the independent ways in which the two phase shifters could act. Nevertheless, further investigations on other models are necessary to draw based and general conclusions in this respect.

Part II

Continuous-time Quantum Walks

CHAPTER 5

Introduction to quantum walks on graphs

Quantum walks [251, 252, 253, 254, 255] represent a wide topic in modern quantum information theory due to their versatility as effective models for very different phenomena, ranging from quantum transport, both in naturally occurring microscopic systems [256] and for quantum technologies, to quantum algorithms and quantum sensing [257, 258]. Some hints of their structure where already recognized by Richard Feynman in 1948 [259] through a construction currently known as *Feynman's checkerboard model*, which was essentially a first attempt to define a discrete model on a lattice which reproduces the free Schrödinger equation by taking the continuum limit in the appropriate way. The term "quantum walk" was first used in its modern meaning in 1993 by Yakir Aharonov et al. [260, 261, 262, 263] to describe what we now call *discrete-time quantum walks* (DTQWs) and turned out to be equal to Feynman's checkerboard model: the significance of their work was also to prove the ballistic motion, compute the average velocity of the walker to be $1/\sqrt{2}$ and derive other analytic results, particularly for the case where the infinite 1-dimensional lattice is interrupted by an hard wall, and asymptotics for the infinite case. Around the same years, *continuous-time quantum walks* (CTQWs) were introduced by E. Farhi and S. Gutmann [264] and the outstanding differences between their behaviour and that of diffusive, classical random walks were remarked [265], hinting at possible quantum overheads in exploring graphs (algorithms involving decision trees) and related problems. A breakthrough came with the papers by Andrew Childs proving first, in 2003, an exponential overhead of quantum walks over classical algorithms for a computational problem in graph theory [266] and then, in 2004, the application of quantum walks to *quantum search* on unstructured (or partially structured) databases modelled by graphs [267, 268, 269]. The application of quantum walks to quantum search quickly developed [268, 270, 271, 272, 273, 274] and it was also applied theoretically to real discrete structures, e.g. graphene [275], tested in experiments [276] and even proposals about the role of quantum search in naturally occuring processes were put forward [256]. The scaling law of $O(\sqrt{N})$ for the quantum walk-based search on an unstructured database of N entries, as opposed to the $O(N)$ scaling of classical algorithms, was proved to be optimal and achievable on vast families of graphs [277, 278]. Still in the early 2000s, *quantum spin chains* were independently studied [279, 280, 281, 282] to address the problem of *quantum transport*, i.e. the transport of quantum coherence and/or quantum information through an ordered quantum medium: these systems are indeed equivalent to quantum walks in their single-particle subspace that is relevant for transport problems, where they have been also considered as purported models for excitonic quantum transport between molecules involved in the photosynthesis [283, 284]. In 2009, A. Childs also

showed that continuous-time quantum walks can serve as models for *universal quantum computation* [285]. Albeit inefficient for single-particle quantum walks, adding more particles with interactions between them on appropriately chosen graphs can model universal quantum computation efficiently [286, 287, 288]. Relevantly, the initial interest sparkled by Feynman for quantum walks as discrete models for relativistic field theories, such as the Klein-Gordon Equation and the Dirac Equation has persisted up to the recent years [289, 290, 291]. As a final introductory remark, let us stress that discrete-time quantum walks and continuous-time quantum walks seem to be related in certain limits [292], although no universal relation between them has been proved on generic, non-regular graphs.

5.1 Classical vs. quantum discrete evolutions in one dimension

5.1.1 Diffusion processes on discrete structures

To introduce the subject, we will start by picturing a classical particle which can sit at discrete positions on a 1-dimensional lattice, labelled by an integer $n \in \mathbb{Z}$. In the most general case, the state of the particle will be described by a probability distribution p_n, such that $\sum_{n=-\infty}^{+\infty} p_n = 1$. A classical stochastic process would then describe the update of this discrete probability distribution with time, and this can happen either at discrete time intervals or continuously in the time domain. In the former case, we can for example define the following updating rule:

$$p_n(t+1) = \gamma(t)p_{n-1}(t) + (1-\gamma(t))p_{n+1}(t) \tag{5.1}$$

where $\gamma(t) \in [0,1]$ is the probability of jumping one step to the right at time t, whereas $1-\gamma(t)$ is the probability of jumping to the right[1]. This updating rule preserves the total probability and spreads stochastically (if $0 < \gamma < 1$) an initially localized particle on the lattice. If we assume a symmetric and time-homogeneous process, $\gamma = 1/2$, a particle initially sitting in $n = 0$ at $t = 0$ will spread, alternating between even and odd sites, according to a binomial distribution:

$$p_n(t) \;=\; \frac{1}{2^t}\binom{t}{\frac{t+n}{2}} \;\simeq\; \frac{2}{\sqrt{2\pi t}}e^{-\frac{n^2}{2t}} \tag{5.2}$$

with a variance $\langle \Delta n^2 \rangle = t$ so that the width of the bell-shaped distribution, after a long time, will be proportional to $\sqrt{t}$.

This behaviour characterizes *diffusive* systems in which external drivers are of secondary importance while a stochastic dynamics (of either internal or external origin, e.g. in Brownian motion) gives rise to an evolution without a preferred direction. Indeed, the continuous version of this model is the central idea of Einstein's theory of Brownian motion [293].

5.1.2 Discrete-time Markov chains

Generalizing the simple hopping model on a 1-dimensional lattice to more complex discrete structures requires some preliminary definitions. Given a finite set of cardinality

[1] Even more generally, one could include a probability of staying in the initial site

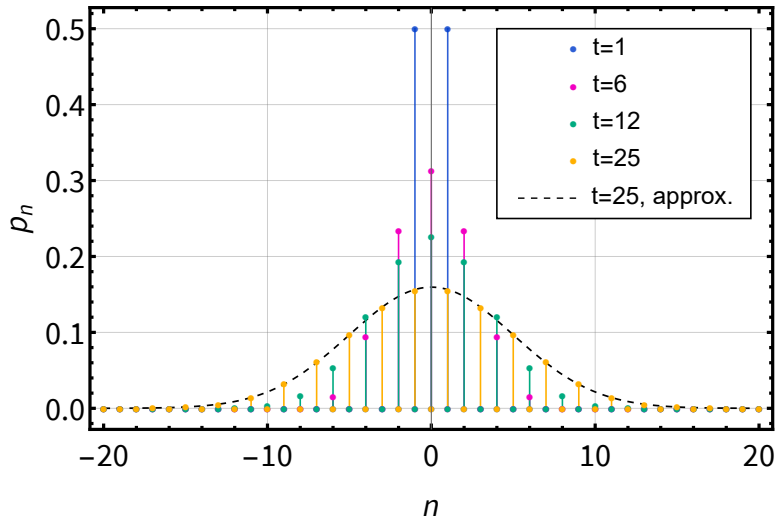

Figure 5.1: Probability distributions for a classical random walk on a 1-dimensional lattice at different times (dots and vertical lines) and Gaussian approximation at $t = 25$ (dashed black curve).

n of possible *deterministic, mutually exclusive states* for a classical system to be found in, we can describe a generic state of the classical system as a vector $\vec{p} \in (\mathbb{R}^+)^n$ of positive numbers summing up to 1. A *discrete-time, homogeneous Markov chain* is a stochastic process in which the vector $\vec{p}$ is updated in discrete steps in such a way that if the state was in the deterministic state j at time t, the probability of ending up in the deterministic state k, $P^t_{j,k}$ at time $t+1$ depends solely on j and k and *not* on t (homogeneity) or on the previous history of the system (Markovian, or memorylessness property). Notice that, in general, $P_{j,k} \neq P_{k,j}$ and $P_{j,j} \neq 0$, so that a transition probability between two deterministic states can be asymmetric, and there can be a non-vanishing probability of staying in the previous state. Clearly, then, the transition probabilities can be arranged into an $n \times n$ matrix P that completely defines the Markov chain. Since the total probability of transitioning out of any given state plus the probability of staying in that state must add up to 1, we have $\sum_k P_{j,k} = 1$, so that the matrix P is *right-stochastic*. The entries of the m-power of P encode the probabilities of transitioning between two states in m steps. Of particular interest is the case when P is symmetric (hence bistochastic) and the transition probabilities from a vertex j are all either 0 or $1/d_j$, where d_j is exactly the number of states that can be reached from j in one step: in other words, all states one-step away from j are equally probable. In these instances one can prove that, whatever the initial state, the long time limit of the Markov chain is stationary and, under further commonly considered conditions, it is *flat*: if we let it evolve for a sufficiently long time, the system will be found with equal probability in any one of the allowed states.

5.1.3 Some facts about graphs

The structure of Markov chains naturally suggests to represent the states as points and the allowed transitions encoded in the matrix by weighted arrows connecting them. In this thesis we will only focus on cases where all the *instantaneous* transitions are equally probable among themselves and both in one way and in the opposite one. In this case, the weighted arrows are replaced by simple arcs. The mathematical structures that cap-

ture this construction are *graphs*:

Definition 5.1.1: Graphs

A *graph* $\mathcal{G} = (V, E)$ is defined by an ordered pair of discrete sets: the elements of the set V are called *vertices*, and its cardinality is called the *order* of the graph and it can be infinite. The elements of the E set are (ordered or unordered) pair of vertices called *edges*. The graph is *directed* if the pairs in E are ordered and *undirected* otherwise. It is *simple* if all the pairs in E are distinct and contain distinct vertices (no two vertices are connected by more than one edge and no vertex is connected to itself by an edge). It is called *connected* if every vertex can be reached from any other vertex following the edges. The number of edges exiting from a vertex v is called the *degree* of v, $\deg(v)$. The graph $\mathcal{G}$ is *m-regular* if each vertex has degree $m \in \mathbb{N}$ and it is *bipartite* if its vertices can be partitioned into two subsets such that all the edges only connect vertices from different subsets. The *topological distance* between two vertices in a graph $\mathcal{G}$ is the number of edges in any shortest path in $\mathcal{G}$ connecting the two vertices.

As remarked above, we will only consider undirected, simple and connected graphs, because we want to model a spontaneous process with no external drivers.

Let us take such a graph $\mathcal{G} = (V, E)$ with $|V| = N$ and label the vertices in such a way that they can be addressed by a natural number. A statistical state of a classical particle on the graph can again be described by a probability distribution over the set V. To find the right bistochastic matrix that will generate the discrete-time homogeneous Markov chain on $\mathcal{G}$, notice that we may associate to the graph a real symmetric $N \times N$ matrix called the *Laplacian* whose entries are defined according to:

$$\begin{cases} j \neq k: & \mathrm{L}_{jk} = -1 \iff (v_j, v_k) \in E \\ j \neq k: & \mathrm{L}_{jk} = 0 \quad \text{otherwise} \\ & \mathrm{L}_{jj} = \deg(v_j) \end{cases} \tag{5.3}$$

where $v_j \in V$ and $j, k \in \mathbb{N}$ are the labels of the vertices. As a shorter notation to indicate that vertices v_j and v_k share an edge, in place of $(v_j, v_k) \in E$ we will also use $j \frown k$, where an unambiguous numbering of the vertices is implied. The Laplacian can be decomposed into a diagonal matrix and an off-diagonal matrix according to:

$$\mathrm{L} = \mathrm{D} - \mathrm{A} \tag{5.4}$$

where the diagonal matrix D encodes the degrees of all the vertices and the off-diagonal matrix A is named the *adjacency matrix* of $\mathcal{G}$. By construction, A is symmetric and traceless, since a simple graph cannot have self-loops. As a consequence, the sum of the entries in each row and the sum of the entries in each column of L is 0. Clearly, both the Laplacian and the adjacency matrix are sufficient to reconstruct the undirected graph: they contain, however, some additional information, namely the labeling of the vertices. If the graph is unlabelled, then any permutation of the rows *and* columns of a Laplacian or adjacency matrix of the graph will provide an equally valid Laplacian / adjacency matrix.

The eigenvectors and eigenvalues of the L and A are also quite insightful in studying the properties of a graph [294, 295]. In general, we have the following result:

Theorem 5.1.1

The Laplacian matrix L of any graph $\mathcal{G}$ is positive-semidefinite. The dimension of the null space of L (number of linearly independent eigenvectors with eigenvalue 0) is equal to the number of connected components of $\mathcal{G}$. If the graph is connected, the eigenvector of L with eigenvalue 0 has all its entries equal to $\frac{1}{\sqrt{N}}$, N being the number of vertices in $\mathcal{G}$, while all the other eigenvalues are strictly positive.

The branch of mathematics devoted to the study of these structures is *graph theory* [296], and it has very illuminating connections with e.g. group theory, algebraic topology and linear algebra. Problems such as finding the shortest path connecting two vertices in a large graph, or determining if a given graph contains a closed path traversing each vertex exactly once are traditionally hard to solve numerically. Even seemingly innocent questions, like asking what is the number of *connected* simple graphs that can be constructed with N vertices (not labelled), do not have an analytical answer and they have to be worked out numerically on a case by case basis [297].

Here we will content ourselves with studying the most common families of graphs, both because they are amenable to analytic calculations and because they relate to prominent applications. As a first class, we shall consider m-regular graphs whose adjacency matrices are *circulant*: each row is a cyclic permutation of the first row. It is easy to show that, once the vertices are ordered in such a way that each row corresponds to the row above shifted by one entry to the right and with the last entry replacing the first one, they are all diagonalized by the Fast Fourier Transform, meaning that the entries of their eigenvectors are the N-th roots of unity, N being the number of vertices:

$$v_j^{(n)} = \frac{1}{\sqrt{N}} \exp\left(\frac{2\pi i(n-1)(j-1)}{N}\right) = \omega_N^{(n-1)(j-1)} \tag{5.5}$$

where the index $n \in \{1, ..., N\}$ labels the eigenvector relative to the eigenvalue λ_n and the index $1 \leq j \leq N$ labels the components of each vector, while $\omega_N = e^{2\pi i/N}$ is the fundamental N-root of unity. It is important to stress that this structure is completely fixed by the circulant property of the matrix: any other circulant $N \times N$ real matrix will have these vectors as eigenvectors. The eigenvalues, on the other hand, depend upon the specific graph type. If a generic circulant matrix has first row $\{c_0, c_{n-1}, c_{n-2}, ..., c_1\}$ and it is ordered as defined above such that the second row is $\{c_1, c_0, c_{n-1}, ..., c_2\}$ and so on, then its eigenvalues are:

$$\lambda_n = \sum_{k=0}^{N-1} c_k \, \omega_N^{(n-1)k}, \quad n \in \{1, ..., n\} \tag{5.6}$$

In this class we find some particularly relevant subclasses:

- **Cycle graphs**, whose adjacency matrix has $\mathrm{A}_{j,j+1} = \mathrm{A}_{j+1,j} = 1$ and all other entries are null, with $j = 1, ..., N$, N being the order of the cycle, and vertex $N+1$ is identified with vertex 1. For example, for a simple cycle of 5 vertices:

$$\mathrm{A}_{C5} = \begin{pmatrix} 0 & 1 & 0 & 0 & 1 \\ 1 & 0 & 1 & 0 & 0 \\ 0 & 1 & 0 & 1 & 0 \\ 0 & 0 & 1 & 0 & 1 \\ 1 & 0 & 0 & 1 & 0 \end{pmatrix} \tag{5.7}$$

They are strongly regular with degree of regularity $m = 2$ and they have N edges, equal to the number of vertices. Their eigenvalues are given by:

$$\lambda_n \;=\; 2\cos\left(\frac{2\pi n}{N}\right) \tag{5.8}$$

We will denote them as C_N. See Fig.5.2(a) for an example.

- **Complete graphs**, as the name suggests, are those graphs where every possible edge is there, thus any two vertices are always neighbours. This means that $\forall j \neq k \;:\; \mathrm{A}_{jk} = 1$ for the adjacency matrices of complete graphs. They are strongly regular with degree of regularity $m = N - 1$ and they have $\frac{N(N-1)}{2}$ edges. Their eigenvalues are given by ($N > 1$):

$$\lambda_n \;=\; \sum_{j=1}^{N} e^{\frac{2\pi(j-1)(n-1)}{N}} - 1 \;=\; \begin{cases} N-1 \text{ if } n = 1 \\ -1 \text{ else} \end{cases} \tag{5.9}$$

  Thus they have the eigenvalue -1 which has degeneracy $N-1$ and the eigenvalue $N-1$ whose unique eigenvector is the flat vector $\{1, ..., 1\} \in \mathbb{R}^N$. The standard notation for a complete graph with N vertices is K_N. An example for $N = 11$ is given in Fig.5.2(b).

- **d-dimensional periodic cubic lattices** can be seen as a generalization of the cycles. Their number of vertices is $N = \Lambda^d$, where $\Lambda \in \mathbb{N}$ is a parameter fixing the number of sites along each dimension. To describe them, it is easiest to introduce a multi-index notation: one first defines an arbitrary bijection between $\{1, ..., N\}$ and the set of d-tuples of natural numbers between 1 and Λ, such that to $1 \leq k \leq N$ corresponds the d-tuple $\tau_k = \{j_1^k, ..., j_k^d\}$ with $1 \leq j_k^n \leq \Lambda$. We then postulate that vertices k_a and k_b are connected by an edge if and only if the corresponding tuples differ by 1 in exactly one entry and they are equal in all other entries, or equivalently $|\tau_{k_a} - \tau_{k_b}| = 1$ where $|\bullet|$ is the Euclidean norm of the d-tuple. Moreover, we use addition modulo Λ, such that the entries 1 and Λ are considered as differing by 1: this imposes the periodicity of the lattice. Their eigenvectors are also labelled by d-tuples in Λ^d and they are given by:

$$\lambda_{\alpha_1,...,\alpha_d} \;=\; 2\sum_{n=1}^{d} \cos\left(\frac{2\pi\alpha_n}{\Lambda}\right) \tag{5.10}$$

  They are d-regular and they have $d\Lambda^d$ edges. They are generalized by *torus graphs*, having $\Lambda_1 \times \Lambda_2 \cdots \times \Lambda_d$ vertices and, correspondingly, each Λ_j will appear in the denominator of the cosine in the eigenvalues. They are denoted by $T_{\Lambda_1,...,\Lambda_d}$. An example for $T_{9,2}$ is given in Fig.5.2(e).

Notice that circulant graphs are always regular, since each row of their adjacency matrices has exactly the same number of nonzero entries. For any m-regular graph, labelling with $\{\lambda_n\}_{n=1,...,N}$ the collection of the eigenvalues of their adjacency matrices, we have that the eigenvalues of their Laplacians are:

$$\tilde{\lambda}_n \;=\; m - \lambda_n \;,\;\; n \in \{1, ..., N\} \tag{5.11}$$

Let us also mention an important family of graphs which are regular but not circulant:

- **Hypercube graphs** are the generalization of the graph defined by the vertices and the edges of a three-dimensional cube. Let d be their dimension, then the number of vertices is 2^d and the number of edges is $d2^{d-1}$. Their adjacency matrices can be defined recursively by:

$$\mathrm{A}^{(d)} := \begin{cases} \mathbb{1}_2 \otimes \mathrm{A}^{(d-1)} + \mathbb{1}_{d-1} \otimes \mathrm{A}^{(1)} & \text{if} \quad d > 1 \\ \mathrm{A}^{(1)} := \begin{pmatrix} 0 & 1 \\ 1 & 0 \end{pmatrix} \end{cases} \tag{5.12}$$

  Their eigenvalues and eigenvectors can be readily computed from the tensor products [251]. Here we only mention that the eigenvalues for the adjacency matrix of the d-dimensional hypercube are $\lambda_n = 2n - d$ with $n = 0, ..., d$ and the n-th eigenvalue has multiplicity $\binom{d}{n}$. They are traditionally denoted by Q_d, the standard hypercube for $d = 4$ is drawn in Fig.5.2(d). Notice that they are equivalent to d-dimensional periodic cubic lattices with $\Lambda = 2$.

Finally, let us consider three more examples, this time belonging to the much wider class of non-regular graphs:

- **Path graphs**, denoted by P_N, are the simplest connected graphs with N vertices and they are obtained by simply joining them with an open path of edges. Their adjacency matrix is identical to that of a cycle C_N except for $\mathrm{A}_{1,N} = \mathrm{A}_{N,1} = 0$. Their eigenvalues are given by:

$$\lambda_k = 2\cos\left(\frac{k\pi}{N+1}\right), \quad k \in \{1, \ldots, N\} \tag{5.13}$$

- **Star graphs** with N vertices are defined by a central vertex, conventionally labelled by 1, and $N - 1$ external vertices that are connected exclusively with 1. The star graph with 11 vertices is drawn in Fig.5.2(f) for reference. Their adjacency matrix takes the following form:

$$\mathrm{A}^{(N)} = \begin{pmatrix} 0 & 1 & \ldots & 1 \\ 1 & & & \\ \vdots & & \mathbb{O}_{N-1} & \\ 1 & & & \end{pmatrix} \tag{5.14}$$

  It is simple to check that two (non-normalized) eigenvectors are

$$v_\pm = (\pm\sqrt{N-1}, 1, \ldots, 1)^T$$

  with eigenvalues $\lambda_\pm = \pm\sqrt{N-1}$. The only other eigenvalue is $\lambda_0 = 0$ with degeneracy $N - 2$ and its eigenspace comprises all the vectors whose first entry is 0 and all the other entries sum up to 0. Since this graph is non-regular, the Laplacian has a different set of eigenvectors and eigenvalues: an eigenvector of the form $\tilde{v}_N = (1 - N, 1, \ldots, 1)^T$ with eigenvalue N, the flat eigenvector $(1, ..., 1)^T$, which is *always* an eigenvector of any Laplacian, with eigenvalue 0, and the same eigenspace of the eigenvalue 0 for the adjacency matrix is also the eigenspace of the Laplacian with eigenvalue 1, with the same degeneracy $N - 1$. Analytical results for (continuous-time) quantum walks on these graphs can be found in [298].

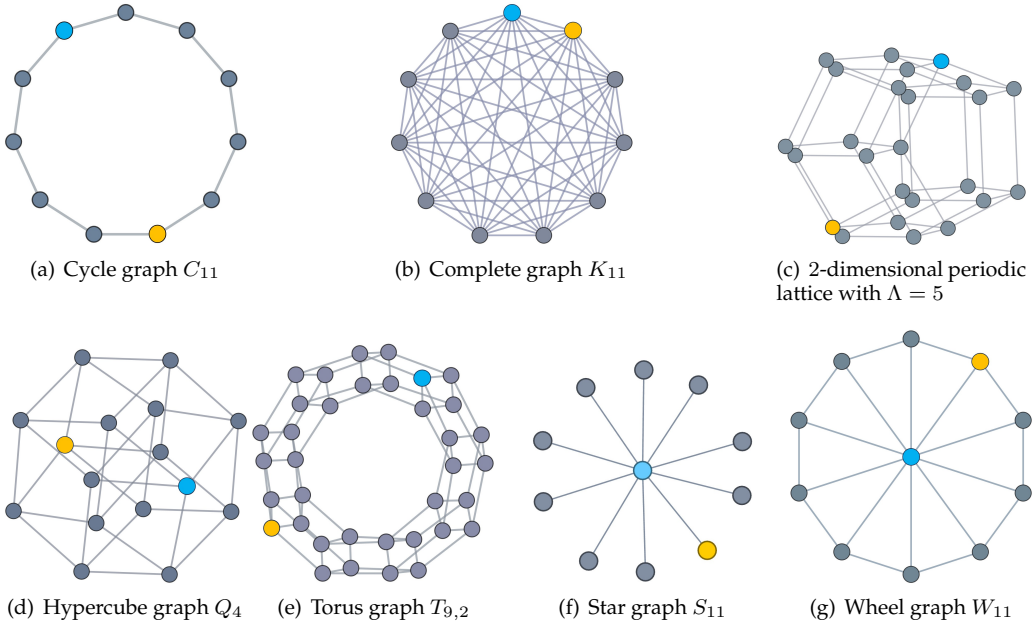

(a) Cycle graph C_{11} (b) Complete graph K_{11} (c) 2-dimensional periodic lattice with $\Lambda = 5$

(d) Hypercube graph Q_4 (e) Torus graph $T_{9,2}$ (f) Star graph S_{11} (g) Wheel graph W_{11}

Figure 5.2: Examples of graphs with 11 vertices. The initial and final vertices for typical transport tasks are colored in light-blue and yellow, respectively. In each case, they are as far apart as possible in terms of topological distance.

- **Wheel graphs** with N vertices consist of a cycle graph C_{N-1} and an additional central vertex which is connected to every vertex in the cycle. The eigenvalues of their adjacency matrices are $\lambda_{\pm} = 1 \pm \sqrt{N}$ and $\lambda_k = 2\cos\frac{2\pi k}{N-1}$ for $k = 1, ..., N-2$, with no degeneracy. They have $2(N-1)$ edges and they will be denoted by W_N. The graph W_{11} is represented in Fig.5.2(g).

Just as a reference, we report here the adjacency matrices of K_5 and S_5 and the Laplacian matrix of W_6:

$$\mathrm{A}_{K_5} = \begin{pmatrix} 0 & 1 & 1 & 1 & 1 \\ 1 & 0 & 1 & 1 & 1 \\ 1 & 1 & 0 & 1 & 1 \\ 1 & 1 & 1 & 0 & 1 \\ 1 & 1 & 1 & 1 & 0 \end{pmatrix} \qquad \mathrm{L}_{W_6} = \begin{pmatrix} 5 & -1 & -1 & -1 & -1 & -1 \\ -1 & 3 & -1 & 0 & 0 & -1 \\ -1 & -1 & 3 & -1 & 0 & 0 \\ -1 & 0 & -1 & 3 & -1 & 0 \\ -1 & 0 & 0 & -1 & 3 & -1 \\ -1 & -1 & 0 & 0 & -1 & 3 \end{pmatrix}$$

$$\mathrm{A}_{S_5} = \begin{pmatrix} 0 & 1 & 1 & 1 & 1 \\ 1 & 0 & 0 & 0 & 0 \\ 1 & 0 & 0 & 0 & 0 \\ 1 & 0 & 0 & 0 & 0 \\ 1 & 0 & 0 & 0 & 0 \end{pmatrix}$$

5.1.4 Discrete-time random walks

We have previously determined that the transition matrix of a discrete-time Markov chain must be right-stochastic (columns summing to 1) in order to preserve probabilities. If we want to define a discrete-time quantum walk on a simple, connected graph $\mathcal{G}$ with adjacency matrix A, the request that the only allowed transitions at each step are those between neighbouring vertices, that these should be equiprobable, together with right-stochasticity lead us to conclude that the transition matrix must have entries:

$$\mathrm{P}_{jk} \;=\; \mathrm{A}_{jk}/d_k \tag{5.15}$$

where $d_k = \mathrm{L}_{kk}$ is the degree of vertex k. Notice that P will not be bistochastic, in general: the probability of transitioning from a vertex of low degree to a vertex of higher degree is higher than the probability of doing the inverse transition. The evolution law is:

$$\vec{p}_t \;=\; \left[\mathrm{P}^t\right]\cdot\vec{p}_0 \;\;,\quad t\in\mathbb{N} \tag{5.16}$$

It can be shown that such Markov chains, under reasonable assumptions, all have an equilibrium distribution such that the probability of finding the walker on vertex j after a long number of steps t converges to:

$$\lim_{t\to\infty}\left[\mathrm{P}^t\right]_{jk} \;=\; \frac{d_j}{\sum_{n=1}^{N} d_n} \tag{5.17}$$

where N is the total number of vertices in $\mathcal{G}$. Notice that the entry $\lim_{t\to\infty}\left[\mathrm{P}^t\right]_{jk}$ does not depend on k, indicating that the equilibrium distribution is the same whatever the initial state. If the graph is m regular, then $d_j = m$ for all vertices and the equilibrium distribution is just the uniform probability distribution over all the vertices.

5.1.5 Discrete-Time Quantum Walks

The most straightforward the generalization of the classical model outlined in the previous subsection is provided by a discrete-time quantum walk (DTQW) [262]; we will just consider the case of a 1-dimensional lattice for convenience of exposition [261]. Such a model is based on an underlying Hilbert space $\mathcal{H}\simeq\mathbb{C}^N\otimes\mathbb{C}^2$, where $\mathbb{C}^N$ is the Hilbert space defining the position of the walker, labelled as usual by an integer such that 0 is the reference starting vertex on the lattice (and $N\to\infty$ in the limit of a true lattice, otherwise we can take periodic boundary conditions $|N+1\rangle\sim|1\rangle$). The second Hilbert space, isomorphic to $\mathbb{C}^2$, describes an accessory quantum degree of freedom, called the *coin*, whose role is to decide where the particle should move at any successive time step: if the coin state is $|\uparrow\rangle$, the walker will move to the right, if it is $|\downarrow\rangle$ it will move to the left and if the coin is in a superposition, then the walker will move differently according to previous rules in each branch of the superposition. The key idea of [261, 262] was to choose a *superposition state* as the initial condition for the coin and a discrete time evolution operator $\hat{\mathrm{U}}_{dt}$ in such a way that not only the walker moves according to the quantum state of the coin, but also the coin state is updated. In this way, successive applications of $\hat{\mathrm{U}}_{dt}$ at consecutive time steps *entangle* the coin and the walker degrees of freedom and they interlace their evolutions. To implement the discrete evolution operator we need first to define a *conditional shift* unitary operator $\hat{\mathrm{U}}_S$ whose role is to implement the shift rules described above for the walker based on the coin state:

$$\hat{\mathrm{U}}_S \;:=\; |j+1\rangle\langle j|\otimes|\uparrow\rangle\langle\uparrow| \;+\; |j-1\rangle\langle j|\otimes|\downarrow\rangle\,\langle\downarrow| \tag{5.18}$$

Now we are free to choose a unitary operation acting on the coin only. Since we are aiming at describing homogeneous hoppings, this unitary should not depend on the position of the walker. A common choice is the *Hadamard coin*, where the coin-updating unitary is equivalent to the Hadamard gate from quantum computation:

$$\hat{\mathrm{U}}_H \;:=\; \frac{1}{\sqrt{2}}\begin{pmatrix} 1 & 1 \\ 1 & -1 \end{pmatrix} \tag{5.19}$$

The full evolution operator is therefore:

$$\hat{\mathrm{U}}_{dt} \;:=\; \left(\mathbb{1}\otimes\hat{\mathrm{U}}_H\right)\hat{\mathrm{U}}_S \tag{5.20}$$

and the evolution from time t to time $t+1$ is given by:

$$|\psi_{t+1}\rangle\!\rangle \;=\; \hat{\mathrm{U}}_{dt}|\psi_t\rangle\!\rangle \tag{5.21}$$

To get an idea of the evolution displayed by such a system, let us take the initial state:

$$|\psi_0\rangle\!\rangle = |j\rangle\otimes(\alpha|\uparrow\rangle+\beta|\downarrow\rangle) \tag{5.22}$$

After the first step, we will have:

$$|\psi_{dt}\rangle\!\rangle \;=\; \hat{\mathrm{U}}_{dt}|\psi_0\rangle\!\rangle \;=\; \alpha|j+1\rangle\otimes\frac{|\uparrow\rangle+|\downarrow\rangle}{\sqrt{2}} \;+\; \beta|j-1\rangle\otimes\frac{|\uparrow\rangle-|\downarrow\rangle}{\sqrt{2}} \tag{5.23}$$

For the second step, one would group all the terms in which the coin is up to apply a right shift and all the terms in which the coin is down will be shifted to the left. Then, again, the coin state in each branch is brought in the corresponding superposition state by the Hadamard gate. As shown in Fig.5.3, such a propagation (red line) is sensibly different from that of a classical random walker starting at the same vertex: the spreading is now linear in time, and the probability to find the walker on a specific site peaks at opposite sites, linearly propagating away from the starting position. We say that discrete-time quantum walks of the Hadamard type on a lattice propagate *ballistically*, in contra position to the diffusive behaviour of classical ones. In [261] the authors provide a proof of this behaviour, showing that the speed of the Hadamard walk is $\frac{1}{\sqrt{2}}$ and that the probability outside the region $[-t/\sqrt{2}, t/\sqrt{2}]$ at time t is exponentially decreasing with the distance from the starting vertex.

It is interesting to note that such a linear relation between the standard deviation and the propagation time is also present in the standard quantum mechanical problem of the dispersion of a Gaussian wavepacket according to the free Schrödinger equation: notwithstanding the similarity with the heat equation, the fact that Schrödinger's equation deals with complex amplitudes means that the wavefunction evolves according to:

$$\psi(x,t) \;=\; \frac{1}{\sqrt{2\pi(1+it/\tau)\sigma_0^2}}e^{-\frac{x^2}{4\sigma_0^2(1+it/\tau)}} \tag{5.24}$$

where σ_0 is the variance of the wavepacket at $t=0$, $\psi(x,0) = (2\pi\sigma_0^2)^{-1/2}\exp(-x^2/2\sigma_0^2)$ and $\tau = 2m\sigma_0^2/\hbar$ is a reference time scale. When we compute the probability as $p(x,t) = |\psi(x,t)|^2$, the complex nature of the exponent leads to a standard deviation at time t given by:

$$\sigma(t) \;=\; \sigma_0\sqrt{1+\frac{t^2}{\tau^2}} \tag{5.25}$$

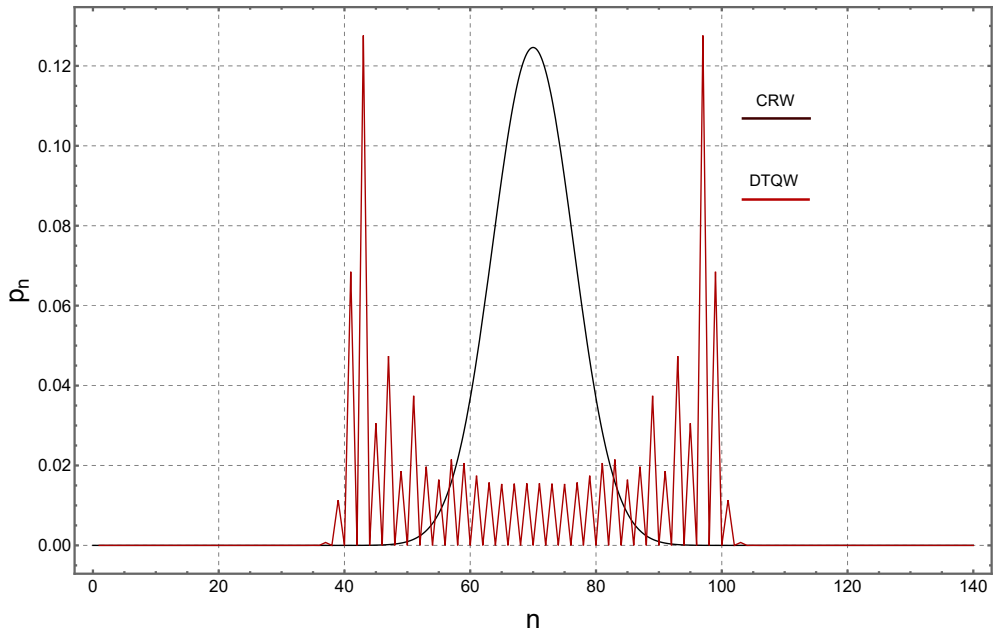

Figure 5.3: Probability distributions for a classical random walk (CRW, black) and a discrete-time quantum walk (DTQW, dark red) on a 1-dimensional path graph with $N = 140$ vertices. The starting vertex is $j = 70$ in both cases and the total propagation time is $T = 25$.

Before leaving the subject of discrete-time quantum walks, we should mention that there are formulations enlarging their underlying Hilbert space to avoid the coin [299], as well as generalizations to other graphs, even non-regular ones [263, 300] which, however, require to associate the states of the walker with the directed edges.

5.2 Continuous-time random walks

Exactly as we did for the discrete-time random walks, we suppose to have a simple connected graph $\mathcal{G} = (V, E)$ with N vertices and a state of the classical system will be described by a probability vector $\vec{p} \in \mathbb{R}_+^N$ over the label space of the vertices. Now, however, we would like to model the evolution of a classical particle which diffusively and continuously flows in and out of the countable allowed states. We will see that the Laplacian matrix is the only valid choice to generate an unbiased continuous-time quantum walk on a given graph, due to the requirement that the total probability must be conserved. In all generality, in place of the discrete-time updating rule of Eq.(5.1), we will now have a differential equation:

$$\frac{d\vec{p}}{dt} = -\gamma \mathrm{M} \cdot \vec{p}(t) \tag{5.26}$$

where M is some $N \times N$ real matrix which is independent of time for an homogeneous process, while γ, measured in hertz, is a rate. During an infinitesimal time lapse dt, the

walker can diffuse into an adjacent vertex with probability γdt. Integrating Eq.(5.26) in a short time interval we then get, in component form:

$$p_j(t+dt) \;=\; p_j(t) \;+\; \left(-\gamma dt \sum_{k=1}^{N} M_{jk} p_k(t)\right) \tag{5.27}$$

This means that $1-\gamma dt M_{jj}$ is the probability for the walker to stay in vertex j in the infinitesimal time dt, while $-\gamma dt M_{jk}$ are the probabilities to diffuse from vertex k to vertex j during dt, and they add to the probability of being found in j at time $t+dt$. Clearly, then, $1-\gamma dt M_{jj}$ must be equal to 1 minus the probability for the walker to *leave* vertex j in the infinitesimal time dt:

$$1-\gamma dt M_{jj} \;=\; 1-\left(-\gamma dt \sum_{k\neq j}^{N} M_{kj}\right) \quad\Longrightarrow\quad \sum_{k=1}^{N} M_{kj} = 0 \tag{5.28}$$

It can be easily checked that this condition already ensures the conservation of total probability, $\sum_{j=1}^{N} p_j(t+dt) = 1$. Up to this point, we did not make explicit reference to the graph structure, and we are just defining a *continous-time homogeneous Markov chain*. If we now insist that instantaneous transitions should all happen with equal probability, but only between neighbouring vertices in $\mathcal{G}$, we must demand that $M_{jk} \neq 0$ if and only if vertices j and k are connected by an edge of $\mathcal{G}$. We can chose, without loss of generality, $M_{jk} = 1 \iff j \frown k$, since an overall scaling is set by γ. This fact, combined with the condition $\sum_{j=1}^{N} M_{jk} = 0$ that we just proved, *forces* the *stochastic generator* M to be the Laplacian matrix L of the graph $\mathcal{G}$. We have therefore the following evolution equation for the continuous-time random walk (CTRW) on $\mathcal{G}$:

$$\frac{d\vec{p}}{dt} \;=\; -\gamma \mathrm{L}\cdot\vec{p}(t) \quad\Longrightarrow\quad \vec{p}(t) \;=\; e^{-\gamma \mathrm{L}}\cdot\vec{p}(0) \tag{5.29}$$

From Theorem 5.1.3 we know that the flat probability distribution $\vec{p}_{eq} = \frac{1}{\sqrt{N}}(1,...,1)^T$ is the unique eigenvector with eigenvalue 0 (assuming $\mathcal{G}$ connected), while all other eigenvalues are strictly positive. Consequently, in the large time limit, the distribution $\lim_{T\to\infty} e^{-\gamma \mathrm{L}}\vec{p}(0)$ will approach the flat one exponentially fast, independently of the initial ensemble $\vec{p}(0)$: the classical continuous-time random walk *thermalize*, even if the graph is not regular.

5.3 Continuous-time quantum walks

In the spirit of this classical construction, one can define a continuous-time quantum walk on the same graph, following [264], by considering an N-dimensional *complex* vector $\vec{\psi}(t) \in \mathbb{C}^N$ which encodes the quantum *amplitudes* for the walker to be found in each vertex of $\mathcal{G}$, and postulate a Schrödinger evolution which closely mimics Eq.(5.29):

$$i\hbar \frac{d}{dt}\vec{\psi}(t) \;=\; -\gamma \mathrm{L}\cdot\vec{\psi}(t) \quad\Longrightarrow\quad \vec{\psi}(t) = e^{i\gamma t \mathrm{L}}\cdot\vec{\psi}(0) \tag{5.30}$$

Hence, we are considering an N-dimensional quantum system whose evolution is governed by the time-independent Hamiltonian $\mathrm{H} = -\gamma \mathrm{L}$ and for which we have a preferred basis, called the localized basis, whose elements are wavevectors of the form $|j\rangle$,

$j = 1, ..., N$, localized at each vertex j of G.

The fact that the Hamiltonian matrix H is real in the localized basis entails nontrivial symmetries. Given any two localized states $|j\rangle$ and $|k\rangle$, the transition probability between them is:

$$P_{j\to k}(t) \;:=\; \left|\left\langle k\right| \exp\left(-\frac{it}{\hbar}\mathrm{H}\right)\left|j\right\rangle\right|^2 \tag{5.31}$$

and it is always time-reversal symmetric:

$$P_{j\to k}(t) = P_{j\to k}(-t) \tag{5.32}$$

This equation, combined with the general fact[2] $P_{j\to k}(t) = P_{k\to j}(-t)$ yields:

$$P_{j\to k}(t) = P_{k\to j}(t) \tag{5.33}$$

Therefore, the transition probabilities (or *transport probabilities*) between pairs of sites of a graph are symmetric under the exchange of the starting and target sites. On graphs that possess a reflection symmetry, the evolution will not exhibit any directionality, or *chirality*, whenever the starting condition is on the reflection axis, meaning that it will not distinguish between left or right. This point is most clearly illustrated by an example involving a cycle graph, as the one shown in Fig. 5.4. The entries of the Laplacian for such a graph are given by $\mathrm{L}_{jj} = 2$ and $\mathrm{L}_{j,j+1} = \mathrm{L}_{j,j-1} = -1$, with $j = 1, ..., N$ and identifying site $N+1$ with site 1 and site -1 with site N, while all other entries are null. Eq.(5.33) then implies that, starting from the localized state $|1\rangle$ at vertex 1, the probability for the quantum walker to be found at vertex k is equal at all times to the probability to be found at vertex $N-k+2$, for any $1 < k < N/2$. In particular, when N is odd, the probability at any site apart from the initial one can never grow larger than $\frac{1}{2}$, since there is always a symmetric site with identical probability. These symmetries also imply that the arbitrary choice of the sign in assigning $\mathrm{H} = \pm\gamma\mathrm{L}$ is immaterial, since they generate the same probabilities.

Whenever the graph is *regular*, i.e. all vertices have the same degree, D is proportional to the identity matrix so that L and A will generate exactly the same quantum evolution, apart for an unobservable overall phase. For non regular graphs, instead, there is no a priori reason to prefer L over A as the generator of the *quantum* evolution, whereas the classical one, as noted before, must be generated by the Laplacian in order to conserve the total probability. In the special instance of cubic lattices, it can be shown that an appropriate continuous limit taken together with $N \to \infty$ Eq.(5.30) yields the Schrödinger equation for a free particle whose mass is inversely proportional to γ, as for Feynman's checkerboard model, but such a relation is not generically meaningful for non regular graphs.

[2] This relation is true even if the initial and final states are not localized, since it is derived merely from unitarity.

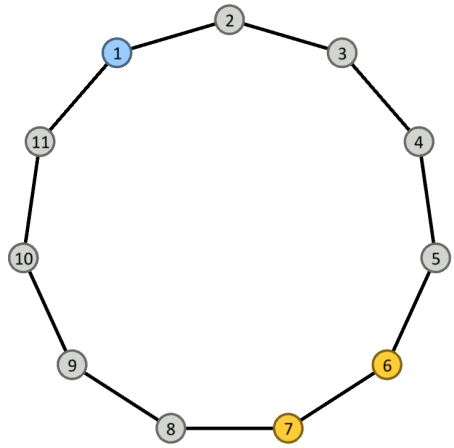

Figure 5.4: Cycle graph with 11 vertices. For a quantum walk starting in a localized state at vertex 1 (light-blue), the probabilities to be observed at vertices 6 and 7 (in yellow) are the same at all times, as a consequence of the time-reversal symmetry of the evolution and the symmetries of the graph.

5.4 Some standard results with continuous-time quantum walks

5.4.1 Perfect state transfer

A typical task that is considered when studying a CTQW on a graph is whether its is possible to achieve an evolution which deterministically sends a localized state $|s\rangle$ into a target state $|f\rangle$, often also localized. If this can be done on the graph $\mathcal{G}$ (using either the Laplacian or the adjacency matrix as generators), we say that $\mathcal{G}$ exhibits *perfect state transfer* (PST) between the vertices s and f. Notice that the symmetries of the evolution imply that, after the same amount of time, $|f\rangle$ will be mapped back to $|s\rangle$. The literature on perfect state transfer is vast and particularly developed on the mathematical side [280, 282, 301, 302, 303]. Without delving into the details, we first observe that PST can be achieved only between vertices that have the same energy with respect to the chosen Hamiltonian: this imposes no restriction if we use the adjacency matrix, since each localized state has energy 0 according to it, but it limits the transfer among vertices of equal degree if the Laplacian is used as the generator. Moreover, given that PST implies a periodic dynamics between the initial and target vertices, all the eigenvectors contributing to this process must have all the eigenvalues in rational ratios one to the other, so that there will exist a finite time after which the evolution goes back to the starting state. A detailed discussion on the conditions needed for PST can be found in [304, 305]. An interesting result, that we should invoke in a later chapter, is that if we consider two distinct connected graphs $\mathcal{G}$ and $\mathcal{G}'$, none of which is trivial (i.e. they contain more than one vertex) and we bridge them by a single edge or a path of length 2, no perfect state transfer is possible between the two vertices connected by the path. In the words of the authors: quantum walks do not like bridges [306].

Another interesting phenomenon is *instantaneous uniform mixing*, which amounts to evolving from a localized state $|j\rangle$ to the uniform, or "flat" state $|F\rangle = \frac{1}{\sqrt{N}} e^{i\phi_k} \sum_{k=1}^{N} |k\rangle$. Importantly, at least when $\mathcal{G}$ is regular, there *must* be relative phases in the target flat

state, otherwise the evolution from a localized state to it would violate its symmetry.

A clear example showcasing both perfect state transfer and fast uniform mixing is provided by the hypercube Q_4. It is convenient to label its $2^4 = 16$ vertices in binary, starting with 0 up to 15. Vertices j and k will be connected by an edge if and only if their binary expansions differ by 1 in a single position, with addition modulo 2. It can be checked that this construction is indeed equivalent to Q_4. Consider now vertex 0 that will correspond to the state $|0000\rangle = |0_2\rangle$ and vertex 15, encoded by the state $|1111\rangle = |15_2\rangle$. For a time $t^* = \frac{\pi}{2}$ the adjacency matrix of the hypercube Q_4 actuates the perfect state transfer between these two states:

$$e^{-i\frac{\pi}{2}\mathrm{A}_{Q_4}}|0_2\rangle \;=\; |15_2\rangle \tag{5.34}$$

Due to the symmetry of the graph, the generic state $|n_2\rangle$ with $n \in \{0, ..., 15\}$ will be transferred to the state $|(15-n)_2\rangle$ in the same time. A convenient way to prove this is to take literally the encoding and rewrite the states in binary form as states of 4 qubits, which is isomorphic to the original $\mathbb{C}^{16}$. By looking at the matrix elements of A_{Q_4} one can then show that this matrix is represented on the (isomorphic) Hilbert space of 4 qubits as:

$$\hat{\mathrm{H}}_{A_{Q4}} \;=\; \sigma_x\otimes\mathbb{1}_2\otimes\mathbb{1}_2\otimes\mathbb{1}_2+\mathbb{1}_2\otimes\sigma_x\otimes\mathbb{1}_2\otimes\mathbb{1}_2+\mathbb{1}_2\otimes\mathbb{1}_2\otimes\sigma_x\otimes\mathbb{1}_2+\mathbb{1}_2\otimes\mathbb{1}_2\otimes\mathbb{1}_2\otimes\sigma_x \tag{5.35}$$

where σ_x is the second Pauli matrix, also known as the NOT gate of quantum computation. Exploiting the fact that all terms in this sum commute, it is simple to show that:

$$e^{-i\frac{\pi}{2}\hat{\mathrm{H}}_{A_{Q4}}} \;=\; \sigma_x\otimes\sigma_x\otimes\sigma_x\otimes\sigma_x \tag{5.36}$$

Therefore the action of this evolution on a state in the computational basis is to negate the computational state of each qubit, as we wanted to show.

The isomorphism that we just constructed also allow us to see that for $\tilde{t} = \frac{\pi}{4}$ the evolution, when applied to any localized state (i.e. any state in the computational basis for the space of 4 qubits), results in instantaneous uniform mixing. Indeed, $e^{-i\frac{\pi}{4}\sigma_x} = \frac{1}{\sqrt{2}}(\mathbb{1}_2 - i\sigma_x) =: \hat{\mathrm{U}}_{\mathrm{mix}}$, which acts on the computational basis as:

$$\hat{\mathrm{U}}_{\mathrm{mix}}|0\rangle = \frac{|0\rangle - i|1\rangle}{2}\,, \quad \hat{\mathrm{U}}_{\mathrm{mix}}|1\rangle = \frac{|1\rangle - i|i\rangle}{2} \tag{5.37}$$

Consequently, $e^{-i\frac{\pi}{4}\hat{\mathrm{H}}_{A_{Q4}}}$ will bring any state of the computational basis into an uniform superposition of *all* the states of the basis, with relative phases chosen among $\{0, \frac{\pi}{2}, \pi, \frac{3\pi}{2}\}$, depending on the initial state, thus realising instantaneous uniform mixing.

The results that we discussed for the hypercube Q_4 actually hold true for any hypercube Q_n, as can be seen by building the corresponding isomorphism with the space of n qubits. Moreover, they clearly do not depend on the choice of the adjacency matrix versus the Laplacian, since the hypercube graphs are regular.

It is worth mentioning that the ideal cases of perfect state transfer and instantaneous uniform mixing also have their approximate counterparts; regarding PST, in any practical scenario having a fidelity with the target state higher than a certain threshold is all that is needed, since noise and experimental errors would be greater than the theoretical

accuracy of transport after a certain point. For this reason, the following definition has been considered:

Definition 5.4.1: Pretty Good State Transfer

Given a connected simple graph $\mathcal{G}$, we say that the graph exhibits *pretty good state transfer* [307, 308] from vertex j to k if, denoting $\hat{\boldsymbol{\rho}}_k = |k\rangle\langle k|$, $\hat{\boldsymbol{\rho}}_j = |j\rangle\langle j|$, we have:

$$\forall \epsilon > 0 \;\; \exists \tau_\epsilon \in \mathbb{R}_+ \quad \text{s.t.} \quad \|e^{-i\mathrm{H}\tau_\epsilon}\hat{\boldsymbol{\rho}}_j e^{i\mathrm{H}\tau_\epsilon} - \hat{\boldsymbol{\rho}}_k\|_1 \; < \; \epsilon \tag{5.38}$$

where H is either the Laplacian or the adjacency matrix of $\mathcal{G}$ and $\|\bullet\|_1$ is the trace-norm.

Several results on pretty good state transfer on quantum spin chains have been derived in recent years (see e.g. [308, 309]).

5.4.2 Grover's algorithm for quantum search on complete graphs

Among the best known applications of continuous-time quantum walks, Grover's algorithm provides a solution for the search of a given entry (and, possibly, more than one) in an unstructured database with a quadratic speedup with respect to the scaling of the optimal classical algorithms. Although a quadratic speedup is not deemed a radical improvement with respect to complexity theory, the case of Grover's algorithm is one of the few in which this advantage is actually proven, since in most other instances, instead, the optimal classical algorithm is not known.

From the point of view of CTQWs, the unstructured database of N entries can be represented by a complete graph K_N: each entry is equally "distant" from any other and there is no intrinsic structure in the database. The starting point of a quantum search algorithm on a graph is the unbiased flat state $|F\rangle = \frac{1}{\sqrt{N}}\sum_{j=1}^{N}|j\rangle$, a uniform superposition over all the states localized at each vertex. The aim is then to construct an Hamiltonian whose evolution will send $|F\rangle$ to the target vertex $|w\rangle$ in the shortest possible time. Let us consider the following ansatz:

$$\hat{\mathrm{H}}_G(\gamma) \;\; = \;\; -\mathrm{L} \; - \gamma|w\rangle\langle w| \tag{5.39}$$

where L is the Laplacian of K_N, $\gamma \in \mathbb{N}$ and the last term is a projector on the target state, also known as an *oracle*. It is imperative to stress that the construction of such an Hamiltonian, despite the presence of the oracle, does *not* entail the previous knowledge of the very state we are looking for: the role of the oracle is to *recognize* the target state any time it is encountered. After all, even in a classical search algorithm, we need to know when we have found the target entry in order to stop the algorithm. It is interesting to note that quantum search is in many senses the *inverse* of instantaneous uniform mixing; indeed, the reverse evolution of a quantum search process will correspond to a localized state coherently spreading over the whole graph to reach the uniform superposition of all localized states.

To find the right value of γ which allows us to perform quantum search with $\hat{\mathrm{H}}_G(\gamma)$ we now introduce a powerful tool in the study of CTQWs: Krylov reduction [310]. The

idea is based on the construction of the Krylov space of an Hermitian matrix from linear algebra: we pick our starting state, in our case $|F\rangle$ and we repeatedly apply the matrix to it, hoping that the space generated by these successive iterations will be a strict subspace of the full Hilbert space, the *Krylov subspace*. If this is the case, we can apply the Gram-Schmidt algorithm to get an orthonormal basis of the subspace, which is called the *Krylov basis*. The full evolution from the original initial state can thus be studied in this reduced space, in which the matrix is represented by a smaller one. In our scenario, we have:

$$\hat{\mathrm{H}}_G(\gamma)|F\rangle = -\frac{\gamma}{\sqrt{N}}|w\rangle \tag{5.40}$$

$$\hat{\mathrm{H}}_G(\gamma)|w\rangle = (N-1-\gamma)|w\rangle - \sum_{j\neq w}^{N}|j\rangle = (N-\gamma)|w\rangle - \sqrt{N}|F\rangle \tag{5.41}$$

Thus, the evolution generated by $\hat{\mathrm{H}}_G(\gamma)$ and starting from $|F\rangle$ happens in a two-dimensional subspace generated by $|w\rangle$ and $|F\rangle$. An orthonormal basis of this space is given by $\{|w\rangle, |\tilde{f}\rangle$, where $|\tilde{F}\rangle = \frac{1}{\sqrt{N-1}}\sum_{j\neq w}^{N}|j\rangle$. The original Hamiltonian $\hat{\mathrm{H}}_G(\gamma)$ can be represented in this basis of the invariant subspace as:

$$\mathrm{H}_G^{\mathrm{red.}}(\gamma) = \begin{pmatrix} N-1-\gamma & -\sqrt{N-1} \\ -\sqrt{N-1} & 1 \end{pmatrix} \tag{5.42}$$

At this point it is only a matter of applying this Hamiltonian to the vector $\left(\frac{1}{\sqrt{N}}, \sqrt{\frac{N-1}{N}}\right)$ representing $|F\rangle$ in the $\{|w\rangle, |\tilde{F}\rangle\}$ basis and find γ such that at a certain time t^* we get $e^{-it^*\mathrm{H}_G^{\mathrm{red.}}}|F\rangle = |w\rangle$. It turns out that the right choice is $\gamma = N$ and the corresponding time is known as *Grover's time* and it is given by $t_G = \frac{\pi}{2\sqrt{N}}$. Had we started from the adjacency matrix, nothing significant would have changed since $-\mathrm{L}-\gamma|w\rangle\langle w|$ and $\mathrm{A}-\gamma|w\rangle\langle w|$ differ by a multiple of the identity matrix, which does not influence the evolution. It might seem quite upsetting that Grover's time *decreases* as the size N of the graph, hence of the database, increases: this has just to do with energy scales, since the energy gap for ever larger complete graphs Laplacians grows linearly. Moreover, the oracle term has to be weighted by $\gamma = N$, thus requiring an energy proportional to N to be implemented. A perhaps more intuitive way of solving the same problem would be to put γ in front of the Laplacian, leading to a Grover's time of $\frac{\pi}{2}\sqrt{N}$ with $\gamma = \frac{1}{N}$ and the expected quadratic speedup with respect to classical search algorithms which take a time proportional to $\frac{N}{2}$ on average. At any rate, whether the quantum search time will increase or decrease with the size of the database in a real scenario will depend upon the specific implementation (i.e., if the couplings are rescaled or not), but from a resource-theoretic viewpoint everything is consistent with the involved energy scales.

Looking beyond complete graphs, quantum search has been generalized to many other graph families and to more elaborate approaches [270, 271, 272, 273, 310, 311, 312, 313]. Independently, the quadratic speedup of Grover's algorithm has been proven to be optimal [277, 278]: no quantum search algorithm on an unstructured database of N entries can achieve its task in a time scaling slower than $\sqrt{N}$ with N. The difference between the Laplacian and the adjacency matrix in quantum search with CTQWs on non-regular graphs have been studied in [274]. At the same time, experimental setups are put forward to empirically investigate quantum search on graphs in view of possible future applications [275, 314, 315].

5.5 A digression on quantum spin chains, the Heisenberg model and the Hubbard model

Continuous-time quantum walks naturally arise in the study of the transport of excitations on ordered systems, such as spin chains. Typically, the starting point is the Bloch theorem, stating that in the presence of a lattice-shaped potential field with a *discrete translation symmetry* represented by the unitary operator $\hat{T}_a$, a being the lattice spacing, the single particle eigenfunctions of the Schrödinger equation are of the form:

$$\psi_k(x) = e^{ikx} u_k(x) \tag{5.43}$$

where $u_k(x)$ is periodic on the lattice:

$$\hat{T}_a u_k(x) = u_k(x+a) = u_k(x) \tag{5.44}$$

and $k \in [-\pi/a, \pi/a]$ is called the *Bloch vector* or *crystal momentum*. From Bloch's eigenfunctions, by Fourier transform, one can build the *Wannier's functions*:

$$w_R(x) = \int \mathrm{d}k e^{-ikR} u_k(x) \tag{5.45}$$

where R is a point on the lattice. These functions are orthogonal for different choices of R and they are localized around R, indeed they are just functions of $x - R$. They form therefore a localized orthonormal basis for the particle in the lattice potential.

Once a basis of localized wavefunctions is in place, the machinery of the so-called *second quantization* can be started to promote the theory for a single electron on a lattice of nuclei into a full interacting, multi-particle theory. Without delving into the details, the core idea is to associate to each Wannier function, labelled by the lattice vector R, a pair of creation and annihilation operators $\hat{c}^\dagger_R, \hat{c}_R$ whose role is to act on the vacuum state of the associated Fock space to create or destroy a particle localized near R. If we are dealing with electrons, they will also be labelled by a spin variable $\sigma = \uparrow, \downarrow$, so that to each particle we have an associated Hilbert space isomorphic to $\mathbb{C}^2$. Moreover, being fermions, their creation and annihilation operators *anti-commute*:

$$\{\hat{c}_{\sigma,R}, \hat{c}^\dagger_{\sigma',R'}\} = \delta_{\sigma\sigma'}\delta_{RR'} \quad , \quad \{\hat{c}_{\sigma,R}, \hat{c}_{\sigma',R'}\} = \{\hat{c}^\dagger_{\sigma,R}, \hat{c}^\dagger_{\sigma',R'}\} = 0 \tag{5.46}$$

which, in particular, implies $\left(\hat{c}^\dagger_{\sigma,R}\right)^2 = 0$, enforcing the Pauli exclusion principle. As per usual, the anticommutator is defined by $\{\hat{A}, \hat{B}\} = \hat{A}\hat{B} + \hat{B}\hat{A}$. The Hamiltonian is then rewritten in terms of matrix elements of the many-body Schrödinger operator between Wannier states, multiplied by the appropriate combination of fermionic creation and annihilation operators. If we start from a standard Hamiltonian for N interacting electrons in an ordered solid[3]:

$$\hat{\mathbf{H}}_{el} = \sum_{j=1}^{N} -\frac{\hbar^2}{2m}\nabla_j^2 + \sum_{j\neq k}^{N} V_C(\vec{x}_j - \vec{x}_k) + \sum_{j=1}^{N} W(\vec{x}_j) \tag{5.47}$$

[3]Here the fermionic nature of the particles is hidden in the assumption that this operator acts on the fully antisymmetrized subspace of the N-particles Hilbert space.

where V_C is an interaction term (e.g. a Coulomb potential) and $W(\vec{x}) = W(\vec{x} + n\vec{R})$ is the periodic lattice potential, with lattice vector $\vec{R}$ and $n \in \mathbb{N}$, we would arrive at a second-quantized many-body Hamiltonian of the form:

$$\begin{aligned}\hat{\mathbf{H}}_{\text{MB}} &= t \sum_{\sigma=\uparrow,\downarrow} \sum_{j} \left(\hat{c}^{\dagger}_{\sigma,j+1} \hat{c}_{\sigma,j} + \hat{c}^{\dagger}_{\sigma,j} \hat{c}_{\sigma,j+1} \right) + \\ &+ \sum_{\sigma=\uparrow,\downarrow} \sum_{j,k} U_{jk} \hat{c}^{\dagger}_{\sigma,j} \hat{c}^{\dagger}_{\sigma',k} \hat{c}_{\sigma,j} \hat{c}_{\sigma',k}\end{aligned} \tag{5.48}$$

where t governs the strength of the kinetic term and U_{jk} are the matrix elements we hinted at before. The periodic potential W only contributes in setting the lattice site, now labelled by j and k, by tunining the exact value of t, and finally by a term proportional to the total number of particles, $\sum_{\sigma=\uparrow,\downarrow} \sum_j \hat{c}^{\dagger}_{\sigma,j} \hat{c}_{\sigma,j}$, having the role of a chemical potential. Since the many-body Hamiltonian preserves the total number of particles and we will consider independently each sector with a given number of electrons, we suppressed this last, irrelevant contribution. Notice that now we are summing over *lattice sites* or, equivalently, Wannier orbitals, and *not* over particles anymore, since in the second quantization the number of particles can be varied. The first two terms in $\hat{\mathbf{H}}_{\text{MB}}$ are *one-body terms*, since they destroy and recreate one particle at a time, while the interaction potential V_C resulted in the third, two-body term. We will proceed by considering some relevant limit cases of this very general expression.

Let us first examine the case where the interaction term can be neglected, $U_{jk} = 0$, and let us assume that the overlap between nearby Wannier functions is so negligible, and the lattice potential so localized, that we can also suppose $W_{jk} = 0$ for $j \neq k$. We will end up with an Hamiltonian for noninteracting particles of the form:

$$\hat{\mathbf{H}}_{free} = t \sum_{\sigma=\uparrow,\downarrow} \sum_{j} (\hat{c}^{\dagger}_{\sigma,j+1} \hat{c}_{\sigma,j} + \hat{c}^{\dagger}_{\sigma,j} \hat{c}_{\sigma,j+1}) \tag{5.49}$$

This kind of Hamiltonian can be fully understood in the single particle subspace, since the many particle states all factorize and they are never mixed by the evolution. We conclude that this limit corresponds to a standard quantum walk on an infinite path, with uniform nearest-neighbours coupling t:

$$\hat{\mathrm{H}}_{QW} = t \sum_{j} (|j\rangle\langle j+1| + |j+1\rangle\langle j|) \tag{5.50}$$

where the spin variable disappeared because it is inconsequential for a single particle.

If instead we keep $U_{jj} \neq 0$, corresponding to a repulsion when the particles are on the same site, we arrive at the well-known *Hubbard model* [316]:

$$\hat{\mathbf{H}}_{\text{Hubbard}} := -t \sum_{\sigma=\uparrow,\downarrow} \sum_{j} \left(\hat{a}^{\dagger}_{\sigma,j+1} \hat{a}_{\sigma,j} + \hat{a}^{\dagger}_{\sigma,j} \hat{a}_{\sigma,j+1} \right) + U \sum_{j} \hat{a}^{\dagger}_{\uparrow,j} \hat{a}_{\uparrow,j} \hat{a}^{\dagger}_{\downarrow,j} \hat{a}_{\downarrow,j} \tag{5.51}$$

where the minus sign in front of t is just a convention.

Before examining some aspecys of this model, it is worth mentioning that a bosonic version of the Hubbard Hamiltonian, going under the name of *Bose-Hubbard model*, is

often used in the theory of superconductors, where Cooper pairs behave effectively as bosons while fulfilling the same Schrödinger equation of electrons as far as their spatial degrees of freedom and mutual repulsion are concerned.

The fermionic Hubbard model plays, in many body theory, a role analogous to the Ising model in statistical physics: although it provides a very crude representation of the complexity of real materials, it embodies the main physical ingredients which drive several important phase transitions. Both the Mott-type metal-insulator transition induced by electron interactions and the paramagnetic-antiferromagnetic transition are indeed described by such a simple model. Unfortunately, no exact and fully general solution of this model is known at present in more than one dimension, and we shall thus focus on limiting cases that will be of interest in our quantum walks oriented perspective. The only relevant coupling constant in the model is the ratio U/t, where the value of t just fixes the units of energy. We will restrict our analysis to the half filled case, i.e. when there is exactly one electron per lattice site. This is a common circumstance, corresponding to the presence of a single valence electron per atom, as in the "ideal", although rather unphysical, case of alkali metals. Furthermore, we will have in mind a simple cubic lattice and the lattice spacing will be denoted by a.

We already studied the case when $U = 0$. When $U/t \ll 1$, the perturbative approach around the free solution is the most convenient and the aforementioned phase transitions can be understood through mean field theory. Of much greater interest for our purposes is the strongly coupled regime, where $U/t \gg 1$. For $t = 0$ at half-filling, the ground state is 2^N degenerate and the corresponding eigenstates can be chosen to be deterministic states with one electron per site and all possible combinations of spins. Since this is equivalent to a string of qubits, we will refer to these states as the *computational basis*. As soon as two electrons with different spin occupy the same site, the energy cost is U, therefore there is a gap and the ground state at half-filling behaves as an insulator. This huge degeneracy is however lifted as soon as t is small but finite. The unique ground state in the limit $t \to 0$ is defined by a suitable linear combination of all computational basis states. Using second order degenerate perturbation theory with respect to the perturbing parameter t, then, it is possible to show that the ground state of the strongly coupled Hubbard model with $t \neq 0$ is equivalent to the ground state of the following Hamiltonian acting on the N-spins systems [316, 317]:

$$\hat{\mathbf{H}}_{\text{Heis.}} = J \sum_{\langle \vec{R}, \vec{R}' \rangle} \left[\hat{\mathbf{S}}_{\vec{R}} \cdot \hat{\mathbf{S}}_{\vec{R}'} - \frac{1}{4} \right] \tag{5.52}$$

where $J = \frac{4t^2}{U}$, the sum is extended over all couples $\langle \vec{R}, \vec{R}' \rangle$ of neighbouring sites on the lattice and $\hat{\mathbf{S}}_{\vec{R}} = (\hat{\mathrm{S}}^x_{\vec{R}}, \hat{\mathrm{S}}^y_{\vec{R}}, \hat{\mathrm{S}}^z_{\vec{R}})$ is the (vector) spin operator for the spin-$\frac{1}{2}$ variable residing at the site with lattice vector $\vec{R}$. The Hamiltonian $\hat{\mathbf{H}}_{\text{Heis.}}$ is known as the Heisenberg Hamiltonian and the corresponding model is the *XXX Heisenberg model* [318]. The nomenclature XXX signifies that the couplings between neighbouring spin variables are homogeneous in every direction, but other possibilities can be considered, depending on the crystal structure of the material under examination. If we focus just on 1-dimensional lattices, we can distinguish several different models:

- **XXX Heisenberg Model**, the one at which we arrived by considering the simplest, spin-independent coupling between nearby electrons, which can be rewritten more

explicitly as:

$$\hat{\mathbf{H}}_{XXX} := J\sum_{n=1}^{N}\hat{\mathbf{S}}_n\cdot\hat{\mathbf{S}}_{n+1} = J\sum_{n=1}^{N}\left[\frac{1}{2}\left(\hat{\mathrm{S}}_n^-\hat{\mathrm{S}}_{n+1}^+ + \hat{\mathbf{S}}_n^+\hat{\mathrm{S}}_{n+1}^-\right) + \hat{\mathbf{S}}_n^z\hat{\mathrm{S}}_{n+1}^z\right] \quad (5.53)$$

with $\hat{\mathrm{S}}_n^{\pm} = \hat{\mathrm{S}}_n^x \pm i\hat{\mathrm{S}}_n^y$ being the raising and lowering operators for spin n. Notice that we are now on a finite lattice with N sites and periodic boundary conditions, such that $N+1 \sim 1$. This model is notoriously solved in an exact way by the *Bethe ansatz* [319, 320, 321] for any N and in all subspaces with a given number of spin $\uparrow$ vs. $\downarrow$, although *practically* computing the eigenstates can still be a challenging numerical task.

- **XXZ Heisenberg Model**, having:

$$\hat{\mathbf{H}}_{XXZ}(\Delta) := J\sum_{n=1}^{N}\left[\frac{1}{2}\left(\hat{\mathrm{S}}_n^-\hat{\mathrm{S}}_{n+1}^+ + \hat{\mathrm{S}}_n^+\hat{\mathrm{S}}_{n+1}^-\right) + \Delta\hat{\mathrm{S}}_n^z\hat{\mathrm{S}}_{n+1}^z\right] \quad (5.54)$$

with a parameter Δ quantifying the coupling bias in the z direction. This model is also solved by more elaborate variations of the Bethe ansatz [322].

- **(Transverse-field) Quantum Ising Model**, which is the quantum analogue of the Ising model of classical statistical mechanics, where spins are treated as binary classical variables. Its Hamiltonian is:

$$\hat{\mathbf{H}}_{\text{Ising}}(g) := J\sum_{n=1}^{N}\hat{\mathrm{S}}_n^z\hat{\mathrm{S}}_{n+1}^z + g\sum_{n=1}^{N}\hat{\mathrm{S}}_n^x \quad (5.55)$$

The coupling is only between the z components of adjacent spins and a transverse homogeneous field in the x direction has been added, with control parameter g. Variants where g is a site-dependent random variable are also often studied to understand the effects of disorder in many-body quantum systems. The model can be solved through a highly-nonlocal mapping to fermionic variables, the *Jordan-Wigner transformations*, which transforms $\hat{\mathrm{H}}_{\text{Ising}}$ into a quadratic Hamiltonian for N fermionic modes that can in turn be diagonalized to solve the initial quantum Ising model [323].

The study of all these systems belong to the large topic of ***quantum spin chains*** [316], whose applications range from theoretical condensed matter and topological materials [324] to models for *quantum information transport* [279, 281, 325, 326, 327] and the study of quantum chaos, to name a few. To rewind our exposition, we started from the very general theory of non-relativistic electrons in an ordered solid and, with the main assumptions of half-filling and strong on-site repulsion, we arrived at a model in which each electron is frozen at one site and they are now the spin orientations, considered as quantum degrees of freedom, those who can hop from one site to the other. In these models, the imbalance between the number of spins $\uparrow$ and the number of spins $\downarrow$ is preserved by the Hamiltonians, therefore one can treat flipped spins as quasi-particles, called *magnons*, whose spin is 1, and *not* $\frac{1}{2}$, since creating a magnon with spin $\uparrow$ from a ground state with all spins $\downarrow$ changes the total spin by $+1$.

5.5.1 The Krawtchouk chain and minimal modulation of weights

Consider the following many-body Hamiltonian on a 1-dimensional lattice with $N = n+1$ sites and *inhomogeneous* nearest-neighbour couplings:

$$\begin{aligned} \hat{H}_K &= \sum_{j=1}^{n} J_K(j) \left(\hat{\mathrm{S}}_j^x \hat{\mathrm{S}}_{j+1}^x + \hat{\mathrm{S}}_j^y \hat{\mathrm{S}}_{j+1}^y \right) \\ J_K(j) &= \frac{J}{4} \sqrt{j(N-j)} \end{aligned} \tag{5.56}$$

acting on a quantum spin chain, where J is a positive real number and $\hat{\mathrm{S}}_j^x, \hat{\mathrm{S}}_j^z, \hat{\mathrm{S}}_j^z$ are the angular momentum operator acting on the spin-$\frac{1}{2}$ degree of freedom at site j. Since this Hamiltonian preserves the number of quasi-particles, meaning that it commutes with the total spin operator $\sum_{j=1}^{N} \hat{\mathbf{S}}_j^2$, we can look at the subspace corresponding to all spin oriented downwards in the z direction except one, where states can be labelled by the position of the spin $\uparrow$ and a natural (weighted) quantum walk on a finite path graph emerges. It turns out that this particular choice of weights achieves perfect state transport between the two ends of the chain, in the sense that:

$$\langle N | e^{-i\hat{H}_K t} | 1 \rangle = \left[-i \sin\left(\frac{Jt}{2} \right) \right]^{N-1} \tag{5.57}$$

so that the transport probability between the antipodes is 1 at $t = \frac{\pi}{J}$. The intuition behind this ideal property comes from recognizing the fact that $\hat{\mathrm{H}}_k$ acts on the invariant subspace generated by 1-particle localized states as the angular momentum operator $\hat{\mathrm{L}}_x$ for a spin-$\frac{n}{2}$ in the $\hat{\mathrm{L}}_z$ eigenbasis. Denoting the 1-particle state with the '1' at position j, $|0...0_{j-1}1_j0_{j+1}...0\rangle$ as $|\{j\}\rangle$, and the spin state $|m\rangle\rangle$ with $\hat{\mathrm{L}}_z = m|m\rangle\rangle$, the identification is:

$$|\{j\}\rangle \longleftrightarrow |m = j - \frac{n}{2}\rangle\rangle$$

Moreover, the spectrum of $\hat{\mathrm{H}}_K$ must then be equal to the spectrum of the spin operator, therefore it will be linear and equispaced:

$$\lambda_k(\hat{\mathrm{H}}_K) = J\left(k - \frac{n}{2}\right) \quad , \qquad k \in \{0, ..., n\} \tag{5.58}$$

In other words, the particular semicircular profile of couplings $J_K(j)$ makes the spectrum linear and equally spaced, with spacing of J: this implies that, whatever the initial state, the dynamics will be $\frac{2\pi}{J}$-periodic. Here we can see at play a key point concerning quantum walks and quantum transport with unitary evolutions: oftentimes, complex or random topologies give rise to incommensurate spectra, which in turn entail a very intricate and never-repeating long time evolution for almost all initial states. One way to approach the task of quantum transport is then to adjust all the free parameters (in this case, the non-uniform, real weights) in order to concoct a combination of eigenvalues and eigenvectors supporting the initial state such that the evolution will end up in the target state. Going back to the Krawtchouk chain, perfect transport can be directly understood by considering the symmetry of the Hamiltonian with respect to reflections about the central link/vertex and the aforementioned periodicity in time: at half the period, the evolution should be at a perfectly symmetrical point with respect to the starting

condition, so that $|\{1\}\rangle \to |\{N\}\rangle$, and actually $|\{j\}\rangle \to |\{N-j+1\}\rangle$ for every $j \leq \lfloor N/2 \rfloor$.

As for the eigenstates, the Krawtchouk chain in the single-particle subspace is diagonalized by the following eigenvectors:

$$|\lambda_k\rangle = \sum_{j=0}^{n} \mathfrak{P}_{k,j}^{(n)} |\{j+1\}\rangle \,, \tag{5.59}$$

$$\mathfrak{P}_{k,j}^{(n)} := \sqrt{\frac{\binom{n}{j}}{\binom{n}{k} 2^n}} \mathfrak{K}_k^{(n)}(j) \,, \tag{5.60}$$

$$\mathfrak{K}_k^{(n)}(j) := \sum_{r=0}^{k} (-1)^r \binom{j}{r} \binom{n-j}{k-r} \tag{5.61}$$

The functions $\mathfrak{K}_k^{(n)}(x)$ are polynomial of order n in their variable x and they are known in the mathematical literature as Krawtchouk polynomial.

Going beyond the single-excitation subspace, the Krawtchouk chain has many other interesting applications. Starting from the state $\otimes_{j=1}^{N} |+\rangle$, where $|+\rangle = \frac{|0\rangle+|1\rangle}{\sqrt{2}}$ and applying the evolution generated by $\hat{\mathrm{H}}_K$ for a time $t^* = \frac{\pi}{J}$ results in the so-called *graph state* of the complete graph of N vertices, which can be converted into the N-qubits GHZ-state $|\mathrm{GHZ}\rangle_N = \frac{|0\rangle^{\otimes N}+|1\rangle^{\otimes N}}{\sqrt{2}}$ by local spin rotations. For a detailed recount of this subject and the applications of quantum spin chains-type interactions to efficiently implement few-qubits gates we refer to [328, 329].

CHAPTER 6

Chiral quantum walks

As we have seen in Eq.(5.32) and Eq.(5.33), Hamiltonians that are real in the localized basis generate evolutions that are constrained by symmetries, often in an undesirable way for quantum transport and other tasks to be tackled with quantum walks. On the other hand, at a variance with classical random walks, the only condition that we have to impose on an Hamiltonian to induce a unitary quantum evolution is Hermitianity. We are therefore naturally led to ask ourselves: given a graph $\mathcal{G}$, what is the most general (Hermitian) Hamiltonian matrix generating a dynamics on the vertices of $\mathcal{G}$ that reflects its topology?

Continuous-time quantum walks generated by complex Hamiltonians have been already introduced in [330, 331, 332] under the name of *chiral quantum walks* and they indeed break the symmetries entailed by real Hamiltonians, at least on a large variety of graphs, allowing for directional biases. However, without further justification, the introduction of chiral quantum walks seems to be a departure from the original spirit of quantum walks. Also, no clear and general connection with the classical RW is obvious from their original definition, and no interpretation of the new degrees of freedom entailed by Hermitian Hamiltonians for chiral CTQW has been discussed, although a partial common ground has been found through the definition of Quantum Stochastic Walks [333] and a connection between classical and quantum random walk was found *for the discrete-time case* [334]. Nonetheless, such a correspondence is a key requisite to compare the performance of chiral quantum walks to classical ones and to establish when they do provide a speedup or a quantum advantage in some tasks. In [335] we provided such a correspondence; specifically, we identified five conditions that any Hamiltonian matrix must fulfill to generate a valid quantum walk on a graph $\mathcal{G}$ and we showed how the set of Hamiltonians solving the corresponding constraints all correspond to the same Laplacian through a general equation. In what follows, we will retrace the same line to illustrate the main arguments.

6.1 Chiral quantum walks as the most general type of continuous-time quantum walks

As a general guideline, an Hermitian operator $\hat{\mathbf{H}}$ acting on $\mathcal{H} \simeq \mathbb{C}^N$ is the Hamiltonian of a CTQW on a graph $\mathcal{G}$ of order N if and only if it respects the topology of the graph, that is to say if:

$$\forall j \neq k \in \{1, ..., N\} : \quad [\mathrm{H}]_{kj} = \langle k|\hat{\mathbf{H}}|j\rangle \neq 0 \qquad \Longleftrightarrow \qquad j \frown k \tag{6.1}$$

where we recall that $j \frown k$ means that vertices j and k are connected by an edge, and the matrix H describes $\hat{\mathbf{H}}$ on the localized basis. It is therefore apparent that the constraints imposed by the structure of the graph are quite loose. If the initial state is localized$\hat{\boldsymbol{\rho}}_0 = |j\rangle\langle j|$, it will stay pure under the unitary evolution induced by $\hat{\mathbf{H}}$:

$$\hat{\boldsymbol{\rho}}(t) \;=\; e^{-i\hat{\mathbf{H}}t}|j\rangle\langle j|e^{i\hat{\mathbf{H}}t} \;=\; |\psi_j(t)\rangle\langle\psi_j(t)| \tag{6.2}$$

where $|\psi_j(t)\rangle = \sum_{k=1}^{n} \alpha_{kj}(t)|k\rangle$ and

$$\alpha_{kj}(t) \;=\; \langle k|e^{-i\hat{\mathbf{H}}t}|j\rangle \;=\; \left[e^{-i\mathrm{H}t}\right]_{kj} \tag{6.3}$$

As we have seen previously, the only classical counterpart to this dynamics is generated by the Laplacian according to Eq.(5.29). Notice that time-homogeneity and Markovianity imply that the classical transition probability matrix $\mathrm{P}(t)$ that transforms the initial probability vector at time 0 to the evolved one at time t satisfies a group structure:

$$\begin{aligned} \mathrm{P}(t) \;&:=\; e^{-t\mathrm{L}} \\ \mathrm{P}(t_2)\mathrm{P}(t_1) \;&=\; \mathrm{P}(t_1+t_2) \quad , \quad \forall t_1, t_2 \geq 0 \end{aligned} \tag{6.4}$$

The unitary evolution of the CTQW, on the other hand, induces an evolution of the probabilities at each vertex of the graph according to Born's rule: $\mathrm{P}_{j\to k}(t) \;=\; |\alpha_{kj}(t)|^2$ exactly as in the case of real Hamiltonians Eq.(5.31), and it should ***not*** be interpreted, a priori, as a standard transition matrix in the sense of Eq.(6.4). Indeed, while it is true that if the initial state $\hat{\boldsymbol{\rho}}_0$ is diagonal, $\hat{\boldsymbol{\rho}}_0 = \sum_j \rho_j^0 |j\rangle\langle j|$, then $\vec{\mathrm{p}}$ evolves according to $\mathrm{p}_k(t) = \sum_j \mathrm{P}_{j\to k}(t)\rho_j^0$, this is no longer true at intermediate times, nor if the initial state is coherent in the localized basis. In fact, we shall now show that *the semigroup structure of Eq.(6.4) can never be fulfilled by the quantum probabilities computed according to the Born rule*. Indeed, we are looking for a real $n \times n$ matrix L fulfilling the equality:

$$\left[e^{-t\mathrm{L}}\right]_{kj} \;=\; \left|\left[e^{-i\mathrm{H}t}\right]_{kj}\right|^2 \quad \forall t \geq 0. \tag{6.5}$$

Expanding both sides to first order in t, we deduce:

$$\begin{aligned} \left[e^{-t\mathrm{L}}\right]_{kj} \;&= \delta_{kj} \;-\; t\mathrm{L}_{kj} \;+\; O(t^2) \\ \left|\left[e^{-i\mathrm{H}t}\right]_{kj}\right|^2 \;&=\; \left[\delta_{kj} - i\mathrm{H}_{kj}t \;+\; O(t^2)\right] \times \left[\delta_{kj} + i\mathrm{H}^*_{kj}t \;+\; O(t^2)\right] \\ -\,t\,\mathrm{L}_{kj} \;&=\; -\,it\,(\mathrm{H}_{jj} - \mathrm{H}^*_{jj})\delta_{jk} \end{aligned}$$

Since H is Hermitian, $\mathrm{H}_{jj} - \mathrm{H}^*_{jj} = 0$ and the equation above can be satisfied if and only if $\mathrm{L} = \not\vdash$ as a matrix. Thus we conclude that, already at first order in time, the dynamics of any CTQW does not resemble that of the classical random walk on the same graph. In particular, the above computation shows that the quantum transition probabilities are always stationary around $t = 0$.

6.1.1 Deriving a quantum-classical correspondence

Going back to our original question, we are seeking a more general equation relating any Hermitian Hamiltonian that generates a CTQW on $\mathcal{G}$ to the Laplacian. Imposing $\mathrm{H} = \pm\mathrm{L}$

forces H to be real, which is not a natural request for an Hamiltonian: this points at the fact that a classical-to-quantum correspondence should be one-to-many, therefore some further structure is required to specify *all* the *Hermitian* Hamiltonians associated with the given classical generator L. Secondly, it is a rather arbitrary and artificial way to define the quantum-classical correspondence, with no physical motivation.

We shall address these issues and find a generalized quantum-classical correspondence between CTQWs and CTRWs by stating reasonable requests to be fulfilled by the equation we would like to derive (T denotes topological requests, A is for algebraic and P for probabilistic):

T0 By definition of continuous-time quantum/classical random walks, both H and L should preserve the topology of the underlying physical system, therefore the equation must enforce that $\mathrm{L}_{jk} \neq 0 \iff \mathrm{H}_{jk} \neq 0$ $(j \neq k)$.

A1 Given H, the equation must admit a unique solution for L with $\sum_j \mathrm{L}_{kj} = 0 \; \forall k$, so that it is a valid Laplacian matrix of a (possibly weighted) graph;

A2 The correspondence should reproduce the simple association $\mathrm{L} = \mathrm{H}$ whenever H is already a Laplacian matrix of an unweighted graph. This is necessary to be consistent with the existing literature on non-chiral CTQWs and it is also a consequence of **T0**.

P3 In compliance with the probabilistic interpretations of quantum mechanics and classical stochastic processes, respectively, the off-diagonal terms of H should be interpreted as transition amplitude rates, while (the negative of) those of L should be the corresponding transition probability rates;

P4 Given H, the diagonals term of the solution L of the equation should maintain the meaning of total probabilities of leaving the corresponding sites.

In general, for $j \neq k$, $\mathrm{H}_{jk} \in \mathbb{C}$ and $\mathrm{L}_{jk} \in \mathbb{R}$. Then Condition **T0** suggests:

$$\mathrm{L}_{jk} \;=\; -|\mathrm{H}_{jk}|^2 \,, \tag{6.6}$$

which also satisfies **P3** for the off-diagonal terms. Conditions **P4** and **A1** for the diagonal terms may be jointly enforced by:

$$\mathrm{L}_{jj} = \sum_{s \neq j}^{n} |\mathrm{H}_{js}|^2 = \langle j|\hat{\mathbf{H}}^2|j\rangle - \langle j|\hat{\mathbf{H}}|j\rangle^2 \,. \tag{6.7}$$

Condition **A2** is also satisfied since one can immediately check that $[\mathrm{L}^2]_{jj}\delta_{jk} - (\mathrm{L}_{kj})^2 = \mathrm{L}_{kj}$ (to be read as a self-consistency equation for the matrix elements of L) whenever H is a Laplacian and the simple identification $\mathrm{L} = \mathrm{H}$ is recovered. Alternative definitions, e.g. $\mathrm{L}_{kj} = -|\mathrm{H}_{jk}|^n$ with $n \neq 2$, would satisfy **T0** and **A2**, and possibly **A1**, but they would unavoidably violate **P3** and **P4**. Indeed, the choice $n = 2$ is naturally suggested by the Born rule *at the level of transition rates*: the classical rate of transition should be the square modulus of the corresponding transition amplitude. In compact form the sought equation is:

$$[\mathrm{L}]_{kj} \;=\; [\mathrm{H}^2]_{jj}\delta_{jk} \;-\; \mathrm{H}_{jk}\mathrm{H}_{kj} \tag{6.8}$$

As stated by this expression, there are many CTQWs corresponding to the same CTRW: the moduli of the off-diagonal entries of H are fixed to the square-root of the moduli of

the corresponding off-diagonal elements of L whereas the phases are completely free. The diagonal elements of H, i.e. the on-site energies of the vertices, are also unconstrained: from a physical point of view, they do not possess a classical analogue, because the corresponding classical system is open and energy is not conserved. On the converse, by Eq.(6.8) the diagonal elements of L are fixed to be the quantum fluctuations of the energy of each site, which are also equal to the total probability of escaping each site, analogously to the connectivity for a Laplacian. We have thus found *all possible continuous-time quantum walks associated with an arbitrary classical random walk on a given graph, assuming the minimal and reasonable requests detailed above.*

6.1.2 Quantum-classical correspondence from intrinsic decoherence

Eq. (6.8) may be also derived by adding a decoherence term with respect to the energy eigenbasis to the Von Neumann evolution equation 1.1 for a chiral CTQW on a graph. To see this, let us consider a temporal coarse-graining, leading to decoherence in the energy eigenbasis, in the spirit of the intrinsic decoherence introduced by G. Milburn [336]. In this way, one prevents the cancellation of the linear term in t in the quantum mechanical evolution by deviating from unitary evolution and introducing decoherence. In particular, let us consider the following Liouville - Von Neumann equation:

$$\frac{\mathrm{d}\hat{\boldsymbol{\rho}}}{\mathrm{d}t} \;=\; -i\left[\hat{\mathrm{H}},\hat{\boldsymbol{\rho}}\right] \;-\frac{\gamma}{2}\left[\hat{\mathrm{H}},\left[\hat{\mathrm{H}},\hat{\boldsymbol{\rho}}\right]\right] \tag{6.9}$$

describing intrinsic decoherence according to [336]. To first order in t we find that the probability of finding the walker on site k at time t when starting on site j at time 0 with the modified quantum evolution Eq.(6.9) is, according to Born's rule:

$$\begin{aligned}\langle k|\hat{\boldsymbol{\rho}}(t)|k\rangle \;&=\; \langle k|j\rangle\langle j|k\rangle \;+\; t\,\frac{\mathrm{d}\langle k|\hat{\boldsymbol{\rho}}|k\rangle}{\mathrm{d}t}\bigg|_0 \;+\; O(t^2) \;=\\ &= \delta_{jk} - \frac{\gamma t}{2}\Big\{\langle k|\hat{\mathrm{H}}\big[\hat{\mathrm{H}},|j\rangle\langle j|\big]|k\rangle \;+\\ &\qquad -\langle k|\big[\hat{\mathrm{H}},|j\rangle\langle j|\big]\hat{\mathrm{H}}|k\rangle\Big\} \;+\; O(t^2) \;=\\ &= \delta_{jk} \;-\; \gamma t\left\{[\mathrm{H}^2]_{jj}\delta_{jk} - |\mathrm{H}_{jk}|^2\right\} \;+\; O(t^2)\end{aligned}$$

where we used $\hat{\boldsymbol{\rho}}_0 = |j\rangle\langle j|$ and the Hermiticity of the matrix H in the last step. Notice that the matrix L defined by the linear term:

$$[\mathrm{L}]_{kj} \;=\; [\mathrm{H}^2]_{jj}\delta_{jk} \;-\; \mathrm{H}_{jk}\mathrm{H}_{kj} \tag{6.10}$$

is a real, symmetric matrix satisfying:

$$\sum_{k=1}^{n}\mathrm{L}_{kj} \;=\; [\mathrm{H}^2]_{jj} \;-\; \sum_{k=1}^{n}\mathrm{H}_{jk}\mathrm{H}_{kj} \;=\; 0$$

hence it generates bi-stochastic transformations. This means that, to first order in t, the probabilities computed with the Born rule for any CTQW *with decoherence* are always compatible with some CTRW and the correspondence equation Eq.(6.8) can be seen, albeit just formally, as a classical limit at short times.

Notice also that, despite the fact that almost any quantum dynamics can be described by a quantum channel with a semi-group structure (at the level of density matrices), this is not generally true for generic classical stochastic processes. However, we just proved that, whenever the classical stochastic process *has* a semi-group structure, it can be simulated by a quantum system with decoherence in the energy basis. We can state the following:

Theorem 6.1.1

Any classical stochastic process that respects the semi-group structure (Eq.6.4) and has finitely many states can be sampled (for short times) by a quantum computer with decoherence in the energy basis.

thus adding physical intuition to the formal consistency implied by conditions **T0-P4**.

6.2 Chiral Hamiltonians and phase configurations

The possibility of choosing *complex* off-diagonal entries in the Hamiltonian H accounts for chirality [330, 337]: the restrictions imposed by the symmetries of Eq.(5.32) and Eq.(5.33) are, in general, no longer true for these Hamiltonians. Concerning classical RWs, instead, time reversal is not meaningful because $e^{-t\mathrm{L}}$ is guaranteed to be a stochastic matrix only if $t \geq 0$, and this is directly related to the irreversible dynamics of classical RWs. We deduce that, whenever H is real, the quantum-classical comparison is unambiguous under time reversal: there is just one possible choice of time direction for the classical walk, and both choices for the quantum walk are equivalent. In contrast, when H is complex the quantities $|\langle k|e^{-i\mathrm{H}t}|j\rangle|^2$ are *not* in general symmetric under $t \to -t$, and a possible ambiguity in the quantum-classical comparison arises. This is resolved when considering all possible Hamiltonians H that are compatible with a given L according to our rule Eq.(6.8). Indeed, if we choose freely the phases of the off-diagonal entries of H we can accommodate both time directions, while the diagonal entries can always be taken to be positive by shifting H by a multiple of the identity.

We will call a *chiral Hamiltonian* generic Hermitian matrix H compatible with the given graph topology, while the CTQW generated by H will be referred to as a *chiral quantum walk* on $\mathcal{G}$. As it is the case for CTQWs generated by real Hamiltonians, the unbiased case in which the *complex moduli* of all the off-diagonal elements of H are either 0 or 1 is the most pertinent for quantum walks. Therefore, a chiral Hamiltonian will have:

$$\text{If } j \frown k: \quad \mathrm{H}_{jk} = \mathrm{H}^*_{kj} = e^{i\phi_{jk}}, \quad \phi_{jk} \in [0, 2\pi) \quad \text{otherwise:} \quad \mathrm{H}_{jk} = 0 \tag{6.11}$$

so that to each *directed* edge (j, k) in $\mathcal{G}$ a complex phase $e^{i\phi_{jk}}$ is assigned, and reversing the orientation of the edge amounts to complex conjugation of the associated phase, in order to maintain the Hermitian constraint for H. A *chiral adjacency matrix* $\tilde{\mathrm{A}}$ on $\mathcal{G}$ is an $N \times N$ Hermitian matrix such that $\mathrm{A}_{jk} = 1 \implies \tilde{\mathrm{A}}_{jk} = e^{i\theta_{jk}}$ with $\theta_{jk} \in [0, 2\pi)$ and $\mathrm{A}_{jk} = 0 \implies \tilde{\mathrm{A}}_{jk} = 0$. A *chiral Laplacian* on $\mathcal{G}$ is an Hermitian matrix $\tilde{\mathrm{L}} = \mathrm{D} - \tilde{\mathrm{A}}$ where $\tilde{\mathrm{A}}$ is a chiral adjacency matrix. We will say that a chiral quantum walk is *of the adjacency type* (resp. *of the Laplacian type*) if it is generated by a chiral adjacency matrix (resp. a chiral Laplacian). An assignment of complex phases to all the edges of a graph $\mathcal{G}$ will be

referred to as a *phase configuration* on $\mathcal{G}$.

Before describing in detail the properties of these phase configurations, we note that the implementation of these systems has been studied in multiple contexts in the recent literature, e.g. under the name of *synthetic gauge fields on lattices* [338, 339, 340, 341, 342], both in cold atoms and in all-optical platforms, moreover for planar graphs (as all the ones considered in our study) they can also be directly realized, at least in principle, as tight-binding models for charged particles hopping between the sites of the graph in an underlying magnetic field, as we shall motivate at the end of the present chapter. Perhaps more in line with typical experimental realizations of non-chiral CTQWs [343, 344], the possibility of reproducing also *complex* couplings between photonic waveguides has been explored [345], hopefully opening the way to future experimental tests of the ideas presented here.

6.3 Quasi-gauge transformations and phase configurations

Distinct configurations of phases on the edges of a graph $\mathcal{G}$, corresponding to different chiral Hamiltonians, can lead to the same transport probabilities between every pair of sites. We can therefore factor the space of all possible phase choices, and therefore the set of all Hamiltonians with the same underlying discrete structure and the same diagonal entries, into equivalence classes such that the Hamiltonians inside each class share the same site-to-site transition probabilities. It can be shown [331] that two chiral Hamiltonians H and H′ on the same graph $\mathcal{G}$ are equivalent in this sense if and only if they are related by a *quasi-gauge transformation*[1]:

$$\mathrm{H} \sim \mathrm{H}' \quad \Longleftrightarrow \quad \mathrm{H}' = \Lambda_{\vec{\alpha}} \mathrm{H} \Lambda_{\vec{\alpha}}^{\dagger} \tag{6.12}$$

where $\Lambda_{\vec{\alpha}}$ is a diagonal unitary matrix with $(\Lambda_{\vec{\alpha}})_{jj} = e^{i\alpha_j}$ and $\vec{\alpha} \in [0, 2\pi)^N$. It is a simple task to show that

$$P_{j\to k}(t) = |\langle k|e^{-i\mathrm{H}t}|j\rangle|^2 = {P'}_{j\to k}(t) = |\langle k|e^{-i\mathrm{H}'t}|j\rangle|^2 \tag{6.13}$$

for $j, k = 1, ..., N$. Moreover, if we take generic pure states as the initial and final states, a quasi-gauge transformation will simply send a transition probability generated by H into *another* transition probability generated by H′, obtained just by application of the quasi-gauge transformation on the initial and final state. We have therefore the following result:

Theorem 6.3.1

Let H and H′ be two chiral Hamiltonians on the same graph $\mathcal{G}$ that are related via a quasi-gauge transformation. Then they will generate the *same* transition probabilities between any two localized states at all times. Moreover, the set of all transition probabilities generated by H for a time t, given *any pure initial and final state*, is a permutation of the same set generated by H′ for the same time t.

In this way, the phases of at most $N - 1$ edges can be cancelled; indeed, if we multiply $\Lambda_{\vec{\alpha}}$ by an additional phase factor $e^{i\theta}$, the transformation in Eq.(6.12) applied to H

[1] Since these transformations do not affect the diagonal elements, H and H′ must already coincide on the diagonal.

will result in the same matrix H′, therefore only $N-1$ among the parameters of $\Lambda_{\vec{\alpha}}$ can matter. A tree graph with N vertices has exactly $N-1$ edges, and it is indeed the case that all chiral Hamiltonians on it belong to the same equivalence class of the adjacency matrix (disregarding the diagonal elements). In particular, on tree graphs the properties in Eq.(5.32) and Eq.(5.33) hold also for chiral quantum walks. However, as soon as the number of edges is larger than $N-1$, there will be at least one loop in the graph, and there will be a phase that cannot be cancelled. This implies different values of the transition probabilities, but *not necessarily* the breaking of the two symmetries. Indeed, the following result holds true:

Theorem 6.3.2

Let $\mathcal{G}$ be a bipartite graph. Then the time-reversal symmetry is preserved by any adjacency-type chiral quantum walk on $\mathcal{G}$. The same holds true for the spatial symmetry, if present in the non-chiral case.

Proof. Let us prove that the time-reversal symmetry is preserved, since spatial symmetry immediately follows if the graph exhibits it. Let us name V_1 and V_2 the two partitions of the set of vertices of $\mathcal{G}$. If we apply a quasi-gauge transformations to all the vertices in V_1 with a phase of π, so that $|j\rangle \mapsto -|j\rangle$ for any $j \in V_1$, then, given that each edge in $\mathcal{G}$ is connected to exactly one vertex in V_1, all the off-diagonal elements of H reverse their sign, so $\mathrm{H} \mapsto -\mathrm{H}$ and time-reversal is realised by a quasi-gauge transformation, thus preserving the transition probabilities. □

It turns out that equivalence classes of chiral Hamiltonians can be characterized by the total phases along each loop of the graph [332], i.e. the product of the phase factors of all the edges involved in the loop, for a given orientation of it: two chiral Hamiltonians with the same diagonal entries are related by a quasi-gauge transformation if and only if all their loops total phases coincide. Loops phases are thus invariants for chiral Hamiltonians, and they will be their central degrees of freedom.

In general, given the graph $\mathcal{G} = (V, E)$ and denoting by $|E|$ its number of edges and by $|V|$ its number of vertices, the actual number of relevant phase parameters for transport will be $|E|-|N|+1$, since each edge can bear a phase and $N-1$ of them are arbitrary under quasi-gauge transformations. For planar graphs, the corresponding independent loops are easily identified, since they are related to the number of regions in which the plane is partitioned by the graph when it is embedded in it without self-intersections. Letting F be this number of *finite* regions[2], thanks to the Euler characteristic of planar graphs we have:

$$|V| - |E| + F = 1 \quad \Rightarrow \quad F = |E| - |V| + 1 \tag{6.14}$$

therefore F is indeed equal to the number of relevant phase parameters.

6.4 Chiral quantum walks on lattices as discretized gauge theories

To provide a physical intuition for the phase degrees of freedom, we remark that the idea of amending for a local change of phase in the wave-function by changing some parameters in the Hamiltonian reminds of local gauge invariance with gauge group $U(1)$, i.e.

[2] In the mathematical literature it is common to include also the outside, infinite region when counting faces of planar graphs. To avoid confusions, we specify that we count only finite regions.

of a coupling between a charged particle described by the wavefunction and a classical abelian gauge field. Indeed, we will now argue that the most general unweighted chiral CTQW on a regular lattice and in any dimension may be interpreted as the discretization of the non-relativistic Schrödinger equation for a scalar charged particle coupled to a classical electromagnetic field. Let us consider an infinite, regular d-dimensional lattice (not necessarily cubic). We require that all the edges have the same weight, reflecting the idea that, apart for the effect of potentials, the transition amplitudes between nearby points in an empty Euclidean space should just depend upon the absolute distance between them. We will refer to a chiral, unweighted QW on a regular lattice as a *homogeneous* chiral CTQW, and these are our natural candidates to be interpreted as spatial discretizations of quantum theories in Euclidean spaces.

Let us start by considering the simple scenario of an infinite 2D square lattice. Referring to some arbitrary vertex, we can label each point with a pair of integers $(n, m) \in \mathbb{Z}^2$ and the corresponding localized state will be $|n, m\rangle$. We will denote by $\Psi_{n,m}(t) = \langle n, m|\Psi(t)\rangle$ the amplitude of the walker at time t to be found at site (n, m), and by $\Psi(t)$ the vector of the amplitudes over all the sites of the lattice. It is also convenient to explicitly write the rate γ that governs the time evolution, so that the Schrödinger equation would be symbolically written as ($\hbar = 1$)

$$i\partial_t \vec{\Psi} \;=\; \gamma \mathrm{H} \cdot \vec{\Psi} \tag{6.15}$$

The most general Hamiltonian matrix H for a CTQW on this lattice will be an infinite, sparse matrix specified by the following entries [3]:

$$\begin{aligned}\frac{1}{\gamma}\langle n', m'|\mathrm{H}|n, m\rangle \;=\; & [4 + d(n, m)]\, \delta_{n',n}\delta_{m',m} + \\ & - \; e^{if_x(n'-1,m')}\delta_{n',n+1}\delta_{m',m} \;-\; e^{-if_x(n',m')}\delta_{n',n-1}\delta_{m',m} + \\ & - \; e^{if_y(n',m'-1)}\delta_{n',n}\delta_{m',m+1} \;-\; e^{-if_y(n',m')}\delta_{n',n}\delta_{m',m-1}\end{aligned} \tag{6.16}$$

where $\delta_{p,n}$ is the Kronecker delta and $f_x(n, m)$, $f_y(n, m)$ and $d(n, m)$ are real valued functions of the nodes coordinates. Now let a be the lattice spacing, which can be assumed to be the same in all directions without loss of generality. By exploring all possible scaling laws of the functions f_x, f_y and d with a, a slight variation of an argument by Feynman (see the last Chapter of [346]) shows that the only nontrivial continuous limit ($a \to 0$) of this model leads to an Hamiltonian operator $\hat{\mathrm{H}}_c(\vec{x})$ of the following form:

$$\hat{\mathrm{H}}_c(\vec{x})\Psi(\vec{x}) \;=\; -K\left(\nabla - i\vec{F}(\vec{x})\right)^2 \Psi(\vec{x}) + U(\vec{x})\Psi(\vec{x}) \tag{6.17}$$

where now:

$$\vec{x} \in \mathbb{R}^2\,, \quad U(\vec{x}) = \gamma d(\vec{x})\,, \quad K = \lim_{a\to 0} a^2\gamma \tag{6.18}$$

$$\vec{F}(\vec{x}) = \lim_{a\to 0} \frac{1}{a}\left(f_x(\vec{x}), f_y(\vec{x})\right) \tag{6.19}$$

and $d(\vec{x})$, $f_x(\vec{x})$, $f_y(\vec{x})$ are the continuum generalizations of $d(n, m)$, $f_x(n, m)$ and $f_y(n, m)$, respectively.

[3] Since the functions $f_x(n, m)$, $f_y(n, m)$ and $d(n, m)$ are completely unconstrained, this is indeed the most general Hamiltonian with nearest neighbor interactions on a square 2D lattice.

To prove this, let us relabel the lattice points as $(n, m) \mapsto (x_n, y_m)$ where $x_n = na$ and $y_m = ma$. By considering f_y and f_x to be independent functions, we can indeed take the same lattice spacing along x and along y, without loss of generality. Now we imagine to extend Ψ to a smooth complex-valued function on the whole $\mathbb{R}^2$ plane, that interpolates between the values of the amplitude at the lattice sites and do the same for the real valued functions $d(x, y)$, $f_x(x, y)$ and $f_y(x, y)$. With this notation, the action of the Hamiltonian on Ψ could be written as:

$$\begin{aligned}\frac{1}{\gamma}\left[\mathrm{H}\cdot\Psi\right](x,y) \;=\; &\left[4+d(x,y)\right]\Psi(x,y) + \\ &- \; e^{if_x(x-a,y)}\Psi(x-a,y) \;-\; e^{-if_x(x,y)}\Psi(x+a,y) + \\ &- \; e^{if_y(x,y-a)}\Psi(x,y-a) \;-\; e^{-if_y(x,y)}\Psi(x,y+a).\end{aligned} \tag{6.20}$$

First, let us focus on the terms with translations along the x direction, the second line of Eq.(6.20). Since we have to *define* a continuum limit, we can freely postulate the scaling of f_x with a. If we take f_x to be $O(1)$, by expanding the second line up to first order in a we find:

$$\begin{aligned}&- e^{if_x}e^{-ia\partial_x f_x}\left[\Psi - a\partial_x\Psi\right] - e^{if_x}\left[\Psi + a\partial_x\Psi\right] + O(a^2) \;= \\ &= \; -2\left(\cos f_x\right)\Psi + ae^{if_x}\left(\partial_x f_x\right)\Psi + 2ia\left(\sin f_x\right)\partial_x\Psi + O(a^2)\end{aligned} \tag{6.21}$$

where we wrote $f_x \equiv f_x(x, y)$ and $\Psi \equiv \Psi(x, y)$ for shortness. Taking the limit $a \to 0$ yields a contribution which is diagonal in the position, so it is just a correction to the scalar potential $d(x, y)$. Analogously, if we expanded the last line assuming f_y of $O(1)$ in a, we would have found a correction term to $d(x, y)$ of the form $-2\cos f_y$. Now suppose that f_x is $O(a)$, so that we can write $f_x(x, y) = aF(x, y)$. Expanding again the second line of Eq.(6.20), this time up to $O(a^2)$, we find:

$$\begin{aligned}&- \left(1 + iaF_x - ia^2\partial_x F_x - \frac{1}{2}a^2F_x^2\right)\left(\Psi - a\partial_x\Psi + \frac{1}{2}a^2\partial_x^2\Psi\right) + \\ &- \left(1 - iaF_x - \frac{1}{2}a^2F_x^2\right)\left(\Psi + a\partial_x\Psi + \frac{1}{2}a^2\partial_x^2\Psi\right) + O(a^3) \;= \\ &= \; -2\Psi - a^2\Big(\partial_x - iF_x\Big)^2\Psi \;+\; O(a^3)\end{aligned} \tag{6.22}$$

and $F_x \equiv F_x(x, y)$. Doing the same for the third line of Eq.(6.20), with $f_y = aF_y$, the net result is:

$$\left[\mathrm{H}\cdot\Psi\right](x,y) \;=\; -\gamma a^2\left(\nabla - i\vec{F}(x,y)\right)^2\Psi(x,y) \;+\; \gamma d(x,y)\Psi(x,y) \;+\; O(a^3) \tag{6.23}$$

where $\vec{F} = (F_x, F_y)$. If we naively take $a \to 0$ at this point, the result would again be trivial. However, unlike the previous case, here we can take $\gamma = K/a^2$, with $K \sim O(1)$ and constant, and also $\lim_{a\to 0}\gamma d(x, y) = U(x, y)$, where we are forced to assume $d(x, y) \sim O(a^2)$ to get a finite continuum limit with a potential field landscape. For these choices, the continuum limit is no longer trivial and we arrive at the desired result:

$$\lim_{a\to 0}\;\left[\mathrm{H}\cdot\Psi\right](x,y) \;=\; -K\left(\nabla - i\vec{F}(x,y)\right)^2\Psi(x,y) \;+\; U(x,y)\Psi(x,y) \tag{6.24}$$

We also remark that taking $f_x \sim O(1)$ and $f_y \sim O(a)$, or vice versa, would prevent γ to be $O(a^{-2})$, otherwise the $-2\gamma \cos f_x$ term would diverge as $a \to 0$. Therefore, a mixed choice of scaling laws for f_x and f_y yields a diagonal action of H on Ψ, hence a trivial result. The last option is to postulate $f_x \sim O(a^{2+\epsilon})$ for $\epsilon > 0$. The only option to find a nontrivial continuum limit is again for $\gamma = K/a^2$ and the result is the same as neglecting f_x altogether to begin with. We have thus proved that the only nontrivial continuum limit of a generic chiral CTQW on a square 2D lattice is given by Eq.(6.24). To conclude, let us highlight the fact that the scaling laws $f_x \sim O(a)$ and $f_y \sim O(a)$ are, in a sense, the most natural choice: these functions define the phases for the hopping amplitudes between neighbors on the lattice, and it is reasonable to require that these phases should go to 0 as the distance between neighboring points is reduced.

We have thus seen that the existence of all these limits is a prerequisite to find a nontrivial theory as $a \to 0$. We can now restore $\hbar$, write $U(x) = qV(x)$, $F(x) = qA(x)$ and $K = \frac{\hbar^2}{2m}$ in order to arrive at the standard nonrelativistic Schrödinger equation for a scalar particle with mass m and charge q in the presence of an electromagnetic field:

$$i\hbar \frac{\partial}{\partial t}\Psi(\vec{x}) = -\frac{\hbar^2}{2m}\left(\nabla - iq\vec{A}(\vec{x})\right)^2 \Psi(\vec{x}) + qV(\vec{x})\Psi(\vec{x}) \tag{6.25}$$

where $\vec{A}(\vec{x})$ is the vector potential and $V(\vec{x})$ is the scalar potential. The derivation can be readily generalized to cubic lattices and, even more generally, to regular lattices in any dimension by introducing the appropriate vector potential $\vec{A}(x)$ and with suitable discretizations of the Laplacian [258], showing that homogeneous chiral CTQWs, despite being the most general of their kind, are in fact always equivalent to discretizations of the Schrödinger equation for a scalar particle in the presence of an electromagnetic field, also suggesting a practical implementation for chiral CTQWs, especially with *synthetic* gauge fields [338]. Notice that the reasoning can also be inverted to deduce the form of the phases $f(n, m)$ from a given vector potential. The result is known as Peierls substitution [340, 342, 347, 348, 349], and in our case for a d-dimensional cubic lattice it reduces to:

$$f_j(\vec{x}) \;=\; q \int_\gamma \vec{A}(\vec{r}(t))dt \tag{6.26}$$

where $\gamma : t \in [0, 1] \to \mathbb{R}^d$ is a path from $\vec{x} \in \mathbb{Z}^d$ to $\vec{x} + a\vec{e}_j$ and $\vec{e}_j$ is the versor in the j-th direction. Notice that this is consistent with $F(\vec{x}) = qA(\vec{x}) = \lim_{a\to 0} \frac{1}{a} f(\vec{x})$ via the integral mean value theorem.

This construction also suggests that we can interpret *any* chiral CTQW on any graph $\mathcal{G}$ in this way. Indeed, any graph can be embedded in 3-dimensional space without intersections between the edges. By Peierl's substitution, given a phases configuration on $\mathcal{G}$, the sum of the phases along any loop in the graph can be interpreted as the total flux of a magnetic field through the face defined by that loop. The only hindrance to this interpretation is that any acceptable magnetic field should have zero divergence. In our discrete case, this requires that the total flux through any closed surface must be zero. But this is indeed guaranteed by the fact that any valid phases configuration will assign a certain phase ϕ to a directed link (j, k) and the opposite phase to the reversed link (k, j). If we consider some loops in $\mathcal{G}$ defining a closed volume in the 3D embedding of the graph, each edge of each loop will be shared by at least another loop and it will be traversed in opposite directions, so that its total contribution to the outgoing flux of

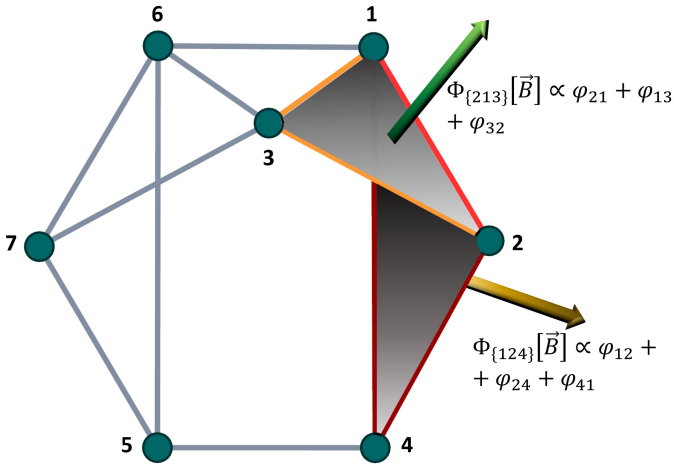

Figure 6.1: A graph with 7 vertices embedded in 3D space and enclosing a volume. Faces $F_a = \{1,3,2\}$, $F_b = \{1,6,3\}$, $F_c = \{3,6,7\}$, and $F_d = \{2,3,7,5,4\}$, oriented outwards with respect to the enclosed volume, are on the foreground. Considering F_a together with the face $F_e\{1,2,4\}$ in the background, we see that the edges $(1,2)$ contributes with a phase φ_{21} to the flux through F_a and with the inverse phase $\varphi_{12} = -\varphi_{21}$ to the flux through F_e. Applying the same reasoning to all edges, we conclude that the net flux through all the (outward-oriented) faces defined by the graph is 0, therefore the phase configuration is compatible with a magnetic field configuration.

$\vec{B}$ is zero. This is illustrated in Fig.6.1 for a simple graph embedded in space. If the graph is also planar and we consider its embedding on the plane, we saw that Euler's formula Eq.(6.14) implies that the number of independent loops is equal to the number of free phase parameters and also to the number of finite faces defined by the planar embedding: this has a clear physical interpretation in terms of magnetic fields since the only invariant quantities can be seen as the fluxes of the magnetic field through each face.

Finally, let us return to gauge invariance. For the 2D square lattice, for each vertex we can cancel the phase of one link attached to it by a phase rotation of the corresponding localized state, therefore we can always set $f_x(n,m) = 0\ \forall n,m \in \mathbb{Z}^2$, for example. The discretized magnetic field is then given by $B(n,m) = [f_y(n+1,m) - f_y(n-1,m)]/2a$ [4], assuming a symmetric discrete derivative. $B(n,m)$ is to be understood as the component of the magnetic field at position (n,m), in the *orthogonal direction to the plane*. As an example, assuming a constant B such that $f_y(n,m) = nB$, the spectrum of the corresponding H as a function of the parameter B is the Hofstadter butterfly [349]. However, our result is much more general, since it can be stated in any dimension and for any choice of the gauge field and, correspondingly, of the magnetic field. It also offers a nice interpretation of the *chiral* behavior of chiral CTQWs: in the presence of magnetic fields, the dynamics of a charged particle can be directional and asymmetric under time reversal.

[4] This is a discretized version of $B_z = \frac{\partial A_y}{\partial x} - \frac{\partial A_x}{\partial y}$ for the gauge choice $A_x = 0$.

CHAPTER 7

Applications and characterization of chiral quantum walks

Given the theoretical construction of chiral quantum walks outlined in the previous chapter, it is natural to ask whether these new phases degrees of freedom can be exploited to push further the success of CTQWs compared to classical ones for certain tasks. In this chapter, we shall pursuit this direction starting in Section 7.1, where we present original results [350] aimed at clarifying what kind of behaviours can be altered and designed through phase configurations. In Section 7.2 [351] we will study a figure of merit, the quantum-classical distance, which is often successful at identifying optimal phases configurations when the graph is fixed but generic. We will conclude by presenting two examples of applications of chiral quantum walks: directed transport, in Section 7.3 [352], and robust transport of quantum information over long (topological) distances in Section 7.4 [353].

7.1 Swift chiral quantum walks

A number of recent results for both Laplacian and adjacency type *non-chiral* CTQWs [354, 355] indicate that the evolution starting from maximally connected vertices can be plagued by a sedentary behaviour, meaning that the return probability to the initial vertex stays close to 1 at all times if its degree is sufficiently large. Let us lay down a basic definition:

Definition 7.1.1: Cone graphs

A *cone* on a graph $\mathcal{G}'$ is a graph $\mathcal{G}$ obtained by adding a vertex v to the vertex set of $\mathcal{G}'$ and connecting it to every vertex in $\mathcal{G}'$. The maximally connected vertex v will be called the *apex* of the cone.

For Laplacian quantum walks the statement is very general, since their evolution from a maximally connected vertex in any graph with $N+1$ vertices is the same as the one from the center (labelled by 1) of an N-pointed star graph S_{N+1}, whose return probability is [298]:

$$p^L_{1\to 1}(t) \;=\; 1 - 2\frac{N-2}{(N-1)^2}\left[1-\cos(Nt)\right] \tag{7.1}$$

and it is clearly sedentary, since $p^L_{1\to1}(t) \to 1\ \forall t \in \mathbb{R}$ as $N \to +\infty$. This general result was proved in [355]. Concerning adjacency CTQWs, instead, the situation is currently less clear. The dynamics starting from the central vertex of the N-pointed star graph in this case is not sedentary, nor it is the one which starts from the center of the wheel graph. Moreover, each adjacency CTQW starting from a maximally connected vertex could yield a different evolution, depending upon the connectivity of the remaining vertices. However, it was shown in [354] that adjacency quantum walks from the apex of cones over several infinite families of graphs are sedentary. Importantly, this is the case when the cone is over m-regular graphs with N vertices and the degree m grows faster than linearly with N. It is self-evident that this behaviour is often undesirable, since the typical overhead of CTQWs over their classical counterpart relies on their ability to spread faster over the graph, either for a transport task or for quantum search (whose time-reversed evolution describes precisely the spreading of a localized state into a flat state).

In this section we will show that appropriate phase configurations can be chosen on many graph families to cure sedentarity to arrived at the so-called *swift chiral quantum walks* of the adjacency type, where the returning probability goes to zero in the shortest time possible, while we also provide a no-go theorem for swift chiral CTQWs of the Laplacian type.

7.1.1 Results for adjacency quantum walks

Let us consider a quantum walk starting at the apex of a cone graph $\mathcal{G}$ over an m-regular graph of N vertices, whose state vector will be labelled $|1\rangle$. Since this vertex is maximally connected, the adjacency matrix A of the full graph will have the following structure:

$$\mathrm{A} = \left(\begin{array}{c|ccc} 0 & 1 & 1 & \dots \\ \hline 1 & & & \\ 1 & & \mathrm{A}' & \\ \vdots & & & \end{array}\right) \tag{7.2}$$

where A′ is the adjacency matrix of the m-regular graph $\mathcal{G}'$. Since each vertex in $\mathcal{G}'$ has exactly m neighbours, calling $|\bar{1}\rangle = \sum_{j=2}^{N+1}|j\rangle$ with support in the subspace of $\mathcal{G}'$, we have:

$$\mathrm{A}|\bar{1}\rangle = N|1\rangle + m|\bar{1}\rangle \tag{7.3}$$

Therefore, calling $|e\rangle = \frac{1}{\sqrt{N}}|\bar{1}\rangle$ the normalized associated with $|\bar{1}\rangle$, A reduces to a simple 2×2 block in the space spanned by $\{|1\rangle, |e\rangle\}$ [310]:

$$\mathrm{A}_{\mathrm{red}} = \begin{pmatrix} 0 & \sqrt{N} \\ \sqrt{N} & m \end{pmatrix} \tag{7.4}$$

This is easily diagonalized, and the resulting return probability starting from $|1\rangle$ is given by:

$$p^{\mathrm{A}}_{1\to1}(t) = 1 - \frac{2N}{m^2+4N}\left[1-\cos(\sqrt{m^2+4N}t)\right] \tag{7.5}$$

whereas, with probability $1-p^{\mathrm{A}}_{1\to1}(t)$ the walker will be in the state $|e\rangle$ orthogonal to $|1\rangle$, from which all the other site-to-site transition probabilities follow.

Eq.(7.5) can be regarded as a partial result on the adjacency version of the general Theorem 7.1 for Laplacian quantum walks. It states that the dynamics starting from the apex of a cone over *any* m-regular graph is fully specified by m and the number of vertices of the underlying graph N (notice that the full graph has $N+1$ vertices instead). If we define a family of regular graphs such that the degree scales as $m \sim O(N^{\frac{1}{2}+\alpha})$ with $\alpha > 0$, it follows that $p^{\mathrm{A}}_{1\to 1}$ stays very close to 1 at all times, for large enough N. This construction leads to a result originally presented in [354].

7.1.2 Constructing swift chiral quantum walks

Now suppose that we can attach complex phases to the edges of the m-regular graph $\mathcal{G}'$ such that the resulting chiral adjacency matrix $\tilde{\mathrm{A}}$, which would substitute A' in Eq.(7.2), fulfils the following condition:

$$\tilde{\mathrm{A}}|\bar{1}\rangle \;=\; 0 \tag{7.6}$$

that is to say, the phases conjure in such a way that the sum of each row of $\tilde{\mathrm{A}}$ is zero. Retracing the steps to arrive at Eq.(7.5), we find the following reduced Hamiltonian for the chiral QW on the cone in the subspace spanned by $\{|1\rangle, |e\rangle\}$:

$$\mathrm{H}_{\mathrm{red}} = \begin{pmatrix} 0 & \sqrt{N} \\ \sqrt{N} & 0 \end{pmatrix} \tag{7.7}$$

from which the return probability to the starting, maximally connected vertex is calculated to be:

$$p^{\tilde{\mathrm{A}}}_{1\to 1}(t) \;=\; \cos^2(\sqrt{N}t) \tag{7.8}$$

Notice that this is the same return probability that would result from the adjacency quantum walk starting from the center of an N-pointed star graph, which cannot support chiral quantum walks since it is a tree graph. This equation motivates the following definition:

Definition 7.1.2

Let $\mathcal{G} = (V, E)$ be a simple, connected and undirected graph, let $v \in V$ be a vertex of $\mathcal{G}$ and denote by N the cardinality of the set of neighbours of v in $\mathcal{G}$. Given a chiral Hamiltonian H on $\mathcal{G}$, it is said to generate a ***swift chiral quantum walk*** starting from v in $\mathcal{G}$ if:

$$\forall t \geq 0: \;\; |\langle v|e^{-i\mathrm{H}t}|v\rangle|^2 \;=\; \cos^2\left(\sqrt{N}t\right) \tag{7.9}$$

Therefore, whenever it is possible to attach phases to the edges such that Eq.(7.6) is fulfilled, we obtain a similar result to the one which is valid for the Laplacian quantum walks, in the sense that all the adjacency-type *swift* chiral quantum walks starting from a maximally connected vertex have the same dynamics as that of the adjacency quantum walk on the star graph. Notice, however, that Laplacian quantum walks tend to stay on the initial vertex, if this has maximal degree, whereas swift quantum walks abandon it fast. In the following, we will formalize this observation and the nomenclature of *swift chiral quantum walks* with rigorous and general results.

If $\mathcal{G}'$ has a vertex of degree 1, then Eq.(7.6) cannot be fulfilled by any assignment of phases on its edges.

Theorem 7.1.1

Let $\mathcal{G}$ be a graph and let v be a vertex of $\mathcal{G}$ with degree N. Out of all the chiral quantum walks starting from v in $\mathcal{G}$ (with generic diagonal entries of the chiral Hamiltonian), a *swift chiral quantum walk*, when it exists, is the fastest at leaving v, in the sense that it evolves to a state orthogonal to v in a time $\tau_s = \frac{\pi}{2\sqrt{N}}$ which achieves the **shortest** quantum speed limit among all chiral evolutions starting from v on $\mathcal{G}$.

Proof. The speed limit to completely leave v is the speed limit to go to a generic state orthogonal to $|v\rangle$. Using Eq.(1.29), we easily find:

$$\tau_{QSL} := \max\left\{\frac{\pi}{2\Delta \mathrm{H}}\,,\ \frac{\pi}{2(\langle \mathrm{H}\rangle - E_0)}\right\} \tag{7.10}$$

where $\Delta \mathrm{H} = \sqrt{\langle \mathrm{H}^2\rangle - \langle \mathrm{H}\rangle^2}$ is the standard deviation of energy on the orbit of $|v\rangle$, $\langle \mathrm{H}\rangle = \langle v|\mathrm{H}|v\rangle$ its average energy and E_0 is the ground state's energy. Notice that the quantum speed limit is defined for a *fixed* Hamiltonian, and we are looking for the *smallest* quantum speed limit over all chiral Hamiltonians on $\mathcal{G}$.

For any localized state $|v\rangle$ with degree N and any chiral Hamiltonian H on $\mathcal{G}$, it is always true that $\Delta \mathrm{H} = \sqrt{N}$. Indeed, let $\langle v|\mathrm{H}|v\rangle = d$, then $\langle v|\mathrm{H}^2|v\rangle = \vec{h}_v^{\dagger}\vec{h}_v = d^2 + N$ where $\vec{h}_v$ is the v-th row of H, whose v-th entry is d and all the other non-zero entries are precisely N complex phases. Therefore we can rewrite:

$$\tau_{QSL} := \max\left\{\frac{\pi}{2\sqrt{N}}\,,\ \frac{\pi}{2(-E_0)}\right\} \ = \ \max\left\{\tau_s\,,\ \frac{\pi}{2(-E_0)}\right\} \tag{7.11}$$

To conclude the proof, let us suppose that there is a better chiral Hamiltonian for which the second expression of Eq.(7.11) applies, which, because of the max, implies that $\tau_{QSL} > \tau_s$. But since we supposed that a swift chiral quantum walk exists, we know that τ_s can be achieved by the swift chiral Hamiltonian, which shows that the second expression in Eq.(7.11) is never the best quantum speed limit whenever a swift chiral quantum walk exists. As a byproduct, we deduce that for swift chiral quantum walks the ground state energy fulfils $E_0 \leq -\sqrt{N}$. □

It is not immediate to conclude that any chiral quantum walk which achieves this limit τ_s must be a swift chiral quantum walk since, a priori, the specific form of the return probability need not be given by Eq.(7.9). It is a very interesting question to ask when is it possible to construct a swift chiral quantum walk (of the adjacency type) starting from maximally connected vertices in any graph $\mathcal{G}$ having no vertex with degree 2 or, equivalently, to find a chiral adjacency matrix fulfilling Eq.(7.6) on any graph $\mathcal{G}'$ having no vertex of degree 1. We shall introduce the following definition:

Definition 7.1.3

Let $\mathcal{G}'$ be a graph of order N and suppose there exists a chiral Hamiltonian H on $\mathcal{G}'$ with eigenvector $\mathbf{1}_N$ and eigenvalue 0 (where $\mathbf{1}_N \in \mathbb{R}^N$ is the vector of all ones) or, equivalently, such that the sum of each row of H is zero. We will say that the phases assigned to the edges of $\mathcal{G}'$ by H provide a ***swift phases configuration*** for $\mathcal{G}'$.

We could not provide general criteria for a graph (with minimal degree ≥ 2) to admit a swift phases configuration. Nevertheless, we shall prove that many infinite families of graphs admit such a construction. Again, full proofs can be found in the original paper [350].

Theorem 7.1.2

If all the vertices of $\mathcal{G}'$ have even degree, then it admits a swift phases configuration.

Theorem 7.1.3

A 3-regular graph $\mathcal{G}'$ admits a swift phases configuration if and only if one of the following equivalent conditions is met:

1. $\mathcal{G}'$ has a perfect matching
2. $\mathcal{G}'$ can be covered with vertex disjoint cycles (it has a 2-factor)

We recall that a perfect matching of $\mathcal{G}'$ is a 1-factor, i.e. a partition of all the vertices in pairs such that the vertices in each pair are adjacent in $\mathcal{G}'$ and each vertex appears in just a single pair. Moreover, we say that $\mathcal{G}'$ can be covered with vertex disjoint cycles if there exists a set of cycles that are subgraphs of $\mathcal{G}'$, whose union covers all the vertices of $\mathcal{G}'$ and such that each vertex of $\mathcal{G}'$ belongs to a single cycle. This is also called a 2-factor of $\mathcal{G}'$. Notice that Theorem 7.1.2 also implies that there are regular graphs not admitting a swift phases configuration: an example is provided by the graph in Fig. 7.1.

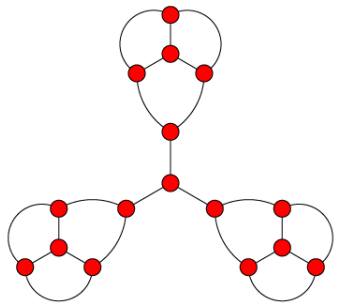

Figure 7.1: A 3-regular graph having no perfect matching and therefore no swift phases configuration.

Corollary 7.1.1

A bridgeless 3-regular graph always admits a swift phases configuration.

Proof. Recall that a graph is k-edge connected if k is the minimum number of edges to be deleted in order to make the graph disconnected. A non connected graph is bridgless if $k > 1$ for each connected component. Petersen theorem ensures that bridgless 3-regular graphs admit perfect matching and the thesis follows from Theorem 7.1.2. □

Notice that the converse is not true: there exist 3-regular graphs with perfect matching and with bridges. An example is provided in Fig. 7.2.

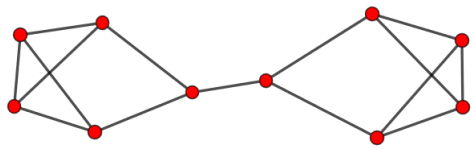

Figure 7.2: A 3-regular graph with a bridge and a perfect matching, thus admitting a swift phases configuration.

Corollary 7.1.2

An hamiltonian 3-regular graph always admits a swift phases configuration.

Proof. A graph $\mathcal{G}'$ is said to be hamiltonian if it admits a hamiltonian cycle, a closed path passing through each vertex of $\mathcal{G}'$ exactly once. The thesis is then a direct consequence of Theorem 7.1.2 □

Theorem 7.1.4

Complete graphs K_N and bipartite complete graphs K_{N_1,N_2} admit a swift phases configuration for all integers $N \geq 3$ and $N_1, N_2 \geq 2$.

Lemma 7.1.1

Let $\mathcal{G}_1$ and $\mathcal{G}_2$ be two graphs such that a cone with apex v on $\mathcal{G}_1$ (resp. $\mathcal{G}_2$) admits a swift chiral quantum walk starting from v. Then also the cone over their disjoint union $\mathcal{G} = \mathcal{G}_1 \bigcup \mathcal{G}_2$ admits a swift chiral quantum walk starting from its apex.

7.1.3 Gauge fixing and uniqueness

Let us consider the case of a cone $\mathcal{G}$, with apex labelled by 1, over a graph $\mathcal{G}'$ of order N. The first column $\vec{h}_1$ of a chiral Hamiltonian $\tilde{\mathrm{H}}$ on $\mathcal{G}$ will have the following structure $\vec{h}_1 = (d_1, \vec{h'}_1)^T$ where $d_1 \in \mathbb{R}$ and $\vec{h}'_1 \in \mathbb{C}^N$ is a vector whose entries are all complex numbers of modulus 1. Then, a quasi-gauge-fixing can be imposed by asking that $\vec{h'}_1 = (1, 1, ..., 1)^T \in \mathbb{R}^N$; indeed, in any class of quasi-gauge-equivalent chiral Hamiltonians, there will be just one representative fulfilling this condition. With this quasi-gauge

choice, a chiral adjacency matrix $\tilde{\mathrm{A}}$ on $\mathcal{G}$ will generate a swift chiral quantum walk from $|1\rangle$ if and only if the corresponding submatrix $\tilde{\mathrm{A}}'$ (which is a chiral adjacency matrix on $\mathcal{G}'$) is such that the sum of each of its rows (and therefore of each column) is zero.

Theorem 7.1.5

Let $\mathcal{G} = (V, E)$ be a simple, connected and undirected graph with $|V| = N$ vertices. Let $v \in V$ be a generic vertex of $\mathcal{G}$ and denote $\mathcal{G}_v$ the subgraph of $\mathcal{G}$ obtained by keeping v and all its neighbours, and deleting every other vertex and the respective edges. Then there exists a *swift chiral quantum walk* (of the adjacency type) starting from v in $\mathcal{G}$ if and only if the following conditions hold:

(a) There is a swift chiral quantum walk starting from v in the cone $\mathcal{G}_v$

(b) Any vertex $v' \in \mathcal{G}$ which is not a neighbour of v has either 0 or ≥ 2 common neighbours with v.

The proof of this result can be found in our original paper [350]

7.1.4 No-go theorems for Laplacian quantum walks

As was reminded in the introduction, continuous-time quantum walks generated by the Laplacian and starting from a vertex with maximal degree all have the same dynamics and they are sedentary. If we allow for an oracle, this behaviour can be easily fixed to get a swift (non-chiral) quantum walk. Indeed, let L be the Laplacian of a graph $\mathcal{G}$ which is a cone over some other graph $\mathcal{G}'$, let us label with 1 the apex of the cone, with a corresponding state vector $|1\rangle$, and call N its degree. Then if we define:

$$\tilde{\mathrm{L}} := \mathrm{L} - (N-1)\mathrm{P}_1 \tag{7.12}$$

where P_1 is the orthogonal projector on $|1\rangle$, it is straightforward to see that in the reduced basis generated from $|1\rangle$ the matrix $\tilde{\mathrm{L}}$ takes the same form of Eq.(7.7), apart for the addition of an immaterial identity matrix and a sign difference, therefore the returning probability is that of a swift quantum walk, Eq.(7.8). Notice that this is equivalent to Grover's Hamiltonian for quantum search on a graph, generalized to the case where just the target vertex has maximal degree [274].

However, in the spirit of using chiral quantum walks and the phases degrees of freedom, it is interesting to ask whether the oracle of Eq.(7.12) can be replaced by a suitable phases configuration while keeping the swift dynamics. In general, this is not possible. Indeed, we already proved that to get the swift evolution, the reduced Hamiltonian in the reduced basis of the starting state vector $|1\rangle$ should be 2×2, and by enforcing the diagonal elements of the Laplacian and attributing generic phases to the links, this matrix must have the following structure:

$$\tilde{\mathrm{H}}_k = \begin{pmatrix} N & \sqrt{N} \\ \sqrt{N} & k \end{pmatrix} \tag{7.13}$$

where we chose the second vector of the reduced basis to be the $|e\rangle = \frac{1}{\sqrt{N}}(|\vec{h}_1\rangle - N|1\rangle)$, where $\vec{h}_1$ is the first column of the full chiral Hamiltonian we are considering (with

diagonal elements fixed by the Laplacian) and the number k is the only parameter we may try to adjust by choosing a phases configuration. For simplicity, suppose that the graph $\mathcal{G}'$ is m-regular. Then clearly $|k| \leq 2m+1$, since the matrix minor of the chiral Hamiltonian pertaining to $\mathcal{G}'$ has all the diagonal elements equal to $m+1$ and exactly m nonzero off-diagonal entries in every row, each of which is a complex phase. But by looking at the dynamics generated by the reduced Hamiltonian (7.13) we get a returning probability of:

$$p_{1\to 1}^{\tilde{\mathrm{H}}_k}(t) \;=\; 1 - \frac{2N}{(k-N)^2+4N}\left(1-\cos\sqrt{(k-N)^2+4N}t\right) \tag{7.14}$$

which is sedentary unless $(k-N) \sim O(\sqrt{N})$. Therefore, on cones over m-regular graphs whose degree does not grow with the number of vertices, chiral quantum walks of the Laplacian type starting from the apex cannot be swift. Despite its generality, this result relies on the assumption that the dynamics reduces to a 2×2 subspace, which would be needed to achieve the exact swift evolution. In fact, a more general no-go theorem holds.

Theorem 7.1.6

Let $\mathcal{G} = (V, E)$ be a cone over a subgraph $\mathcal{G}'$ of order N (then $|V| = N+1$) and denote by $|1\rangle$ the characteristic vector of the apex of the cone, labelled by 1. Let $d^{\max}$ be the largest degree for the vertices of $\mathcal{G}'$. Then, if $d^{\max} \sim o(N)$ for large N, any chiral quantum walk of the Laplacian type starting from 1 is sedentary[a]; more generally, if $\tilde{\mathrm{L}}$ is a chiral Laplacian on $\mathcal{G}$:

$$p_{1\to 1}^{\tilde{\mathrm{L}}}(t) \;\geq\; 1 - \frac{\sqrt{N}}{N-2d^{\max}} \tag{7.15}$$

(assuming $2d^{\max} < N$).

[a] In the original definition by C. Godsil [354], sedentarity requires that the return probability has the asymptotic form $1-\frac{k}{N}$ for constant k and large order N. Here we slightly relax this definition by allowing asymptotic scaling of the form $1-\frac{k}{N^\alpha}$ for $\alpha > 0$, such that it is still true that the return probability is close to 1 as $N \to \infty$. In particular, Theorem 7.1.4 implies sedentarity with $\alpha = 1/2$.

Again, the proof can be found in [350]. The fact that $\mathcal{G}$ is a cone is not strictly necessary for the theorem above to hold. Indeed, it is sufficient that the starting vertex has the largest degree (N) and that the degrees of all the other vertices are $o(N)$. In this sense, this result indicates that the diagonal elements of the chiral Laplacians strongly hinder the transport between vertices with highly different degrees, and this issue cannot be overcome by leveraging on chirality.

7.2 Quantum-classical distance as a guide for optimal phase configurations

Given the considerable amount of new degrees of freedom introduced by chiral quantum walks, especially on large graphs, it is desirable to have some figures of merit that can hint at the optimal phase configuration for a given task. Indeed, we already saw an instance of this for CTQWs starting at a maximally connected vertex, for which the addition of phases can strongly improve the spreading of the walker over the whole structure. In general, as outlined in Section 5.4, the distinctive quantum features of continuous-time quantum walks belong to one of the following classes: coherent quantum transport (and, in the best case scenario, perfect state transfer), instantaneous uniform mixing and quantum search. We therefore seek a quantity that will point at an optimized phase configuration for one of these tasks that is achievable on a given topology.

The idea of the quantum-classical distance was first introduced in [356] as an attempt to quantify the difference in behaviour between a CTQW and the corresponding CTRW on the same graph. To do this, it is first necessary to embed the classical evolution in the formalism of quantum states, so that a quantitative comparison can be constructed from there. For a quantum walk, the basis of localized states is the most classical, in the sense that we expect decoherence with respect to it whenever they are implemented through a spatial structure and we consider localized states to be deterministic, distinguishable and not further resolvable. It is consequent to ask that the classical evolution should not generate coherences in the localized basis. The embedding of the classical evolution $\mathcal{E}_t$, for a graph $\mathcal{G} = (V, E)$ with N vertices, can then be realized by imposing:

$$\mathcal{E}_t\left[\sum_{j=1}^{N}\rho_j^0|j\rangle\langle j|\right] \;=\; \sum_{j,k=1}^{N}\rho_j^0\left(e^{-t\mathrm{L}}\right)_{kj}|k\rangle\langle k| \tag{7.16}$$

where L is the Laplacian of $\mathcal{G}$, so that the probabilities of finding the walker in each vertex evolve exactly as in Eq.(5.29) with $\vec{p}(0) = (\rho_1^0, ..., \rho_N^0)^T$. Combining Eq.(7.16) and Eq.(6.2,6.3) for a localized initial state $\hat{\boldsymbol{\rho}}_j^0 = |j\rangle\langle j|$ and using the notation $\mathcal{U}_t$ for the superoperator acting on $\hat{\boldsymbol{\rho}}_j^0$ and corresponding to the quantum unitary evolution, we can compare the states at each time by looking at their fidelity. We define the *quantum-classical distance* as [356]:

$$\mathcal{D}_{QC}^j(t) \;:=\; 1 - \mathcal{F}\left[\mathcal{E}_t(\hat{\boldsymbol{\rho}}_j^0), \mathcal{U}_t(\hat{\boldsymbol{\rho}}_j^0)\right] \;= \tag{7.17}$$

$$= \; 1 - \sum_{k=1}^{N} p_{kj}(t)|\langle k|\psi_j(t)\rangle|^2. \tag{7.18}$$

with $p_{kj}(t) = \left(e^{-t\mathrm{L}}\right)_{kj}$ and $|\psi_j(t)\rangle = e^{-it\hat{\mathbf{H}}}|j\rangle$, while $\mathcal{F}[\bullet,\bullet]$ is the fidelity, defined as in Eq.(1.15. Eq.(7.18) follows from Eq.(7.17) when the initial state is localized, but it is clearly not valid when the initial state is mixed, in which case Eq.(7.17) should be used directly. Notice that $\mathcal{D}_{QC}^j(t)$ is zero at a given time if and only if the classically and quantum evolved states are exactly the same at that time. Despite becoming uninformative whenever one of the states is proportional to the identity, being equal to $1 - \frac{1}{N}$ in this instance[1], this quantity should be considered throughout its whole time evolution,

[1] This is true also for the relative entropy of the (pure) quantum evolved state with respect to the classical one, which can be used as an alternative measure of the distance between the two dynamics, leading to essentially identical conclusions.

showing the departure between the quantum and the classical dynamics. It is still true, by the same token as in [356], that the maximum value of the quantum-classical distances over all possible *classical* initial states can be attained by a single localized state, at any given time. Therefore we can still define a global quantum-classical distance by:

$$\mathcal{D}_{QC}(t) \;:=\; \max_{j\in V}\left\{\mathcal{D}^{j}_{QC}(t)\right\} \tag{7.19}$$

which is independent of the initial state, but only depends upon the graph (specified by L) and the choice of H compatible with the topology. Notice that, among pure initial states, the maximum has to be restricted over localized ones, since the classical evolution cannot be defined on superpositions.

Checking for a few graphs with different topologies and number of vertices, the overall behaviour of this quantity in time seems very similar to the simpler scenario where L is a Laplacian and the straightforward identification $\mathrm{H} = \mathrm{L}$ can be applied. In particular, the asymptotic value in the long time limit takes the same expression for any connected graph of size N and it is given by:

$$\mathcal{D}^{j}_{QC}(t \gg 1) \simeq 1 - 1/N. \tag{7.20}$$

Because of this saturation effect of $\mathcal{D}_{QC}$ at large times, fluctuations of the quantum-classical distance can be significant only if they happen before the classical evolution gets close to equilibrium. This is a valuable property: indeed, since the quantum evolution is aperiodic on general graphs, unpredictable behaviors can occur at sufficiently long times and it is therefore mandatory, from a physical point of view, to impose a cutoff on the relevant time scale to perform the required task. A natural choice is precisely the time scale of the classical evolution, especially if a quantum advantage is sought.

7.2.1 Quantum-classical distance at short times

To understand the behavior of the quantum-classical distance at short times, instead, we may expand $p_{kj}(t)$ and $|\langle k|\psi_j(t)\rangle|^2$ up to second order in t and obtain

$$\begin{aligned}\mathcal{D}^{j}_{QC}(t) = t\left(\left[\mathrm{H}^2\right]_{jj} - [\mathrm{H}]^2_{jj}\right) - t^2\Bigg(&- \left[\mathrm{H}^2\right]_{jj} + [\mathrm{H}]^2_{jj} + \frac{1}{2}\left[\mathrm{H}^2\right]^2_{jj} + \\ &- \left[\mathrm{H}^2\right]_{jj}[\mathrm{H}]^2_{jj} + \frac{1}{2}\sum_s |\mathrm{H}_{js}|^4\Bigg) \;+\; O(t^3)\end{aligned} \tag{7.21}$$

If we focus on unweighted graphs, which means that we assume $|\mathrm{H}_{jk}|$ to be either 1 or 0 depending on whether vertices j and k are neighbours or not, we have that $\left[\mathrm{H}^2\right]_{jj} - [\mathrm{H}]^2_{jj} = (\Delta\mathrm{H}^2)_{jj} = d_j$ where d_j is the degree of j. Moreover:

$$\frac{1}{2}\left[\mathrm{H}^2\right]^2_{jj} - \left[\mathrm{H}^2\right]_{jj}[\mathrm{H}]^2_{jj} + \frac{1}{2}\sum_s |\mathrm{H}_{js}|^4 \;= \tag{7.22}$$

$$= \frac{1}{2}\left(\left[\mathrm{H}^2\right]_{jj} - [\mathrm{H}]^2_{jj}\right)^2 + \frac{1}{2}\sum_{s\neq j} |\mathrm{H}_{js}|^4 \;= \tag{7.23}$$

$$= \frac{d_j^2 + d_j}{2} \tag{7.24}$$

where in the last step we used the fact that $\sum_{s\neq j}|\mathrm{H}_{js}|^4$ gets a contribution of 1 for any s connected to j and 0 otherwise. Therefore, the short-time expansion of the quantum-classical distance to second order is:

$$\mathcal{D}^j_{QC}(t) \;=\; d_j t \;-\; d_j(d_j-1)\frac{t^2}{2} \;+\; O(t^3). \tag{7.25}$$

and it depends just upon the degree of the starting vertex: *neither the on-site average energies nor the phases of the off-diagonal entries of* H *affect the short-time behavior of the quantum-classical distance*; however, the time scale at which the second order expansion can be trusted is typically orders of magnitude smaller than the timescale at which we maximize its value in the following examples, therefore we could still expect a contribution due to phases when the maximization is carried out at the appropriate timescale.

7.2.2 1-norm of Coherence and Inverse Participation Ratio

In order to understand what type of properties of the quantum walk contribute to the quantum-classical distance, and how $\mathcal{D}_{QC}$ relates to other figure of merits that are suitable to characterize the behaviour of CTQWs, we will turn our attention to two additional quantities, the 1-norm of coherence and the inverse participation ratio (IPR), to be later compared with Eq.(7.25).

Let us start with the 1-norm of coherence. With respect to the localized basis, the coherence of the pure state $|\psi_j(t)\rangle$ given by Eq.(6.2) can be written as [356]:

$$\mathcal{C}_j(t) \;=\; \left(\sum_k |\alpha_{kj}(t)|\right)^2 - 1 \tag{7.26}$$

with $\alpha_{jk}(t)$ defined according to Eq.(6.3). Here and in the following, it will be helpful to start from the fourth-order short time expansion of $|\alpha_{kj}(t)|^2$:

$$\begin{aligned}|\alpha_{kj}(t)|^2 \;&=\delta_{jk} \;-\; t^2\left(\delta_{jk}\left[\mathrm{H}^2\right]_{jj} - |\mathrm{H}_{jk}|^2\right) \;+\; t^3\mathrm{Im}\left[\mathrm{H}_{jk}\left[\mathrm{H}^2\right]_{kj}\right] \;+ \\ &+\; t^4\left(\frac{1}{12}\delta_{jk}\left[\mathrm{H}^4\right]_{jj} - \frac{1}{3}\mathrm{Re}\left[\mathrm{H}_{jk}\left[\mathrm{H}^3\right]_{kj}\right] \;+\; \frac{1}{4}|\left[\mathrm{H}^2\right]_{jk}|^2\right) \;+\; O(t^5)\end{aligned} \tag{7.27}$$

From this, it follows that:

$$\begin{aligned}\sum_k |\alpha_{kj}(t)| \;&=\; \sqrt{1-d_j t^2 + O(t^4)} \;+\; t\sum_{k\neq j}|\mathrm{H}_{jk}|\sqrt{1 - t\mathrm{Im}\left[\mathrm{H}_{jk}\left[\mathrm{H}^2\right]_{kj}\right] + O(t^2)} \;+ \\ &+\; \frac{t^2}{2}\sum_{k\neq j,\mathrm{H}_{jk}=0}|\left[\mathrm{H}^2\right]_{jk}| \;+\; O(t^3)\end{aligned}$$

where we splitted the initial sum over k in a first term with $k=j$, a second sum with $k\neq j$ but which gets contributions only for terms having $\mathrm{H}_{jk}\neq 0$, and a final sum that takes into account the last terms with $k\neq j$ and $\mathrm{H}_{jk}=0$. Expanding the square roots and collecting powers of t, one obtains:

$$\sum_k |\alpha_{kj}(t)| \;=\; 1 + t d_j - \frac{1}{2}t^2\left(d_j \;+\; \sum_{k\neq j}\mathrm{Im}\left[\mathrm{H}_{jk}\left[\mathrm{H}^2\right]_{kj}\right] + \sum_{\substack{k\neq j\\ \mathrm{H}_{jk}=0}}|\left[\mathrm{H}^2\right]_{jk}|\right) + O(t^3).$$

Further simplifying the imaginary part:

$$\sum_{k\neq j} \mathrm{Im}\left[\mathrm{H}_{jk}\left[\mathrm{H}^2\right]_{kj}\right] \;=\; \sum_{k} \mathrm{Im}\left[\mathrm{H}_{jk}\left[\mathrm{H}^2\right]_{kj}\right] \;=\; \mathrm{Im}\left[\mathrm{H}^3\right]_{jj} \;=\; 0.$$

we arrive at:

$$\mathcal{C}_j(t) \;=\; 2d_j t \;+\; \Big[d_j(d_j-1) - \sum_{\substack{k\neq j \\ \mathrm{H}_{jk}=0}} |\left[\mathrm{H}^2\right]_{jk}|\Big]t^2 \;+O(t^3).$$

Thus coherence behaves similarly to quantum-classical distance at short times, but it is also affected by other degrees of freedom of H; the term $\sum_{\substack{k\neq j \\ \mathrm{H}_{jk}=0}} |\left[\mathrm{H}^2\right]_{jk}|$ has a simple graphical interpretation: $|\left[\mathrm{H}^2\right]_{jk}|$ for $k \neq j$ and for $\mathrm{H}_{jk} = 0$ is a sum over all possible paths of length 2 connecting vertex j with a vertex k at distance 2 from j, where each path is weighted by the product of the phases of its two links in the direction from j to k. Since this is the modulus of a sum of phases, interference may happen. Therefore $\mathcal{C}_j$ can get a phase-dependent second order contribution in t only if the graph contains a 4-cycle passing through j and beacycle a non-zero overall phase, so that there will be at least two paths joining the same k with j and weighted by different phase factors.

The *inverse participation ratio* (IPR), on the other hand, is a measure of how spread is the walker with respect to the initial vertex:

$$\mathcal{I}_j(t) \;=\; \sum_k |\alpha_{kj}(t)|^4 \tag{7.28}$$

Indeed, $|\alpha_{kj}(t)|^2 = P_{j\to k}(t)$ are the transition probabilities, and summing their squares is a way of quantifying how peaked the probability distribution over the vertices is at time t: the higher the IPR, the more peaked the distribution is, with a maximum value of 1 ($t = 0$) and a minimum value of $1/N$. which decreases while the QW spreads over the vertices of the graph. The second-order short time expansion of $\mathcal{I}_j(t)$ is derived from Eq.(7.27):

$$\mathcal{I}_j(t) \;=\; 1 - 2d_j t^2 \;+\; O(t^4). \tag{7.29}$$

Unlike the 1-norm of coherence and D^j_{QC}, the IPR has no linear term in t. Moreover, up to second order it is dependent just upon the degree of j.

7.2.3 Cycle graphs

As a test case, let us study the behaviour of the quantum-classical distance for cycle graphs. The most general chiral Hamiltonian on C_N is:

$$\mathrm{H} \;=\; \begin{pmatrix} d_1 & e^{i\theta} & 0 & 0 & \dots & e^{-i\theta} \\ e^{-i\theta} & d_2 & e^{i\theta} & 0 & \dots & 0 \\ 0 & e^{-i\theta} & d_3 & e^{i\theta} & \dots & 0 \\ \vdots & \vdots & & & \vdots & \vdots \\ e^{i\theta} & 0 & 0 & \dots & e^{-i\theta} & d_N \end{pmatrix} \tag{7.30}$$

where $\theta \in [0, 2\pi)$ is the only relevant phase, which has been distributed equally over all links for convenience, while $d_1, ..., d_N \in \mathbb{R}^+$. We will restrict our attention to the role

of phases, thus we put $d_1 = ... = d_N = d$ and further impose $d = 0$ without loss of generality. The eigenvectors of H will still be Bloch states:

$$|\lambda_j\rangle \;:=\; \frac{1}{\sqrt{N}}\sum_{k=1}^{N} e^{i\frac{2\pi jk}{N}}|k\rangle \tag{7.31}$$

while the eigenvalues will be shifted according to:

$$\lambda_j \;:=\; 2\cos\left(\theta+\frac{2\pi j}{N}\right) \tag{7.32}$$

where $j = 1, ..., N$. Notice that, although for $\theta = 0$ the spectrum is doubly degenerate, for almost every $\theta \neq 0$ the degeneracy is lifted. Moreover, despite $\theta \in [0, 2\pi)$, one can always choose a representative phase in the reduced scheme, that is $\theta \in [0, \frac{2\pi}{N})$, much like the first Brillouin zone for crystal momentum, without affecting transition probabilities between sites (see below). When N is large, the effect of θ on the spectrum is clearly minor. The transition probabilities associated with this chiral quantum walk on a cycle are:

$$P_{j\to k}(t) \;=\; \frac{1}{N^2}\left|\sum_{s=1}^{N} e^{2i\left[\frac{\pi(k-j)s}{N}-t\cos\left(\theta+\frac{2\pi s}{N}\right)\right]}\right|^2 \tag{7.33}$$

We again emphasize that, by virtue of quasi-gauge invariance, any other phases configuration on the cycle with phases ϕ_j along each edge $(j, j+1)$ is related to the configuration with homogeneous phase by simply putting $\theta = \frac{1}{N}\sum_{j=1}^{N}\phi_j$ in Eq.(7.33): transition probability between localized states and all the other quantities that we will be interested in attain the same value for both configurations. Another, still equivalent option is to put a phase of $N\theta$ on just one edge: the choice does not matter, only the orientation should respect the sign of the total phase. In the large cycle limit $N \to \infty$, then, transition probabilities will be the same as those computed for a path graph, at least up to a timescale proportional to $N/2$: indeed the only chiral edge can be placed at the opposite end of the cycle with respect to the starting vertex and the respective phase cannot influence the evolution before the amplitude has had the time to reach that edge. Thus we have:

$$\lim_{N\to\infty} P_{j\to k}(t) \;=\; |J_{|k-j|}(2t)|^2 \tag{7.34}$$

where $J_n(x)$ is the n-th Bessel function. The same result can also be derived directly from Eq.(7.33).When the probability will have reached the opposite side of the cycle with respect to the initial vertex,then phase-dependent interference can happen. Since the initial propagation on the cycle is known to be ballistic with velocity 2, in order to reach the opposite side of the cycle the walker will take a time approximately given by $\tau = N/4$, which therefore is also the time it takes for $\theta \neq 0$ to have some appreciable effect on the on-site probabilities. However, this prediction can be inaccurate for small cycles, because of the non-negligible tails of the ballistic wavefronts.

To understand the influence of phases on quantum transport on the cycle after this minimal time, let us first consider the standard $\theta = 0$ case. We previously argued that the probability of finding the walker on each site except the starting one (and the one opposite to it in the case of even cycles) cannot exceed $\frac{1}{2}$ at any time, because of the spatial symmetry of the non-chiral CTQW Eq.(5.33). Additionally, if N is even the cycle is a bipartite graph and we know that any θ will still preserve the spatial symmetry.

The only vertex to which the transport probability can be higher than $\frac{1}{2}$ for even cycles is the opposite one to the starting vertex, which is indeed interesting as a target for transport. At fixed time, the optimal phase to maximize the probability $P_{j\to j+N/2}(t)$ can be different from zero. However, it seems that the highest peaks of $P_{j\to j+N/2}(t)$ for a wide range of times are always attained for $\theta = 0$. This can be appreciated in Fig.7.3, where we plotted the transition probabilities between opposite sites vs. time for cycles of 8 and 10 sites and for different values of θ. We restricted the plotting region to probability values in $[0.7, 1]$, choosing 0.7 as a cutoff defining the accepted transport events.

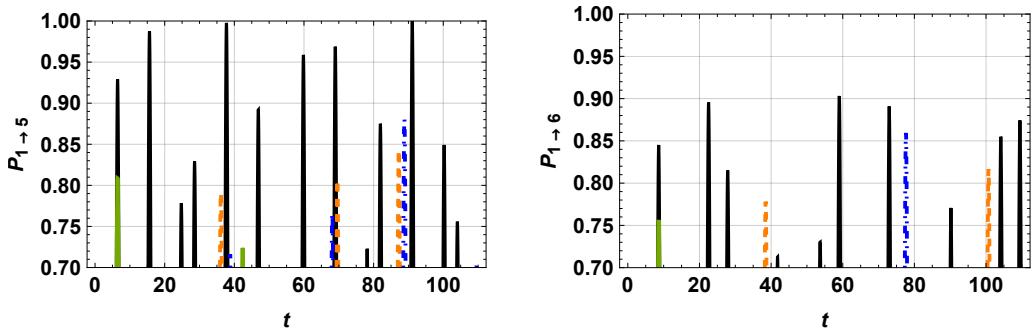

Figure 7.3: Transition probability from initial site 1 to site 5 of a 8-cycle (left) and to site 6 of a 10-cycle (right) as functions of time and for different values of the phases. The non-chiral $\theta = 0$ case is plotted in black. For the 8-cycle the other phases are $\theta = 0.04$ (solid light green), $\theta = 0.13$ (dashed orange) and $\theta = 0.23$ (dotted-dashed blue). For the 10-cycle we chose $\theta = 0.027$ (solid, light green), $\theta = 0.13$ (dashed, orange) and $\theta = 0.28$ (dot-dashed, blue). Notice that the probability axis plot range is restricted to $[0.7, 1]$ because it is the most informative region for quantum transport.

These observations suggest that chiral CTQWs provide no advantage for optimal quantum transport on even cycles over their non-chiral counterparts. Nevertheless, we highlight the fact that $P_{j\to j+N/2}(t)$ can be completely suppressed at all times by choosing $\theta = \pi/N$ (or, equivalently, a phase of π on a single, generic link), a phenomenon that, together with the unbroken reflection symmetry for generic θ, has already been attributed to the fact that even cycles are *bipartite* graphs. We notice that, in the context of excitonic transport in biochemical complexes, this sets a possible prediction to be contrasted with observations, since finding a cycle-like structure with an even number of units could exclude that complex couplings play a role.

When the cycle is odd, instead, there is no opposite vertex to the starting one. At a variance with even cycles, almost every $\theta \neq 0$ now breaks the spatial symmetry with respect to the starting point, opening the possibility for enhanced quantum site-to-site transport. In Fig.7.4 we plotted the transition probabilities from site 1 to various other sites of a 7-cycle for $\theta = \frac{\pi}{14}$ (a). For any other value of the phase in the relevant range $[0, \frac{2\pi}{7}]$, in each case the highest peaks are considerably lowered, and the same happens for all other examined odd values of $N \geq 7$. It seems that the phase $\frac{\pi}{2N}$ is *resonant*, although the pattern is very disordered and small changes in the precise value of the phase induce considerable shifts in the peaks at long times, which is a signature of chaos. This is illustrated by Fig.7.4 (b), where we displayed the same set of transition probabilities again for C_7, but with a slightly off-resonant value of $\theta = 0.21$, to be compared with the resonant value of $\frac{\pi}{14} \simeq 0.22$. We stress that all the peaks displayed by odd cycles are

entirely due to the introduction of the phase degree of freedom, since *non-chiral* CTQW on odd cycles starting in a localized state will never be found with probability higher than $\frac{1}{2}$ on other sites.

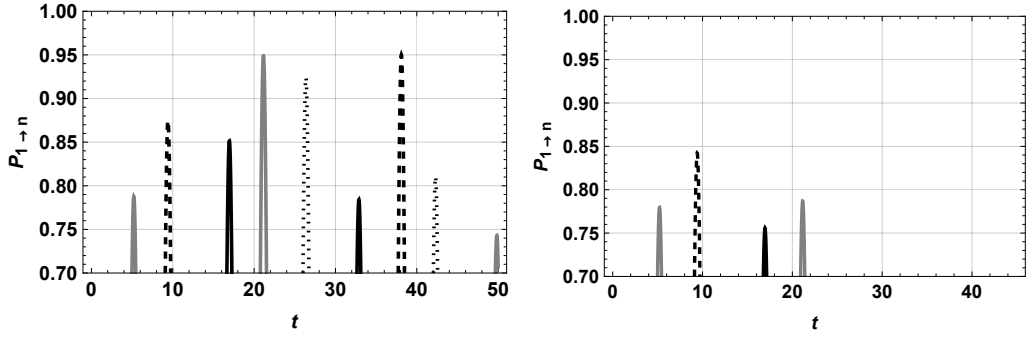

Figure 7.4: Transition probability from initial site 1 to site n on a 7-cycle as functions of time, for the resonant phase value $\frac{\pi}{14}$ and for slightly off-resonant phase value 0.21. Different stroke styles represent different target sites: $n = 2$ in solid black, $n = 3$ in gray, $n = 4$ in dashed black and $n = 5$ in dotted black.

We will now see how the quantum-classical distance captures these results for the prototypical example of cycle graphs and how it can indicate the optimal phase, putting order to the opaque relationship between the values of θ and the transition probabilities. A reasonably compact expression for the quantum-classical distance at time t as a function of θ can be derived from Eq.(7.33) and the standard formulas for a continuous-time classical random walk on cycles:

$$\mathcal{D}_{QC}(t;\theta) := 1 - \frac{e^{-2t}}{N^2} \times \sum_{k,s=1}^{N} \exp\left[2t\cos\frac{2\pi k}{N} + \right. \\ \left. - 4it\sin\left(\theta + \frac{\pi(2s+k)}{N}\right)\sin\frac{\pi k}{N}\right]. \tag{7.35}$$

Since the dynamics is the same independently of the starting vertex, the expression for the quantum-classical distance can be computed for any localized initial state $|j\rangle$ and maximization over j is not necessary. It is a simple task to show that

$$\mathcal{D}_{QC}\left(t;\frac{\pi}{N}+\phi\right) = \mathcal{D}_{QC}\left(t;\frac{\pi}{N}-\phi\right)$$

and, when N is odd, also

$$\mathcal{D}_{QC}\left(t;\frac{\pi}{2N}+\phi\right) = \mathcal{D}_{QC}\left(t;\frac{\pi}{2N}-\phi\right).$$

Therefore, when N is even $\mathcal{D}_{QC}(t;\theta)$ attains all its possible values, at fixed t, for θ in the range $[0,\frac{\pi}{N}]$ and when N is odd for θ in the range $[0,\frac{\pi}{2N}]$. Already for modestly sized cycles ($N \geq 7$), the variations of $\mathcal{D}_{QC}(t)$ with θ are very small. Indeed one can expand $\mathcal{D}_{QC}(t)$ around $t = 0$ and notice that all terms up to order $N-1$ in t when N is even, and up to order $2N-1$ in t when N is odd, are independent of θ, while an oscillatory θ

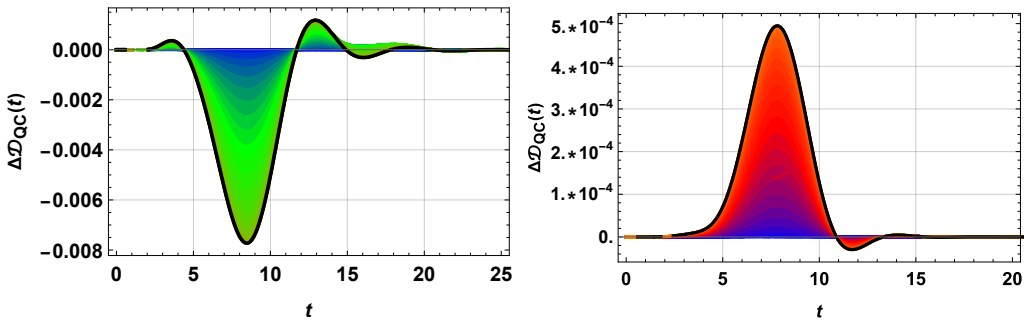

Figure 7.5: Gain in quantum-classical distance $\Delta\mathcal{D}_{QC}(t)$ vs. time for a 10-cycle (left) and a 7-cycle (right), with respect to the quantum-classical distance for the standard evolutions generated by the Laplacian (blue, horizontal baseline in both plots). For the 10-cycle phases are increasing in the relevant range $[0, \frac{\pi}{10}]$ with a corresponding color hue from blue to green (from darker to lighter shade). For the 7-cycle the relevant range of phases is $[0, \frac{\pi}{14}]$ and θ increases from blue to red hues (from darker to lighter shade). Notice that the maximum in time of $\mathcal{D}_{QC}$ is not necessarily related with the time at which transport occurs, because the former quantity is also influenced by the time scale of the classical evolution.

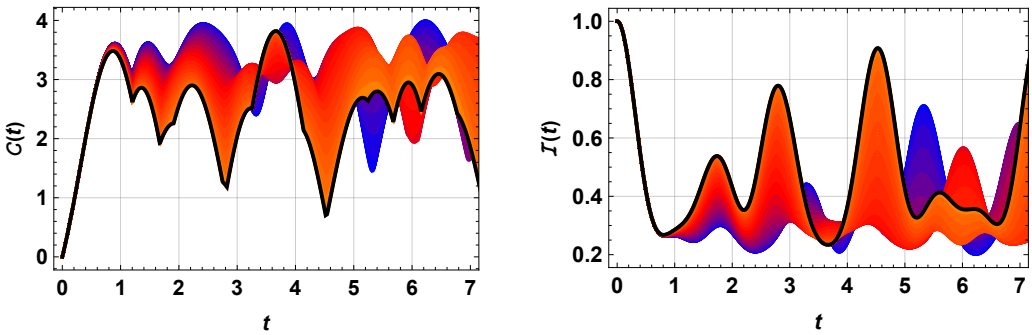

Figure 7.6: Coherence and IPR vs. time for a 5-cycle and for different values of $\theta \in [0, \frac{\pi}{10})$, corresponding to color shades from blue to orange (from darker to lighter shade). The black (solid) line represents the resonant phase $\frac{\pi}{10}$.

dependence starts at higher orders. Because of this feeble θ dependence, we considered the difference between the quantum-classical distance with phase θ and the same quantity with zero phase, i.e. $\Delta\mathcal{D}_{QC}(t;\theta) = \mathcal{D}_{QC}(t;\theta) - \mathcal{D}_{QC}(t;0)$. As can be appreciated in Fig.7.5, this quantity brings a clear order to the irregular behaviour that was seen in the transition probabilities. For even cycles, $\mathcal{D}_{QC}(t;\theta) - \mathcal{D}_{QC}(t;0)$ has a negative, significant dip at approximately the same time for all values of θ, and it is the lowest at $\theta = \frac{\pi}{N}$, the phase which fully suppresses transport to the opposite vertex; conversely, for odd cycles we find that the same quantity *peaks* at approximately the same time, with the highest peak for $\theta = \frac{\pi}{2N}$, again the resonant phase, which optimizes transport for odd cycles. Moreover, the heights of the peaks are monotonically increasing in absolute value with $\theta \in [0, \frac{\pi}{2N})$, while the depths of the dips for even N are monotonically increasing with $\theta \in [0, \frac{\pi}{N})$. Therefore we see that finding the global maximum of $\Delta\mathcal{D}_{QC}$, with respect to θ and t, at a maximum (resp. minimum) of $\mathcal{D}_{QC}(t;\theta)$ in time, correctly spots the least

classical (resp. the nearest to classical) evolution among all possible chiral CTQW on the same cycle. Intuitively, we can understand the reason of its effectiveness: $\mathcal{D}_{QC}(t)$ is maximized for the quantum evolution that departs the most from the classical one, the latter being slowly and diffusively spreading towards the homogeneous distribution. Therefore, a chiral CTQW which evolves to nearly localized states and could be optimal for transport, will also maximizes $\mathcal{D}_{QC}(t)$. To further support this claim, we can look at the phase dependence of the functions $\mathcal{C}(t)$ and $\mathcal{I}(t)$, as in Fig.7.6 for a 5-cycle. Again, the resonant phase (black line, $\theta = \frac{\pi}{10}$) is associated with higher localization (lower coherence and higher IPR values) especially at short times, and also the overall trend seen for the quantum-classical distance is respected at least at short times, with values of θ close to 0 leading to the opposite behavior. We conclude by noting that some results about so-called *pretty good universal transport* for chiral CTQW on cycles with a prime number of vertices are known in the mathematical literature [357], although they have little role in a physical context since no bound on the time needed for transport is considered there.

7.2.4 Complete graphs

To test the behaviour of the DQC at the extremes, let us now take on the complete graphs, having maximal connectivity as opposed to cycles. For them, just a minority of phases of H can be ignored by quasi-gauge invariance: according to the general results from the previous chapter, we expect $|E| - N + 1 = \frac{N(N-3)}{2} + 1$ free phases parameters, growing quadratically in the number of vertices.

We already know that the action of phases can radically change the dynamics on complete graphs when starting from a localized state given that their non-chiral evolution, being sedentary, is equivalent to that of a star graph S_N starting at the core vertex [298, 355]while the swift phases configuration makes them evolve away from it at the quantum speed limit. In other words, if the Hamiltonian is real, many links of the complete graph can be eliminated without changing the evolution. This is intuitive by symmetry arguments: since all vertices are connected to the initial one, the amplitudes in all the vertices except the first will be equal at all times and probability will never flow through links that connect these vertices, therefore they are irrelevant for the dynamics.

We initially investigate the effect of randomly added phases on the quantum-classical distance, 1-norm of coherence and IPR. Because of the large number of free parameters, we adopt a few selected strategies to better explore the parameters space. In Fig.7.7 a comparison between the averaged coherence and IPR for different phase choices on the complete graph with $N = 13$ is shown. The blue curves corresponds to the non-chiral choice with $\mathrm{H} = \mathrm{L}$. The orange curves are averages over 400 configurations where a single randomly generated phase $e^{i\phi}$ is applied to all the links of the complete graph in the direction $j \to k$ for $k > j$. We infer that a typical phase different from $\phi = 0$ attached to each link increases the average coherence and decreases the IPR with respect to $\mathrm{H} = \mathrm{L}$. If, instead, we distribute with equal probabilities two random phases $e^{i\phi_1}, e^{i\phi_2}$ among the edges in the given direction, there is an even greater increase in the coherence and decrease in the IPR (dark green curves, again averaging over 400 random configurations). Finally, if an independent, randomly generated phase is applied to each link independently, the resulting average behaviour is described by the black curves. Notice that now the order is irrelevant, since all orders will be explored if the phase of each link is independent and sampled in the full range $[0, 2\pi)$. Clearly this rule entails all the

previous ones, but the *typical* configuration contributing to the black curve will be one in which there is no correlation between phases on different links and there is essentially full *disorder* in the phase degrees of freedom of the Hamiltonian. Now the IPR stabilizes to the lowest values between the examined ones, while the coherence is maximal with respect to the previous cases. These two quantities therefore hints at a *phase-disorder-induced delocalization* in the evolution of a localized state on a complete graph [2]. These results were checked also for $N = 16$ and $N = 17$ and appear robust irrespective of the number of sites. We stress that these are not artifacts of the averaging, since the quantities are all positive and the black curves clearly set apart from the other trends: they thus display the *typical* behaviour of a random phase configuration, and not just the average trend.

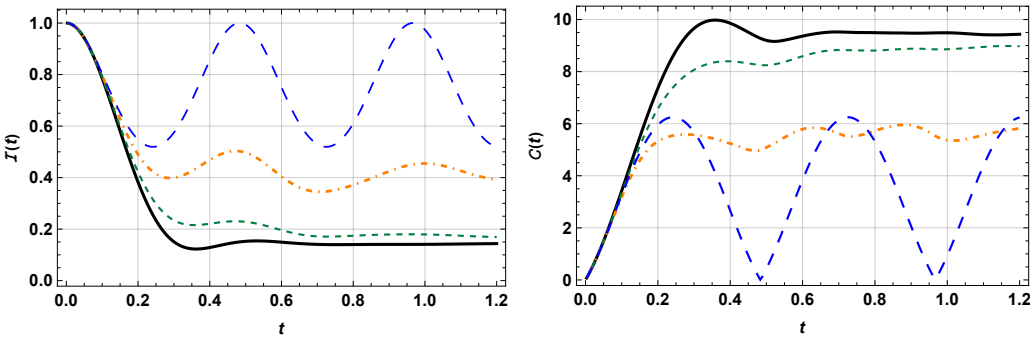

Figure 7.7: IPR $\mathcal{I}(t)$ and coherence $\mathcal{C}(t)$ vs. time of a continuous-time quantum walker on a complete graph with $N = 13$ sites with localized initial condition. The standard evolution generated by $\mathrm{H} = \mathrm{L}$ is depicted by the blue curves (spaced-dashed). The orange curves (dotted-dashed) are averages over 400 Hamiltonians with a single, randomly generated phase attached to all links in the "positive" direction. The dark-green curves (dashed) resulted from the average of 400 Hamiltonians with two, independent randomly generated phase randomly attributed to each link in positive direction. Black curves (solid) correspond to the random assignment of independent phases to each link, still averaged over 400 runs.

Looking now at $\Delta\mathcal{D}_{QC}$, the difference between the quantum-classical distance for these different averaged evolutions and the quantum-classical distance for the reference, non-chiral case $\mathrm{H} = \mathrm{L}$ (Fig.7.8, same color code), we see a glaring relation between this quantity and IPR or coherence: any addition of non-zero phase seems to add to the quantum-classical distance (at least *on average*), and the increase goes along with the higher delocalization, as signaled by large values of the coherence and low values of the IPR. Mind that, strictly speaking, we are considering the quantum-classical distance *at fixed initial state* $|j\rangle$, since the full $\mathcal{D}_{QC}(t)$ would require maximization over all initial states at each time, once H and its phases have been specified. A crucial point here is the correlation between $\Delta\mathcal{D}_{QC}$ and localization (high values of $\mathcal{I}$ and low values of $\mathcal{C}$), which is opposite with respect to the relation found for cycle graphs. Here those dynamics leading to less localized states are more quantum, according to the quantum-classical distance. This fact could be partially predicted from the short-time expansion of Eq.(7.25)

[2] Here by *phase disorder* we mean the randomness in the choice of phases for each link, much like the disorder of the on-site potential in Anderson localization, and *not* the disorder induced by uncertainty on the values of the Hamiltonian's parameters.

which is not monotonic in the connectivity d_j, unlike the expansions for $\mathcal{C}(t)$ and $\mathcal{I}(t)$ to the same order in t. This is another evidence that $\mathcal{D}_{QC}(t)$ stands out against other dynamical quantities in the successful recognition of optimal chiral quantum evolutions. Of course, the relevant task is graph-dependent, being either an hitting-type or a mixing-type task, but remarkably the quantum-classical distance seems able to optimize the parameters in both scenarios.

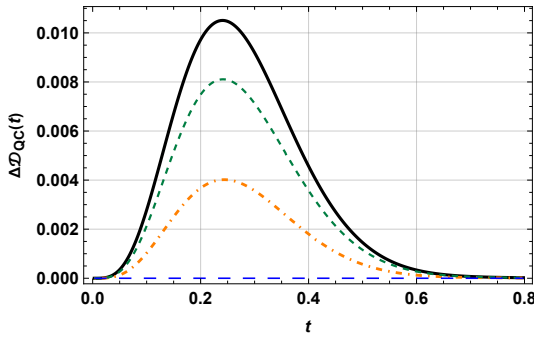

Figure 7.8: Difference $\Delta\mathcal{D}_{QC}(t)$ between the quantum-classical distances of the various, averaged chiral evolutions and the non-chiral H = L one, for a complete graph with $N = 13$ sites and localized initial condition of the CTQW. Color code and meaning as for Fig.7.7. The reference case with H = L is the base line in blue.

7.2.5 Optimization of the quantum-classical distance

Guided by these observations, the next natural step is to maximize $\mathcal{D}_{QC}(t)$ over all possible phases degrees of freedom in H for the complete graph. This has to be performed at a fixed time, that we chose afterwards by identifying the time at which $\mathcal{D}_{QC}$ attains its maximum, as suggested by our analysis of the cycle grpahs; it seems, however, that the resulting optimal configuration is time-independent for complete graphs (as suggested by Fig.7.8). Starting with random guesses, the optimization converges to different Hamiltonians each time. However, a common feature of these optimal matrices is easy to spot:

1. The first column of an optimal H_O on the complete graph of N sites is orthogonal, with respect to the Hermitian product on $\mathbb{C}^N$, to all the rows of H except the first one (assuming that all the diagonal elements have been fixed to 0, without loss of generality)

The first column is singled out because of the choice of $|1\rangle$ as the (arbitrary) initial condition. Let us call $\vec{h}$ the first column of an optimal Hamiltonian H_O. Because of the topology and the choice of diagonal elements, its entries will be:

$$h_1 = 0\,, \quad h_j = e^{i\phi_j} \;\; \forall j = 2, ..., N \tag{7.36}$$

and, since H_O is Hermitian, its first row will be $\left(\vec{h}^*\right)^T$, so that the scalar product between the first row and the first column is $N-1$. Let us denote by $\vec{e}_1$ the localized state $|1\rangle$ in matrix notation, which is the first vector of the canonical basis. Then we have:

$$\begin{aligned} \mathrm{H}_O^{2n} \cdot \vec{e}_1 &= (N-1)^n \vec{e}_1 \\ \mathrm{H}_O^{2n+1} \cdot \vec{e}_1 &= (N-1)^n \, \mathrm{H}_O \cdot \vec{e}_1 = (N-1)^n \vec{h} \end{aligned} \tag{7.37}$$

The evolution of the initial state localized at site 1 then follows immediately:

$$\begin{aligned} e^{-it\mathrm{H}_O}\cdot\vec{e}_1 \;&=\\ &= \cos[\sqrt{N-1}t]\vec{e}_1 - \frac{i}{\sqrt{N-1}}\sin[\sqrt{N-1}t]\vec{h} \end{aligned} \tag{7.38}$$

Notice that $\vec{h}$, as a vector of amplitudes, represents a state which is balanced between all sites except the first, to which it is orthogonal. Therefore, the evolution of Eq.(7.38) is a cyclic rotation between the initial state localized at site 1 and an equally distributed state over all other sites except the initial one, necessarily passing through an intermediate flat state:

$$|f\rangle \;=\; \frac{1}{\sqrt{N}}\Big(|1\rangle \;+\; \sum_{j=2}^{N} e^{i\phi_j}|j\rangle\Big) \tag{7.39}$$

where the amplitude to find the walker in any site of the graph is equal to $N^{-1/2}$. The time needed to reach $|f\rangle$ for the first time is given by:

$$t_f \;=\; \frac{1}{\sqrt{N-1}}\arccos\frac{1}{\sqrt{N}} \tag{7.40}$$

while the time needed to reach the state $|\vec{h}\rangle \;=\; \frac{1}{\sqrt{N-1}}\sum_{j=2}^{N} h_j|j\rangle$ associated with the vector $\vec{h}$ and orthogonal to the initial state $|1\rangle$ is:

$$t_h \;=\; \frac{\pi}{2\sqrt{N-1}}. \tag{7.41}$$

It should be emphasized that $|f\rangle$, as for any flat state, has maximal coherence value of $N-1$ and minimal IPR value of $\frac{1}{N}$. Exploiting the simple structure of these optimal evolutions, an exact expression for their quantum-classical distance can also be derived:

$$\mathcal{D}^{O}_{QC}(t) = 1 - \frac{1-e^{-Nt}}{N} - e^{-Nt}\frac{1+\cos[2\sqrt{N-1}t]}{2}. \tag{7.42}$$

7.2.6 Search to the quantum speed limit without an oracle

From Condition 1 one can appreciate that the optimal evolution singled out by the maximization of the quantum-classical distance is precisely the *swift chiral quantum walk* on a cone graph with apex in $|1\rangle$: indeed, the complete graph with N vertices is a cone over a complete graph with $N-1$ vertices with respect to any one of its N initial vertices taken as the apex. In the appendix of [351] we provide an explicit construction of the swift configuration for all complete graphs.

Let us now pick $|\vec{h}\rangle \;=\; \frac{i}{\sqrt{N-1}}\sum_{j=1}^{N}|j\rangle$, i.e. all the phases of the first column of H_O equal to i, which can be done starting from any swift chiral Hamiltonian with apex in 1 by applying a quasi-gauge transformation. By evolving $|1\rangle$ for a time t_f as in Eq.(7.40), we find:

$$e^{-i\mathrm{H}_O t_f}|1\rangle \;=\; |f\rangle \;:=\; \frac{1}{\sqrt{N}}\sum_{j=1}^{N}|j\rangle \tag{7.43}$$

so that the final state is the flat state with zero relative phases. Reversing this evolution, we have $e^{i\mathrm{H}_O t_f}|f\rangle = |1\rangle$: in other words, the evolution generated by $-\mathrm{H}_O$ starting from

the flat state $|f\rangle$ and for a time t_f is a *solution to the search problem* with target vertex 1 and it reaches the respective *quantum speed limit*. The oracle of Grover's algorithm has been replaced by a swift phases configuration.

Since coherence and IPR for a localized initial condition are quasi-gauge invariant quantities, the blue curves in Fig.7.7 imply that it is not possible to reach a flat state from a localized one with any H which is quasi-gauge-equivalent to L. Thus, Condition 1 and also our result for the search problem *require* a *nontrivial phases configuration*. It is interesting to compare our search time t_f with Grover's time and with the quantum speed limit for this evolution. We previously saw that Grover's time for the complete graph K_N is $t_G = \frac{\pi}{2\sqrt{N}}$; for any $N > 2$, then, $t_f < t_G < t_h$, therefore our search Hamiltonian is *faster* than Grover's one and it does not require an oracle. Of course, in order for this result to hold, a bias has to be present in the *phases* of our optimal H so that the target vertex can be singled out during the evolution. This bias is in fact embodied by the swift CTQW condition 1. In particular, one can contrast this result with the one in [358], where the oracle was preserved but only unbiased choices of phases were considered, concluding that no improvement of search time was possible. We will now show that t_f is actually the quantum speed limit for our task[3]. Using Eq.(1.29), we have again that the variance $\Delta\hat{\mathrm{H}}$ does not depend on the phases and it is equal to $\sqrt{N-1}$, as we observed for swift quantum walks. Then, with $|a\rangle = |f\rangle$ and $|b\rangle = |1\rangle$ the first quantity inside the max of Eq.(1.29):

$$\frac{\arccos|\langle 1|f\rangle|}{\Delta\hat{\mathrm{H}}} = \frac{1}{\sqrt{N-1}}\arccos\frac{1}{\sqrt{N}} = t_f \tag{7.44}$$

Since we already know that t_f cannot be smaller than τ_{QSL}, the max in the definition (1.29) of τ_{QSL} and the result of Eq.(7.44) already imply that $\tau_{QSL} = t_f$. This was verified by computing the second quantity in Eq.(1.29) and checking that it is always smaller than the first for $N > 3$ [4]. It can be shown that τ_{QSL} is also the quantum speed limit for Grover's Hamiltonian. Indeed, we highlight that $\Delta\hat{\mathrm{H}}$ attains its largest value for the complete graph, among all the topologies that connect N vertices in a simple, connected graph. We conclude that our construction exploits phases to achieve quantum search between N orthogonal states without an oracle and in the least possible time allowed by quantum mechanics, without altering the on-site energies at will. We remark that the scaling behaviour $O(N^{-1/2})$ of Grover's time is known to be already the best one, and indeed our search time t_f follows the same asymptotic scaling for large N. The construction that we provided, on the other hand, achieves the goal of optimizing the constant pre-factor, which is sub-optimal for Grover's algorithm. The comparison in log-scale is shown in Fig.7.9.

To further illustrate the differences between the evolution induced by Grover's Hamiltonian H_G and the optimal solution H_O that we found, we plotted in Fig.7.10 the time behavior of the quantities $\mathcal{C}(t), \mathcal{I}(t)$ and also the gain in quantum-classical distance $\Delta\mathcal{D}_{QC}$ with respect to the reference $\mathrm{H} = \mathrm{L}$, again for a complete graph with $N = 13$ sites and starting at vertex $|1\rangle$. Black curves depict the evolution generated by H_O, while Grover's evolution is in light-green. The blue curves correspond to the non-chiral $\mathrm{H} = \mathrm{L}$ choice. The insets show a magnification of the regions where the relevant times happen: the

[3] Previously we only showed that the swift construction achieves the quantum speed limit at fully leaving the initial vertex.

[4] The check was performed numerically because E_0 depends on the phases in a non trivial way, so that the second quantity is harder to compute in general.

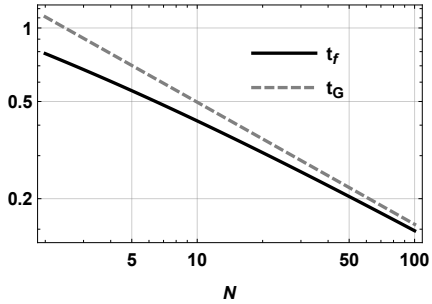

Figure 7.9: Optimal search time exploiting phases t_f (black line) and Grover's time t_G as functions of the number of sites N, with log scale on both axes. t_f is always smaller than t_G, and it is also equal to the quantum speed limit τ_{QSL}

red circle indicates the time t_f, the red square designates time t_G and finally the rotated square indicates t_h.

Importantly, the gain in quantum-classical distance with respect to the non-chiral H = L choice is also maximal for the evolution generated by H_O, even when compared with Grover's evolution, a non obvious fact since the maximization was performed without considering diagonal degrees of freedom. Moreover, the optimal evolution outperforms the best evolutions found in Fig.7.7 by randomly generating phases according to IPR and coherence, and correspondingly $\Delta\mathcal{D}_{QC}$ is in fact higher at all times.

Condition 1 can indeed be fulfilled by the swift chiral quantum walk construction, but it should be clear that in this section it arose solely from the maximization of the quantum-classical distance, thereby corroborating the power of this method.

To conclude with this class of examples, let us remark that with non-chiral CTQWs on complete graphs with N vertices it is impossible to observe *instantaneous uniform mixing* [359], where the walker completely delocalizes to a uniform superposition of all basis states at a certain instant during its evolution, except for $N = 2, 3, 4$. Our result shows that, with the generalization to *chiral* quantum walks, but retaining unitarity, instantaneous uniform mixing is achievable on *any* complete graph in a remarkably short time t_f given by Eq. (7.40), which is $O(1/\sqrt{N})$ for large N. Importantly, this is a quadratic speedup with respect to the $O(1)$ scaling of mixing on hypercube graphs [269] [5] and it also holds for generic number of sites, whereas the hypercube protocol applies only if N is a power of 2.

7.2.7 Cube graph

As remarked before, on the hypercube graphs perfect state transfer between opposite vertices [268] and instantaneous uniform mixing [269] are achieved by the standard CTQW: we thus expect to find no improvement with chiral configurations on them. Notice also that, once the phases degrees of freedom are taken into account, instantaneous uniform mixing and the time-reversed process, which is quantum search without an oracle, are achieved by quasi-gauge equivalent Hamiltonians, since the hypercube

[5] In the literature on quantum algorithms, it is common wisdom to rescale the adjacency matrix of regular graphs by their connectivity to compare evolution times. With that convention, the time needed to achieve uniform mixing with the scaled adjacency matrix on hypercube graphs is $O(N)$, while the time to perform the same task on complete graphs with our *chiral* protocol is $O(\sqrt{N})$.

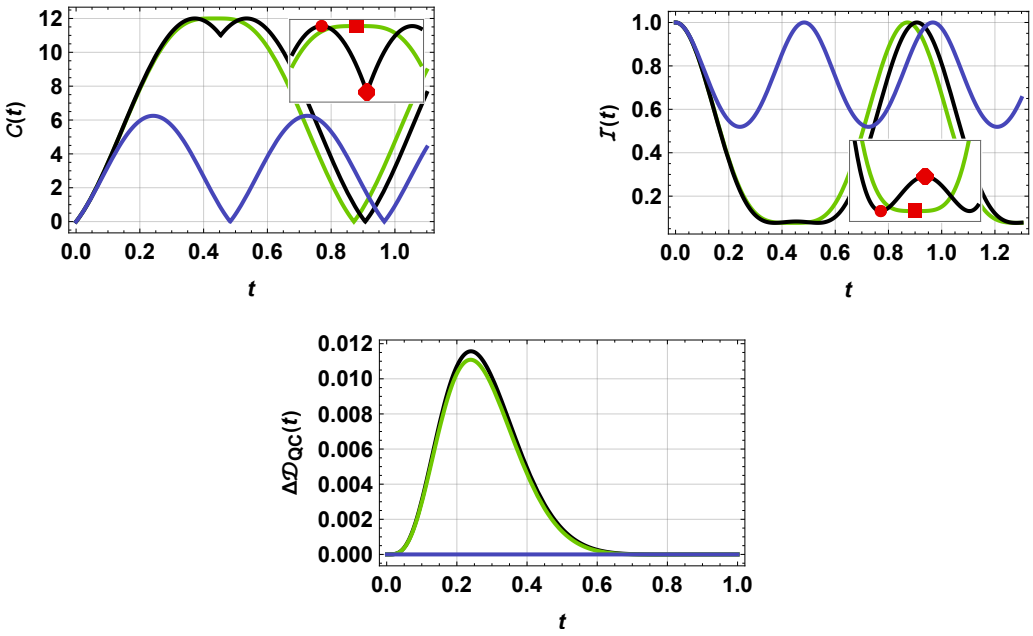

Figure 7.10: Comparison for coherence $\mathcal{C}(t)$, IPR $\mathcal{I}(t)$ and gain in quantum-classical distance $\Delta\mathcal{D}_{QC}(t)$ for evolutions generated by H_O (black curves), H_G (light-green curves) and $\mathrm{H} = \mathrm{L}$ (blue curves) for a complete graph of $N = 13$ sites and starting with a localized state. The insets in plots of $\mathcal{C}(t)$ and $\mathcal{I}(t)$ show a magnification of the region for $0.3 < t < 0.5$, where times t_f (red circle), t_G (red square) and t_h (rotated red square) are located.

graphs are bipartite and one can find a quasi-gauge transformation sending any chiral Hamiltonian H on them to $-\mathrm{H}$. Also, the $\mathcal{D}_{QC}$ will attain the same value in both cases and it is for all purposes equivalent to the initial non-chiral CTQW. In accordance with these observations, the optimization of the quantum-classical distance over the phases degrees of freedom on the cube graph does not provide better options: the best case for quantum search and uniform mixing is already the non-chiral one. On the other hand, by minimizing $\mathcal{D}_{QC}(t)$ at short times, one finds a choice of phases that completely suppresses transport to half of the vertices of the cube, more precisely to those that are not connected to the starting one.

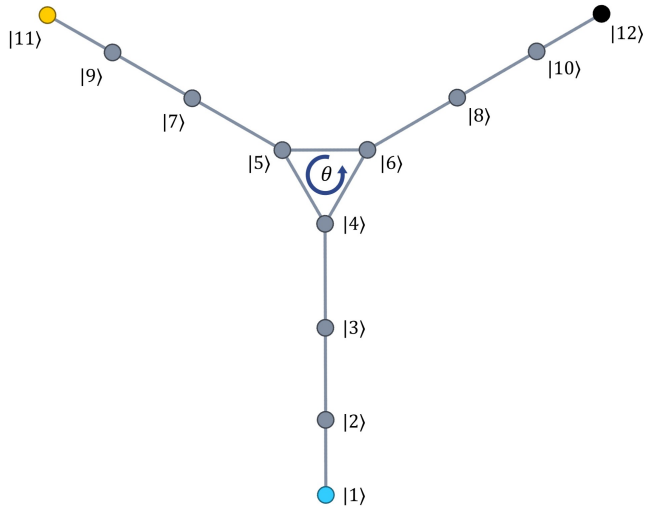

Figure 7.11: Graph of the quantum switch with 12 sites. The walker starts at site 1 (in light-blue). The target is site 11, in yellow, while its symmetrical, site 12, is represented in black. The central phase θ, oriented as indicated by the circular arrow, enhances transport from the starting site to the target for the resonant value $\theta = \pi/2$, while at the same time suppressing the transport probability $1 \to 12$.

7.3 The Quantum Switch Graphs

In this section we will consider graphs like the one depicted in Fig.7.11, which are seldom referred to as *quantum switches* [351, 352], as paramount examples of directional quantum transport with chiral continuous-time quantum walks. Since the graph is planar and there is a single loop, just one phase will affect transition probabilities between sites. Calling θ the total phase in the central loop, we will distribute it on oriented edges $(5,4)$, $(6,5)$ an $(7,6)$ such that each of them is associated with an entry equal to $e^{i\frac{\theta}{3}}$ in the upper half of the chiral Hamiltonian. If $\theta = 0$ and the diagonal elements respect the rotational invariance of the graph, clearly:

$$P_{1\to 11}(t) \;=\; P_{1\to 12}(t) \;\leq\; \frac{1}{2} \tag{7.45}$$

at all times because of the spatial symmetry of Eq.(5.33) that we discussed in the context of non-chiral quantum walks. Our first aim will be to explore the effect of θ in achieving *directional transport*, i.e. the strongest possible imbalance between $P_{1\to 11}$ and $P_{1\to 12}$ at the first time instant in which one of the two transport probabilities reaches its first maximum in time.

7.3.1 Quantum-classical distance for the quantum switch graphs

These graphs were already considered in [330] as examples of the advantage provided by *chiral* quantum walks over the ones defined by the Laplacian or the adjacency matrix. Indeed, it was shown that a resonant value of $\theta = \frac{\pi}{2}$ suppresses transport from vertex 1 to vertex 12, with reference to Fig.7.11, while enhancing transport from vertex 1 to

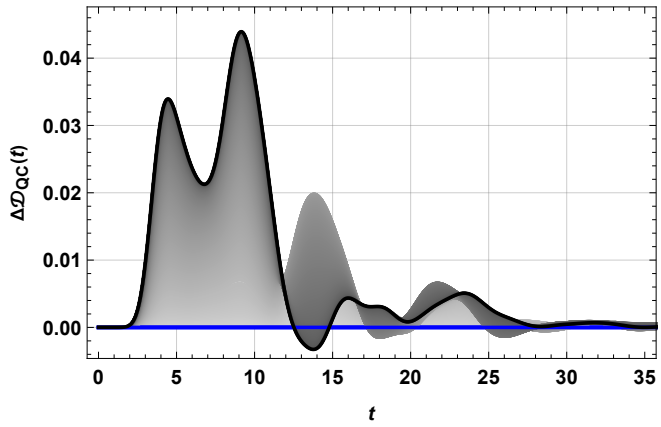

Figure 7.12: Difference between $\mathcal{D}_{QC}$ for the adjacency matrix of the 12-sites quantum switch with an adjoined phase and the same quantity for the standard adjacency matrix. The value of θ ranges from 0 to $\frac{\pi}{2}$ for increasingly darker shades of gray. The black line results from the resonant phase $\theta = \frac{\pi}{2}$ and the blue baseline (horizontal) is the non-chiral evolution.

vertex 11. Notice that the quantum switch graphs are non-regular, meaning that the connectivity is not the same for all sites and the Laplacian or the adjacency matrix of the graph generate different quantum evolutions. Here we first consider the adjacency matrix A for a 12-sites switch and the corresponding chiral adjacency matrix $\tilde{\mathrm{A}}_\theta$, where the phase on the loop is assigned as prescribed above. In Fig.7.12 we again plot the difference between $\mathcal{D}_{QC}(t)$ for the Hamiltonian with such a phase and the same quantity without the phase. The value of θ is increasing between 0 and $\frac{\pi}{2}$ from light gray to black curves, and we checked that larger values of θ are redundant.

The comparison with coherence and IPR shows a similar relation to that seen for cycle graphs: more localized evolutions, leading to higher values of IPR and lower values of coherence, are associated with higher gains in $\Delta\mathcal{D}_{QC}$. The resonant phase $\theta = \frac{\pi}{2}$ is clearly identified as the black curve which maximizes $\Delta\mathcal{D}_{QC}$. It achieves a transport fidelity of ~ 0.77 to the target state $|11\rangle$ when starting in $|1\rangle$ in a time $t \sim 5$. Surprisingly, this transport probability is considerably higher than the value that would be reached in a comparable time range for a simple chain of 8 sites, i.e. if the third arm of the triangle, composed of vertices 6, 8, 10 and 12, were not there to begin with, if we assume the Laplacian as generator in this latter case.

When we take the Laplacian in place of the adjacency matrix as the starting point, instead, the result differs qualitatively. Now for any choice of the free phase, localization on one branch of the switch is never as effective as the previous case. Accordingly, $\mathcal{D}_{QC}$ attains lower values now and its variations with phases are smaller, favoring the non-chiral choice $\mathrm{H} = \mathrm{A}$ for quantum transport on this topology. This example also provides further motivation in favor of the use of the adjacency matrix in place of the Laplacian for CTQWs on finite, non-regular graphs. Indeed, while having the connectivities on the diagonal is natural if the differential form of the Laplacian has to be recovered in the continuum limit (without an additional potential field landscape), this request is not so meaningful for small, non-regular graphs that do not embody a discretization of a continuous space in any obvious way.

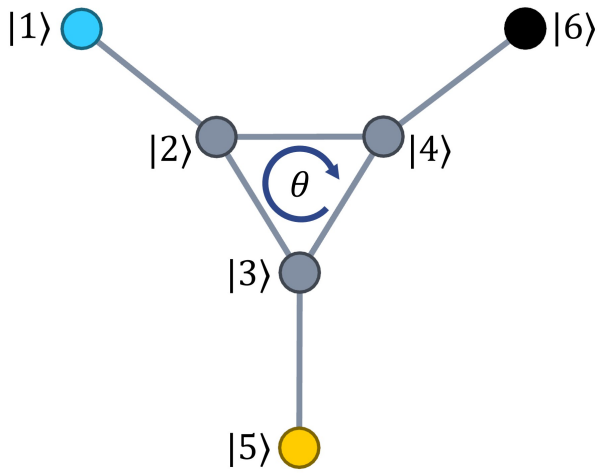

Figure 7.13: Graph of the quantum switch with 6 sites. The walker starts at site 1 (in light-blue). The target is site 5, in yellow, while its symmetrical, site 6, is represented in black. The central phase θ is defined and oriented as before.

7.3.2 Exact solutions for the quantum switch with 6 vertices

An explicit formula for the (chiral) transport probabilities on the quantum switch graphs requires the diagonalization of the corresponding chiral Hamiltonians H_θ, whose diagonal elements will be assumed to be symmetric with respect to the rotational symmetry of these graphs from now on. Since this $\mathbb{Z}3$ rotational symmetry is preserved even in presence of a phase θ on the central loop, we can build an ansatz for the eigenstates using the representation of this group. To fix the ideas, we will consider the simplest quantum switch, with just 6 vertices, as represented in Fig.7.13. The most general chiral Hamiltonian respecting the rotational symmetry on this graph is given by:

$$\mathrm{H}_{\theta,\gamma} = \begin{pmatrix} 0 & 1 & 0 & 0 & 0 & 0 \\ 1 & \gamma & e^{-i\frac{\theta}{3}} & e^{i\frac{\theta}{3}} & 0 & 0 \\ 0 & e^{i\frac{\theta}{3}} & \gamma & e^{-i\frac{\theta}{3}} & 1 & 0 \\ 0 & e^{-i\frac{\theta}{3}} & e^{i\frac{\theta}{3}} & \gamma & 0 & 1 \\ 0 & 0 & 1 & 0 & 0 & 0 \\ 0 & 0 & 0 & 1 & 0 & 0 \end{pmatrix} \tag{7.46}$$

apart for an overall rescaling factor, which is immaterial since we did not fix any time unit.

Using the rotational ansatz, the problem of diagonalizing $\mathrm{H}_{\theta,\gamma}$ reduces to the eigenproblem for a 2×2 matrix. In the end, the eigenvalues of the Hamiltonian are easily found as [352]:

$$E_n = S_n + (-1)^{\mathrm{mod}(n,2)}\sqrt{1+S_n^2} \tag{7.47}$$

$$S_n = \frac{\gamma}{2} + \cos\left[\frac{\theta}{3} + \frac{4\pi}{3}\mathrm{mod}(n-1,3)\right] . \tag{7.48}$$

and they are plotted in Fig.7.14 as functions of θ, for different values of γ. The corre-

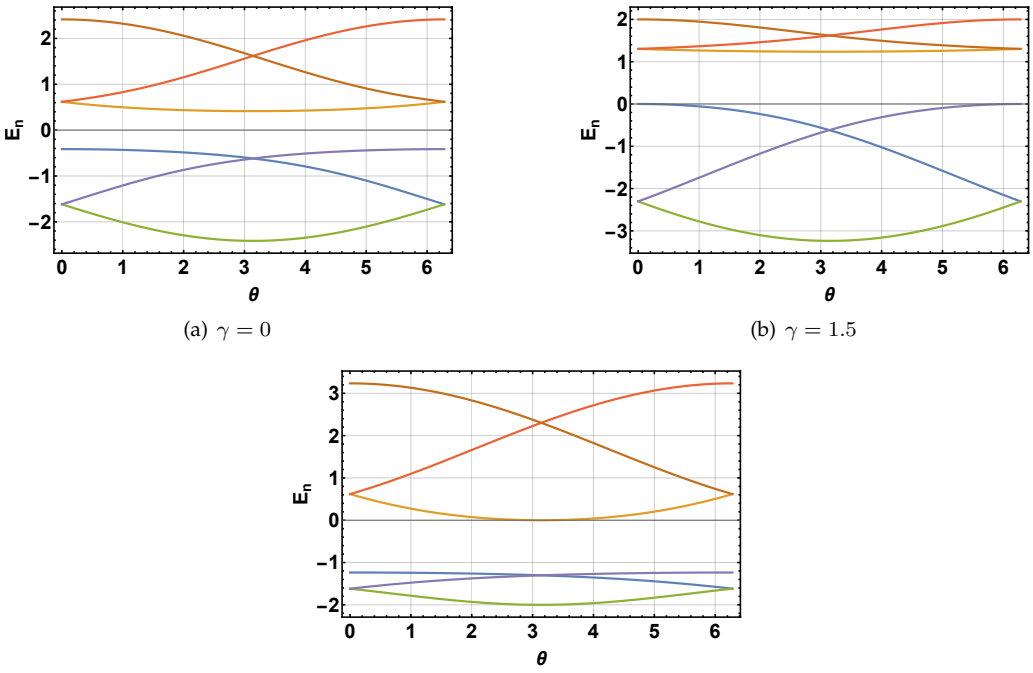

(a) $\gamma = 0$ (b) $\gamma = 1.5$

(c) $\gamma = -1.5$

Figure 7.14: Eigenvalues of $\mathrm{H}_{\theta,\gamma}$ as functions of θ for three different values of γ.

sponding eigenvectors are given by:

$$|E_n\rangle = \frac{1}{\sqrt{3(1+E_n^2)}} \begin{pmatrix} 1 \\ E_n \\ e^{i\frac{2\pi(n-1)}{3}} E_n \\ e^{i\frac{4\pi(n-1)}{3}} E_n \\ e^{i\frac{2\pi(n-1)}{3}} \\ e^{i\frac{4\pi(n-1)}{3}} \end{pmatrix}. \tag{7.49}$$

Interestingly, E_n^2 is exactly the ratio of the occupation probabilities of the inner sites (2, 3 and 4) over the outer sites (1, 5 and 6). The transport probability can be finally computed as:

$$P_{15}(t,\theta,\gamma) = \left| \sum_{n=1}^{6} e^{-iE_n t} \frac{e^{-i\frac{2\pi}{3}(n-1)}}{3(1+E_n^2)} \right|^2 \tag{7.50}$$

$$P_{16}(t,\theta,\gamma) = \left| \sum_{n=1}^{6} e^{-iE_n t} \frac{e^{-i\frac{4\pi}{3}(n-1)}}{3(1+E_n^2)} \right|^2 \tag{7.51}$$

For $t \simeq 2.629$ and $\gamma = 0$ we obtain $P_{1\to5}(t^*, \frac{\pi}{2}) \simeq 0.88$ and $P_{1\to6}(t^*, \frac{\pi}{2}) \simeq 3\cdot10^{-3}$, thus achieving a good performance of directional transport at short times. A more detailed discussion on the optimization of the γ parameter and the quantum metrology aspects of this problem can be found in [352].

7.4 Chirally-enhanced quantum transport on chain graphs

As a last example of the applications of chiral CTQWs, we shall consider how the addition of complex phases could enhance the transport probability in chain graphs. Our benchmark will be the path graphs P_n, whose transport probability from site 1 to site N at its first maximum in time asymptotically falls off with N as [281]:

$$J_N\left(\frac{1}{2}(N+0.8089N^{1/3})\right) \;\simeq\; 1.3499N^{-1/3} \tag{7.52}$$

As for the chain structures, we will limit our analysis to triangle chains, as in Fig.7.15. The choice of these specific structures is not fortuitous: in [353] we considered many ways of constructing chains out of smaller graph units with one of two loops, also exploring various ways to bridge them. In accordance to the result in [306], it was found that the graph units should be directly glued by one vertex, instead of bridging them with an additional edge which disfavors transport across it. Additionally, two types of chains that emerged as best candidates for quantum transport were precisely the triangle chain and the barred-square chain which, for transport purposes, reduces to the former upon a local change of basis inside each unit.

7.4.1 Definition of the quantum transport task

To be able to tackle the optimization of quantum transport on more complex structures, we first need to pick the right figure of merit. In general, the long time behaviour of CTQWs is burdened by highly fine-detailed interference patterns arising from the various spectral components of the starting state, whose ratios of eigenvalues are typically irrational. On the other hand, on chain graphs we expect a ballistic behaviour, i.e. a linear relationship between the topological distance $\mathrm{dist}(s,f)$ from the starting site $|s\rangle$ to the target final site $|f\rangle$ and the time of the transport event that we would like to pick. In [353] we performed extensive numerical analysis on various topologies to deduce that the maximization of the transport probability $P_{s\to f}(t)$ with respect to $t\in[0,\mathrm{dist}(s,f)/v]$ yields the most predictable and reliable results for $v\sim O(1)$ and the selected transport events with these maximization essentially always coincide with the first local maximum of $P_{s\to f}(t)$ in time. We therefore adopt as a measure of transport performance of a chiral Hamiltonian on a chain graph the value of the transport probability $P_{s\to f}(t^*)$ at the first time instant in which the following conditions hold simultaneously:

$$P_{s\to f}(t^*) \;\geq\; \frac{1}{2} \tag{7.53}$$

$$\left.\frac{\mathrm{d}P_{s\to f}}{\mathrm{d}t}\right|_{t=t^*} = 0\,, \qquad \left.\frac{\mathrm{d}^2P_{s\to f}}{\mathrm{d}t^2}\right|_{t=t^*} < 0 \tag{7.54}$$

7.4.2 Results for the chiral triangle chain

Numerical simulations show that, when joining identical units as in Fig.7.15, the optimal phase configuration for transport between the two ends of the chain is obtained by putting all the phases equal to each other and at the value established by maximizing the transport performance for the single-unit chain [353]. For the triangle chain, this

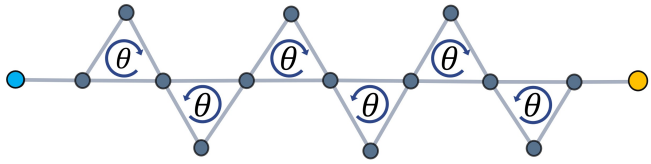

Figure 7.15: Triangle chain with 6 units. The starting vertex is colored in light-blue, while the target vertex is in yellow.

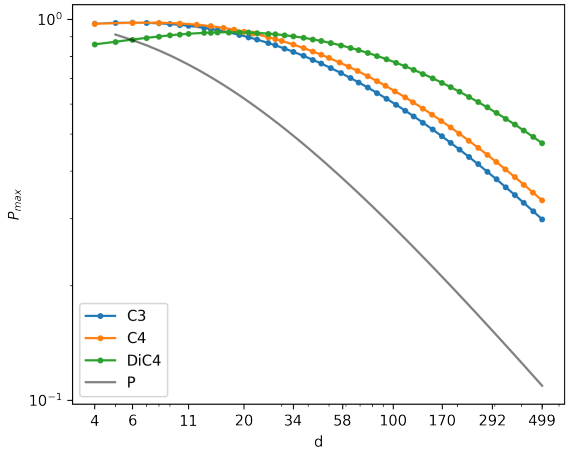

Figure 7.16: Transport performances for triangle chains (light-blue), square chains (orange) and barred-square chains (green). The transport performances of the path graphs (gray) are shown for reference. The horizontal axis displays the topological distance between the first and last site of each chain.

corresponds again to putting $\theta = \pi/2$ as a total phase for each unit, with the orientations specified as in Fig.7.15. The transport performance as a function of the topological distance for triangle chains (C3) with the optimal phase configurations are plotted in Fig.7.16 in loglog scale, together with the corresponding transport performances of path graphs (P), barred-square chains (DiC4) and square chains (C4). The barred-square chains also achieve their best performances with a chiral configuration, while the square chains transport at their best with the ordinary adjacency matrix as generator.

7.4.3 Analysis of quantum transport mechanisms in chain graphs

Going to the Krlyov basis with respect to the initial site $|s\rangle$, the (non-chiral) square chain is mapped into a path graph whose exterior edges have an ordinary weight of 1, while all the interior edges are weighted by $\sqrt{2}$; importantly, this mapping is *local*, in the sense that it is performed by a unitary operation that only mixes the vertices inside the same square, therefore the transport performances of the original chain and the one of the weighted path graph can be directly compared [353]. In [327] the authors analyzed quantum trans-

port on path graphs with modulation of the external edges[6] and they advanced a mechanism to justify their greatly improved performance with respect to ordinary path graphs, which was already observed in [360]. Indeed, it seems that weighting the exterior edges of P_N by $w_0^{opt} = 1.030 \times N^{-1/6}$ significantly improves the asymptotic performance, from the decreasing power-law of Eq.(7.52) to a constant asymptotic value of $P_{s\to f}(t^*) \simeq 0.847$ for a transport time t^* that is still linearly scaling with N, apart for subleading $O(N^{1/3})$ corrections; this should be contrasted with the Krawtchouk chain we discussed before, which achieved perfect transport, but at the cost of modulating *all* the edges of the path.

The mechanics advanced in [327] to explain this improvement can be understood as follows. Whenever the Hamiltonian H is real, it can be diagonalized by an orthogonal matrix O, such that $\mathrm{O}^T \mathrm{H} \mathrm{O} = \Lambda$ and $\Lambda = \mathrm{diag}(\lambda_1, ..., \lambda_N)$. Moreover, for chain graphs, the mirror symmetry that reflects the chain around a plane perpendicular to it and passing through the middle vertex/edge, there is a relation of the type $\mathrm{O}_{k,j} = \pm \mathrm{O}_{k,N+1-j}$ for $j = 1, ..., N$, N being the total number of vertices; if n labels the eigenvalues in increasing order, the relative sign is alternating with n; therefore, the transport probability from the first to the last site becomes:

$$P_{1\to N}(t) \;=\; |\sum_n R_n e^{i\pi n - i\lambda_n t}|^2 \tag{7.55}$$

where $R_n = |\mathrm{O}_{n,1}|^2$ and therefore $\sum_n R_n = 1$. In order for this to be close to 1, the phases should all interfere constructively at a certain time: this implies that $\lambda_n = \nu n + s_0$ for some constant shift s_0 and some speed ν. It is therefore clear that whenever the chain has a mirror symmetry and the Hamiltonian is real, optimal transport from the first to the last site requires an equispaced spectrum, of the type that can be achieved with appropriate weights as in the Krawtchouk chain [329]. On the other hand, it is quantitatively obvious that minimal modulation of the weights of exterior edges cannot significantly alter the spectrum for N large. In general, instead, it has the effect of modulating the values of R_n around the centre of the spectrum, where $\lambda_n = 0$, whereas the spectrum itself is essentially unaffected; indeed, the coefficients R_n are strongly influenced by the matrix elements of O involving the first and the last sites, and therefore will significantly change with the modulation of the weights on the external edges. Thus, by appropriately choosing the weight w, one can tweak the values of R_n so that only those integers n for which λ_n is linear with n give a significant contribution to the sum in Eq.(7.55).

Conversely, in [353] we showed that the C3 chain with the optimal phase configurations has a spectrum which is closer to a linear one, when compared with the spectrum of P or its variation with modified, equal weights on the first and last edge: interestingly, then, although minimal modulation of the weights cannot significantly alter the spectrum in favor of transport for large N, chiral effects do help in this regard without breaking the homogeneity of the chain. However, the C3 optimal chain is chiral: its Hamiltonian is not real and some of its eigenvectors are necessarily complex. For these reasons, looking at the linearity of the spectrum is not fully sufficient to deduce a transport enhancement in itself. In general, letting $\mathrm{U_H}$ be the unitary matrix that diagonalizes the Hamiltonian H for the chiral triangle chain and λ_k its eigenvalues, the transport amplitude will be:

$$A_{1\to M}(t) \;=\; \sum_{k=1}^{M} \mathrm{U}^*_{k,M} \mathrm{U}_{k,1} e^{-i\lambda_k t} \tag{7.56}$$

[6] Which is equivalent, up to a time rescaling, to modulating by the same weight only the interior edges

where N is the number of triangle units and $M = 2N + 3$ is the total number of sites (therefore site $2N + 3$ is the target for transport). Let us call $\phi_k = \arg(\mathrm{U}^*_{k,M}\mathrm{U}_{k,1})$. We see that the condition of optimal transport at time $\tilde{t}$ requires:

$$\lambda_k \tilde{t} \simeq \phi_k + s_0 \quad \forall k = 1, ..., M \tag{7.57}$$

where s_0 is a possible constant phase shift.

For the optimal value of the total phase on the triangle units, the Hamiltonian of the chain has a characteristic symmetry that allows us to better explore the condition in Eq.(7.57). Indeed one can easily check that a reflection about the middle of the chain (defined by a permutation matrix Π) combined with an appropriate quasi-gauge transformation U_D gives a unitary transformation $\mathrm{U}_S = \mathrm{U}_D\Pi$ such that:

$$\mathrm{U}_S^\dagger \, \mathrm{H} \, \mathrm{U}_S = -\mathrm{H} \tag{7.58}$$

This equation implies, in particular, that the spectrum of H is symmetric around the zero of the energy. Clearly:

$$A_{1\to M}(t) = \langle M|e^{-i\mathrm{H}t}|1\rangle = \langle M|\mathrm{U}_S^\dagger e^{i\mathrm{H}t}\mathrm{U}_S|1\rangle = e^{i\varphi}\langle 1|e^{i\mathrm{H}t}|M\rangle = e^{i\varphi}A_{M\to 1}(-t) \tag{7.59}$$

where φ is a constant phase determined by $\arg(\mathrm{U}_D)_{1,1} - \arg(\mathrm{U}_D)_{M,M}$ and we exploited the fact that $\Pi|1\rangle = |M\rangle$ and $\Pi|M\rangle = |1\rangle$. But now notice that $A_{M\to 1}(-t)$ is the complex conjugate of $A_{1\to M}(t)$, therefore the previous chain of equalities leads us to conclude that:

$$A_{1\to M}(t) = e^{i\varphi/2}\sqrt{P_{1\to M}(t)} \tag{7.60}$$

or in words, that the phase of the transport amplitude is constant in time. It is important to stress that this is a consequence of the special symmetry of H in Eq.(7.58): whenever the value of the phase is different from the optimal one, this symmetry will not be respected. Notice that if there exists a time $\tilde{t}$ such that $\forall k : \phi_k - \lambda_k\tilde{t} = s_0$, then $s_0 = \varphi/2$ would be the constant phase of the amplitude; since we can argue that this constant phase must be zero, we conclude that we can assume $s_0 = 0$ in Eq.(7.57). The same reasoning can be applied to the transport amplitudes $A_{k\to M-k}(t)$ for a walker initially localized at site $|k\rangle$ to be found in the localized state $|M-k\rangle$ at time t: also in this case the phase will be constant in time. Therefore, provided that the transport probabilities are optimized, these chains also allow for transport of superposition states of a few sites of the chain. As was recently argued [361] for a spin-chain analogue model, the transport of superposition states can be exploited to transport entanglement; indeed, our argument about the time-independence of the amplitude's phase also explains the results in [361], at the same time backing up the role of chirality in achieving this property. On the other hand, if the goal is the transport of a quantum bit, the pure quantum walk model encoding the qubit state in a spatial superposition of the first two sites of the chain-graph can be more convenient in a practical implementation, since it requires a much smaller Hilbert space, thus being less sensitive to decoherence sources [7].

[7] Indeed, in the spin-chain model, coherent transport would require to preserve both the spatial coherence between different sites *and* the local coherence in the spin basis.

7.5 On the maximal gap of chiral Hamiltonians

An interesting point to be addressed if one hopes to exploit chiral CTQWs for quantum metrology is the following: what is the maximal energy difference between two eigenstates of a chiral (adjacency-type) Hamiltonian on a given graph? Indeed, a balanced superposition of the ground state and the highest excited state offers the greatest precision when measuring the rate γ or other properties related to the Hamiltonian.

A first bound is given by the following result:

Theorem 7.5.1: Spectral bounds for chiral adjacency matrix and Laplacian

Let $\mathcal{G}$ be a connected simple graph, let $d_{\max}$ be the maximal degree among all vertices of $\mathcal{G}$ and let $\tilde{\mathrm{A}}$ be a generic chiral adjacency matrix on $\mathcal{G}$. If $\lambda^{\tilde{A}}_{\min}$ and $\lambda^{\tilde{A}}_{\max}$ are, respectively, the smallest and largest eigenvalues of $\tilde{\mathrm{A}}$, then the following bounds hold:

$$-d_{\max} \leq \lambda^{\tilde{A}}_{\min} \tag{7.61}$$

$$\lambda^{\tilde{A}}_{\max} \leq d_{\max} \tag{7.62}$$

Moreover, let $\tilde{\mathrm{L}}$ be a generic chiral Laplacian on $\mathcal{G}$ and let $\tilde{\lambda}_{\min}$ and $\tilde{\lambda}_{\max}$ be its smallest and largest eigenvalues, respectively. Then:

$$0 \leq \lambda^{\tilde{L}}_{\min} \tag{7.63}$$

$$\lambda^{\tilde{L}}_{\max} \leq 2d_{\max} \tag{7.64}$$

In particular, chiral Laplacians are always positive-semidefinite matrices.

Proof. To prove the first statement, let $\vec{v}$ be an eigenvector of $\tilde{\mathrm{A}}$ with eigenvalue $\lambda^{\tilde{A}}$ and let $|v_{j_0}| = \sup_j |v_j|$ be the largest entry of $\vec{v}$ (in absolute value). Then:

$$|\lambda^{\tilde{A}}||v_{j_0}| = |(\tilde{\mathrm{A}}\vec{v})_{j_0}| \leq \sum_k |\tilde{\mathrm{A}}_{j_0 k} x_k| \leq |v_{j_0}| \sum_k |\tilde{\mathrm{A}}_{j_0 k}| \leq |v_{j_0}| d^{\max} \tag{7.65}$$

where in the last inequality we used $\sum_k |\tilde{\mathrm{A}}_{j_0 k}| = d_{j_0} \leq d^{\max}$. Thus, as claimed, $|\lambda^{\tilde{A}}| \leq d^{\max}$ for any eigenvalue λ of $\tilde{\mathrm{A}}$. The same reasoning applied to a chiral Laplacian gives the other bound, since $\sum_k |\tilde{\mathrm{L}}_{j_0 k}|$ is upper bounded by $2d^{\max}$, counting the diagonal contribution. Notice also that chiral Laplacians are still positive-semidefinite; indeed, let $\vec{v}$ be an eigenvector of $\tilde{\mathrm{L}}$, v_{j_0} be its entry with largest absolute value as before and $\lambda^{\tilde{L}}$ the corresponding eigenvalue. Then:

$$\begin{aligned} &\lambda^{\tilde{L}} v_{j_0} = \left(\tilde{\mathrm{L}}\vec{v}\right)_{j_0} = d_{j_0} v_{j_0} + \sum_{k \neq j_0} \tilde{\mathrm{L}}_{j_0 k} v_k \implies \\ &\implies |d_{j_0} - \lambda^{\tilde{L}}||v_{j_0}| = |\sum_{k \neq j} \tilde{\mathrm{L}}_{jk} v_k| \leq d_{j_0}|v_{j_0}| \implies \\ &\implies \lambda^{\tilde{L}} \geq 0 \end{aligned} \tag{7.66}$$

once again exploiting the fact that $\sum_{k \neq j_0} |\tilde{\mathrm{L}}_{j_0 k}| = d_{j_0}$. □

In both cases, then, the maximal gap for *any* graph and any phases configuration is equal to twice the maximal degree. This theoretical maximum is indeed achieved by the family of hypercube graphs Q_d, whose adjacency matrices have $2d$ as their maximal gap, in the non-chiral configuration. On the other hand, there are cases in which one can show that no chiral configuration can achieve this value. For example, on a wheel graph with an odd number of vertices, W_{2n+1}, the maximal gap is $2\sqrt{2n+4}$ and it is attained by a chiral configuration, whereas the non-chiral adjacency matrix has $\Delta_{\max} = 2\sqrt{2n+1}$ (see Subsection 5.1.3). In general, we have the following result:

Theorem 7.5.2

Let $\mathcal{G}$ be a connected simple graph with $d_{\max}$ the maximum of the degrees of all its vertices. Let $\tilde{\mathrm{A}}$ be any chiral adjacency matrix on it and $\Delta_{\max}$ be the difference between the largest and the smallest eigenvalue of $\tilde{\mathrm{A}}$. Then:

$$\Delta_{\max} \leq 2d_{\max} \tag{7.67}$$

Moreover, if $\mathcal{G}$ admits a swift chiral quantum walk starting from v with $\deg(v) = d^{\max}$, with chiral Hamiltonian $\tilde{\mathrm{A}}^{\text{swift}}$, the corresponding largest spectral gab $\Delta^{\text{swift}}_{\max}$ is lower bounded by:

$$2\sqrt{d_{\max}} \leq \Delta^{\text{swift}}_{\max} \tag{7.68}$$

Proof. The first bound directly derives from Theorem 7.5 and it also applies to any chiral Laplacian on $\mathcal{G}$. As for the second bound, let us recall that admitting a swift chiral quantum walk starting from v means that $\tilde{\mathrm{A}}^{\text{swift}}|v\rangle = \sqrt{d^{\max}}|e\rangle$, where $|e\rangle = \frac{1}{\sqrt{d^{\max}}}\sum_{j=1}^{d^{\max}}|v_j\rangle$ is the uniform superposition over all vertices connected to v, and $\tilde{\mathrm{A}}^{\text{swift}}|e\rangle = \sqrt{d^{\max}}|v\rangle$. Therefore:

$$\tilde{\mathrm{A}}^{\text{swift}}\frac{|v\rangle \pm |e\rangle}{\sqrt{2}} = \pm\sqrt{d^{\max}}\frac{|v\rangle \pm |e\rangle}{\sqrt{2}} \tag{7.69}$$

so that we can explicitly construct two eigenvectors with eigenvalue $\sqrt{d^{\max}}$ and the thesis follows. □

As a closing example, let us consider by how much the swift phase configuration can improve $\Delta_{\max}$ on complete graphs. We will limit ourselves to graphs with an even number of sites, K_{2N}. For those, the swift adjacency matrix has entries:

$$\forall 1 \leq j < k \leq 2N : \tilde{\mathrm{A}}^{\text{swift}}_{jk} = (-1)^{j+k} i \tag{7.70}$$

$$\forall j,k \in \{1,\dots,2N\} : \quad \tilde{\mathrm{A}}^{\text{swift}}_{kj} = -\tilde{\mathrm{A}}^{\text{swift}}_{jk} \tag{7.71}$$

The vectors $\vec{v}^{\pm} \in \mathbb{C}^{2N}$ with entries $v_j^{\max} = \frac{(-1)^j}{\sqrt{2N}} e^{\pm i\frac{\pi j}{2N}}$ are eigenvectors of $\tilde{\mathrm{A}}^{\max}$ with eigenvalues given by:

$$-i\sum_{j=2}^{N} e^{i\pm\frac{\pi(j-1)}{2N}} = \pm\coth\left(\frac{\pi}{4N}\right) \tag{7.72}$$

and it can be verified numerically that these are the extremal eigenvalues of $\tilde{\mathrm{A}}^{\max}$, so that $\Delta^{\text{swift}}_{\max} = 2\coth\frac{\pi}{4N}$, while the gap for the standard adjacency matrix of K_{2N} is $\Delta_{\max} = 2N$.

Already for K_4 we find that $\Delta_{\text{max}}^{\text{swift}} > \Delta_{\text{max}}$, while asymptotically for large N we have:

$$2\coth\left(\frac{\pi}{4N}\right) \;=\; \frac{8}{\pi}N + O\left(\frac{1}{N}\right) \tag{7.73}$$

which is greater than $2N$ since $8/\pi \simeq 2.55$. We thus find a multiplicative improvement of the maximal gap by a factor of $\Delta_{\text{max}}^{\text{swift}}/\Delta_{\text{max}} = 4/\pi \simeq 1.27$ for sufficiently large complete graphs. Thus far, however, we did not find any example of a family of graphs whose asymptotic scaling of Δ_{max} with d^{max} can be changed by some chiral phase configurations (e.g. from $\propto \sqrt{d^{\text{max}}}$ to $\propto d^{\text{max}}$).

Future directions

7.6 Novel developments in CV quantum steering

Concerning the notions of quantum steering that were discussed in Part I of this thesis, the natural development would consist in generalizing them to non-Gaussian states. In particular, it is known that entanglement is necessary to remotely generate quantum non-Gaussianity starting from a bipartite Gaussian state, while the relation with steerability is less obvious [362]; a partial result in this direction indicates that quantum steerability from mode A to mode B is necessary and sufficient to be able to induce Wigner negativity on mode A by photon-subtraction on mode B, starting from a two-mode Gaussian state $\hat{\boldsymbol{\rho}}_{AB}$ (notice the reversed directions) [363]. In general, one can also consider the differences between remote generation of quantum non-Gaussianity or the more demanding Wigner negativity [362, 364], plausibly arriving at different notions of quantum correlations on the set of Gaussian-entangled states. The topic of Gaussian vs. non-Gaussian entanglement, which we completely glossed over, is of paramount importance in recent developments, as it appears to be also related to the possibility of achieving quantum advantage with CV quantum computation [365, 366].

7.7 Future directions for chiral quantum walks

In many ways, the exploration of the potential applications of chiral quantum walks is still at its beginning. Although our works partially restrict their aims and can help in the characterization of their evolutions, much is left to future explorations. Their application in the analogy with quantum computation has not been explored, despite the fact that directional transport seems to be a valuable feature to be added to Child's construction [285]. For example, the problem of scattering on a version of the chiral quantum switch with infinite arms has been studied in [367] and again for the resonant phase value $\theta = \pi/2$ it was shown that a Gaussian wavepacket prepared on one arm and with a group velocity directed towards the central triangle is preferentially scattered into a single one of the outer arms, a fact that could be directly applied to the quantum walks model for quantum computation. On a different note, one could consider quantizing the phases of chiral quantum walks in a similar fashion to the derivation of the toric code from the quantum Ising model: there, one usually promotes the global $\mathbb{Z}2$ invariance of the Ising model to a local one by adding binary degrees of freedom on the edges; by quantizing these new degrees of freedom as quantum bits and defining operators on the plaquettes, the toric code can be derived. For chiral quantum walks, a similar process

should be carried out with the local $\mathrm{U}(1)$ invariance. The addition of more than one particle on the same graph with a given phase configuration and a local interaction could also be explored, since little is known about the effect of the phases on the entangling power of the corresponding interacting chiral Hamiltonians. Finally, let us mention that we have preliminary results indicating a solid connection between chiral quantum walks with random phase configurations and random matrix theory; the hope is that, much in the same way as one can map the N-particle subspace of the Hubbard model to a quantum walk for a single particle on a sufficiently large graph, some features of *quantum chaos* could be understood via mappings to chiral quantum walks with random phase configurations.

Bibliography

[1] P. Busch, "Quantum states and generalized observables: A simple proof of gleason's theorem," *Phys. Rev. Lett.*, vol. 91, p. 120403, Sep 2003. [Online]. Available: https://link.aps.org/doi/10.1103/PhysRevLett.91.120403

[2] J. von Neumann, *Mathematical Foundations of Quantum Mechanics*, ser. Goldstine Printed Materials. Princeton University Press, 1955. [Online]. Available: https://books.google.it/books?id=JLyCo3RO4qUC

[3] B. C. Hall, *Quantum Theory for Mathematicians*. Springer New York, 2013. [Online]. Available: https://doi.org/10.1007/978-1-4614-7116-5

[4] C. Cohen-Tannoudji, B. Diu, F. Laloë, and S. R. Hemley, *Quantum mechanics*, ser. A Wiley-Interscience publication. New York, NY [u.a.]: Wiley [u.a.], 1977.

[5] L. D. Landau and L. M. Lifshitz, *Quantum Mechanics Non-Relativistic Theory, Third Edition: Volume 3*, 3rd ed. Butterworth-Heinemann, Jan. 1981. [Online]. Available: http://www.worldcat.org/isbn/0750635398

[6] J. Preskill, "Lecture notes for physics 229: Quantum information and computation," 1998.

[7] M. M. Wilde, *Quantum Information Theory*. Cambridge University Press, Apr. 2013. [Online]. Available: https://doi.org/10.1017/cbo9781139525343

[8] J. J. Sakurai, *Modern quantum mechanics; rev. ed.* Reading, MA: Addison-Wesley, 1994. [Online]. Available: https://cds.cern.ch/record/1167961

[9] D. Walls and G. J. Milburn, Eds., *Quantum Optics*. Springer-Verlag Berlin, January 2008. [Online]. Available: https://doi.org/10.1007/978-3-540-28574-8

[10] M. E. Peskin and D. V. Schroeder, *An introduction to quantum field theory*. Boulder, CO: Westview, 1995.

[11] J. A. Wheeler and W. H. Zurek, *Quantum Theory and Measurement*. Princeton University Press, 1983. [Online]. Available: http://www.jstor.org/stable/j.ctt7ztxn5

[12] J. A. Barrett, *The Quantum Mechanics of Minds and Worlds*. Oxford, GB: Oxford University Press UK, 1999.

[13] S. M. Carroll and C. T. Sebens, "Many worlds, the born rule, and self-locating uncertainty," in *Quantum Theory: A Two-Time Success Story*. Springer Milan, 2014, pp. 157–169. [Online]. Available: https://doi.org/10.1007/978-88-470-5217-8_10

[14] Zurek, W. H., "Pointer basis of quantum apparatus: Into what mixture does the wave packet collapse?" *Phys. Rev. D*, vol. 24, pp. 1516–1525, Sep 1981. [Online]. Available: https://link.aps.org/doi/10.1103/PhysRevD.24.1516

[15] W. H. Zurek, "Environment-induced superselection rules," *Phys. Rev. D*, vol. 26, pp. 1862–1880, Oct 1982. [Online]. Available: https://link.aps.org/doi/10.1103/PhysRevD.26.1862

[16] Wojciech H. Zurek, "Decoherence and the transition from quantum to classical," *Physics Today*, vol. 44, no. 10, pp. 36–44, Oct. 1991. [Online]. Available: https://doi.org/10.1063/1.881293

[17] Zurek, Wojciech Hubert, "Decoherence, einselection, and the quantum origins of the classical," *Rev. Mod. Phys.*, vol. 75, pp. 715–775, May 2003. [Online]. Available: https://link.aps.org/doi/10.1103/RevModPhys.75.715

[18] C. A. Fuchs, N. D. Mermin, and R. Schack, "An introduction to QBism with an application to the locality of quantum mechanics," *American Journal of Physics*, vol. 82, no. 8, pp. 749–754, Aug. 2014. [Online]. Available: https://doi.org/10.1119/1.4874855

[19] R. E. Kastner, *The Transactional Interpretation of Quantum Mechanics*. Cambridge University Press, Apr. 2022. [Online]. Available: https://doi.org/10.1017/9781108907538

[20] C. Rovelli, "Relational quantum mechanics," *International Journal of Theoretical Physics*, vol. 35, no. 8, pp. 1637–1678, Aug. 1996. [Online]. Available: https://doi.org/10.1007/bf02302261

[21] P. C. Hohenberg, "Colloquium: An introduction to consistent quantum theory," *Reviews of Modern Physics*, vol. 82, no. 4, pp. 2835–2844, Oct. 2010. [Online]. Available: https://doi.org/10.1103/revmodphys.82.2835

[22] G. Bacciagaluppi and A. Valentini, *Quantum Theory at the Crossroads: Reconsidering the 1927 Solvay Conference*. Cambridge University Press, 2009.

[23] A. Valentini, "De Broglie-Bohm Pilot-Wave Theory: Many Worlds in Denial?" in *Many Worlds?* Oxford University PressOxford, Jun. 2010, pp. 476–509. [Online]. Available: https://doi.org/10.1093/acprof:oso/9780199560561.003.0019

[24] R. W. Spekkens, "Evidence for the epistemic view of quantum states: A toy theory," *Phys. Rev. A*, vol. 75, p. 032110, Mar 2007. [Online]. Available: https://link.aps.org/doi/10.1103/PhysRevA.75.032110

[25] N. Harrigan and R. W. Spekkens, "Einstein, incompleteness, and the epistemic view of quantum states," *Foundations of Physics*, vol. 40, no. 2, pp. 125–157, Jan. 2010. [Online]. Available: https://doi.org/10.1007/s10701-009-9347-0

[26] M. F. Pusey, J. Barrett, and T. Rudolph, "On the reality of the quantum state," *Nature Physics*, vol. 8, no. 6, pp. 475–478, May 2012. [Online]. Available: https://doi.org/10.1038/nphys2309

[27] W. K. Wootters and W. H. Zurek, "A single quantum cannot be cloned," *Nature*, vol. 299, no. 5886, pp. 802–803, Oct. 1982. [Online]. Available: https://doi.org/10.1038/299802a0

[28] G. Carcassi, L. Maccone, and C. A. Aidala, "Four postulates of quantum mechanics are three," *Phys. Rev. Lett.*, vol. 126, p. 110402, Mar 2021. [Online]. Available: https://link.aps.org/doi/10.1103/PhysRevLett.126.110402

[29] M. A. Nielsen and I. L. Chuang, *Quantum Computation and Quantum Information*. Cambridge University Press, Jun. 2012. [Online]. Available: https://doi.org/10.1017/cbo9780511976667

[30] W. F. Stinespring, "Positive Functions on C ∗ -Algebras," *Proceedings of the American Mathematical Society*, vol. 6, no. 2, p. 211, Apr. 1955. [Online]. Available: https://doi.org/10.2307/2032342

[31] E. H. Lieb and M. B. Ruskai, "Proof of the strong subadditivity of quantum-mechanical entropy," *Journal of Mathematical Physics*, vol. 14, no. 12, pp. 1938–1941, Dec. 1973. [Online]. Available: https://doi.org/10.1063/1.1666274

[32] R. Cheng, "Quantum geometric tensor (fubini-study metric) in simple quantum system: A pedagogical introduction," 2010. [Online]. Available: https://arxiv.org/abs/1012.1337

[33] A. Uhlmann, "The transition probability in the state space of a star-algebra," *Reports on Mathematical Physics*, vol. 9, no. 2, pp. 273–279, Apr. 1976. [Online]. Available: https://doi.org/10.1016/0034-4877(76)90060-4

[34] I. Bengtsson and K. Zyczkowski, *Geometry of Quantum States*. Cambridge University Press, May 2006. [Online]. Available: https://doi.org/10.1017/cbo9780511535048

[35] D. Markham, J. A. Miszczak, Z. Puchała, and K. Życzkowski, "Quantum state discrimination: A geometric approach," *Phys. Rev. A*, vol. 77, p. 042111, Apr 2008. [Online]. Available: https://link.aps.org/doi/10.1103/PhysRevA.77.042111

[36] H.-P. Breuer and F. Petruccione, *The Theory of Open Quantum Systems*. Oxford University PressOxford, Jan. 2007. [Online]. Available: https://doi.org/10.1093/acprof:oso/9780199213900.001.0001

[37] H.-P. Breuer, E.-M. Laine, J. Piilo, and B. Vacchini, "Colloquium: Non-markovian dynamics in open quantum systems," *Rev. Mod. Phys.*, vol. 88, p. 021002, Apr 2016. [Online]. Available: https://link.aps.org/doi/10.1103/RevModPhys.88.021002

[38] B. Vacchini, A. Smirne, E.-M. Laine, J. Piilo, and H.-P. Breuer, "Markovianity and non-markovianity in quantum and classical systems," *New Journal of Physics*, vol. 13, no. 9, p. 093004, Sep. 2011. [Online]. Available: https://doi.org/10.1088/1367-2630/13/9/093004

[39] V. Gorini, A. Kossakowski, and E. C. G. Sudarshan, "Completely Positive Dynamical Semigroups of N-Level Systems," *Journal of Mathematical Physics*, vol. 17, no. 5, pp. 821–825, May 1976. [Online]. Available: https://doi.org/10.1063/1.522979

[40] G. Lindblad, "On the generators of quantum dynamical semigroups," *Communications in Mathematical Physics*, vol. 48, no. 2, pp. 119–130, Jun. 1976. [Online]. Available: https://doi.org/10.1007/bf01608499

[41] C. W. Gardiner, *Stochastic methods*, ser. Springer Series in Synergetics. Berlin, Germany: Springer, October 2010.

[42] H.-P. Breuer, E.-M. Laine, and J. Piilo, "Measure for the Degree of Non-Markovian Behavior of Quantum Processes in Open Systems," *Phys. Rev. Lett.*, vol. 103, p. 210401, Nov 2009. [Online]. Available: https://link.aps.org/doi/10.1103/PhysRevLett.103.210401

[43] D. Chruściński, A. Kossakowski, and Á. Rivas, "Measures of non-Markovianity: Divisibility versus backflow of information," *Physical Review A*, vol. 83, no. 5, p. 052128, 2011.

[44] H.-P. Breuer, "Foundations and measures of quantum non-Markovianity," *Journal of Physics B: Atomic, Molecular and Optical Physics*, vol. 45, no. 15, p. 154001, 2012.

[45] B. Bylicka, D. Chruściński, and S. Maniscalco, "Non-markovianity and reservoir memory of quantum channels: a quantum information theory perspective," *Scientific reports*, vol. 4, p. 5720, 2014.

[46] B. Bellomo, R. Lo Franco, and G. Compagno, "Non-markovian effects on the dynamics of entanglement," *Phys. Rev. Lett.*, vol. 99, p. 160502, Oct 2007. [Online]. Available: https://link.aps.org/doi/10.1103/PhysRevLett.99.160502

[47] A. D'Arrigo, G. Benenti, R. L. Franco, G. Falci, and E. Paladino, "Hidden entanglement, system-environment information flow and non-Markovianity," *International Journal of Quantum Information*, vol. 12, no. 02, p. 1461005, Mar. 2014. [Online]. Available: https://doi.org/10.1142/s021974991461005x

[48] A. Orieux, A. D'Arrigo, G. Ferranti, R. L. Franco, G. Benenti, E. Paladino, G. Falci, F. Sciarrino, and P. Mataloni, "Experimental on-demand recovery of entanglement by local operations within non-Markovian dynamics," *Scientific Reports*, vol. 5, no. 1, Feb. 2015. [Online]. Available: https://doi.org/10.1038/srep08575

[49] P. A. Camati, J. F. G. Santos, and R. M. Serra, "Employing non-markovian effects to improve the performance of a quantum otto refrigerator," *Phys. Rev. A*, vol. 102, p. 012217, Jul 2020. [Online]. Available: https://link.aps.org/doi/10.1103/PhysRevA.102.012217

[50] A. U. Devi, A. Rajagopal *et al.*, "Open-system quantum dynamics with correlated initial states, not completely positive maps, and non-markovianity," *Physical Review A*, vol. 83, no. 2, p. 022109, 2011.

[51] M. M. Wolf, J. Eisert, T. Cubitt, and J. I. Cirac, "Assessing non-markovian quantum dynamics," *Physical Review Letters*, vol. 101, no. 15, p. 150402, 2008.

[52] R. Vasile, S. Maniscalco, M. G. A. Paris, H.-P. Breuer, and J. Piilo, "Quantifying non-Markovianity of continuous-variable Gaussian dynamical maps," *Phys. Rev. A*, vol. 84, p. 052118, Nov 2011. [Online]. Available: https://link.aps.org/doi/10.1103/PhysRevA.84.052118

[53] A. Rivas, S. F. Huelga, and M. B. Plenio, "Entanglement and non-markovianity of quantum evolutions," *Phys. Rev. Lett.*, vol. 105, p. 050403, Jul 2010. [Online]. Available: https://link.aps.org/doi/10.1103/PhysRevLett.105.050403

[54] Rivas, Angel and Huelga, Susana F and Plenio, Martin B, "Quantum non-Markovianity: characterization, quantification and detection," *Reports on Progress in Physics*, vol. 77, no. 9, p. 094001, 2014.

[55] B.-H. Liu, S. Wißmann, X.-M. Hu, C. Zhang, Y.-F. Huang, C.-F. Li, G.-C. Guo, A. Karlsson, J. Piilo, and H.-P. Breuer, "Locality and universality of quantum memory effects," *Scientific Reports*, vol. 4, no. 1, Sep. 2014. [Online]. Available: https://doi.org/10.1038/srep06327

[56] H.-P. Breuer, E.-M. Laine, J. Piilo, and B. Vacchini, "*Colloquium:* non-markovian dynamics in open quantum systems," *Reviews of Modern Physics*, vol. 88, p. 021002, 2016.

[57] S. Luo, S. Fu, and H. Song, "Quantifying non-markovianity via correlations," *Physical Review A*, vol. 86, no. 4, p. 044101, 2012.

[58] S.-L. Chen, N. Lambert, C.-M. Li, A. Miranowicz, Y.-N. Chen, and F. Nori, "Quantifying non-markovianity with temporal steering," *Physical Review Letters*, vol. 116, no. 2, p. 020503, 2016.

[59] J. Svozilík, R. Hidalgo-Sacoto, and I. I. Arkhipov, "Universal non-markovianity detection in hybrid open quantum systems," *Scientific Reports*, vol. 10, no. 18258, 2020.

[60] K.-D. Wu, Z. Hou, G.-Y. Xiang, C.-F. Li, G.-C. Guo, D. Dong, and F. Nori, "Detecting non-markovianity via quantified coherence: theory and experiments," *npj Quantum Information*, vol. 6, no. 55, 2020.

[61] P. Liuzzo-Scorpo, W. Roga, L. A. M. Souza, N. K. Bernardes, and G. Adesso, "Non-Markovianity Hierarchy of Gaussian Processes and Quantum Amplification," *Physical Review Letters*, vol. 118, p. 050401, 2017.

[62] S. Maniscalco, S. Olivares, and M. G. A. Paris, "Entanglement oscillations in non-Markovian quantum channels," *Phys. Rev. A*, vol. 75, p. 062119, Jun 2007. [Online]. Available: https://link.aps.org/doi/10.1103/PhysRevA.75.062119

[63] A. M. Gleason, *Measures on the Closed Subspaces of a Hilbert Space*. Dordrecht: Springer Netherlands, 1957, pp. 123–133. [Online]. Available: https://doi.org/10.1007/978-94-010-1795-4_7

[64] R. W. Spekkens, "Contextuality for preparations, transformations, and unsharp measurements," *Phys. Rev. A*, vol. 71, p. 052108, May 2005. [Online]. Available: https://link.aps.org/doi/10.1103/PhysRevA.71.052108

[65] S. Kochen and E. P. Specker, "The problem of hidden variables in quantum mechanics," *Journal of Mathematics and Mechanics*, vol. 17, no. 1, pp. 59–87, 1967. [Online]. Available: http://www.jstor.org/stable/24902153

[66] J. S. Bell, "On the Einstein Podolsky Rosen paradox," *Physics Physique Fizika*, vol. 1, pp. 195–200, Nov 1964. [Online]. Available: https://link.aps.org/doi/10.1103/PhysicsPhysiqueFizika.1.195

[67] J. S. BELL, "On the Problem of Hidden Variables in Quantum Mechanics," *Rev. Mod. Phys.*, vol. 38, pp. 447–452, Jul 1966. [Online]. Available: https://link.aps.org/doi/10.1103/RevModPhys.38.447

[68] A. Peres, *Quantum Theory: Concepts and Methods*. Springer Netherlands, 2002. [Online]. Available: https://doi.org/10.1007/0-306-47120-5

[69] J. S. Bell and A. Aspect, *Speakable and Unspeakable in Quantum Mechanics*. Cambridge University Press, Jun. 2004. [Online]. Available: https://doi.org/10.1017/cbo9780511815676

[70] A. Aspect, J. Dalibard, and G. Roger, "Experimental Test of Bell's Inequalities Using Time-Varying Analyzers," *Phys. Rev. Lett.*, vol. 49, pp. 1804–1807, Dec 1982. [Online]. Available: https://link.aps.org/doi/10.1103/PhysRevLett.49.1804

[71] M. Giustina, M. A. M. Versteegh, S. Wengerowsky, J. Handsteiner, A. Hochrainer, K. Phelan, F. Steinlechner, J. Kofler, J.-A. Larsson, C. Abellán, W. Amaya, V. Pruneri, M. W. Mitchell, J. Beyer, T. Gerrits, A. E. Lita, L. K. Shalm, S. W. Nam, T. Scheidl, R. Ursin, B. Wittmann, and A. Zeilinger, "Significant-Loophole-Free Test of Bell's Theorem with Entangled Photons," *Phys. Rev. Lett.*, vol. 115, p. 250401, Dec 2015. [Online]. Available: https://link.aps.org/doi/10.1103/PhysRevLett.115.250401

[72] G. C. Ghirardi, A. Rimini, and T. Weber, "A general argument against superluminal transmission through the quantum mechanical measurement process," *Lettere al Nuovo Cimento*, vol. 27, no. 10, pp. 293–298, Mar. 1980. [Online]. Available: https://doi.org/10.1007/bf02817189

[73] G. C. Ghirardi and T. Weber, "Quantum mechanics and faster-than-light communication: Methodological considerations," *Il Nuovo Cimento B Series 11*, vol. 78, no. 1, pp. 9–20, Nov. 1983. [Online]. Available: https://doi.org/10.1007/bf02721378

[74] G. C. Ghirardi, R. Grassi, A. Rimini, and T. Weber, "Experiments of the EPR Type Involving CP-Violation Do not Allow Faster-than-Light Communication between Distant Observers," *Europhysics Letters (EPL)*, vol. 6, no. 2, pp. 95–100, May 1988. [Online]. Available: https://doi.org/10.1209/0295-5075/6/2/001

[75] P. H. Eberhard and R. R. Ross, "Quantum field theory cannot provide faster-than-light communication," *Foundations of Physics Letters*, vol. 2, no. 2, pp. 127–149, Mar. 1989. [Online]. Available: https://doi.org/10.1007/bf00696109

[76] S. Popescu, "Nonlocality beyond quantum mechanics," *Nature Physics*, vol. 10, no. 4, pp. 264–270, Apr. 2014. [Online]. Available: https://doi.org/10.1038/nphys2916

[77] G. Grynberg, A. Aspect, C. Fabre, and C. Cohen-Tannoudji, *Introduction to Quantum Optics*. Cambridge University Press, Sep. 2010. [Online]. Available: https://doi.org/10.1017/cbo9780511778261

[78] Z.-D. Li, Y.-L. Mao, M. Weilenmann, A. Tavakoli, H. Chen, L. Feng, S.-J. Yang, M.-O. Renou, D. Trillo, T. P. Le, N. Gisin, A. Acín, M. Navascués, Z. Wang, and J. Fan, "Testing real quantum theory in an optical quantum network," *Phys. Rev. Lett.*, vol. 128, p. 040402, Jan 2022. [Online]. Available: https://link.aps.org/doi/10.1103/PhysRevLett.128.040402

[79] V. Giovannetti, S. Lloyd, and L. Maccone, "Quantum limits to dynamical evolution," *Phys. Rev. A*, vol. 67, p. 052109, May 2003. [Online]. Available: https://link.aps.org/doi/10.1103/PhysRevA.67.052109

[80] Vittorio Giovannetti and Seth Lloyd and Lorenzo Maccone, "The quantum speed limit," in *Fluctuations and Noise in Photonics and Quantum Optics*, D. Abbott, J. H. Shapiro, and Y. Yamamoto, Eds., vol. 5111, International Society for Optics and Photonics. SPIE, 2003, pp. 1 – 6. [Online]. Available: https://doi.org/10.1117/12.507486

[81] ——, "The speed limit of quantum unitary evolution," *Journal of Optics B: Quantum and Semiclassical Optics*, vol. 6, no. 8, pp. S807–S810, jul 2004. [Online]. Available: https://doi.org/10.1088/1464-4266/6/8/028

[82] S. Deffner and S. Campbell, "Quantum speed limits: from heisenberg's uncertainty principle to optimal quantum control," *Journal of Physics A: Mathematical and Theoretical*, vol. 50, no. 45, p. 453001, oct 2017. [Online]. Available: https://doi.org/10.1088/1751-8121/aa86c6

[83] M. Horodecki, P. Horodecki, and R. Horodecki, "Separability of mixed states: necessary and sufficient conditions," *Physics Letters A*, vol. 223, no. 1-2, pp. 1–8, Nov. 1996. [Online]. Available: https://doi.org/10.1016/s0375-9601(96)00706-2

[84] R. F. Werner, "Quantum states with einstein-podolsky-rosen correlations admitting a hidden-variable model," *Phys. Rev. A*, vol. 40, pp. 4277–4281, Oct 1989. [Online]. Available: https://link.aps.org/doi/10.1103/PhysRevA.40.4277

[85] W. K. Wootters, "Entanglement of formation of an arbitrary state of two qubits," *Phys. Rev. Lett.*, vol. 80, pp. 2245–2248, Mar 1998. [Online]. Available: https://link.aps.org/doi/10.1103/PhysRevLett.80.2245

[86] Wootters, William K., "Entanglement of formation and concurrence," *Quantum Info. Comput.*, vol. 1, no. 1, p. 27–44, jan 2001.

[87] A. Peres, "Separability criterion for density matrices," *Phys. Rev. Lett.*, vol. 77, pp. 1413–1415, Aug 1996. [Online]. Available: https://link.aps.org/doi/10.1103/PhysRevLett.77.1413

[88] R. F. Werner and M. M. Wolf, "Bound entangled gaussian states," *Phys. Rev. Lett.*, vol. 86, pp. 3658–3661, Apr 2001. [Online]. Available: https://link.aps.org/doi/10.1103/PhysRevLett.86.3658

[89] L.-M. Duan, G. Giedke, J. I. Cirac, and P. Zoller, "Inseparability criterion for continuous variable systems," *Phys. Rev. Lett.*, vol. 84, pp. 2722–2725, Mar 2000. [Online]. Available: https://link.aps.org/doi/10.1103/PhysRevLett.84.2722

[90] G. Adesso, M. Cianciaruso, and T. R. Bromley, "Quantum discord and nonclassical correlations beyond entanglement," pp. 175–194, Apr. 2016. [Online]. Available: https://doi.org/10.1002/9783527805785.ch9

[91] H. Ollivier and W. H. Zurek, "Quantum discord: A measure of the quantumness of correlations," *Phys. Rev. Lett.*, vol. 88, p. 017901, Dec 2001. [Online]. Available: https://link.aps.org/doi/10.1103/PhysRevLett.88.017901

[92] A. Streltsov, *Quantum Correlations Beyond Entanglement*. Springer International Publishing, 2015. [Online]. Available: https://doi.org/10.1007/978-3-319-09656-8

[93] D. Girolami, A. M. Souza, V. Giovannetti, T. Tufarelli, J. G. Filgueiras, R. S. Sarthour, D. O. Soares-Pinto, I. S. Oliveira, and G. Adesso, "Quantum discord determines the interferometric power of quantum states," *Phys. Rev. Lett.*, vol. 112, p. 210401, May 2014. [Online]. Available: https://link.aps.org/doi/10.1103/PhysRevLett.112.210401

[94] H. Barnum, C. M. Caves, C. A. Fuchs, R. Jozsa, and B. Schumacher, "Noncommuting mixed states cannot be broadcast," *Phys. Rev. Lett.*, vol. 76, pp. 2818–2821, Apr 1996. [Online]. Available: https://link.aps.org/doi/10.1103/PhysRevLett.76.2818

[95] G. Adesso, T. R. Bromley, and M. Cianciaruso, "Measures and applications of quantum correlations," *Journal of Physics A: Mathematical and Theoretical*, vol. 49, no. 47, p. 473001, Nov. 2016. [Online]. Available: https://doi.org/10.1088/1751-8113/49/47/473001

[96] G. S. Agarwal, *Quantum Optics*. Cambridge University Press, Nov. 2012. [Online]. Available: https://doi.org/10.1017/cbo9781139035170

[97] C. Cohen-Tannoudji, J. Dupont-Roc, and G. Grynberg, *Photons and atoms: introduction to quantum electrodynamics*. New York, NY: Wiley, 1989, trans. of : Photons et atomes. Paris, InterEditions, 1987. [Online]. Available: https://cds.cern.ch/record/113864

[98] S. Olivares, "Introduction to generation, manipulation and characterization of optical quantum states," *Phys. Lett. A*, vol. 418, p. 127720, 2021. [Online]. Available: https://www.sciencedirect.com/science/article/pii/S0375960121005843

[99] A. Serafini, *Quantum Continuous Variables*. Boca Raton: CRC Press, Jul. 2017. [Online]. Available: https://doi.org/10.1201/9781315118727

[100] A. Ferraro, S. Olivares, and M. G. A. Paris, *Gaussian States in Quantum Information*. Napoli: Bibliopolis, 2005.

[101] M. Walschaers, "Non-gaussian quantum states and where to find them," *PRX Quantum*, vol. 2, p. 030204, Sep 2021. [Online]. Available: https://link.aps.org/doi/10.1103/PRXQuantum.2.030204

[102] H. Groenewold, "On the principles of elementary quantum mechanics," *Physica*, vol. 12, no. 7, pp. 405–460, Oct. 1946. [Online]. Available: https://doi.org/10.1016/s0031-8914(46)80059-4

[103] L. V. Hove, "Sur le problème des relations entre les transformations unitaires de la mécanique quantique et les transformations canoniques de la mécanique classique," *Acad. Roy. Belgique Bull. Cl. Sci.*, no. 37, 1951. [Online]. Available: https://api.semanticscholar.org/CorpusID:126172588

[104] D. Giulini, "That strange procedure called quantisation," in *Quantum Gravity*. Springer Berlin Heidelberg, 2003, pp. 17–40. [Online]. Available: https://doi.org/10.1007/978-3-540-45230-0_2

[105] D. J. Simms and N. M. J. Woodhouse, *Lectures on Geometric Quantization*. Springer Berlin Heidelberg, 1976. [Online]. Available: https://doi.org/10.1007/3-540-07860-6

[106] T. L. Curtright, D. B. Fairlie, and C. K. Zachos, *A Concise Treatise on Quantum Mechanics in Phase Space*. WORLD SCIENTIFIC, Imperial College Press, Jun. 2013. [Online]. Available: https://doi.org/10.1142/8870

[107] D. A. Dubin, M. A. Hennings, and T. B. Smith, *Mathematical Aspects of Weyl Quantization and Phase*. WORLD SCIENTIFIC, Jun. 2000. [Online]. Available: https://doi.org/10.1142/4140

[108] R. J. Glauber, "The quantum theory of optical coherence," *Phys. Rev.*, vol. 130, pp. 2529–2539, Jun 1963. [Online]. Available: https://link.aps.org/doi/10.1103/PhysRev.130.2529

[109] K. E. Cahill and R. J. Glauber, "Density operators and quasiprobability distributions," *Phys. Rev.*, vol. 177, pp. 1882–1902, Jan 1969. [Online]. Available: https://link.aps.org/doi/10.1103/PhysRev.177.1882

[110] E. C. G. Sudarshan, "Equivalence of semiclassical and quantum mechanical descriptions of statistical light beams," *Phys. Rev. Lett.*, vol. 10, pp. 277–279, Apr 1963. [Online]. Available: https://link.aps.org/doi/10.1103/PhysRevLett.10.277

[111] K. E. Cahill and R. J. Glauber, "Ordered expansions in boson amplitude operators," *Phys. Rev.*, vol. 177, pp. 1857–1881, Jan 1969. [Online]. Available: https://link.aps.org/doi/10.1103/PhysRev.177.1857

[112] L. Mandel, "Non-classical states of the electromagnetic field," *Physica Scripta*, vol. T12, pp. 34–42, jan 1986. [Online]. Available: https://doi.org/10.1088/0031-8949/1986/t12/005

[113] C. T. Lee, "Measure of the nonclassicality of nonclassical states," *Phys. Rev. A*, vol. 44, pp. R2775–R2778, Sep 1991. [Online]. Available: https://link.aps.org/doi/10.1103/PhysRevA.44.R2775

[114] N. Lütkenhaus and S. M. Barnett, "Nonclassical effects in phase space," *Phys. Rev. A*, vol. 51, pp. 3340–3342, Apr 1995. [Online]. Available: https://link.aps.org/doi/10.1103/PhysRevA.51.3340

[115] G. S. Agarwal and K. Tara, "Nonclassical character of states exhibiting no squeezing or sub-poissonian statistics," *Phys. Rev. A*, vol. 46, pp. 485–488, Jul 1992. [Online]. Available: https://link.aps.org/doi/10.1103/PhysRevA.46.485

[116] T. Kiesel, W. Vogel, V. Parigi, A. Zavatta, and M. Bellini, "Experimental determination of a nonclassical glauber-sudarshan p function," *Phys. Rev. A*, vol. 78, p. 021804, Aug 2008. [Online]. Available: https://link.aps.org/doi/10.1103/PhysRevA.78.021804

[117] U. M. Titulaer and R. J. Glauber, "Correlation functions for coherent fields," *Phys. Rev.*, vol. 140, pp. B676–B682, Nov 1965. [Online]. Available: https://link.aps.org/doi/10.1103/PhysRev.140.B676

[118] W. Vogel, "Nonclassical states: An observable criterion," *Phys. Rev. Lett.*, vol. 84, pp. 1849–1852, Feb 2000. [Online]. Available: https://link.aps.org/doi/10.1103/PhysRevLett.84.1849

[119] T. Kiesel and W. Vogel, "Nonclassicality filters and quasiprobabilities," *Phys. Rev. A*, vol. 82, p. 032107, Sep 2010. [Online]. Available: https://link.aps.org/doi/10.1103/PhysRevA.82.032107

[120] S. Ryl, J. Sperling, E. Agudelo, M. Mraz, S. Köhnke, B. Hage, and W. Vogel, "Unified nonclassicality criteria," *Phys. Rev. A*, vol. 92, p. 011801, Jul 2015. [Online]. Available: https://link.aps.org/doi/10.1103/PhysRevA.92.011801

[121] F. m. c. Damanet, J. Kübler, J. Martin, and D. Braun, "Nonclassical states of light with a smooth p function," *Phys. Rev. A*, vol. 97, p. 023832, Feb 2018. [Online]. Available: https://link.aps.org/doi/10.1103/PhysRevA.97.023832

[122] N. Biagi, M. Bohmann, E. Agudelo, M. Bellini, and A. Zavatta, "Experimental certification of nonclassicality via phase-space inequalities," *Phys. Rev. Lett.*, vol. 126, p. 023605, Jan 2021. [Online]. Available: https://link.aps.org/doi/10.1103/PhysRevLett.126.023605

[123] M. Bohmann, E. Agudelo, and J. Sperling, "Probing nonclassicality with matrices of phase-space distributions," *Quantum*, vol. 4, p. 343, Oct. 2020. [Online]. Available: https://doi.org/10.22331/q-2020-10-15-343

[124] A. Serafini, "Detecting entanglement by symplectic uncertainty relations," *J. Opt. Soc. Am. B*, vol. 24, no. 2, pp. 347–354, Feb 2007. [Online]. Available: http://www.osapublishing.org/josab/abstract.cfm?URI=josab-24-2-347

[125] A. Einstein, B. Podolsky, and N. Rosen, "Can quantum-mechanical description of physical reality be considered complete?" *Phys. Rev.*, vol. 47, pp. 777–780, May 1935. [Online]. Available: https://link.aps.org/doi/10.1103/PhysRev.47.777

[126] R. A. Horn and C. R. Johnson, *Matrix Analysis*. Cambridge University Press, 1985.

[127] S. D. Bartlett, T. Rudolph, and R. W. Spekkens, "Reconstruction of Gaussian quantum mechanics from Liouville mechanics with an epistemic restriction," *Phys. Rev. A*, vol. 86, p. 012103, Jul 2012. [Online]. Available: https://link.aps.org/doi/10.1103/PhysRevA.86.012103

[128] S. Pirandola, G. Spedalieri, S. L. Braunstein, N. J. Cerf, and S. Lloyd, "Optimality of Gaussian Discord," *Phys. Rev. Lett.*, vol. 113, p. 140405, Oct 2014. [Online]. Available: https://link.aps.org/doi/10.1103/PhysRevLett.113.140405

[129] P. Giorda and M. G. A. Paris, "Gaussian quantum discord," *Phys. Rev. Lett.*, vol. 105, p. 020503, Jul 2010. [Online]. Available: https://link.aps.org/doi/10.1103/PhysRevLett.105.020503

[130] G. De Palma, D. Trevisan, and V. Giovannetti, "Gaussian states minimize the output entropy of one-mode quantum gaussian channels," *Phys. Rev. Lett.*, vol. 118, p. 160503, Apr 2017. [Online]. Available: https://link.aps.org/doi/10.1103/PhysRevLett.118.160503

[131] M. M. Wolf, G. Giedke, and J. I. Cirac, "Extremality of gaussian quantum states," *Phys. Rev. Lett.*, vol. 96, p. 080502, Mar 2006. [Online]. Available: https://link.aps.org/doi/10.1103/PhysRevLett.96.080502

[132] A. S. Holevo, M. Sohma, and O. Hirota, "Capacity of quantum gaussian channels," *Phys. Rev. A*, vol. 59, pp. 1820–1828, Mar 1999. [Online]. Available: https://link.aps.org/doi/10.1103/PhysRevA.59.1820

[133] R. W. Spekkens, "Quasi-quantization: Classical statistical theories with an epistemic restriction," in *Fundamental Theories of Physics*. Springer Netherlands, Dec. 2015, pp. 83–135. [Online]. Available: https://doi.org/10.1007/978-94-017-7303-4_4

[134] S. Lloyd and S. L. Braunstein, "Quantum computation over continuous variables," *Phys. Rev. Lett.*, vol. 82, pp. 1784–1787, Feb 1999. [Online]. Available: https://link.aps.org/doi/10.1103/PhysRevLett.82.1784

[135] D. Gottesman, A. Kitaev, and J. Preskill, "Encoding a qubit in an oscillator," *Phys. Rev. A*, vol. 64, p. 012310, Jun 2001. [Online]. Available: https://link.aps.org/doi/10.1103/PhysRevA.64.012310

[136] A. Mari and J. Eisert, "Positive wigner functions render classical simulation of quantum computation efficient," *Phys. Rev. Lett.*, vol. 109, p. 230503, Dec 2012. [Online]. Available: https://link.aps.org/doi/10.1103/PhysRevLett.109.230503

[137] R. W. Spekkens, "Negativity and contextuality are equivalent notions of nonclassicality," *Phys. Rev. Lett.*, vol. 101, p. 020401, Jul 2008. [Online]. Available: https://link.aps.org/doi/10.1103/PhysRevLett.101.020401

[138] R. Hudson, "When is the wigner quasi-probability density non-negative?" *Reports on Mathematical Physics*, vol. 6, no. 2, pp. 249–252, 1974. [Online]. Available: https://www.sciencedirect.com/science/article/pii/003448777490007X

[139] F. Soto and P. Claverie, "When is the Wigner function of multidimensional systems nonnegative?" *Journal of Mathematical Physics*, vol. 24, no. 1, pp. 97–100, Jan. 1983. [Online]. Available: https://doi.org/10.1063/1.525607

[140] S. L. Braunstein and P. van Loock, "Quantum information with continuous variables," *Rev. Mod. Phys.*, vol. 77, pp. 513–577, Jun 2005. [Online]. Available: https://link.aps.org/doi/10.1103/RevModPhys.77.513

[141] M. G. Genoni, M. G. A. Paris, and K. Banaszek, "Measure of the non-gaussian character of a quantum state," *Phys. Rev. A*, vol. 76, p. 042327, Oct 2007. [Online]. Available: https://link.aps.org/doi/10.1103/PhysRevA.76.042327

[142] ——, "Quantifying the non-gaussian character of a quantum state by quantum relative entropy," *Phys. Rev. A*, vol. 78, p. 060303, Dec 2008. [Online]. Available: https://link.aps.org/doi/10.1103/PhysRevA.78.060303

[143] M. G. Genoni and M. G. A. Paris, "Quantifying non-gaussianity for quantum information," *Phys. Rev. A*, vol. 82, p. 052341, Nov 2010. [Online]. Available: https://link.aps.org/doi/10.1103/PhysRevA.82.052341

[144] A. Kenfack and K. yczkowski, "Negativity of the wigner function as an indicator of non-classicality," *Journal of Optics B: Quantum and Semiclassical Optics*, vol. 6, no. 10, pp. 396–404, aug 2004. [Online]. Available: https://doi.org/10.1088/1464-4266/6/10/003

[145] M. G. Genoni, M. L. Palma, T. Tufarelli, S. Olivares, M. S. Kim, and M. G. A. Paris, "Detecting quantum non-gaussianity via the wigner function," *Phys. Rev. A*, vol. 87, p. 062104, Jun 2013. [Online]. Available: https://link.aps.org/doi/10.1103/PhysRevA.87.062104

[146] M. Barbieri, N. Spagnolo, M. G. Genoni, F. Ferreyrol, R. Blandino, M. G. A. Paris, P. Grangier, and R. Tualle-Brouri, "Non-gaussianity of quantum states: An experimental test on single-photon-added coherent states," *Phys. Rev. A*, vol. 82, p. 063833, Dec 2010. [Online]. Available: https://link.aps.org/doi/10.1103/PhysRevA.82.063833

[147] M. Walschaers, C. Fabre, V. Parigi, and N. Treps, "Entanglement and wigner function negativity of multimode non-gaussian states," *Phys. Rev. Lett.*, vol. 119, p. 183601, Oct 2017. [Online]. Available: https://link.aps.org/doi/10.1103/PhysRevLett.119.183601

[148] ——, "Statistical signatures of multimode single-photon-added and -subtracted states of light," *Phys. Rev. A*, vol. 96, p. 053835, Nov 2017. [Online]. Available: https://link.aps.org/doi/10.1103/PhysRevA.96.053835

[149] V. Cimini, M. Barbieri, N. Treps, M. Walschaers, and V. Parigi, "Neural networks for detecting multimode wigner negativity," *Phys. Rev. Lett.*, vol. 125, p. 160504, Oct 2020. [Online]. Available: https://link.aps.org/doi/10.1103/PhysRevLett.125.160504

[150] U. Chabaud, D. Markham, and F. Grosshans, "Stellar representation of non-gaussian quantum states," *Phys. Rev. Lett.*, vol. 124, p. 063605, Feb 2020. [Online]. Available: https://link.aps.org/doi/10.1103/PhysRevLett.124.063605

[151] C. Hughes, M. G. Genoni, T. Tufarelli, M. G. A. Paris, and M. S. Kim, "Quantum non-gaussianity witnesses in phase space," *Phys. Rev. A*, vol. 90, p. 013810, Jul 2014. [Online]. Available: https://link.aps.org/doi/10.1103/PhysRevA.90.013810

[152] L. c. v. Lachman, I. Straka, J. Hloušek, M. Ježek, and R. Filip, "Faithful hierarchy of genuine n-photon quantum non-gaussian light," *Phys. Rev. Lett.*, vol. 123, p. 043601, Jul 2019. [Online]. Available: https://link.aps.org/doi/10.1103/PhysRevLett.123.043601

[153] U. Chabaud, G. Roeland, M. Walschaers, F. Grosshans, V. Parigi, D. Markham, and N. Treps, "Certification of non-gaussian states with operational measurements," *PRX Quantum*, vol. 2, p. 020333, Jun 2021. [Online]. Available: https://link.aps.org/doi/10.1103/PRXQuantum.2.020333

[154] E. Schrödinger, "Discussion of probability relations between separated systems," *Mathematical Proceedings of the Cambridge Philosophical Society*, vol. 31, no. 4, p. 555–563, 1935.

[155] H. M. Wiseman, S. J. Jones, and A. C. Doherty, "Steering, entanglement, nonlocality, and the einstein-podolsky-rosen paradox," *Phys. Rev. Lett.*, vol. 98, p. 140402, Apr 2007. [Online]. Available: https://link.aps.org/doi/10.1103/PhysRevLett.98.140402

[156] S. J. Jones, H. M. Wiseman, and A. C. Doherty, "Entanglement, einstein-podolsky-rosen correlations, bell nonlocality, and steering," *Phys. Rev. A*, vol. 76, p. 052116, Nov 2007. [Online]. Available: https://link.aps.org/doi/10.1103/PhysRevA.76.052116

[157] M. T. Quintino, T. Vértesi, D. Cavalcanti, R. Augusiak, M. Demianowicz, A. Acín, and N. Brunner, "Inequivalence of entanglement, steering, and bell nonlocality for general measurements," *Phys. Rev. A*, vol. 92, p. 032107, Sep 2015. [Online]. Available: https://link.aps.org/doi/10.1103/PhysRevA.92.032107

[158] C. Branciard, E. G. Cavalcanti, S. P. Walborn, V. Scarani, and H. M. Wiseman, "One-sided device-independent quantum key distribution: Security, feasibility, and the connection with steering," *Phys. Rev. A*, vol. 85, p. 010301, Jan 2012. [Online]. Available: https://link.aps.org/doi/10.1103/PhysRevA.85.010301

[159] P. Skrzypczyk, M. Navascués, and D. Cavalcanti, "Quantifying einstein-podolsky-rosen steering," *Phys. Rev. Lett.*, vol. 112, p. 180404, May 2014. [Online]. Available: https://link.aps.org/doi/10.1103/PhysRevLett.112.180404

[160] S. Wollmann, N. Walk, A. J. Bennet, H. M. Wiseman, and G. J. Pryde, "Observation of Genuine One-Way Einstein-Podolsky-Rosen Steering," *Phys. Rev. Lett.*, vol. 116, p. 160403, Apr 2016. [Online]. Available: https://link.aps.org/doi/10.1103/PhysRevLett.116.160403

[161] S. L. W. Midgley, A. J. Ferris, and M. K. Olsen, "Asymmetric gaussian steering: When alice and bob disagree," *Phys. Rev. A*, vol. 81, p. 022101, Feb 2010. [Online]. Available: https://link.aps.org/doi/10.1103/PhysRevA.81.022101

[162] J. Bowles, T. Vértesi, M. T. Quintino, and N. Brunner, "One-way Einstein-Podolsky-Rosen steering," *Physical Review Letters*, vol. 112, no. 20, p. 200402, 2014.

[163] D. Cavalcanti and P. Skrzypczyk, "Quantum steering: a review with focus on semidefinite programming," *Reports on Progress in Physics*, vol. 80, no. 2, p. 024001, dec 2016. [Online]. Available: https://doi.org/10.1088/1361-6633/80/2/024001

[164] R. Uola, A. C. S. Costa, H. C. Nguyen, and O. Gühne, "Quantum steering," *Rev. Mod. Phys.*, vol. 92, p. 015001, Mar 2020. [Online]. Available: https://link.aps.org/doi/10.1103/RevModPhys.92.015001

[165] Frigerio, Massimo and Olivares, Stefano and Paris, Matteo G. A., "Steering nonclassicality of Gaussian states," *Phys. Rev. A*, vol. 103, p. 022209, Feb 2021. [Online]. Available: https://link.aps.org/doi/10.1103/PhysRevA.103.022209

[166] Massimo Frigerio and Claudio Destri and Stefano Olivares and Matteo G.A. Paris, "Quantum steering with Gaussian states: A tutorial," *Physics Letters A*, vol. 430, p. 127954, Apr. 2022. [Online]. Available: https://doi.org/10.1016/j.physleta.2022.127954

[167] I. Kogias, A. R. Lee, S. Ragy, and G. Adesso, "Quantification of gaussian quantum steering," *Phys. Rev. Lett.*, vol. 114, p. 060403, Feb 2015. [Online]. Available: https://link.aps.org/doi/10.1103/PhysRevLett.114.060403

[168] M. D. Reid, "Demonstration of the einstein-podolsky-rosen paradox using nondegenerate parametric amplification," *Phys. Rev. A*, vol. 40, pp. 913–923, Jul 1989. [Online]. Available: https://link.aps.org/doi/10.1103/PhysRevA.40.913

[169] M. D. Reid, P. D. Drummond, W. P. Bowen, E. G. Cavalcanti, P. K. Lam, H. A. Bachor, U. L. Andersen, and G. Leuchs, "Colloquium: The einstein-podolsky-rosen paradox: From concepts to applications," *Rev. Mod. Phys.*, vol. 81, pp. 1727–1751, Dec 2009. [Online]. Available: https://link.aps.org/doi/10.1103/RevModPhys.81.1727

[170] Z. Y. Ou, S. F. Pereira, H. J. Kimble, and K. C. Peng, "Realization of the einstein-podolsky-rosen paradox for continuous variables," *Phys. Rev. Lett.*, vol. 68, pp. 3663–3666, Jun 1992. [Online]. Available: https://link.aps.org/doi/10.1103/PhysRevLett.68.3663

[171] J. Kiukas, C. Budroni, R. Uola, and J.-P. Pellonpää, "Continuous-variable steering and incompatibility via state-channel duality," *Phys. Rev. A*, vol. 96, p. 042331, Oct 2017. [Online]. Available: https://link.aps.org/doi/10.1103/PhysRevA.96.042331

[172] V. D'Auria, S. Fornaro, A. Porzio, S. Solimeno, S. Olivares, and M. G. A. Paris, "Full characterization of gaussian bipartite entangled states by a single homodyne detector," *Phys. Rev. Lett.*, vol. 102, p. 020502, Jan 2009. [Online]. Available: https://link.aps.org/doi/10.1103/PhysRevLett.102.020502

[173] S. Cialdi, C. Porto, D. Cipriani, S. Olivares, and M. G. A. Paris, "Full quantum state reconstruction of symmetric two-mode squeezed thermal states via spectral homodyne detection and a state-balancing detector," *Phys. Rev. A*, vol. 93, p. 043805, Apr 2016. [Online]. Available: https://link.aps.org/doi/10.1103/PhysRevA.93.043805

[174] S. Olivares, "Introduction to generation, manipulation and characterization of optical quantum states," *Physics Letters A*, vol. 418, p. 127720, 2021. [Online]. Available: https://www.sciencedirect.com/science/article/pii/S0375960121005843

[175] L. Lami, C. Hirche, G. Adesso, and A. Winter, "Lindblad- and non-lindblad-type dynamics of a quantum brownian particle," *Physical Review Letters*, vol. 117, p. 220502, 2016.

[176] V. Giovannetti and D. Vitali, "Phase-noise measurement in a cavity with a movable mirror undergoing quantum brownian motion," *Phys. Rev. A*, vol. 63, p. 023812, Jan 2001. [Online]. Available: https://link.aps.org/doi/10.1103/PhysRevA.63.023812

[177] F. Intravaia, S. Maniscalco, and A. Messina, "Density-matrix operatorial solution of the non-Markovian master equation for quantum Brownian motion," *Physical Review A*, vol. 67, no. 4, p. 042108, 2003.

[178] L. A. Souza, H. S. Dhar, M. N. Bera, P. Liuzzo-Scorpo, and G. Adesso, "Gaussian interferometric power as a measure of continuous-variable non-Markovianity," *Physical Review A*, vol. 92, no. 5, p. 052122, 2015.

[179] S. Maniscalco, J. Piilo, F. Intravaia, F. Petruccione, and A. Messina, "Lindblad-and non-lindblad-type dynamics of a quantum brownian particle," *Physical Review A*, vol. 70, no. 3, p. 032113, 2004.

[180] S. Maniscalco, F. Intravaia, J. Piilo, and A. Messina, "Misbeliefs and misunderstandings about the non-markovian dynamics of a damped harmonic oscillator," *Journal of Optics B: Quantum and Semiclassical Optics*, vol. 6, no. 3, pp. S98–S103, mar 2004. [Online]. Available: https://doi.org/10.1088/1464-4266/6/3/016

[181] U. Weiss, *Quantum dissipative systems*. World scientific, 2012, vol. 13.

[182] Gaetana Spedalieri, "Quantum Hypothesis Testing: Theory and Applications to Quantum Sensing and Data Readout," Ph.D. dissertation, University of York, Department of Computer Science, March 2016.

[183] S. M. Barnett and S. Croke, "Quantum state discrimination," *Advances in Optics and Photonics*, vol. 1, no. 2, p. 238, Feb. 2009. [Online]. Available: https://doi.org/10.1364/aop.1.000238

[184] A. Chefles, "Quantum state discrimination," *Contemporary Physics*, vol. 41, no. 6, pp. 401–424, Nov. 2000. [Online]. Available: https://doi.org/10.1080/00107510010002599

[185] A. Acín, "Statistical distinguishability between unitary operations," *Phys. Rev. Lett.*, vol. 87, p. 177901, Oct 2001. [Online]. Available: https://link.aps.org/doi/10.1103/PhysRevLett.87.177901

[186] A. M. Childs, J. Preskill, and J. Renes, "Quantum information and precision measurement," *Journal of Modern Optics*, vol. 47, no. 2-3, pp. 155–176, Feb. 2000. [Online]. Available: https://doi.org/10.1080/09500340008244034

[187] C. W. Helstrom, *Quantum detection and estimation theory*. Academic Press, New York, 1976.

[188] M. G. A. Paris, "Quantum estimation for quantum technology," *Int. J. Quantum Inf.*, vol. 7, pp. 125–137, Jan. 2009. [Online]. Available: https://doi.org/10.1142/s0219749909004839

[189] V. Giovannetti, S. Lloyd, and L. Maccone, "Quantum-Enhanced Measurements: Beating the Standard Quantum Limit," *Science*, vol. 306, no. 5700, pp. 1330–1336, Nov. 2004. [Online]. Available: https://doi.org/10.1126/science.1104149

[190] Vittorio Giovannetti and Seth Lloyd and Lorenzo Maccone, "Advances in quantum metrology," *Nature Phot.*, vol. 5, no. 4, pp. 222–229, Mar. 2011. [Online]. Available: https://doi.org/10.1038/nphoton.2011.35

[191] S. L. Braunstein, C. M. Caves, and G. Milburn, "Generalized Uncertainty Relations: Theory, Examples, and Lorentz Invariance," *Annals of Physics*, vol. 247, no. 1, pp. 135–173, Apr. 1996. [Online]. Available: https://doi.org/10.1006/aphy.1996.0040

[192] G. Y. Xiang, B. L. Higgins, D. W. Berry, H. M. Wiseman, and G. J. Pryde, "Entanglement-enhanced measurement of a completely unknown optical phase," *Nature Photonics*, vol. 5, no. 1, pp. 43–47, Dec. 2010. [Online]. Available: https://doi.org/10.1038/nphoton.2010.268

[193] L. Pezzè, A. Smerzi, M. K. Oberthaler, R. Schmied, and P. Treutlein, "Quantum metrology with nonclassical states of atomic ensembles," *Rev. Mod. Phys.*, vol. 90, p. 035005, Sep 2018. [Online]. Available: https://link.aps.org/doi/10.1103/RevModPhys.90.035005

[194] D. Braun, G. Adesso, F. Benatti, R. Floreanini, U. Marzolino, M. W. Mitchell, and S. Pirandola, "Quantum-enhanced measurements without entanglement," *Rev. Mod. Phys.*, vol. 90, p. 035006, Sep 2018. [Online]. Available: https://link.aps.org/doi/10.1103/RevModPhys.90.035006

[195] B. L. Higgins, D. W. Berry, S. D. Bartlett, H. M. Wiseman, and G. J. Pryde, "Entanglement-free Heisenberg-limited phase estimation," *Nature*, vol. 450, no. 7168, pp. 393–396, Nov. 2007. [Online]. Available: https://doi.org/10.1038/nature06257

[196] Abbott, B. P. *et al.*, LIGO Scientific Collaboration and Virgo Collaboration, "Observation of Gravitational Waves from a Binary Black Hole Merger," *Phys. Rev. Lett.*, vol. 116, p. 061102, Feb 2016. [Online]. Available: https://link.aps.org/doi/10.1103/PhysRevLett.116.061102

[197] R. Schnabel, N. Mavalvala, D. E. McClelland, and P. K. Lam, "Quantum metrology for gravitational wave astronomy," *Nature Communications*, vol. 1, no. 1, Nov. 2010. [Online]. Available: https://doi.org/10.1038/ncomms1122

[198] M. A. Taylor and W. P. Bowen, "Quantum metrology and its application in biology," *Physics Reports*, vol. 615, pp. 1–59, Feb. 2016. [Online]. Available: https://doi.org/10.1016/j.physrep.2015.12.002

[199] S.-H. Tan, B. I. Erkmen, V. Giovannetti, S. Guha, S. Lloyd, L. Maccone, S. Pirandola, and J. H. Shapiro, "Quantum Illumination with Gaussian States," *Phys. Rev. Lett.*, vol. 101, p. 253601, Dec 2008. [Online]. Available: https://link.aps.org/doi/10.1103/PhysRevLett.101.253601

[200] S. Guha and B. I. Erkmen, "Gaussian-state quantum-illumination receivers for target detection," *Phys. Rev. A*, vol. 80, p. 052310, Nov 2009. [Online]. Available: https://link.aps.org/doi/10.1103/PhysRevA.80.052310

[201] S. Barzanjeh, S. Guha, C. Weedbrook, D. Vitali, J. H. Shapiro, and S. Pirandola, "Microwave Quantum Illumination," *Phys. Rev. Lett.*, vol. 114, p. 080503, Feb 2015. [Online]. Available: https://link.aps.org/doi/10.1103/PhysRevLett.114.080503

[202] E. D. Lopaeva, I. Ruo Berchera, I. P. Degiovanni, S. Olivares, G. Brida, and M. Genovese, "Experimental Realization of Quantum Illumination," *Phys. Rev. Lett.*, vol. 110, p. 153603, Apr 2013. [Online]. Available: https://link.aps.org/doi/10.1103/PhysRevLett.110.153603

[203] S. S. Mizrahi and V. V. Dodonov, "Creating quanta with an annihilation operator," *Journal of Physics A: Mathematical and General*, vol. 35, no. 41, pp. 8847–8857, oct 2002. [Online]. Available: https://doi.org/10.1088/0305-4470/35/41/315

[204] M. F. B. Cenni, L. Lami, A. Acin, and M. Mehboudi, "Thermometry of gaussian quantum systems using gaussian measurements," 2021.

[205] A. Ourjoumtsev, R. Tualle-Brouri, J. Laurat, and P. Grangier, "Generating optical schrödinger kittens for quantum information processing," *Science*, vol. 312, no. 5770, pp. 83–86, 2006.

[206] A. Ourjoumtsev, A. Dantan, R. Tualle-Brouri, and P. Grangier, "Increasing entanglement between gaussian states by coherent photon subtraction," *Phys. Rev. Lett.*, vol. 98, p. 030502, Jan 2007. [Online]. Available: https://link.aps.org/doi/10.1103/PhysRevLett.98.030502

[207] J. Wenger, R. Tualle-Brouri, and P. Grangier, "Non-gaussian statistics from individual pulses of squeezed light," *Phys. Rev. Lett.*, vol. 92, p. 153601, Apr 2004. [Online]. Available: https://link.aps.org/doi/10.1103/PhysRevLett.92.153601

[208] J. Fiurášek, R. García-Patrón, and N. J. Cerf, "Conditional generation of arbitrary single-mode quantum states of light by repeated photon subtractions," *Phys. Rev. A*, vol. 72, p. 033822, Sep 2005. [Online]. Available: https://link.aps.org/doi/10.1103/PhysRevA.72.033822

[209] S. Olivares and M. G. A. Paris, "Squeezed fock state by inconclusive photon subtraction," *J. Opt. B*, vol. 7, no. 12, pp. S616–S621, nov 2005.

[210] V. Parigi, A. Zavatta, M. Kim, and M. Bellini, "Probing quantum commutation rules by addition and subtraction of single photons to/from a light field," *Science*, vol. 317, no. 5846, pp. 1890–1893, 2007.

[211] A. Zavatta, V. Parigi, M. S. Kim, and M. Bellini, "Subtracting photons from arbitrary light fields: experimental test of coherent state invariance by single-photon annihilation," *New J. Phys.*, vol. 10, no. 12, p. 123006, dec 2008. [Online]. Available: https://doi.org/10.1088/1367-2630/10/12/123006

[212] S. Olivares and M. G. A. Paris, "Enhancement of nonlocality in phase space," *Phys. Rev. A*, vol. 70, p. 032112, Sep 2004. [Online]. Available: https://link.aps.org/doi/10.1103/PhysRevA.70.032112

[213] Stefano Olivares and Matteo G A Paris, "Photon subtracted states and enhancement of nonlocality in the presence of noise," *J. Opt. B*, vol. 7, no. 10, pp. S392–S397, sep 2005.

[214] C. Invernizzi, S. Olivares, M. G. A. Paris, and K. Banaszek, "Effect of noise and enhancement of nonlocality in on/off photodetection," *Phys. Rev. A*, vol. 72, p. 042105, Oct 2005. [Online]. Available: https://link.aps.org/doi/10.1103/PhysRevA.72.042105

[215] T. Opatrný, G. Kurizki, and D.-G. Welsch, "Improvement on teleportation of continuous variables by photon subtraction via conditional measurement," *Phys. Rev. A*, vol. 61, p. 032302, 2000.

[216] S. Olivares, M. G. A. Paris, and R. Bonifacio, "Teleportation improvement by inconclusive photon subtraction," *Phys. Rev. A*, vol. 67, p. 032314, Mar 2003. [Online]. Available: https://link.aps.org/doi/10.1103/PhysRevA.67.032314

[217] S. M. Barnett, G. Ferenczi, C. R. Gilson, and F. C. Speirits, "Statistics of photon-subtracted and photon-added states," *Phys. Rev. A*, vol. 98, p. 013809, Jul 2018. [Online]. Available: https://link.aps.org/doi/10.1103/PhysRevA.98.013809

[218] L. Zhang, A. Datta, and I. A. Walmsley, "Precision metrology using weak measurements," *Phys. Rev. Lett.*, vol. 114, p. 210801, May 2015. [Online]. Available: https://link.aps.org/doi/10.1103/PhysRevLett.114.210801

[219] D. Braun, P. Jian, O. Pinel, and N. Treps, "Precision measurements with photon-subtracted or photon-added gaussian states," *Phys. Rev. A*, vol. 90, p. 013821, Jul 2014. [Online]. Available: https://link.aps.org/doi/10.1103/PhysRevA.90.013821

[220] S. Alipour and A. T. Rezakhani, "Extended convexity of quantum fisher information in quantum metrology," *Phys. Rev. A*, vol. 91, p. 042104, 2015.

[221] D. R. M. Arvidsson-Shukur, N. Y. Halpern, H. V. Lepage, A. A. Lasek, C. H. W. Barnes, and S. Lloyd, "Quantum advantage in postselected metrology," *Nature Comm.*, vol. 11, no. 1, Jul. 2020. [Online]. Available: https://doi.org/10.1038/s41467-020-17559-w

[222] J. Combes and C. Ferrie, "Cost of postselection in decision theory," *Phys. Rev. A*, vol. 92, p. 022117, Aug 2015. [Online]. Available: https://link.aps.org/doi/10.1103/PhysRevA.92.022117

[223] J. Rubio, J. Anders, and L. A. Correa, "Global quantum thermometry," *Phys. Rev. Lett.*, vol. 127, p. 190402, Nov 2021. [Online]. Available: https://link.aps.org/doi/10.1103/PhysRevLett.127.190402

[224] J. Fiurášek, "Optimal probabilistic estimation of quantum states," *New J. Phys.*, vol. 8, no. 9, pp. 192–192, sep 2006. [Online]. Available: https://doi.org/10.1088/1367-2630/8/9/192

[225] B. Gendra, E. Ronco-Bonvehi, J. Calsamiglia, R. Muñoz Tapia, and E. Bagan, "Quantum metrology assisted by abstention," *Phys. Rev. Lett.*, vol. 110, p. 100501, Mar 2013. [Online]. Available: https://link.aps.org/doi/10.1103/PhysRevLett.110.100501

[226] J. Calsamiglia, B. Gendra, R. Muñoz-Tapia, and E. Bagan, "Probabilistic metrology or how some measurement outcomes render ultra-precise estimates," *New J. Phys.*, vol. 18, no. 10, p. 103049, 2016. [Online]. Available: https://doi.org/10.1088/1367-2630/18/10/103049

[227] O. S. Magaña-Loaiza, J. Harris, J. S. Lundeen, and R. W. Boyd, "Weak-value measurements can outperform conventional measurements," *Phys. Scripta*, vol. 92, no. 2, p. 023001, dec 2016. [Online]. Available: https://doi.org/10.1088/1402-4896/92/2/023001

[228] G. Li, L.-B. Chen, T. Wang, Z.-H. He, and H.-S. Song, "Precision metrology of weak measurement with a thermal state pointer," *J. Phys. B*, vol. 52, no. 15, p. 155501, jul 2019. [Online]. Available: https://doi.org/10.1088/1361-6455/ab1500

[229] G. Chen, P. Yin, W.-H. Zhang, G.-C. Li, C.-F. Li, and G.-C. Guo, "Beating standard quantum limit with weak measurement," *Entropy*, vol. 23, no. 3, p. 354, Mar 2021. [Online]. Available: http://dx.doi.org/10.3390/e23030354

[230] S. Tanaka and N. Yamamoto, "Information amplification via postselection: A parameter-estimation perspective," *Phys. Rev. A*, vol. 88, p. 042116, Oct 2013. [Online]. Available: https://link.aps.org/doi/10.1103/PhysRevA.88.042116

[231] C. Ferrie and J. Combes, "Weak value amplification is suboptimal for estimation and detection," *Phys. Rev. Lett.*, vol. 112, p. 040406, Jan 2014. [Online]. Available: https://link.aps.org/doi/10.1103/PhysRevLett.112.040406

[232] J. Combes, C. Ferrie, Z. Jiang, and C. M. Caves, "Quantum limits on postselected, probabilistic quantum metrology," *Phys. Rev. A*, vol. 89, p. 052117, May 2014. [Online]. Available: https://link.aps.org/doi/10.1103/PhysRevA.89.052117

[233] H. Adnane, F. Albarelli, A. Gharbi, and M. G. A. Paris, "Characterizing non-deterministic noiseless linear amplifiers at the quantum limit," *J. Phys. A*, vol. 52, no. 49, p. 495302, nov 2019. [Online]. Available: https://doi.org/10.1088/1751-8121/ab28b3

[234] R. Coto, H. T. Dinani, A. Norambuena, M. Chen, and J. R. Maze, "Probabilistic magnetometry with a two-spin system in diamond," *Quantum Sci. Tech.*, vol. 6, no. 3, p. 035011, jun 2021. [Online]. Available: https://doi.org/10.1088/2058-9565/abfce1

[235] S. Das, S. Modak, and M. N. Bera, "Saturating quantum advantages in postselected metrology with the positive kirkwood-dirac distribution," *Phys. Rev. A*, vol. 107, p. 042413, Apr 2023. [Online]. Available: https://link.aps.org/doi/10.1103/PhysRevA.107.042413

[236] L. M. Johansen, "Nonclassicality of thermal radiation," *Journal of Optics B: Quantum and Semiclassical Optics*, vol. 6, no. 12, pp. L21–L24, oct 2004. [Online]. Available: https://doi.org/10.1088/1464-4266/6/12/l01

[237] F. Albarelli, M. Barbieri, M. Genoni, and I. Gianani, "A perspective on multiparameter quantum metrology: From theoretical tools to applications in quantum imaging," *Physics Letters A*, vol. 384, no. 12, p. 126311, Apr. 2020. [Online]. Available: https://doi.org/10.1016/j.physleta.2020.126311

[238] A. Uhlmann, "Parallel transport and "quantum holonomy" along density operators," *Reports on Mathematical Physics*, vol. 24, no. 2, pp. 229–240, Oct. 1986. [Online]. Available: https://doi.org/10.1016/0034-4877(86)90055-8

[239] T. Frankel, *The Geometry of Physics: An Introduction*. Cambridge University Press, Nov. 2011. [Online]. Available: https://doi.org/10.1017/cbo9781139061377

[240] M. Nakahara, *Geometry, Topology and Physics*. CRC Press, Oct. 2018. [Online]. Available: https://doi.org/10.1201/9781315275826

[241] M. V. Berry, "Quantal phase factors accompanying adiabatic changes," *Proceedings of the Royal Society of London. A. Mathematical and Physical Sciences*, vol. 392, no. 1802, pp. 45–57, Mar. 1984. [Online]. Available: https://doi.org/10.1098/rspa.1984.0023

[242] A. Holevo, *Probabilistic and Statistical Aspects of Quantum Theory*. Pisa: Edizioni della Normale, 2011. [Online]. Available: https://doi.org/10.1007/978-88-7642-378-9

[243] ——, "Commutation superoperator of a state and its applications to the noncommutative statistics," *Reports on Mathematical Physics*, vol. 12, no. 2, pp. 251–271, Oct. 1977. [Online]. Available: https://doi.org/10.1016/0034-4877(77)90009-x

[244] A. Carollo, B. Spagnolo, A. A. Dubkov, and D. Valenti, "On quantumness in multi-parameter quantum estimation," *Journal of Statistical Mechanics: Theory and Experiment*, vol. 2019, no. 9, p. 094010, Sep. 2019. [Online]. Available: https://doi.org/10.1088/1742-5468/ab3ccb

[245] J. Suzuki, "Information Geometrical Characterization of Quantum Statistical Models in Quantum Estimation Theory," *Entropy*, vol. 21, no. 7, p. 703, Jul. 2019. [Online]. Available: https://doi.org/10.3390/e21070703

[246] D. Šafránek, A. R. Lee, and I. Fuentes, "Quantum parameter estimation using multi-mode gaussian states," *New Journal of Physics*, vol. 17, no. 7, p. 073016, jul 2015. [Online]. Available: https://dx.doi.org/10.1088/1367-2630/17/7/073016

[247] M. G. Genoni, M. G. A. Paris, G. Adesso, H. Nha, P. L. Knight, and M. S. Kim, "Optimal estimation of joint parameters in phase space," *Phys. Rev. A*, vol. 87, p. 012107, Jan 2013. [Online]. Available: https://link.aps.org/doi/10.1103/PhysRevA.87.012107

[248] O. Pinel, J. Fade, D. Braun, P. Jian, N. Treps, and C. Fabre, "Ultimate sensitivity of precision measurements with intense Gaussian quantum light: A multimodal approach," *Phys. Rev. A*, vol. 85, p. 010101, Jan 2012. [Online]. Available: https://link.aps.org/doi/10.1103/PhysRevA.85.010101

[249] D. Šafránek, "Discontinuities of the quantum Fisher information and the Bures metric," *Phys. Rev. A*, vol. 95, p. 052320, May 2017. [Online]. Available: https://link.aps.org/doi/10.1103/PhysRevA.95.052320

[250] D. Šafránek, "Estimation of Gaussian quantum states," *Journal of Physics A: Mathematical and Theoretical*, vol. 52, no. 3, p. 035304, Dec. 2018. [Online]. Available: https://doi.org/10.1088/1751-8121/aaf068

[251] R. Portugal, *Quantum walks and search algorithms*. AG: Springer Nature Switzerland, 2018.

[252] O. Mülken and A. Blumen, "Continuous-time quantum walks: Models for coherent transport on complex networks," *Phys. Rep.*, vol. 502, no. 2-3, pp. 37–87, 2011.

[253] J. Kempe, "Quantum random walks: an introductory overview," *Contemp. Phys.*, vol. 44, no. 4, pp. 307–327, 2003.

[254] A. Ambainis, "Quantum walks and their algorithmic applications," *Int. J. Quantum Inf.*, vol. 1, no. 04, pp. 507–518, 2003.

[255] S. E. Venegas-Andraca, "Quantum walks: a comprehensive review," *Quant. Inf. Process.*, vol. 11, no. 5, pp. 1015–1106, 2012.

[256] M. Roget, S. Guillet, P. Arrighi, and G. Di Molfetta, "Grover search as a naturally occurring phenomenon," *Phys. Rev. Lett.*, vol. 124, p. 180501, May 2020. [Online]. Available: https://link.aps.org/doi/10.1103/PhysRevLett.124.180501

[257] A. Beggi, L. Razzoli, P. Bordone, and M. G. A. Paris, "Probing the sign of the hubbard interaction by two-particle quantum walks," *Phys. Rev. A*, vol. 97, no. 1, p. 013610, 2018.

[258] L. Razzoli, L. Ghirardi, I. Siloi, P. Bordone, and M. G. Paris, "Lattice quantum magnetometry," *Phys. Rev. A*, vol. 99, no. 6, p. 062330, 2019.

[259] S. S. Schweber, "Feynman and the visualization of space-time processes," *Rev. Mod. Phys.*, vol. 58, pp. 449–508, Apr 1986. [Online]. Available: https://link.aps.org/doi/10.1103/RevModPhys.58.449

[260] Y. Aharonov, L. Davidovich, and N. Zagury, "Quantum random walks," *Phys. Rev. A*, vol. 48, no. 2, p. 1687, 1993.

[261] A. Ambainis, E. Bach, A. Nayak, A. Vishwanath, and J. Watrous, "One-dimensional quantum walks," in *Proceedings of the thirty-third annual ACM symposium on Theory of computing*. ACM, 2001, pp. 37–49.

[262] D. Aharonov, A. Ambainis, J. Kempe, and U. Vazirani, "Quantum walks on graphs," in *Proceedings of the thirty-third annual ACM symposium on Theory of computing*. ACM, 2001, pp. 50–59.

[263] V. Kendon, "Quantum walks on general graphs," *Int. J. Quantum Inf.*, vol. 4, no. 05, pp. 791–805, 2006.

[264] E. Farhi and S. Gutmann, "Quantum computation and decision trees," *Phys. Rev. A*, vol. 58, pp. 915–928, Aug 1998. [Online]. Available: https://link.aps.org/doi/10.1103/PhysRevA.58.915

[265] A. M. Childs, E. Farhi, and S. Gutmann, "An example of the difference between quantum and classical random walks," *Quantum Information Processing*, vol. 1, no. 1, pp. 35–43, 2002. [Online]. Available: https://doi.org/10.1023/A:1019609420309

[266] A. M. Childs, R. Cleve, E. Deotto, E. Farhi, S. Gutmann, and D. A. Spielman, "Exponential algorithmic speedup by a quantum walk," in *Proceedings of the thirty-fifth annual ACM symposium on Theory of computing*. ACM, Jun. 2003. [Online]. Available: https://doi.org/10.1145/780542.780552

[267] A. M. Childs and J. Goldstone, "Spatial search by quantum walk," *Phys. Rev. A*, vol. 70, p. 022314, Aug 2004. [Online]. Available: https://link.aps.org/doi/10.1103/PhysRevA.70.022314

[268] A. M. Childs and Y. Ge, "Spatial search by continuous-time quantum walks on crystal lattices," *Phys. Rev. A*, vol. 89, no. 5, p. 052337, 2014.

[269] C. Moore and A. Russell, "Quantum walks on the hypercube," *Proceedings of the 6th Int. Workshop on Randomization and Approximation in Computer Science (RANDOM'02), also in quant-ph/0104137*, 2002.

[270] N. Shenvi, J. Kempe, and K. B. Whaley, "Quantum random-walk search algorithm," *Phys. Rev. A*, vol. 67, no. 5, p. 052307, 2003.

[271] G. Abal, R. Donangelo, F. L. Marquezino, and R. Portugal, "Spatial search on a honeycomb network," *Math. Struct. Comp. Sci.*, vol. 20, no. 6, pp. 999–1009, 2010.

[272] M. G. A. Paris, C. Benedetti, and S. Olivares, "Improving quantum search on simple graphs by pretty good structured oracles," *Symmetry*, vol. 13, no. 1, 2021. [Online]. Available: https://www.mdpi.com/2073-8994/13/1/96

[273] T. G. Wong, "Quantum walk search through potential barriers," *J. Phys. A*, vol. 49, no. 48, p. 484002, 2016.

[274] T. G. Wong, L. Tarrataca, and N. Nahimov, "Laplacian versus adjacency matrix in quantum walk search," *Quantum Inf. Process.*, vol. 15, no. 10, pp. 4029–4048, 2016.

[275] I. Foulger, S. Gnutzmann, and G. Tanner, "Quantum search on graphene lattices," *Phys. Rev. Lett.*, vol. 112, p. 070504, Feb 2014. [Online]. Available: https://link.aps.org/doi/10.1103/PhysRevLett.112.070504

[276] D. Lu, J. Zhu, P. Zou, X. Peng, Y. Yu, S. Zhang, Q. Chen, and J. Du, "Experimental implementation of a quantum random-walk search algorithm using strongly dipolar coupled spins," *Phys. Rev. A*, vol. 81, p. 022308, Feb 2010. [Online]. Available: https://link.aps.org/doi/10.1103/PhysRevA.81.022308

[277] S. Chakraborty, L. Novo, A. Ambainis, and Y. Omar, "Spatial search by quantum walk is optimal for almost all graphs," *Phys. Rev. Lett.*, vol. 116, no. 10, p. 100501, 2016.

[278] S. Chakraborty, L. Novo, and J. Roland, "Optimality of spatial search via continuous-time quantum walks," *Phys. Rev. A*, vol. 102, p. 032214, Sep 2020. [Online]. Available: https://link.aps.org/doi/10.1103/PhysRevA.102.032214

[279] S. Bose, "Quantum communication through an unmodulated spin chain," *Phys. Rev. Lett.*, vol. 91, p. 207901, Nov 2003. [Online]. Available: https://link.aps.org/doi/10.1103/PhysRevLett.91.207901

[280] M. Christandl, N. Datta, A. Ekert, and A. J. Landahl, "Perfect state transfer in quantum spin networks," *Phys. Rev. Lett.*, vol. 92, no. 18, p. 187902, 2004.

[281] S. Bose, "Quantum communication through spin chain dynamics: an introductory overview," *Contemporary Physics*, vol. 48, no. 1, pp. 13–30, Jan. 2007. [Online]. Available: https://doi.org/10.1080/00107510701342313

[282] A. Kay, "A Review of Perfect, Efficient, State Transfer and its Application as a Constructive Tool," *International Journal of Quantum Information*, vol. 08, no. 04, pp. 641–676, Jun. 2010. [Online]. Available: https://doi.org/10.1142/s0219749910006514

[283] M. B. Plenio and S. F. Huelga, "Dephasing-assisted transport: quantum networks and biomolecules," *New J. Phys.*, vol. 10, no. 11, p. 113019, 2008.

[284] M. Mohseni, P. Rebentrost, S. Lloyd, and A. Aspuru-Guzik, "Environment-assisted quantum walks in photosynthetic energy transfer," *J. Chem. Phys.*, vol. 129, no. 17, pp. 174 106–174 106, 2008.

[285] A. M. Childs, "Universal computation by quantum walk," *Phys. Rev. Lett.*, vol. 102, p. 180501, May 2009. [Online]. Available: https://link.aps.org/doi/10.1103/PhysRevLett.102.180501

[286] A. M. Childs, D. Gosset, and Z. Webb, "Universal computation by multiparticle quantum walk," *Science*, vol. 339, no. 6121, pp. 791–794, Feb. 2013. [Online]. Available: https://doi.org/10.1126/science.1229957

[287] Y. Lahini, M. Verbin, S. D. Huber, Y. Bromberg, R. Pugatch, and Y. Silberberg, "Quantum walk of two interacting bosons," *Phys. Rev. A*, vol. 86, no. 1, p. 011603, 2012.

[288] Y. Lahini, G. R. Steinbrecher, A. D. Bookatz, and D. Englund, "Quantum logic using correlated one-dimensional quantum walks," *npj Quantum Inf.*, vol. 4, no. 1, p. 2, 2018.

[289] P. Arrighi and S. Facchini, "Decoupled quantum walks, models of the klein-gordon and wave equations," *EPL (Europhysics Letters)*, vol. 104, no. 6, p. 60004, Dec. 2013. [Online]. Available: https://doi.org/10.1209/0295-5075/104/60004

[290] P. Arrighi, V. Nesme, and M. Forets, "The dirac equation as a quantum walk: higher dimensions, observational convergence," *Journal of Physics A: Mathematical and Theoretical*, vol. 47, no. 46, p. 465302, Nov. 2014. [Online]. Available: https://doi.org/10.1088/1751-8113/47/46/465302

[291] P. Arrighi, G. Di Molfetta, I. Márquez-Martín, and A. Pérez, "Dirac equation as a quantum walk over the honeycomb and triangular lattices," *Phys. Rev. A*, vol. 97, no. 6, p. 062111, 2018.

[292] A. M. Childs, "On the relationship between continuous- and discrete-time quantum walk," *Communications in Mathematical Physics*, vol. 294, no. 2, pp. 581–603, Oct. 2009. [Online]. Available: https://doi.org/10.1007/s00220-009-0930-1

[293] G. E. Uhlenbeck and L. S. Ornstein, "On the Theory of the Brownian Motion," *Physical Review*, vol. 36, no. 5, pp. 823–841, Sep. 1930.

[294] A. E. Brouwer and W. H. Haemers, *Spectra of Graphs*. New York, NY: Springer New York, NY, 2012.

[295] C. Godsil and G. Royle, *Algebraic Graph Theory*. Springer New York, 2001. [Online]. Available: https://doi.org/10.1007/978-1-4613-0163-9

[296] D. B. West, *Introduction to Graph Theory*, 2nd ed. Prentice Hall, September 2000.

[297] A001349 - Number of connected graphs with n nodes. [Online]. Available: http://oeis.org/A123456

[298] X.-P. Xu, "Exact analytical results for quantum walks on star graphs," *Journal of Physics A: Mathematical and Theoretical*, vol. 42, no. 11, p. 115205, feb 2009. [Online]. Available: https://doi.org/10.1088/1751-8113/42/11/115205

[299] R. Portugal, S. Boettcher, and S. Falkner, "One-dimensional coinless quantum walks," *Phys. Rev. A*, vol. 91, p. 052319, May 2015. [Online]. Available: https://link.aps.org/doi/10.1103/PhysRevA.91.052319

[300] C. Godsil and H. Zhan, "Discrete-time quantum walks and graph structures," 2017. [Online]. Available: https://arxiv.org/abs/1701.04474

[301] V. M. Kendon and C. Tamon, "Perfect state transfer in quantum walks on graphs," *J. Comput. Theor. Nanos.*, vol. 8, no. 3, pp. 422–433, 2011.

[302] G. Coutinho, "Quantum state transfer in graphs," 2014. [Online]. Available: http://hdl.handle.net/10012/8623

[303] R. Alvir, S. Dever, B. Lovitz, J. Myer, C. Tamon, Y. Xu, and H. Zhan, "Perfect state transfer in laplacian quantum walk," *J. Algebr. Comb.*, vol. 43, no. 4, pp. 801–826, 2016.

[304] C. Godsil, "State transfer on graphs," *Discrete Mathematics*, vol. 312, no. 1, pp. 129–147, Jan. 2012. [Online]. Available: https://doi.org/10.1016/j.disc.2011.06.032

[305] Chris Godsil, "When can perfect state transfer occur?" *The Electronic Journal of Linear Algebra*, vol. 23, Jan. 2012. [Online]. Available: https://doi.org/10.13001/1081-3810.1563

[306] G. Coutinho, C. Godsil, E. Juliano, and C. M. van Bommel, "Quantum walks do not like bridges," *Linear Algebra and its Applications*, vol. 652, pp. 155–172, Nov. 2022. [Online]. Available: https://doi.org/10.1016/j.laa.2022.07.009

[307] X. Fan and C. Godsil, "Pretty good state transfer on double stars," *Linear Algebra and its Applications*, vol. 438, no. 5, pp. 2346–2358, Mar. 2013. [Online]. Available: https://doi.org/10.1016/j.laa.2012.10.006

[308] L. Banchi, G. Coutinho, C. Godsil, and S. Severini, "Pretty good state transfer in qubit chains—the heisenberg hamiltonian," *Journal of Mathematical Physics*, vol. 58, no. 3, Mar. 2017. [Online]. Available: https://doi.org/10.1063/1.4978327

[309] G. Coutinho, K. Guo, and C. M. Van Bommel, "Pretty good state transfer between internal nodes of paths," *Quantum Info. Comput.*, vol. 17, no. 9–10, p. 825–830, aug 2017.

[310] L. Novo, S. Chakraborty, M. Mohseni, H. Neven, and Y. Omar, "Systematic dimensionality reduction for quantum walks: Optimal spatial search and transport on non-regular graphs," *Sci. Rep.*, vol. 5, p. 13304, 2015.

[311] D. Qu, S. Marsh, K. Wang, L. Xiao, J. Wang, and P. Xue, "Deterministic search on star graphs via quantum walks," *Phys. Rev. Lett.*, vol. 128, p. 050501, Feb 2022. [Online]. Available: https://link.aps.org/doi/10.1103/PhysRevLett.128.050501

[312] S. Apers, S. Chakraborty, L. Novo, and J. Roland, "Quadratic speedup for spatial search by continuous-time quantum walk," *Phys. Rev. Lett.*, vol. 129, p. 160502, Oct 2022. [Online]. Available: https://link.aps.org/doi/10.1103/PhysRevLett.129.160502

[313] A. Candeloro, C. Benedetti, M. G. Genoni, and M. G. A. Paris, "Feedback-assisted quantum search by continuous-time quantum walks," *Advanced Quantum Technologies*, vol. 6, no. 1, Nov. 2022. [Online]. Available: https://doi.org/10.1002/qute.202200093

[314] M. Delvecchio, C. Groiseau, F. Petiziol, G. S. Summy, and S. Wimberger, "Quantum search with a continuous-time quantum walk in momentum space," *Journal of Physics B: Atomic, Molecular and Optical Physics*, vol. 53, no. 6, p. 065301, Feb. 2020. [Online]. Available: https://doi.org/10.1088/1361-6455/ab63ad

[315] I. Foulger, S. Gnutzmann, and G. Tanner, "Quantum walks and quantum search on graphene lattices," *Phys. Rev. A*, vol. 91, no. 6, p. 062323, 2015.

[316] A. Auerbach, *Interacting Electrons and Quantum Magnetism*. Springer New York, 1994. [Online]. Available: https://doi.org/10.1007/978-1-4612-0869-3

[317] C. L. Cleveland and R. M. A., "Obtaining a heisenberg hamiltonian from the hubbard model," *American Journal of Physics*, vol. 44, no. 1, pp. 44–46, Jan. 1976. [Online]. Available: https://doi.org/10.1119/1.10537

[318] W. Heisenberg, "Zur theorie des ferromagnetismus," *Zeitschrift für Physik*, vol. 49, no. 9-10, pp. 619–636, Sep. 1928. [Online]. Available: https://doi.org/10.1007/bf01328601

[319] H. Bethe, "Zur theorie der metalle," *Zeitschrift für Physik*, vol. 71, no. 3-4, pp. 205–226, Mar. 1931. [Online]. Available: https://doi.org/10.1007/bf01341708

[320] M. Karbach, G. Müller, H. Gould, and J. Tobochnik, "Introduction to the bethe ansatz i," *Computers in Physics*, vol. 11, no. 1, p. 36, 1997. [Online]. Available: https://doi.org/10.1063/1.4822511

[321] M. Karbach, K. Hu, and G. Müller, "Introduction to the bethe ansatz II," *Computers in Physics*, vol. 12, no. 6, pp. 565–573, Nov. 1998. [Online]. Available: https://doi.org/10.1063/1.168740

[322] R. J. Baxter, "Exactly solved models in statistical mechanics," in *Series on Advances in Statistical Mechanics*. WORLD SCIENTIFIC, May 1985, pp. 5–63. [Online]. Available: https://doi.org/10.1142/9789814415255_0002

[323] G. B. Mbeng, A. Russomanno, and G. E. Santoro, "The quantum ising chain for beginners," 2020. [Online]. Available: https://arxiv.org/abs/2009.09208

[324] I. Affleck and F. D. M. Haldane, "Critical theory of quantum spin chains," *Phys. Rev. B*, vol. 36, pp. 5291–5300, Oct 1987. [Online]. Available: https://link.aps.org/doi/10.1103/PhysRevB.36.5291

[325] T. J. Osborne and N. Linden, "Propagation of quantum information through a spin system," *Phys. Rev. A*, vol. 69, p. 052315, May 2004. [Online]. Available: https://link.aps.org/doi/10.1103/PhysRevA.69.052315

[326] A. Wójcik, T. Łuczak, P. Kurzyński, A. Grudka, T. Gdala, and M. Bednarska, "Unmodulated spin chains as universal quantum wires," *Phys. Rev. A*, vol. 72, p. 034303, Sep 2005. [Online]. Available: https://link.aps.org/doi/10.1103/PhysRevA.72.034303

[327] L. Banchi, T. J. G. Apollaro, A. Cuccoli, R. Vaia, and P. Verrucchi, "Long quantum channels for high-quality entanglement transfer," *New Journal of Physics*, vol. 13, no. 12, p. 123006, Dec. 2011. [Online]. Available: https://doi.org/10.1088/1367-2630/13/12/123006

[328] Groenland, Koen L., "Quantum protocols for few-qubit devices," PhD thesis, Institute for Logic, Language and Computation (ILLC), Amsterdam, Amsterdam, January 2020. [Online]. Available: https://hdl.handle.net/11245.1/dc65f93d-9c45-4499-aea9-f36091b5735f

[329] K. Groenland and K. Schoutens, "Many-body strategies for multiqubit gates: Quantum control through krawtchouk-chain dynamics," *Phys. Rev. A*, vol. 97, p. 042321, Apr 2018. [Online]. Available: https://link.aps.org/doi/10.1103/PhysRevA.97.042321

[330] Z. Zimborás, M. Faccin, Z. Kádár, J. D. Whitfield, B. P. Lanyon, and J. Biamonte, "Quantum Transport Enhancement by Time-Reversal Symmetry Breaking," *Scientific Reports*, vol. 3, no. 1, Aug. 2013. [Online]. Available: https://doi.org/10.1038/srep02361

[331] D. Lu, J. D. Biamonte, J. Li, H. Li, T. H. Johnson, V. Bergholm, M. Faccin, Z. Zimborás, R. Laflamme, J. Baugh, and S. Lloyd, "Chiral quantum walks," *Phys. Rev. A*, vol. 93, p. 042302, Apr 2016. [Online]. Available: https://link.aps.org/doi/10.1103/PhysRevA.93.042302

[332] J. W. Turner and J. Biamonte, "Topological classification of time-asymmetry in unitary quantum processes," *Journal of Physics A: Mathematical and Theoretical*, vol. 54, no. 23, p. 235301, apr 2021. [Online]. Available: https://doi.org/10.1088/1751-8121/abf9d0

[333] J. D. Whitfield, C. A. Rodríguez-Rosario, and A. Aspuru-Guzik, "Quantum stochastic walks: A generalization of classical random walks and quantum walks," *Phys. Rev. A*, vol. 81, p. 022323, Feb 2010. [Online]. Available: https://link.aps.org/doi/10.1103/PhysRevA.81.022323

[334] M. G. Andrade, F. de Lima Marquezino, and D. R. Figueiredo, "On the equivalence between quantum and random walks on finite graphs," *Quantum Information Processing*, vol. 19, no. 11, Nov. 2020. [Online]. Available: https://doi.org/10.1007/s11128-020-02917-w

[335] M. Frigerio, C. Benedetti, S. Olivares, and M. G. A. Paris, "Generalized quantum-classical correspondence for random walks on graphs," 2021.

[336] G. J. Milburn, "Intrinsic decoherence in quantum mechanics," *Phys. Rev. A*, vol. 44, pp. 5401–5406, Nov 1991. [Online]. Available: https://link.aps.org/doi/10.1103/PhysRevA.44.5401

[337] S. Cameron, S. Fehrenbach, L. Granger, O. Hennigh, S. Shrestha, and C. Tamon, "Universal state transfer on graphs," *Linear Algebra and its Applications*, vol. 455, pp. 115–142, 2014. [Online]. Available: https://www.sciencedirect.com/science/article/pii/S0024379514002845

[338] O. Boada, L. Novo, F. Sciarrino, and Y. Omar, "Quantum walks in synthetic gauge fields with three-dimensional integrated photonics," *Phys. Rev. A*, vol. 95, no. 1, p. 013830, 2017.

[339] L. Novo and S. Ribeiro, "Floquet engineering of continuous-time quantum walks: Toward the simulation of complex and next-nearest-neighbor couplings," *Phys. Rev. A*, vol. 103, p. 042219, Apr 2021. [Online]. Available: https://link.aps.org/doi/10.1103/PhysRevA.103.042219

[340] M. Aidelsburger, *Artificial gauge fields with ultracold atoms in optical lattices*. New York: Springer, 2015.

[341] J. Dalibard, F. Gerbier, G. Juzeliūnas, and P. Öhberg, "Colloquium: Artificial gauge potentials for neutral atoms," *Rev. Mod. Phys.*, vol. 83, no. 4, p. 1523, 2011.

[342] C. Cedzich, T. Geib, A. H. Werner, and R. F. Werner, "Quantum walks in external gauge fields," *Journal of Mathematical Physics*, vol. 60, no. 1, p. 012107, 2019.

[343] J. Wang and K. Manouchehri, *Physical implementation of quantum walks*. New York: Springer, 2013.

[344] C. Benedetti, D. Tamascelli, M. G. Paris, and A. Crespi, "Quantum spatial search in two-dimensional waveguide arrays," *Phys. Rev. Appl.*, vol. 16, p. 054036, Nov 2021. [Online]. Available: https://link.aps.org/doi/10.1103/PhysRevApplied.16.054036

[345] S. Longhi, "Aharonov–bohm photonic cages in waveguide and coupled resonator lattices by synthetic magnetic fields," *Optics Letters*, vol. 39, no. 20, p. 5892, Oct. 2014. [Online]. Available: https://doi.org/10.1364/ol.39.005892

[346] R. P. Feynman, R. B. Leighton, and M. Sands, *The Feynman Lectures on Physics, Vol. III: The New Millennium Edition: Quantum Mechanics*, ser. The Feynman Lectures on Physics. New York: Basic Books, 2011.

[347] İ. Yalçınkaya and Z. Gedik, "Two-dimensional quantum walk under artificial magnetic field," *Phys. Rev. A*, vol. 92, no. 4, p. 042324, 2015.

[348] B. A. Bernevig and T. L. Hughes, *Topological insulators and topological superconductors*. Princeton: Princeton university press, 2013.

[349] D. R. Hofstadter, "Energy levels and wave functions of bloch electrons in rational and irrational magnetic fields," *Phys. Rev. B*, vol. 14, no. 6, p. 2239, 1976.

[350] Massimo Frigerio and Matteo G.A. Paris, "Swift chiral quantum walks," *Linear Algebra and its Applications*, vol. 673, pp. 28–45, Sep. 2023. [Online]. Available: https://doi.org/10.1016/j.laa.2023.05.007

[351] M. Frigerio, C. Benedetti, S. Olivares, and M. G. A. Paris, "Quantum-classical distance as a tool to design optimal chiral quantum walks," *Phys. Rev. A*, vol. 105, p. 032425, Mar 2022. [Online]. Available: https://link.aps.org/doi/10.1103/PhysRevA.105.032425

[352] A. Bottarelli, M. Frigerio, and M. G. A. Paris, "Quantum routing of information using chiral quantum walks," *AVS Quantum Science*, vol. 5, no. 2, Apr. 2023. [Online]. Available: https://doi.org/10.1116/5.0146805

[353] E. Annoni, M. Frigerio, and M. G. A. Paris, "Enhanced quantum transport in chiral quantum walks," 2023. [Online]. Available: https://arxiv.org/abs/2308.14747

[354] C. Godsil, "Sedentary quantum walks," *Linear Algebra and its Applications*, vol. 614, pp. 356–375, 2021, special Issue ILAS 2019. [Online]. Available: https://www.sciencedirect.com/science/article/pii/S0024379520304067

[355] L. Razzoli, P. Bordone, and M. G. A. Paris, "Universality of the fully connected vertex in laplacian continuous-time quantum walk problems," *Journal of Physics A: Mathematical and Theoretical*, vol. 55, no. 26, p. 265303, jun 2022. [Online]. Available: https://doi.org/10.1088/1751-8121/ac72d5

[356] V. Gualtieri, C. Benedetti, and M. G. A. Paris, "Quantum-classical dynamical distance and quantumness of quantum walks," *Phys. Rev. A*, vol. 102, p. 012201, Jul 2020. [Online]. Available: https://link.aps.org/doi/10.1103/PhysRevA.102.012201

[357] S. Cameron, S. Fehrenbach, L. Granger, O. Hennigh, S. Shrestha, and C. Tamon, "Universal state transfer on graphs," *Linear Algebra and its Applications*, vol. 455, pp. 115–142, 2014. [Online]. Available: https://www.sciencedirect.com/science/article/pii/S0024379514002845

[358] T. G. Wong, "Quantum walk search with time-reversal symmetry breaking," *Journal of Physics A: Mathematical and Theoretical*, vol. 48, no. 40, p. 405303, sep 2015. [Online]. Available: https://doi.org/10.1088/1751-8113/48/40/405303

[359] A. Ahmadi, R. Belk, C. Tamon, and C. Wendler, "On mixing in continuous-time quantum walks on some circulant graphs," *Quantum Info. Comput.*, vol. 3, no. 6, p. 611–618, Nov. 2003.

[360] L. Campos Venuti, S. M. Giampaolo, F. Illuminati, and P. Zanardi, "Long-distance entanglement and quantum teleportation in xx spin chains," *Phys. Rev. A*, vol. 76, p. 052328, Nov 2007. [Online]. Available: https://link.aps.org/doi/10.1103/PhysRevA.76.052328

[361] U. Sağlam, M. Paternostro, and Özgür E. Müstecaplıoğlu, "Entanglement transfer via chiral and continuous-time quantum walks on a triangular chain," *Physica A: Statistical Mechanics and its Applications*, vol. 612, p. 128480, 2023. [Online]. Available: https://www.sciencedirect.com/science/article/pii/S0378437123000353

[362] M. Walschaers, "On quantum steering and wigner negativity," *Quantum*, vol. 7, p. 1038, Jun. 2023. [Online]. Available: https://doi.org/10.22331/q-2023-06-07-1038

[363] M. Walschaers and N. Treps, "Remote generation of wigner negativity through einstein-podolsky-rosen steering," *Phys. Rev. Lett.*, vol. 124, p. 150501, Apr 2020. [Online]. Available: https://link.aps.org/doi/10.1103/PhysRevLett.124.150501

[364] Y. Xiang, S. Liu, J. Guo, Q. Gong, N. Treps, Q. He, and M. Walschaers, "Distribution and quantification of remotely generated wigner negativity," *npj Quantum Information*, vol. 8, no. 1, Mar. 2022. [Online]. Available: https://doi.org/10.1038/s41534-022-00533-3

[365] U. Chabaud and M. Walschaers, "Resources for bosonic quantum computational advantage," *Phys. Rev. Lett.*, vol. 130, p. 090602, Mar 2023. [Online]. Available: https://link.aps.org/doi/10.1103/PhysRevLett.130.090602

[366] M. Walschaers, J. Kuipers, J.-D. Urbina, K. Mayer, M. C. Tichy, K. Richter, and A. Buchleitner, "Statistical benchmark for BosonSampling," *New Journal of Physics*, vol. 18, no. 3, p. 032001, Mar. 2016. [Online]. Available: https://doi.org/10.1088/1367-2630/18/3/032001

[367] Y.-C. Yu and X. Cai, "Controlled transport in chiral quantum walks on graphs," *New Journal of Physics*, vol. 25, no. 8, p. 083034, Aug. 2023. [Online]. Available: https://doi.org/10.1088/1367-2630/acec90

Acknowledgments

I would like to express deep gratitude to my supervisor Matteo G. A. Paris. Besides guiding me in my first research experiences, he cared for my academic and human development in ways that often only became clear to me long afterwards. He has been enlightening, patient, empathetic and always available for discussions, without ever refusing to engage in the tricky foundational questions I am often concerned with. He also gave me some of the best advises to find my way in an increasingly competitive academic environment. I am convinced that I have been really lucky to have had the opportunity and the privilege to work with him. I am also grateful to the rest of our research group, in particular to professors Claudia Benedetti and Stefano Olivares, PhD students Davide Ferracin, Daniele Morrone and Michele Notarnicola, and currently postdoctoral researchers Alessandro Candeloro and Luca Razzoli: they have been to me the living proof that the scientific community can truly be supportive, cooperative and friendly.